# Reaction of Glucose Catalyzed by Framework and Extraframework Tin Sites in Zeolite Beta

Thesis by

Ricardo Bermejo-Deval

In Partial Fulfillment of the Requirements for the

degree of

Doctor of Philosophy


CALIFORNIA INSTITUTE OF TECHNOLOGY

Pasadena, California

2014

(Defended 12 May 2014)

## ACKNOWLEDGEMENTS

The past years at Caltech have been one of the most challenging periods of my life, learning to be a better person and being part of the world of science. I feel privileged to have interacted with such talented and inspiring colleagues and scientists, as well as those I have disagreed with. The variety of people I have encountered and the experiences I have gathered have helped me to gain scholarship, wisdom, confidence and critical thinking, as much as to become an open-minded person to any opinion or people.

First and foremost, I am very grateful to my advisor and mentor, Professor Mark E. Davis, for his financial, scientific and personal support. I appreciate his patience, flexibility, advice and scientific discussions, helping me to grow and mature scientifically. I would like to thank the thesis committee Professors Richard Flagan, Jay Labinger and Theodor Agapie, for their discussions and kindness. I appreciate everyone in the Davis group for helping me in the lab throughout these years. Special thanks to Yasho for helping me get started in the lab, to Bingjun and Raj for scientific advice, and to Marat for helpful talks. I am also very thankful to Sonjong Hwang for SS NMR, David Vandervelde for NMR and Mona Shahgholi for mass spectrometry. In addition, I would like to express my gratitude to the people at Chevron R&D at Richmond, for conceding me an internship with them during July-October 2012, especially to C.Y. Chen.

I would like to thank all of my classmates, professors and mentors in my home city Valencia, Spain, who believed and trusted in me to pursue a PhD at Caltech. I am greatly indebted to Professors Carmen Gabaldon and Paula Marzal, for mentoring me during my undergraduate degree and research fellowship. I am greatly honored to be

guided in my research career by Professor Avelino Corma, who has aided with both scientific and personal advice. I would also like to express my gratitude to “la Caixa” fellowship program for paying part of my PhD studies, as well as granting me the opportunity to meet great people.

I feel truly fortunate to have met and become friends with a great number of people throughout these years: Marilena, Matt Coggon, Matt Shanner, Vanessa, Kathy, Carlos, Alejandro, Pablo & others… I feel really lucky to have shared such great times with the Caltech Masters Swimteam and their friends: Andrew, Evelyn, Sean, Tobias, AJ and Dubi. I will never forget the support and friendship that Charlie Slominski and Matt Lalli have provided me with, during both good and bad times. To all of you, thank you.

Last but not least, I would like to express my deepest gratitude to my family who have always supported and believed in my goals. To my dad, Toni, for being patient in all aspects of my life; to my brother, John, for providing me with laughter and joy since the day he was born; and to my mum, Helen, for guiding me in my life and pushing me to become the person I am.

# ABSTRACT

The isomerization of glucose into fructose is a large-scale reaction for the production of high-fructose corn syrup, and is now being considered as an intermediate step in the possible route of biomass conversion into fuels and chemicals. Recently, it has been shown that a hydrophobic, large pore, silica molecular sieve having the zeolite beta structure and containing framework $Sn^{4+}$ (Sn-Beta) is able to isomerize glucose into fructose in aqueous media. Here, I have investigated how this catalyst converts glucose to fructose and show that it is analogous to that achieved with metalloenzymes. Specifically, glucose partitions into the molecular sieve in the pyranose form, ring opens to the acyclic form in the presence of the Lewis acid center (framework $Sn^{4+}$), isomerizes into the acyclic form of fructose and finally ring closes to yield the furanose product. Akin to the metalloenzyme, the isomerization step proceeds by intramolecular hydride transfer from C2 to C1. Extraframework tin oxides located within hydrophobic channels of the molecular sieve that exclude liquid water can also isomerize glucose to fructose in aqueous media, but do so through a base-catalyzed proton abstraction mechanism. Extraframework tin oxide particles located at the external surface of the molecular sieve crystals or on amorphous silica supports are not active in aqueous media but are able to perform the isomerization in methanol by a base-catalyzed proton abstraction mechanism. Post-synthetic exchange of $Na^{+}$ with Sn-Beta alters the glucose reaction pathway from the 1,2 intramolecular hydrogen shift (isomerization) to produce fructose towards the 1,2 intramolecular carbon shift (epimerization) that forms mannose. $Na^{+}$ remains exchanged onto silanol groups during reaction in methanol solvent, leading to a near complete shift in selectivity towards glucose epimerization to mannose. In contrast,

decationation occurs during reaction in aqueous solutions and gradually increases the reaction selectivity to isomerization at the expense of epimerization. Decationation and concomitant changes in selectivity can be eliminated by addition of NaCl to the aqueous reaction solution. Thus, framework tin sites with a proximal silanol group are the active sites for the 1, 2 intramolecular hydride shift in the isomerization of glucose to fructose, while these sites with Na-exchanged silanol group are the active sites for the 1, 2 intramolecular carbon shift in epimerization of glucose to mannose.

# TABLE OF CONTENTS

# LIST OF FIGURES

## Chapter 1



## Chapter 2

**Chapter 4**

**Chapter 6**

# LIST OF TABLES

## Chapter 2



## Chapter 3



## Chapter 4

# Chapter 1: Introduction and Thesis Organization

## 1. Biomass Conversion into Biofuels and Fine Chemicals

### 1.1 Biomass Components

Climate change and dwindling fossil fuel resources have made industry look at biomass as a renewable feedstock for the synthesis of chemicals and transportation fuels.[1] Previous studies from the U.S. Department of Agriculture (USDA) and Oak Ridge National Laboratory calculated that the U.S. would be able to sustain producing $1.3x10^9$ metric tons on an annual basis, resulting in an energy production of $3.8x10^9$ barrels of oil.[2] Since carbohydrates represent 75% of the annual renewable biomass,[3] chemical companies such as Shell, UOP, Petrobas, Conoco-Phillips, Dupont, Dow and BP are already using carbohydrates as part of their economy.[1] Hence, developing new chemical synthetic routes from carbohydrates is of current interest for Industry.

Currently, the catalytic transformation of biomass into fuels and chemicals is done by gasification, pyrolysis and hydrolysis.[4] While gasification is achieved by means of biomass reaction with a controlled amount of oxygen and/or steam without combustion, pyrolysis is done via thermochemical decomposition of organic material at elevated temperatures in the absence of oxygen. In gasification a gas mixture is obtained, syngas (carbon monoxide, hydrogen and carbon dioxide), and in pyrolysis the products include biochar, bio-oil and gases (methane, hydrogen, carbon monoxide and carbon dioxide). In contrast, hydrolysis attempts to breakdown the polymers of biomass into its individual components.

Lignocellulosic biomass is the most abundant raw material available for the synthesis of biofuels, composed of 3 constituents:[5] lignin (15-20%), hemicellulose (25-35%) and cellulose (40-50%). Lignin is an integral part of the plant secondary cell

walls,[6] composed of three methoxylated monolignol monomers: p-coumaryl alcohol, coniferyl alcohol and sinapsyl alcohol. Hemicellulose is an amorphous polysaccharide found in the cell wall of plants, formed mainly of $C_5$ (D-xylose and D-arabinose) and $C_6$ (D-glucose, D-mannose and D-galactose) sugar monomers. Cellulose is a structural component from the primary cell wall of green plants, consisting of thousands of glucose units. The liberation of cellulose from the lignin composite and the breakdown of its rigid structure have been a priority in biomass research,[7] since glucose together with xylose are considered as two important platform molecules for the biomass conversion into fuels and fuels additives, as can be seen in Figure 1.1.

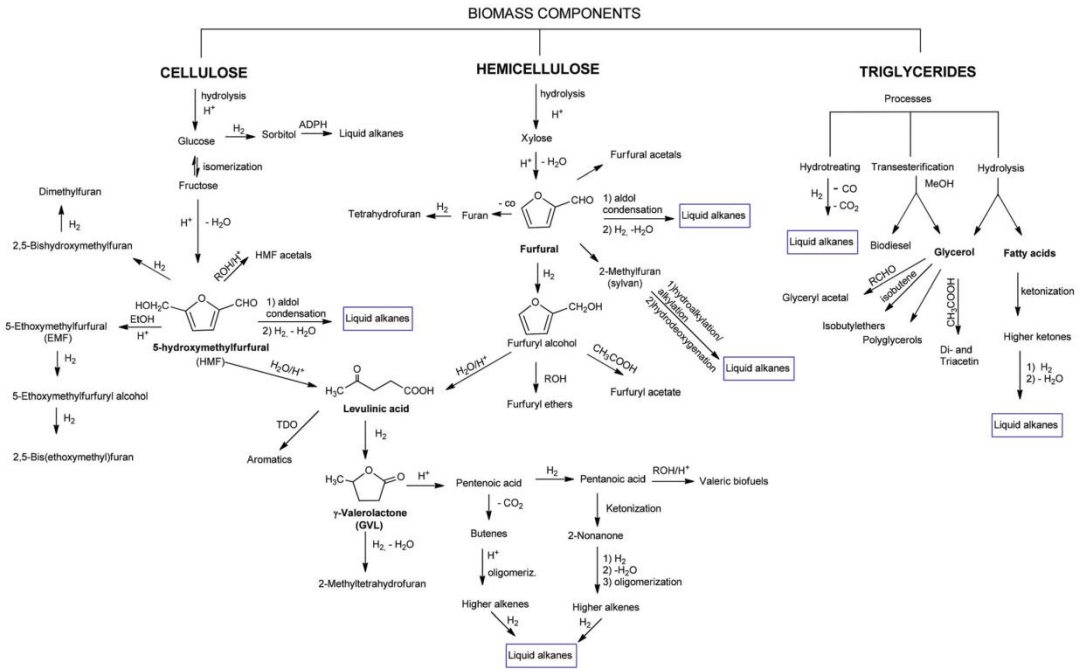


**Figure 1.1 Biomass conversion into fuels and fuel additives[5].**

## 2.2 Biomass Hydrolysis

Liquid acid catalysts have been used in the hydrolysis of lignocellulosic biomass, with higher catalytic performance at low concentrations, higher temperatures and short residence times to avoid further degradation of its monomers.[8,9] Inorganic Brønsted acids such as hydrochloric, sulfuric and phosphoric acid are very effective in

the depolymerization of lignocellulose, but the severe corrosion, costly separation and acid waste neutralization seem an expensive process.[4] Carbonic acid seems to be more environmentally friendly, due to the low corrosion and depressurization of the carbon dioxide, resulting in no acid waste residues after reaction.[10,11] Other alternatives have been the use of organic acids, such as oxalic and maleic acid,[12] and ionic liquids, the latter being the most effective with nearly 90% yield of glucose from cellulose.[13] However, the high cost and low recyclability of ionic liquids prevent the scale-up of this process.

Solid acid-catalyzed hydrolysis has the advantage of easy catalyst separation from the liquid mixture after reaction and its reusability. Sulfonated activated carbon results in a highly active catalyst for the hydrolysis of cellulose,[14,15] with 40.5% glucose yields, in comparison to other solid Brønsted acids like zeolites, sulfonated zirconia and Amberlyst sulfonated resin . The strong acidity of the $–SO_3H$ functional groups together with the hydrophobic planes on the surfaces of the activated carbon at mildly hydrothermal conditions seem favorable for cellulose hydrolysis. Heteropoly acids are also active in the hydrolysis of cellulose, with 50.5% yield of glucose over $H_3PW_{12}O_{40}$. However, the poor solid-solid interaction between the catalyst and cellulose results in a low activation of the β-1,4-glycosidic bonds that connect the monosaccharides, leading to a moderate depolymerization.

## 2.3 Biomass Applications

For these simple sugars to be able to produce transportation fuels and chemicals, they need be broken down and have oxygen atoms removed without deteriorating their energy value.[3] Although microorganisms seem to have found a path to convert the sugars into chemical compounds of interest,[16] the relatively slow

kinetics of fermentation and the expensive post-processing of these products have made heterogeneous catalysis a viable option to develop a sustainable carbohydrate industry.

Currently, "The Biofine"[17,18] process is in pilot level production, converting lignocellulose into platform molecule levulinic acid.[19] In a first step, biomass hydrolysis into 5-hydroxymethylfurfural (HMF) takes place in a plug-flow reactor using sulfuric acid as a Brønsted acid for short residence times to minimize product degradation. In the second step, intermediates are converted into levulinic acid, separating the formic acid formed as well as the intermediates. The low efficiency of biomass converted into levulinic acid, 50% yield, has driven scientists to design catalysts and processes that are more efficient throughout the pathway described in Figure 1.1.

Biphasic reactors can increase the selectivity of HMF and furfural (e.g., 90%) from fructose and xylose,[20–22] respectively. In these cases side reactions, such as condensations, are minimized extracting the HMF or furfural from the aqueous layer using organic solvents like THF, 2-butanol or methyl isobutyl ketone. HMF is also considered a platform molecule for the synthesis of transportation fuels. Hydrogenolysis of HMF over Cu-Ru/C or $CuCrO_4$ catalysts results in 79% and 61% yields of 2,5-dimethyl furan (DMF), respectively.[23] Aldol condensation of HMF and furfural with ketones can be coupled with hydrogenation/dehydration over a Pd/MgO-$ZrO_2$ catalyst, obtaining high yields of condensation products.[24] Nevertheless, HMF hydration produces equimolar amounts of formic acid and levulinic acid, the latter being a molecule in the selected list of platform molecules derived from biomass.[25]

Levulinic acid serves as the platform molecule for the synthesis of γ-valerolactone (GVL), having to use external hydrogen. Levulinic acid is dehydrated into angelica lactone and reduced to γ-valerolactone, or reduced to 4-hydroxy-pentanoic acid and subsequent dehydration.[5] Using a Ru/C catalyst at 423 K and 34.5 bar in dioxane, 97% yield of GVL is achieved.[26] The *in situ* decomposition of formic acid (a byproduct in the synthesis of levulinic acid) to form hydrogen has been proposed as an alternative source.[19,27] Monosaccharide conversion into GVL with external hydrogen or formic acid has been achieved using Ru/C catalyst together with trifluoroacetic acid,[28] preventing the poisoning of the metal from other acids, like sulfuric acid. This process resulted in yields of 52% and 46% from D-fructose and D-glucose, respectively, with formic acid and of 62% and 38% from same reactants with external hydrogen.[29]

The applications of γ-valerolactone are varied, from being a platform molecule for the synthesis of fuels and chemicals to its direct use as a fuel additive or solvent.[30] Methyltetrahydrofuran (MTHF), a fuel extender which can be blended up to 70% with gasoline without modification of current internal combustion engines,[19] can be synthesized by the reduction of GVL into 1,4-pentanediol and consequent dehydration,[31] resulting in 63% yield of MTHF with bimetallic catalyst Pd (5%)Re(5%)/C.[32] The ring opening of GVL results in a mixture of pentenoic acids, the precursors in the synthesis of alkanes and alkenes. Ketonization of pentanoic acids and consequent hydrogenation forms $C_9$ alkanes, while decarboxylation of a mixture of pentenoic acids leads to butenes that can be oligomerized to $C_{8+}$ alkenes

Liquid biofuels are also currently being produced from vegetable oils and animal fats which have a high content of tryglycerides.[33] These triglycerides can go

through transesterification with methanol to produce biodiesel and glycerol as a byproduct. The 3 hydroxyl groups in glycerol can functionalize other molecules, producing acetals, ethers and polyglycerols among others.[5] Transition metals, such as platinum and rhenium, supported on microporous materials[34,35] or molybdenum supported on alumina[36,37] are good catalyst for the hydrotreating of triglycerides to produce liquid alkanes.

## 2. Introduction to Zeolites, Lewis Acids and Zeolite Sn-Beta

### 2.2 Introduction to Zeolites and Molecular Sieves

Zeolites are microporous inorganic materials with diverse applications in industrial relevant processes, ranging from petrochemical and purification processes to medicine and agriculture.[38] Their structure arises from a three-dimensional network with pores and cavities between 0.2-2 nm in diameter formed by tetrahedral heteroatoms, mainly $Si^{+4}$ and $Al^{+3}$, coordinated through oxygen atoms.[39] The defect charge resulting from the tetrahedral coordination of the $Al^{+3}$ ions requires an extra-framework cation to balance the net charge of the framework. These cations can be inorganic cations, organic cations, ammonium ions or protons, being in some cases the nature of the catalytic active site.[40] This results in the following general formula composition of a zeolite: $Al_2O_3 \cdot x\ SiO_2 \cdot y\ H_2O \cdot M_{2/n}O$, being M the cation compensating the defect charge created by the alumina. A proton located in the proximity of a framework aluminum introduces a strong Brønsted acid site, which is required in multiple catalyzed chemical reactions.[38]

The topology and micropore system allows zeolites to be molecular sieves, selective in the size of reactants entering the framework as well as the products

leaving it. The inter-diffusion of molecules into the zeolite can be tuned by crystal size (ranging from 5-20 μm), pore size distribution and number of different pore openings where molecules enter (one-, two, and/or three-dimensional pores). In addition, these pores are interconnected through cages and channels, resulting in a high surface area where active sites are situated, to enhance the rate of chemical reactions and selectivity to a desired product.[40] Their physicochemical features together with the high hydrothermal stability and "nontoxic" character has originated in a wide application of zeolites in industry.

Zeolites have been traditionally described as crystalline microporous aluminosilicates with the physicochemical abilities previously described. Over time, zeolite-type materials have been synthesized with different composition, having the same framework topology. The compositions of these materials are varied: silicates, silicoaluminophosphates, aluminophosphates, metallosilicates, etc. Although their physical properties are analogous to zeolites, their chemical features are different, providing a unique catalytic site for a desired reaction. Also, the electronic environment might change, like the case of defect free silicates with high hydrophobicity and low ion exchange capacity.

The zeolite nomenclature is assigned to its topology with a three letter code, whether it is a natural or synthetic zeolite, designated by the International Union of Pure and Applied Chemistry (IUPAC) Commission on Zeolite Nomenclature and the International Zeolite Association (IZA). Zeolites with the same topology but with different chemical composition may be named differently. A well-known example of this is MFI, composed of a three-dimensional framework with 10 member ring mouth pores. The most common synthetic material with MFI topology is zeolite ZSM-5,

which can have different cations compensating the defect charge created by the aluminum, like a proton, and therefore, named H-ZSM-5. In addition, the isomorphic substitution of metals in tetrahedral coordination of pure silicate MFI frameworks has led to different materials: titanium[41] (TS-1), iron[42] (FeS-1), Sn[43,44] (Sn-MFI or Tin-Silicate-1),… Due to the large number of zeolites, they have been divided in different groups according to the size of their mouth pores: small (8 or less member rings), medium (10 member rings), and large (12 member rings) and extra-large (higher than 12). In the case of this work we will concentrate only on a large zeolite, zeolite beta, with isomorphically substituted Sn in tetrahedral coordination.

## 2.3 Lewis Acids

A Lewis acid is defined by the IUPAC as a molecular entity that is an electron-pair acceptor and therefore able to react with a Lewis base to form a Lewis adduct, by sharing the electron pair furnished by the Lewis base.[45] Figure 1.2 shows a typical schematic representation of a Lewis acid catalyst[46] with a Lewis base, such as a carbonyl group. The cycle begins when the Lewis acid coordinates to the Lewis base with the formation of an adduct. The energy difference and degree of overlap between the occupied orbitals of the base and the empty orbitals of the acid is proportional to electron density transferred from the Lewis basic site to the Lewis acid site. In the case of a carbonyl group, the polarization increases the electrophilicity of its C atom, making it more susceptible to nucleophilic attack. Following the chemical transformation, the Lewis acid-complex dissociates.

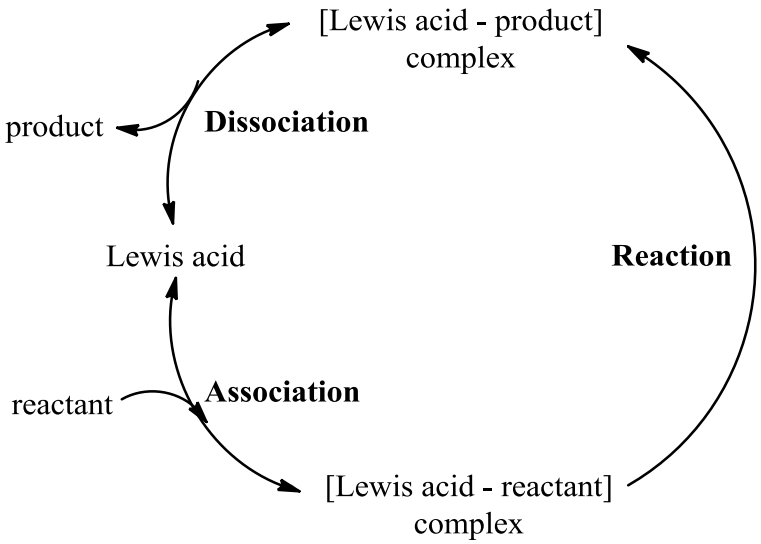


**Figure 1.2 Lewis acid catalyst schematic representation of a typical catalytic cycle[46].**

The strength of a Lewis acid can be assessed with different theories. The charge and size of a Lewis acid cation is one of them. Those cations with higher positive charges and smaller size have a greater tendency to accept electrons.[47] Another theory is the hard-soft acid-base (HSAB) theory, where both Lewis acids and bases are divided into hard and soft groups.[48] In the case for Lewis acids, small and low polarizable cations with highly localized charges are known to fall in the category of hard species ( like $H^+$, $Ti^{4+}$ and $Sn^{4+}$), while those molecules that are large and polarizable with delocalized charges are considered soft species (like $Cd^{2+}$, $Ag^+$ and $Au^+$). These theories have been established for homogeneous Lewis acids, being in some cases limited in their applications. Hence, numerical and quantum chemical calculations have been used.[49] In the case of solid Lewis acids, the diversity in site distribution between Brønsted and Lewis acidity makes it harder to establish a strong relationship.[46]

The efficiency of a Lewis acid is influenced by its interaction with the solvent media. In the presence of water, the reactivity of a Lewis acid is diminished. Upon dissolution in water, metal salts with strong Lewis acid character, such as $AlCl_3$, $TiCl_4$

and $BF_3$, complex with water molecules forming aqua ions due to their ability to attract electron pairs.[50] In the case of cations with oxidation states of 1, 2, or 3, these ions follow the chemical formula of $(M(H_2O)_n)^{z+}$, where n is the solvation number (ranging from four to six) and z+ is the charge of the cation. Those cations with higher oxidation states will undergo hydrolysis reactions to produce hydroxide or oxide species, decreasing its Lewis acidity. Cations with higher electrical charge result in stronger bonds with water molecules and those with smaller radius have weaker bond interactions.[47] Due to the efficiency decrease of Lewis acids in aqueous media, anhydrous conditions are preferred.

## 2.4 Microporous and Mesoporous Lewis Acids

Titanium silicate-1 (TS-1) was the first crystalline microporous material with isolated Lewis acid sites incorporated in a "zeotype" framework.[41] In contrast to conventional zeolites, TS-1 does not have Brønsted sites. The isomorphic substitution of isolated $Ti^{4+}$ sites in tetrahedral coordination with pure silica, in a bidirectional medium pore with MFI structure, gives TS-1 a unique Lewis acid character. TS-1 in aqueous hydrogen peroxide is currently used in varied industrial processes, including phenol hydroxylation, cyclohexanone ammoxidation, and propene oxidation synthesis.[51–53] Since the framework is primarily silicon dioxide, it provides a unique hydrophobic environment capable to maintain activity in the presence of a bulk water phase. In consequence, using TS-1 derives in a greener and more efficient chemical process, in contrast to homogenous catalysts and expensive organic hydroperoxides or peracids.

The selective oxidation of hydrocarbons with TS-1 is attributed to its isolated tetrahedral Ti atoms in MFI framework, coordinating to $H_2O_2$ to form a Ti-OOH

species. The $Ti^{4+}$ center can act as a Lewis acid by using empty $d^0$ orbitals to accept electron pairs from reactants.[46] However, the topology of TS-1 (3-dimensional 10 member ring with effective diameter of 0.55 nm) limits its application to non-bulky molecules which are not diffusion limited. Therefore, to accommodate larger substrates, titanium silicates with larger pore openings have also been synthesized.

Ti-Beta is also a Lewis acid microporous material with larger pore openings, 12 member rings in a three-dimensional framework.[54] Corma *et al.*[55] have studied the hydrophobicity of Ti-Beta, changing the synthesis gel composition. Ti-Beta synthesized in fluoride media, Ti-Beta(F), is a hydrophobic microporous material with minimum internal defects having a fivefold coordination. The fluoride-containing media synthesis is at near neutral pH, increasing the stability and balancing the charges introduced by the organic structure directing agent. In contrast, Ti-Beta synthesized in hydroxide media, Ti-Beta(OH), leads to a more hydrophilic microporous material with a higher amount of internal defects having a highly six-fold distorted coordination. The activity of both of these catalysts with the epoxidation of 1-hexene using methanol and acetonitrile as solvents, demonstrates the necessity of a highly hydrophobic media, preventing the deactivation of the Lewis acid site.

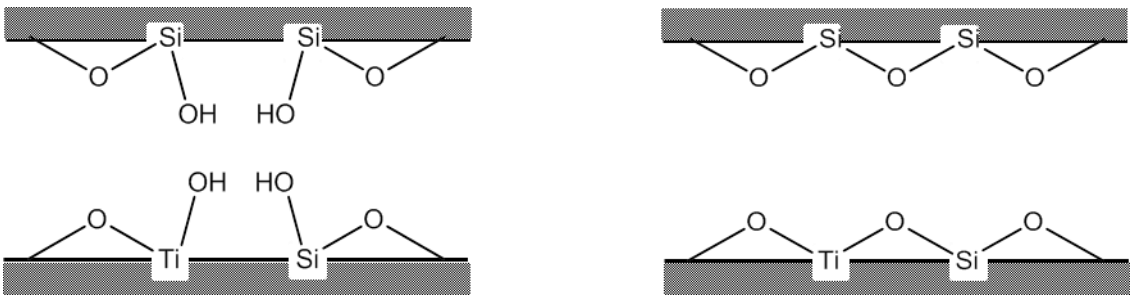


**Figure 1.3 Ti-silicates Ti-Beta(OH) (left) and Ti-Beta(F) (right)**

The high activities of the Ti-containing silicates have led scientists to incorporate other metals in these frameworks, introducing different Lewis acid sites that could catalyze other reactions. Examples of these are tin (Sn),[56,57] zirconium (Zr)[58,59] in Beta and tantalum (Ta)[60] and niobium (Nb)[61] in MCM-41 . The introduction of these metals in the crystalline framework depends on the ionic radius of the metal, the rigidity of the zeolitic crystalline framework and the synthesis conditions (composition and pH).[40]

## 2.5 Zeolite Sn-Beta

Zeolite Beta is a large pore zeolite with a faulted intergrowth of two distinct zeolite frameworks: polymorphs A and B.[62] These are composed of perpendicular channels, which intersect to form a three-dimensional array of cages with 12 ring apertures with mean diameters of 0.67 nm.[63] Polymorph A results in a tetragonal crystal lattice with cages arranged in helical fashion around a fourfold screw axis, being either right or left-handed (space groups $P4_122$ or $P4_322$). In contrast, polymorph B is monoclinic C2/c having achiral structure.

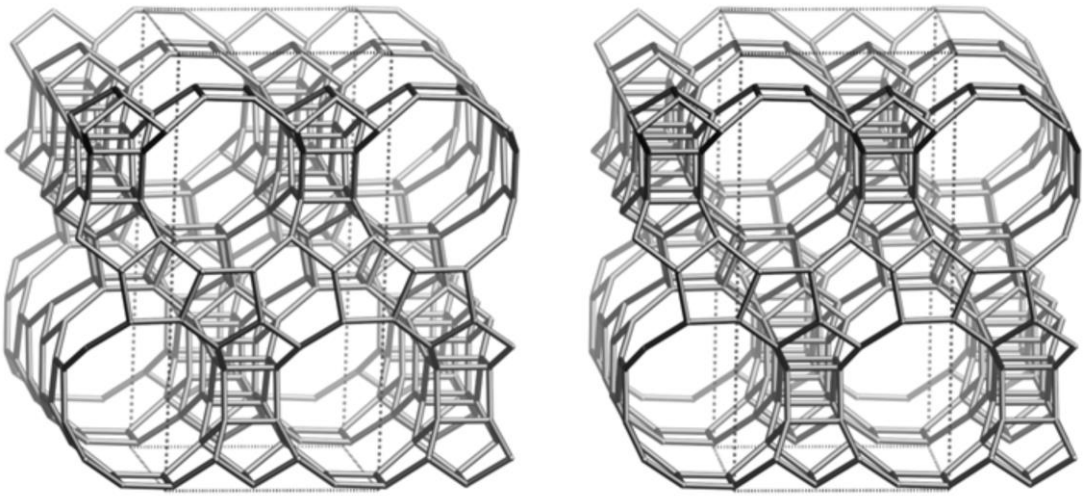

**Figure 1.4 Zeolite Beta framework along {010}[64].**

Zeolite Sn-Beta was first synthesized by Corma *et al*.,[65] having isolated Sn sites tetrahedrally coordinated to silicon atoms by oxygen bridges.[57] This tin silicate was synthesized for the Baeyer-Villiger oxidation of ketones with hydrogen peroxide, $H_2O_2$, to form the corresponding lactones. Until the synthesis of Sn-Beta, other catalysts have increased the nucleophilicity of $H_2O_2$ to react with the ketone, binding the peroxide to other functional groups present in the molecule and, consequently, reducing the chemoselectivity towards lactones.[66] Instead, activating the desired functional group (the carbonyl group of the ketone) with a Lewis acid seems a better idea to enhance the chemoselectivity to lactones. Therefore, the high electronegativity of Sn polarizes the carbonyl group making it more susceptible to a nucleophilic attack from the peroxide. In addition, the hydrophobicity and the Beta zeolite structure allows the diffusion of reactants through its large pores.[57] Therefore, Sn-Beta is able to oxidize cyclic ketones to its corresponding lactones (Figure 1.5) with 30-95% conversions and almost 100% selectivity.[67] Similarly, enriched R-enantiomer δ-decalactone can be synthesized by oxidation of delfone with $H_2O_2$ in solvent free conditions.[68]

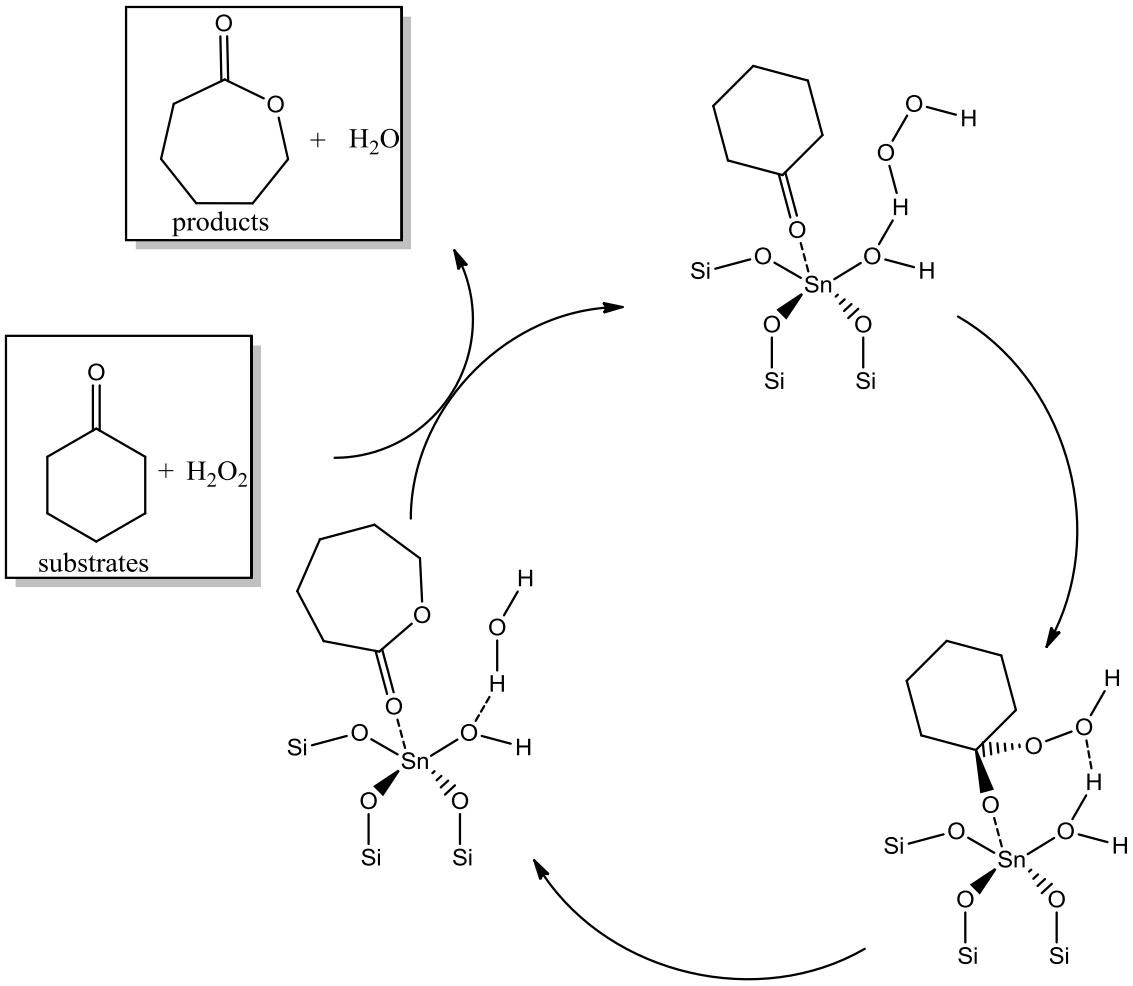


**Figure 1.5 Proposed mechanism of the Baeyer-Villiger oxidation of cyclohexanone with hydrogen peroxide and catalyzed by Sn-Beta[69].**

The activation of a carbonyl group with Sn-Beta has also been used in other reactions. The Meerwein-Ponndorf-Verley reduction of aldehydes and ketones and Oppenauer's oxidation of alcohols (MPVO reactions) requires a Lewis acid metal center to which both reactants (the aldehyde/ketone and alcohol) are coordinated, performing a hydride transfer from the alcohol to the carbonyl group.[70,71] The high electronegativity of Sn makes Sn-Beta obtain high activity and selectivity in MPV reactions like the reduction of cyclohexanone with isopropanol or 2-butanol (Figure 6), obtaining almost 100% conversion and selectivity.[72] Although the presence of water in Sn-Beta decreases the activity, surface organic modification can make the

catalyst more hydrophobic and good results are still obtained in the MPVO reaction with 10% water in the reaction medium.[73]

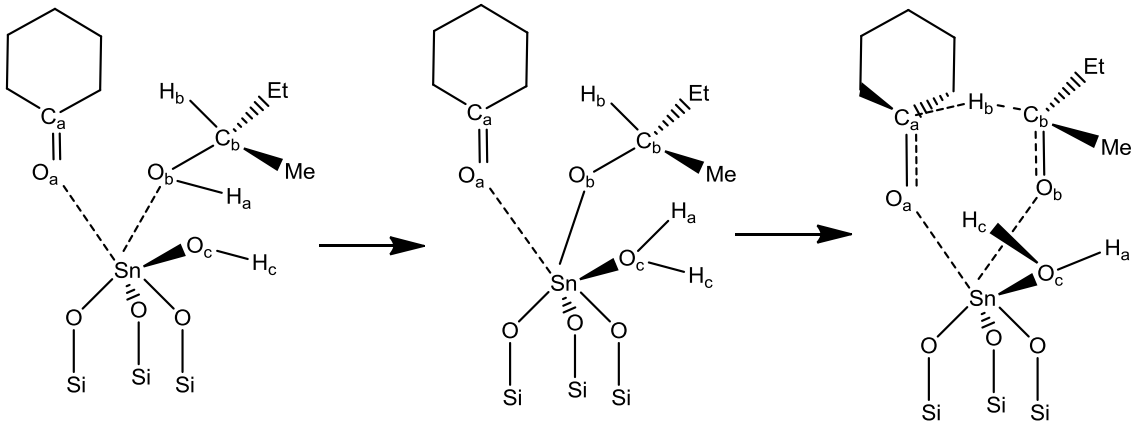


**Figure 1.6 Proposed reaction mechanism for the MPV reaction using Sn-Beta catalyst[74].**

Through a combination of theoretical and Infrared (IR) studies, Boronat *et al.*[69,75] suggest two types of Sn sites. The Sn centers could be bonded to four silicon atoms of the zeolite framework through bridging oxygens, being called the "closed" site, or the Sn centers could be bonded to three of these and one bond hydrolyzed becoming Sn-OH, being called the "opened" site. The closed site happens to be 80% of the tin incorporated in the zeolite framework. They claim the open site is the more active one for several reasons: 1) lengthening the four Sn-$O_{framework}$ distances is difficult in the zeolite through the donor-acceptor interactions between HOMO and LUMO of the adsorbed molecule and the catalyst, respectively, 2) the calculated adsorption enthalpy of the open site is higher than the closed site, and 3) the calculated distance from the carbonyl oxygen to the tin center is lower for the open site. In addition, by multishell fit to extended X-ray absorption fine structure (EXAFS) data, it is believed that a symbiotic relationship exists between the structure directing agent in the zeolite synthesis and the Sn heteroatoms during the framework formation, suggesting Sn to be located at T5/T6 sites of opposite sides of the six-member rings.[76]

In both the Baeyer-Villiger oxidation and MPV reaction, the "open" site plays a fundamental role as the active site,[69] as it can be seen in Figure 1.5 and Figure 1.6. In the first case, the Lewis acid Sn atom activates the carbonyl group of the cyclic ketone, while the oxygen atom of the Sn-OH interacts with the $H_2O_2$ through hydrogen bonding to then attack the carbonyl group and form the corresponding lactone and water. In the second case, the Sn-OH aids in the hydride shift from the alcohol to the cyclic ketone, which are both bonded to the Sn atom, to form the corresponding ketone and cyclohexanol, respectively.[73,74]

Sn-Beta has also been of current interest in aldol condensation for the fine chemical industry. The condensation of cyclohexanone with malonitrile results in the formation of cyclohexylidenemalononitrile with a 46% yields after 6 hours.[77] Other applications of Sn-Beta with $C_6$ and $C_5$ sugars will be thoroughly discussed in the following chapters.

## 3. Motivation and Thesis Organization

In the first section of this chapter a review has been presented on the conversion of biomass into liquid biofuels. 5-hydromethylfurfural (HMF), levulinic acid and γ-valerolactone (GVL) have been extensively applied as platform molecules in the different routes (dehydration, decarboxylation, hydrogenation…) for the synthesis of transportation fuels. The limiting factor of these pathways is the low carbon balance reached up to these platform molecules. In the Biofine process, there is a 50% mass loss corresponding to the mass of $C_6$ sugars.[19] Therefore, a higher yield will be needed in the conversion of $C_6$ sugars into the platform molecules to make biomass an efficient raw material in the synthesis of transportation fuels.

The conversion of cellulose into the platform molecules mentioned goes through fructose, an isomer of glucose which is more reactive. Previous to the beginning of this thesis work, Sn-Beta showed superior activity in the conversion of glucose into fructose in solvent water,[78] competing with the industrial process which uses a metalloenzyme. Herein, we study the isomerization of glucose into fructose and epimerization of glucose into mannose with framework tin and extraframework tin sites in zeolite beta to understand the activity of these. In addition, both of these Sn sites can cause carbon-carbon cleavage in glucose and fructose, to form different carboxylic acids which are of interest in the synthesis of biopolymers.

In Chapter 2 the isomerization of glucose into fructose with Sn-Beta zeolite is discussed, highlighting the applications of such system in comparison to enzymes which are not active at high temperature and low pH. The active site of Sn-Beta is studied by Solid State Nuclear Magnetic Resonance (SS NMR), with corresponding results as those seen previously through infrared spectroscopy. The reaction pathway of the glucose isomerization into fructose with zeolite Sn-Beta is elucidated. Finally, the formation of mannose with Sn-Beta is identified as a byproduct formed from fructose.

In the following chapter, Chapter 3, extraframework tin sites, located within the hydrophobic channels of zeolite Beta, show the isomerization of glucose to fructose in both, water and methanol through a different mechanism, as the one seen by framework Sn. $SnO_2$ particles, located at external zeolite crystal surfaces or supported on amorphous silica, catalyze isomerization in methanol but not in water, suggesting that contact with bulk water inhibits isomerization at $SnO_2$ surfaces. In addition, the types and locations of the Sn site are discussed through X-ray diffraction, $N_2$ adsorption, $^{119}$Sn SS NMR and UV-VIS diffuse reflectance.

In Chapter 4, the neighboring silanol group of the open Sn site is examined, exchanging its proton with a sodium cation, $Na^+$, to enhance the epimerization rate. Na-exchanged Sn-Beta catalyzes the epimerization of glucose to mannose in methanol and in concentrated NaCl aqueous solutions via a 1, 2 carbon shift, while in water, the $Na^+$ leaves the active site, reverting to the isomerization of glucose into fructose. The data and the mechanistic evidence presented herein show a shift in the pathway to the epimerization into mannose with a new Lewis acid site. In this chapter Ricardo Bermejo-Deval and Marat Orazov equally contributed to this work.

In Chapter 5, glucose with Sn-Beta at longer reaction times, 2-10 hours, is shown to be an active catalyst in the synthesis of lactic acid and methyl lactate from glucose in solvent water and methanol, respectively. These two products result from the retro-aldol condensation from fructose. However, glucose can analogously form undesired byproducts vinylglycolic acid and methyl vinylglycolate in solvent water and methanol, respectively. In contrast, extraframework $SnO_2$/Si-Beta, selectively forms lactic acid over vinylglycolic acid in water and methyl lactate over methyl vinylglycolate in methanol. With the use of $^{13}C$ as an isotopic tracer at different positions of the glucose backbone, the mechanism of the formation of lactic acid and vinylglycolic acid is elucidated.

Finally, in Chapter 6, an overall conclusion of the thesis will be presented, discussing the different isomerization and epimerization reactions with Sn-Beta and $SnO_2$/Si-Beta at short reaction times, and retro-aldol reactions at long reaction times. In addition, future research will be outlined to gather a better understanding on the glucose reactions with Lewis acid silicates at short and long reaction times.

## 4. References


1. Huber, G. W., Iborra, S. & Corma, A. Synthesis of transportation fuels from biomass: chemistry, catalysts, and engineering. *Chem. Rev.* **106,** 4044–98 (2006).

2. Klass, D. L. Biomass for Renewable Energy and Fuels. *Renew. Energy* **1,** (2004).

3. Schmidt, L. D. & Dauenhauer, P. J. NEWS & VIEWS Hybrid routes to biofuels. *Nature* **447,** (2007).

4. Zhou, C.-H., Xia, X., Lin, C.-X., Tong, D.-S. & Beltramini, J. Catalytic conversion of lignocellulosic biomass to fine chemicals and fuels. *Chem. Soc. Rev.* **40,** 5588–617 (2011).

5. Climent, M. J., Corma, A. & Iborra, S. Conversion of biomass platform molecules into fuel additives and liquid hydrocarbon fuels. *Green Chem.* (2013). doi:10.1039/c3gc41492b

6. Freudenberg, K. & Neish, A. C. Constitution and Biosynthesi of Lignin. *Science (80-. ).* **165,** 784 (1969).

7. Lange, J.-P. Lignocellulose conversion: an introduction to chemistry, process and economics. *Biofuels, Bioprod. Biorefining* **1,** 39–48 (2007).

8. Zhao, H. *et al.* Effects of Crystallinity on Dilute Acid Hydrolysis of Cellulose by Cellulose Ball-Milling Study. *Energy & Fuels* **20,** 807–811 (2006).

9. Hamelinck, C. N., van Hooijdonk, G. & Faaij, A. P. C. Ethanol from lignocellulosic biomass: techno-economic performance in short-, middle- and long-term. *Biomass and Bioenergy* **28,** 384–410 (2005).

10. Rogalinski, T., Liu, K., Albrecht, T. & Brunner, G. Hydrolysis kinetics of biopolymers in subcritical water. *J. Supercrit. Fluids* **46,** 335–341 (2008).

11. Schacht, C., Zetzl, C. & Brunner, G. From plant materials to ethanol by means of supercritical fluid technology. *J. Supercrit. Fluids* **46,** 299–321 (2008).

12. Vom Stein, T. *et al.* Salt-assisted organic-acid-catalyzed depolymerization of cellulose. *Green Chem.* **12,** 1844–1849 (2010).

13. Binder, J. B. & Raines, R. T. Fermentable sugars by chemical hydrolysis of biomass. *Proc. Natl. Acad. Sci. U. S. A.* **107,** 4516–21 (2010).

14. De Vyver, S. *et al.* Sulfonated silica/carbon nanocomposites as novel catalysts for hydrolysis of cellulose to glucose. *Green Chem.* **12,** 1560–1563 (2010).

15. Yamaguchi, D. *et al.* Hydrolysis of Cellulose by a Solid Acid Catalyst under Optimal Reaction Conditions. *J. Phys. Chem. C* **113,** 3181–3188 (2009).

16. Stephanopoulos, G. Challenges in engineering microbes for biofuels production. *Science* **315,** 801–4 (2007).

17. Fitzpatrick, S. W. Lignocellulose Degradation to Furfural and Levulinic Acid. (1990).

18. Fitzpatrick, S. Production of Levulinic Acid from carbohydrate-contaning materials. (1997).

19. Alonso, D. M., Bond, J. Q. & Dumesic, J. a. Catalytic conversion of biomass to biofuels. *Green Chem.* **12,** 1493 (2010).

20. Chheda, J. N., Rom?n-Leshkov, Y. & Dumesic, J. a. Production of 5-hydroxymethylfurfural and furfural by dehydration of biomass-derived mono- and poly-saccharides. *Green Chem.* **9,** 342 (2007).

21. Chheda, J. N. & Dumesic, J. a. An overview of dehydration, aldol-condensation and hydrogenation processes for production of liquid alkanes from biomass-derived carbohydrates. *Catal. Today* **123,** 59–70 (2007).

22. Román-Leshkov, Y., Chheda, J. N. & Dumesic, J. a. Phase modifiers promote efficient production of hydroxymethylfurfural from fructose. *Science* **312,** 1933–7 (2006).

23. Román-Leshkov, Y., Barrett, C. J., Liu, Z. Y. & Dumesic, J. a. Production of dimethylfuran for liquid fuels from biomass-derived carbohydrates. *Nature* **447,** 982–5 (2007).

24. Barrett, C. J., Chheda, J. N., Huber, G. W. & Dumesic, J. A. Single-reactor process for sequential aldol-condensation and hydrogenation of biomass-derived compounds in water. *Appl. Catal. B Environ.* **66,** 111–118 (2006).

25. Bozell, J. J. & Petersen, G. R. Technology development for the production of biobased products from biorefinery carbohydrates—the US Department of Energy's "Top 10" revisited. *Green Chem.* **12,** 539 (2010).

26. Manzer, L. E. Catalytic synthesis of α-methylene-γ-valerolactone: a biomass-derived acrylic monomer. *Appl. Catal. A Gen.* **272,** 249–256 (2004).

27. Deng, L., Li, J., Lai, D.-M., Fu, Y. & Guo, Q.-X. Catalytic conversion of biomass-derived carbohydrates into gamma-valerolactone without using an external H2 supply. *Angew. Chem. Int. Ed. Engl.* **48,** 6529–32 (2009).

28. Heeres, H. *et al.* Combined dehydration/(transfer)-hydrogenation of C6-sugars (D-glucose and D-fructose) to γ-valerolactone using ruthenium catalysts. *Green Chem.* **11,** 1247 (2009).

29. Girisuta, B., Janssen, L. P. B. M. & Heeres, H. J. Kinetic Study on the Acid-Catalyzed Hydrolysis of Cellulose to Levulinic Acid. *Ind. Eng. Chem. Res.* **46,** 1696–1708 (2007).

30. Tuck, C. O., Pérez, E., Horváth, I. T., Sheldon, R. a & Poliakoff, M. Valorization of biomass: deriving more value from waste. *Science* **337,** 695–9 (2012).

31. Bozell, J. J. *et al.* Production of levulinic acid and use as a platform chemical for derived products. *Resour. Conserv. Recycl.* **28,** 227–239 (2000).

32. Elliot, D. C. & Frye, J. G. Hydrogenated 5-carbon compound and method making. (1999).

33. Leung, D. Y. C., Wu, X. & Leung, M. K. H. A review on biodiesel production using catalyzed transesterification. *Appl. Energy* **87,** 1083–1095 (2010).

34. Murata, K., Liu, Y., Inaba, M. & Takahara, I. Production of Synthetic Diesel by Hydrotreatment of Jatropha Oils Using Pt−Re/H-ZSM-5 Catalyst. *Energy & Fuels* **24,** 2404–2409 (2010).

35. Wang, C. *et al.* One-Step Hydrotreatment of Vegetable Oil to Produce High Quality Diesel-Range Alkanes. *ChemSusChem* **5,** 1974–1983 (2012).

36. Sousa, L. A., Zotin, J. L. & da Silva, V. T. Hydrotreatment of sunflower oil using supported molybdenum carbide. *Appl. Catal. A Gen.* **449,** 105–111 (2012).

37. Krár, M., Kovács, S., Kalló, D. & Hancsók, J. Fuel purpose hydrotreating of sunflower oil on CoMo/Al2O3 catalyst. *Bioresour. Technol.* **101,** 9287–9293 (2010).

38. Bhatia, S. *Zeolite Catalysis: principles and applications*. (CRC Press, 1990).

39. Corma, A. & Zones, S. *Zeolites and Catalysis*. (Wiley-VCH Verlag GmbH & Co. KGaA, 2010). doi:10.1002/9783527630295

40. Moliner, M. Direct Synthesis of Functional Zeolitic Materials. *ISRN Mater. Sci.* **2012,** 1–24 (2012).

41. Taramasso, M., Perego, G. & Notari, B. No Title. (1983).

42. Ristic, A., Lazar, K., Solt, H. & Kaucic, V. The influence of microwave-assisted synthesis on nanocrystalline iron silicalite-1 particles. *CrystEngComm* **13,** 1946–1952 (2011).

43. Niphadkar, P., Kotwal, M., Deshpande, S., Bokade, V. & Joshi, P. Tin-silicalite-1: Synthesis by dry gel conversion, characterization and catalytic performance in phenol hydroxylation reaction. *Mater. Chem. Phys.* **114,** 344–349 (2009).

44. Niphadkar, P. S., Patil, K. R. & Joshi, P. N. Characterization of surface acid sites in tin-silicalite-1 (Sn-MFI) molecular sieve by X-ray photoelectron spectroscopy. *Microporous Mesoporous Mater.* **141,** 236–240 (2011).

45. IUPAC Gold Book. at <http://goldbook.iupac.org/L03508.html>

46. Román-Leshkov, Y. & Davis, M. E. Activation of Carbonyl-Containing Molecules with Solid Lewis Acids in Aqueous Media. *ACS Catal.* **1,** 1566–1580 (2011).

47. Wulfsberg, F. Principles of Descriptive Inorganic Chemsitry. *Brooks/Cole Monterey, CA* (1987).

48. Pearson, R. G. Hard and Soft Acids and Bases. *J. Am. Chem. Soc.* **265,** (1963).

49. Parr, R. G., Donnelly, R. A., Levy, M. & Palke, W. E. Electronegativity: The density functional viewpoint. *J. Chem. Phys.* **68,** (1978).

50. Corma, A. & García, H. Lewis acids: from conventional homogeneous to green homogeneous and heterogeneous catalysis. *Chem. Rev.* **103,** 4307–65 (2003).

51. Huybrechts, D. R. C., Bruycker, L. De & Jacobs, P. A. Oxyfunctionalization of alkanes with hydrogen peroxide on titanium silicate. *Nature* **345,** 240 (1990).

52. Perego, C., Carati, A., Ingallina, P., Mantegazza, M. A. & Bellussi, G. Production of titanium containing molecular sieves and their application in catalysis. *Appl. Catal. A Gen.* **221,** 63–72 (2001).

53. Notari, B. Titanium silicalites. *Catal. Today* **18,** 163–172 (1993).

54. Blasco, T. *et al.* Unseeded synthesis of Al-free Ti-Beta zeolite in fluoride medium: a hydrophobic selective oxidation catalyst. *Chem. Commun.* 2367 (1996). doi:10.1039/cc9960002367

55. Blasco, T. *et al.* Direct Synthesis and Characterization of Hydrophobic Aluminum-Free Ti−Beta Zeolite. *J. Phys. Chem. B* **102,** 75–88 (1998).

56. Mal, N., Ramaswamy, V., Rajamohanan, P. & Ramaswamy, a. Sn-MFI molecular sieves: synthesis methods, 29Si liquid and solid MAS-NMR, 119Sn static and MAS NMR studies. *Microporous Mater.* **12,** 331–340 (1997).

57. Corma, a, Nemeth, L. T., Renz, M. & Valencia, S. Sn-zeolite beta as a heterogeneous chemoselective catalyst for Baeyer-Villiger oxidations. *Nature* **412,** 423–5 (2001).

58. Wang, X. X., Lefebvre, F., Patarin, J. & Basset, J.-M. Synthesis and characterization of zirconium containing mesoporous silicas: I. Hydrothermal synthesis of Zr-MCM-41-type materials. *Microporous Mesoporous Mater.* **42,** 269–276 (2001).

59. Nie, Y., Jaenicke, S. & Chuah, G.-K. Zr–Zeolite Beta: A New Heterogeneous Catalyst System for the Highly Selective Cascade Transformation of Citral to (±)-Menthol. *Chem. – A Eur. J.* **15,** 1991–1999 (2009).

60. Antonelli, D. M. & Ying, J. Y. Synthesis and Characterization of Hexagonally Packed Mesoporous Tantalum Oxide Molecular Sieves. *Chem. Mater.* **8,** 874–881 (1996).

61. Ziolek, M. & Nowak, I. Synthesis and characterization of niobium-containing MCM-41. *Zeolites* **18,** 356–360 (1997).

62. Newsam, J. M., Treacy, M. M. J., Koetsier, W. T. & Gruyter, C. B. D. Structural Characterization of Zeolite Beta. *Proc. R. Soc. A Math. Phys. Eng. Sci.* **420,** 375–405 (1988).

63. Omegna, A., Vasic, M., Anton van Bokhoven, J., Pirngruber, G. & Prins, R. Dealumination and realumination of microcrystalline zeolite beta: an XRD, FTIR and quantitative multinuclear (MQ) MAS NMR study. *Phys. Chem. Chem. Phys.* **6,** 447 (2004).

64. IZA structures. at <http://izasc.ethz.ch/fmi/xsl/IZA-SC/ftc_fw.xsl?-db=Atlas_main&-lay=fw&STC=*BEA&-find>

65. Corma, A. & Valencia, S. Stannosilicate molecular sieves. (1999).

66. Strukul, G. Transition Metal Catalysis in the Baeyer - Villiger Oxidation of Ketones. *Angew. Chem. Int. Ed. Engl.* **37,** 1198–1209 (1998).

67. Renz, M. & Corma, A. Selective and Shape-Selective Baeyer ± Villiger Oxidations of Aromatic. *Chem. A Eur. J.* 4708–4717 (2002).

68. Corma, A., Iborra, S., Mifsud, M., Renz, M. & Susarte, M. A New Environmentally Benign Catalytic Process for the Asymmetric Synthesis of Lactones: Synthesis of the Flavouring δ-Decalactone Molecule. *Adv. Synth. Catal.* **346,** 257–262 (2004).

69. Boronat, M., Concepción, P., Corma, A. & Renz, M. Peculiarities of Sn-Beta and potential industrial applications. *Catal. Today* **121,** 39–44 (2007).

70. Creyghton, E. J., Huskens, J., van der Waal, J. C. & van Bekkum, H. in *Heterog. Catal. Fine Chem. IV Proc. 4th Int. Symp. Heterog. Catal. Fine Chem.* (H.U. Blaser, A. B. & Prins, R.) **108,** 531–537 (Elsevier, 1997).

71. Van der Waal, J. C., Kunkeler, P. J., Tan, K. & van Bekkum, H. in *3rd World Congr. Oxid. Catalaysis Proc. 3rd World Congr. Oxid. Catal.* (R.K. Grasselli S.T. Oyama, A. M. G. & Lyons, J. E.) **110,** 1015–1024 (Elsevier, 1997).

72. Corma, A., Domine, M. E., Nemeth, L. & Valencia, S. Al-free Sn-Beta zeolite as a catalyst for the selective reduction of carbonyl compounds (Meerwein-Ponndorf-Verley reaction). *J. Am. Chem. Soc.* **124,** 3194–5 (2002).

73. Corma, A., Domine, M. & Valencia, S. Water-resistant solid Lewis acid catalysts: Meerwein–Ponndorf–Verley and Oppenauer reactions catalyzed by tin-beta zeolite. *J. Catal.* **215,** 294–304 (2003).

74. Boronat, M., Corma, A. & Renz, M. Mechanism of the Meerwein-Ponndorf-Verley-Oppenauer (MPVO) redox equilibrium on Sn- and Zr-beta zeolite catalysts. *J. Phys. Chem. B* **110,** 21168–74 (2006).

75. Boronat, M., Concepcion, P., Corma, a, Renz, M. & Valencia, S. Determination of the catalytically active oxidation Lewis acid sites in Sn-beta zeolites, and their optimisation by the combination of theoretical and experimental studies. *J. Catal.* **234,** 111–118 (2005).

76. Bare, S. R. *et al.* Uniform catalytic site in Sn-beta-zeolite determined using X-ray absorption fine structure. *J. Am. Chem. Soc.* **127,** 12924–32 (2005).

77. Corma, A. & Renz, M. Experimental Evidence for a Dual Site Mechanism in Sn-Beta and Sn-MCM-41 Catalyst for the Baeyer-Villiger Oxidation. *Collect. Czech. Chem. Commun.* **70,** 1727–1736 (2005).

78. Moliner, M., Román-Leshkov, Y. & Davis, M. E. Tin-containing zeolites are highly active catalysts for the isomerization of glucose in water. *Proc. Natl. Acad. Sci. U. S. A.* **107,** 6164–8 (2010).

# Chapter 2 : The Glucose Isomerization into Fructose Reaction Pathway with Sn-Beta

## 1. Introduction

There is at present a growing interest in the use of renewable carbon sources for the production of chemicals, polymers and fuels. As a result, numerous chemical transformations of biomass into a wide variety of products are currently being explored. The Davis group has been focusing on the isomerizations of sugars, and in particular, the isomerization of glucose to fructose (Figure 2.1),[1–3] as a key reaction that could be incorporated into a large number of pathways to convert biomass into useful products.[4,5] For example, oligomeric carbohydrates can be depolymerized into glucose monomers, that can then be converted to the chemical platform molecule 5-hydroxymethylfurfural (HMF),[4,5] via the fructose intermediate.[3] Analogously, xylose has been converted to furfural via the xylulose intermediate.[6] Additionally, the isomerization of glucose to fructose could be a step further in creating a synthetic glycolysis pathways.[7]

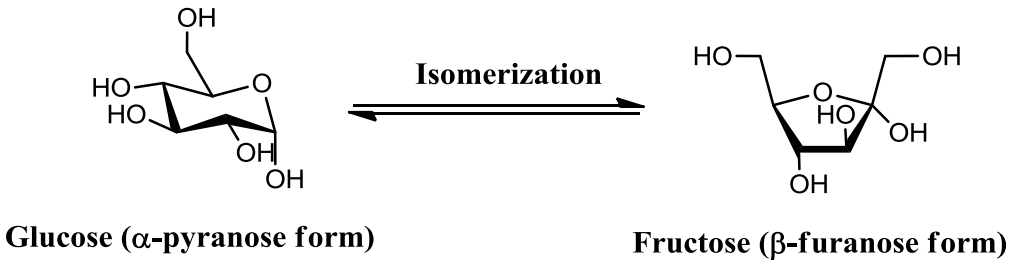


**Figure 2.1 Schematic representation of the glucose isomerization into fructose.**

In the presence of a base catalyst, such as sodium hydroxide, isomerization and epimerization of glucose occurs at 313K. The abstraction of the α-carbonyl protons in glucose results in a tautomeric enediol which forms fructose and mannose

after re-protonation (Lobry de Bruyn-Alberda van Ekenstein rearrangements, LdB-AvE).[8,9] Due to the instability of the monosaccharides in alkaline media at 313K or above, longer residence times lead to 2,3- and 3,4-enediols that are precursors of other ketohexoses and other aldohexoses, in addition to retro-aldol fragmentation and degradation reactions.[10–13] Therefore, high fructose selectivities (> 90%) are only reached at low glucose conversions (< 10%), making base catalysts bad candidates for large-scale glucose processing.

The conversion of glucose to fructose for the production of high-fructose corn syrup is accomplished commercially by immobilized enzyme catalysts, such as D-xylose isomerase (XI). Reaction mechanisms for XI-mediated isomerizations have been investigated for some time because of their relevance to glycolysis and industrial biocatalysis.[14] It is well established that the aldose to ketose interconversion occurs by a three-stage mechanism after binding of the glucose cyclic form takes place. These steps are: (i) aldose ring opening to set the acyclic form of the sugar, (ii) aldose to ketose isomerization of the linear sugar at C-1 and C-2 via a metal assisted hydride transfer; and (iii) ring closure to release the cyclic form of the ketose. Similarly, it has been shown that this metalloenzyme requires two divalent metal ions (M1 and M2) for the enzyme to be active. The preferred metal ions are $Mg^{+2}$ or $Mn^{+2}$. Only recently, complementary X-ray and neutron diffraction techniques aimed at probing the location and dynamics of H/D atoms in XI crystal structures have been exploited to reveal unique insights of the enzyme reaction mechanism.[15] Three important new features have been elucidated: 1) the primary role of M1 (in conjunction with specific amino acid residues) is to destabilize the pyranose structure and promote the ring opening of the sugar, 2) M2 binds and stabilizes O1 and O2 on the acyclic sugar, promoting the hydride shift from C2 to C1, and c) a hydroxyl group bound to M2 is

responsible for the deprotonation/protonation sequences that shuttle protons involved in the interconversion of aldehydes and hydroxyl groups between O2 and O1.

Previous to the beginning of this thesis work, the Davis group had shown that the isomerization of glucose to fructose could be catalyzed in aqueous media by hydrophobic zeolites that contain Lewis acids.[1–3] Specifically, pure-silica zeolites with the zeolite beta structure containing small amounts of framework $Ti^{4+}$ or $Sn^{4+}$ (denoted as Ti-Beta and Sn-Beta, respectively) are able to isomerize glucose to fructose in high yield at relatively low temperatures (383-413 K), as it can be seen in Figure 2.2. The Sn-Beta sample has superior activity to the Ti-Beta material and can even convert solutions that contain 45wt% glucose.[1] The much lower isomerization activity with medium-pore zeolites indicates how much the properties of the large-pore zeolite influence in the reaction. Increasing the pore size, with metal centers incorporated in the silica framework, to ordered mesoporous silica MCM-41 also decreased the isomerization activity. The high activity in an acidic environment (pH = 2), enables the coupling of glucose isomerization into fructose and other acid-catalyzed reactions in a one pot reaction. In addition, Sn-Beta maintains its original activity after four consecutive isomerization cycles at 383K for 30 min each.

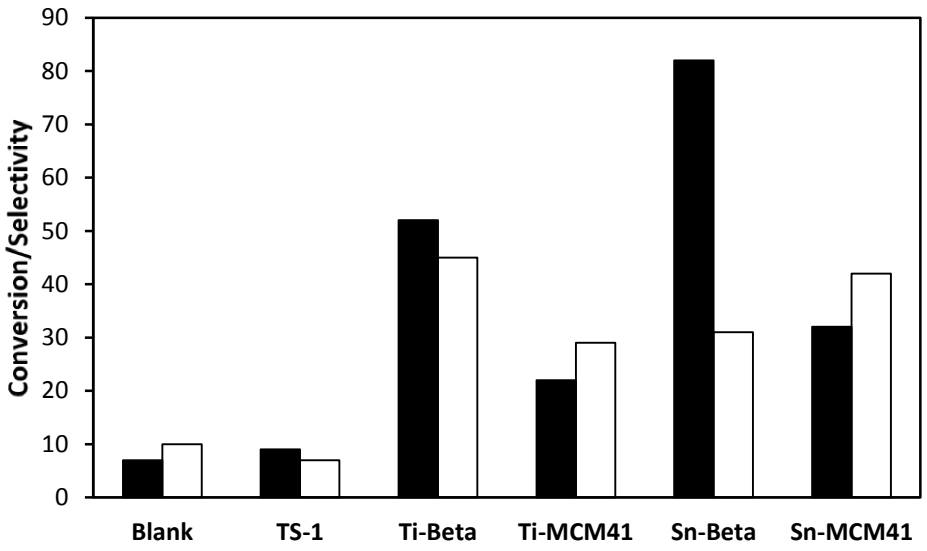


**Figure 2.2 Glucose isomerization reaction catalyzed by various metal-containing solids under the following reaction conditions:[1] 10% (wt/wt) glucose in water, 413K, 90 min and 1:50 metal:glucose molar ratio. Glucose conversion is in black and fructose selectivity is in white.**

Consequently, it was demonstrated that the reaction mechanism in aqueous media was a truly Lewis acid-mediated intramolecular hydride shift.[2] With the use of deuterium as an isotopic tracer in the C-2 position of glucose, both liquid $^{13}C$ and $^{1}H$ NMR show the shift of the deuterium atom to the C-1 position of fructose. Additionally, kinetic experiments reveal a kinetic isotope effect of approximately two, indicating that the intramolecular hydride shift is the rate limiting step of the reaction. Hence, the redistribution of the oxidation states, between carbon atoms in the Meerwein-Ponndorf-Verley (MPV) aldehyde and ketone reduction within the hydrophobic micropores of Sn-Beta is equivalent to the C-1 and C-2 position of the monosaccharide.[16,17] In contrast, the base-catalyzed isomerization loses its proton in the C-2 position of glucose to form the corresponding enolate, reincorporating subsequently a proton from the solution into the molecule.

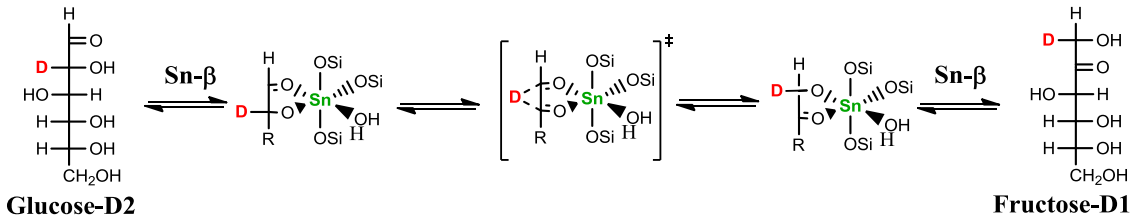


**Figure 2.3 Schematic representation of the intramolecular hydride shift in the isomerization of glucose into fructose with Sn-Beta catalyst in water.**[2]

Additionally, it has been shown that the catalyst activity is maintained in aqueous media saturated with sodium chloride and acidic pH. This allows for the "one pot" conversion of starch to HMF through a reaction sequence, namely involving: the homogeneous acid-catalyzed depolymerization of starch to glucose, the heterogeneous Lewis acid-catalyzed isomerization of glucose to fructose and the homogeneous acid-catalyzed dehydration of fructose to HMF.[3] The high selectivities to HMF (over 70%) with this "one-pot" biphasic water/tetrahydrofuran (THF) reactor system opens up the possibility of complex carbohydrate conversion to HMF.

The activation of carbonyl-containing molecules-more specifically sugars, by solids containing Lewis acid centers is a new area of heterogeneous catalysis. In addition to the isomerization of glucose in aqueous media,[1–3] the isomerization of triose sugars in methanol or water[18] and the conversion of sugars to lactic acid derivatives in methanol have been reported using Sn-containing porous solids.[19] Activation of carbonyl-containing molecules with solid acids has recently been reviewed, including the limited data on solid Lewis acid catalysis (especially in aqueous media).[20] Sn-Beta and Ti-Beta reveal a number of analogous behaviors to metalloenzymes when isomerizing glucose. Given the potential significance of this emerging area of heterogeneous catalysis, it is important to gain further fundamental understanding of the reaction pathways using these solids. In this chapter, the glucose

isomerization reaction catalyzed by hydrophobic zeolites that contain Lewis acid centers is investigated using a number of experimental techniques. The goal of this work is to provide a fundamental understanding of the reaction pathway from an experimental perspective and to elucidate whether or not the entire reaction pathway shows further analogy to the metalloenzyme pathway.

## 2. Results and Discussion

### 2.1 The Ring Opening

The initial step in the enzymatic isomerization of glucose to fructose involves the ring opening of a glucose molecule at M1 (one of the two metal sites in the metalloenzymes).[15] In order to determine if a similar pathway was followed by Sn-Beta, the absorption of $^{13}C$ labeled glucose and fructose into Sn-Beta and Si-Beta (used as control) was investigated using $^{13}C$ NMR. Spectra obtained from glucose and fructose adsorbed into Si-Beta showed that the sugars were in their cyclic configurations (resonances between 100 and 90 ppm are assigned to the alpha and beta anomers of the pyranose and furanose rings). No new resonances were observed when compared to the spectra of pure glucose or fructose solutions. Conversely, upon adsorption of these sugars in Sn-Beta, new resonances at ca. 130, 180 and 214 ppm appeared. The resonance at 214 ppm was at the chemical shift reported for the keto carbonyl carbon of the acyclic form of fructose.[21] Cross polarization (CP) experiments with variable contact times were consistent with an assignment of a keto group for the 214 ppm resonance (Figure 2.4). The CP method is based on $^{1}H$-$^{13}C$ heteronuclear dipolar coupling so the $^{13}C$ signal strongly depends on their internuclear distance. Appearance of the 214 ppm resonance only at longer contact times (0.1 and 1.0 ms) unambiguously ruled out the possibility of the carbonyl carbon having a direct C-H bond as in an aldehyde. Quantitative NMR measurements performed on adsorbed

fructose samples revealed that the amount of the acyclic form is on the same order of magnitude as the amount of Sn present in the sample. Because of the errors in the elemental analyses and NMR experiments, greater precision on the estimate of the amount of the acyclic form was not possible. These measurements indicate that ca. 5% of the fructose was in the acyclic form. This amount is approximately an order of magnitude larger than what is observed in solution.

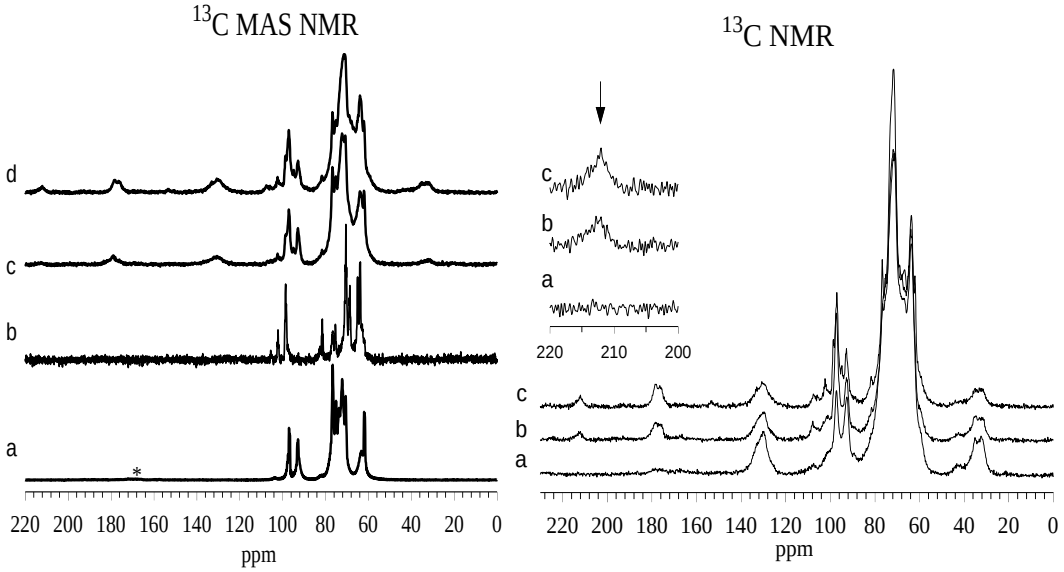


**Figure 2.4 Left: (a) glucose adsorbed into Si-Beta, (b) fructose adsorbed into Si-Beta, (c) glucose adsorbed into Sn-Beta, (d) fructose adsorbed into Sn-Beta. Right: spectra from fructose adsorbed into Sn-Beta, (a) cross polarization contact time of 0.1 ms, (b) cross polarization contact time of 1.0 ms, and (c) no cross polarization.**

IR measurements reveal the presence of a carbonyl band at ca. 1728 $cm^{-1}$ that has been assigned previously to the keto carbonyl of the acyclic form of fructose (Figure 2.5). Altogether, these data provided direct evidence for the presence of ring opened fructose molecules in Sn-Beta, suggesting that Sn not only was necessary to observe the acyclic form of fructose, but also played an important role in stabilizing the acyclic form of fructose.

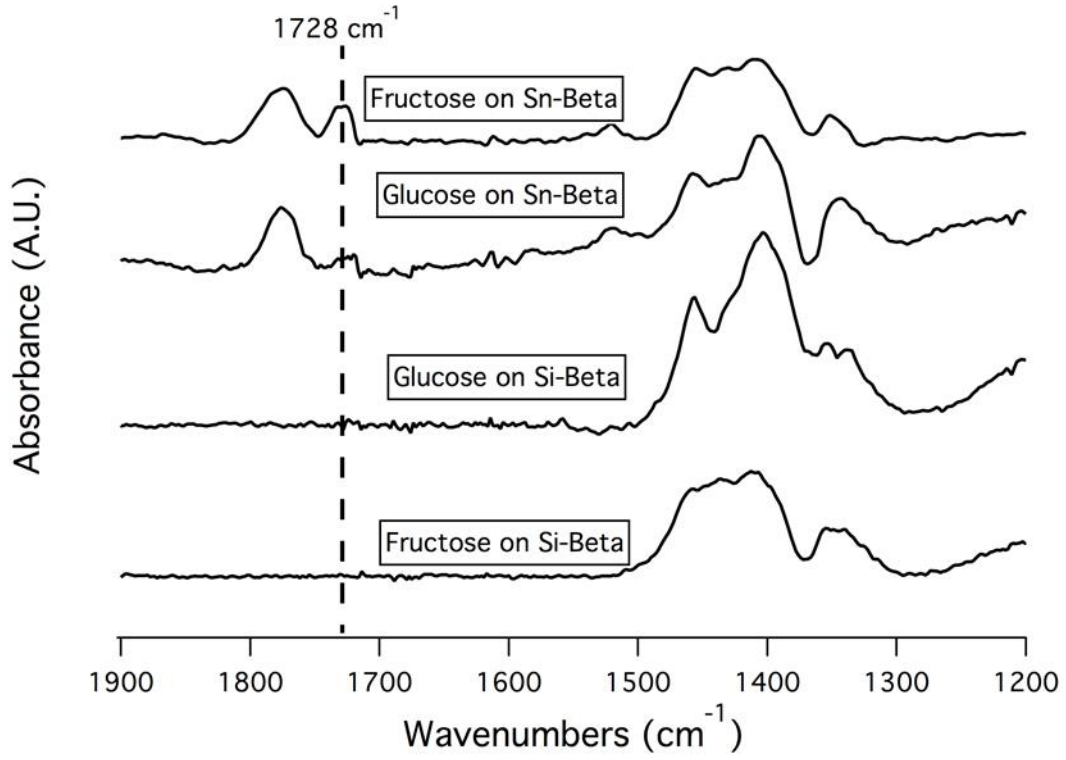


**Figure 2.5 Infrared spectra of glucose and fructose adsorbed in Sn-Beta and Si-Beta. The band at 1775 $cm^{-1}$ was not assigned to either the ketone or aldehyde groups of the acyclic fructose and glucose, respectively.**

The acyclic form of glucose would produce an aldehyde with a chemical shift around 205 ppm.[22] This resonance was not observed in the glucose adsorption experiments. Certainly, if the acyclic forms of glucose and fructose were present in similar proportions as in solution, acyclic glucose would be two-orders of magnitude lower in concentration than acyclic fructose and could not be detected by solid-state NMR.[22] Note that the 214 ppm was present in the sample where glucose was adsorbed into Sn-Beta, in an amount that corresponds to approximately 30% of the amount observed in the fructose adsorption experiment (Figure 2.6).

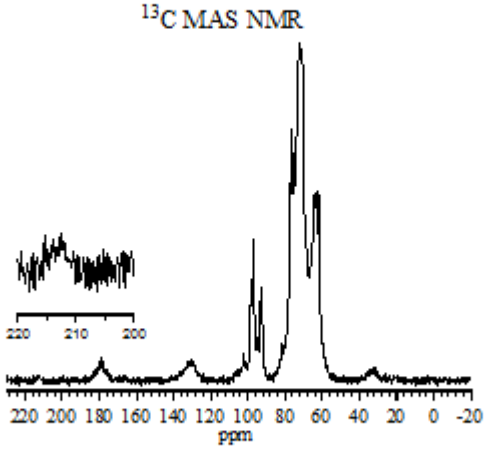


**Figure 2.6 $^{13}$C Solid-State NMR spectra of glucose adsorbed in Sn-Beta.**

The existence of this resonance implied that some of the glucose had ring opened (being able to occupy other Sn sites) and isomerized to the ring open form of fructose. In fact, when this sample was re-analyzed after several months of storage at room temperature, the reaction proceeded further. These NMR data strongly supported the proposed ring open reaction pathway, thus impliying that initial Sn-Beta pathways parallel the initial reaction steps observed in enzymatic systems. While there was an IR assignment of the keto carbonyl of the acyclic form of fructose, no assignment for the acyclic aldehyde carbonyl of glucose has been reported. However, when glucose was adsorbed on Sn-Beta, (but not Si-Beta) there was a broad band at ca. 1730-1720 $cm^{-1}$ that was reasonable to assign to the combination of the 1728 $cm^{-1}$ band from the acyclic fructose and a band from the aldehyde carbonyl (ca. 1720 $cm^{-1}$) of the acyclic glucose (Figure 2.5). These band intensities and assignments were consistent with the $^{13}$C NMR results. Overall, the NMR and IR data from both glucose and fructose adsorbed in Sn-Beta suggested that the reaction pathway paralleled the reaction steps observed in enzymatic steps.

At this time, the resonances at ca. 130 and 180 ppm have not been assigned yet. After reaction with either $^{13}C$ labeled glucose or fructose, these resonances appear as do others (Figure 2.7). The reaction of glucose on either Sn-Beta or Ti-Beta gave ca. 90% yields of glucose, fructose and mannose.[1] From the NMR spectra of the solids after reaction, some of the resonances were assigned to products that could be observed in solution, or remain on the solid and are not observed in solution (Figure 2.7). Further attempts to assign the remaining products in solution and on the solids will be discussed in Chapter 5.

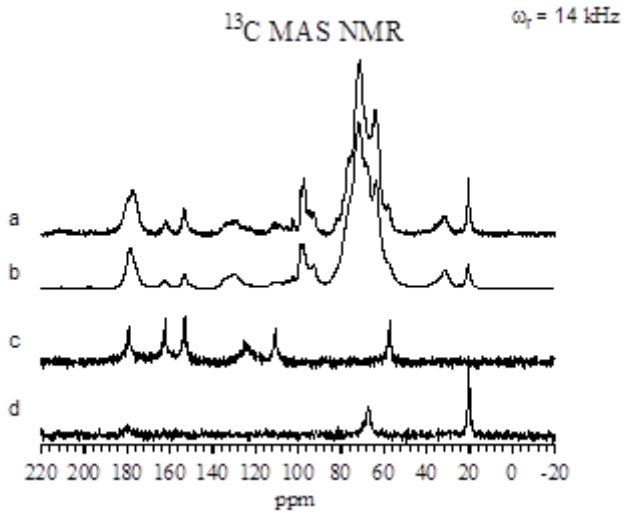


**Figure 2.7 $^{13}C$ Solid-State NMR of Sn-Beta after reaction condition using either labeled fructose (a) or labeled glucose (b) as the reactant. Also, HMF adsorbed into Sn-Beta (c) and lactic acid adsorbed into Si-Beta (d) at room temperature were shown for comparison.**

## 2.2 Isomerization Step

The enzymatic isomerization step is believed to occur primarily at M2. First, a hydroxyl ion bound to M2 promotes deprotonation at O2.[23] Next, M2 forms a bidentate complex with both O1 and O2, withdrawing electron density from the C-O bonds and effectively polarizing the substrate. This leads to a partial positive character on C1, consequently reducing the energetic barrier for hydride shift. Finally,

the protonated hydroxyl group at M2 donates the proton to O1, converting the aldehyde into a hydroxyl group.

Kinetic studies on enzymatic systems suggested that the kinetically limiting factor is the hydride shift. Interestingly, a similar conclusion could be drawn for the isomerizations with Sn-Beta and Ti-Beta. Previously, it has been shown that the mechanism of the glucose isomerization reaction using Sn-Beta involves a Lewis acid-mediated intramolecular hydride shift[2]. A kinetic isotope effect of ca. 2 for both Sn-Beta[2] and Ti-Beta is observed using glucose labeled with deuterium at the C2 position. Activation energies were obtained from initial rate data of glucose to fructose isomerization (Figs. S3 and S4) were 21.2 +/- 0.7 kcal/mol (343-373K) and 37.1 +/- 1.0 kcal/mol (388-403K) for Sn-Beta and Ti-Beta (obtained from Eranda Nikolla, a former Post-Doc in the M. E. Davis group), respectively. These data show that the hydride step is kinetically relevant and that Sn-Beta has a higher activity than Ti-Beta at the reaction conditions used.

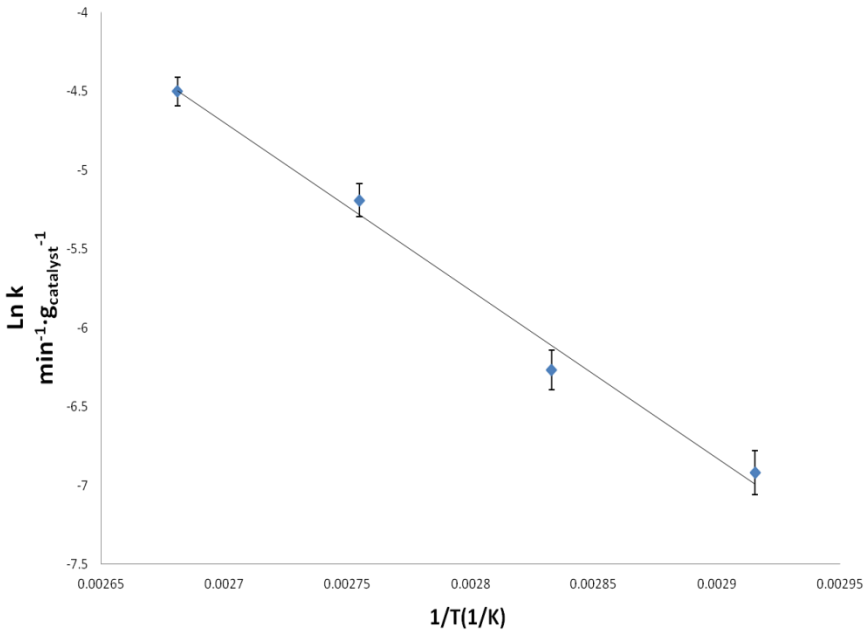


**Figure 2.8 Arrhenius plot for glucose isomerization over Sn-Beta.**

The kinetic parameters were used to confirm if the reaction was possible at room temperature (25ºC), when $^{13}C$ glucose was adsorbed on Sn-Beta. Under the same reaction conditions it was estimated that during the period of 1-4 days, the glucose conversion was in between 0.15-0.63%. Since the rate limiting step is the intramolecular shift, no glucose conversion should be happening at room temperature. Since isomerization is observed through $^{13}C$ NMR, it does not seem that the results are the same for lower temperatures.

## 2.3 Reaction Centers with Sn or Ti Containing Zeolite

The reaction pathway over Sn-Beta and Ti-Beta proceeded via a ring opening, hydride shift, and a ring closing mechanism. To gain further insights into how these conversions proceeded at the metal centers, the state of the Sn in the zeolite was investigated by solid-state NMR methods. Different atomic arrangements of framework Sn were depicted in Figure 2.9. Framework Sn can exist in two different states, octahedral or tetrahedral, depending on whether it is hexacoordinated or tetracoordinated. Also, Boronat *et al.*[24] proposed that framework Sn can be located in two different types of sites, closed or open, depending if the Sn centers have four bonds to the silicon atoms of the zeolite framework through bridging oxygens or if the Sn centers have three such bonds to the framework and one bond that has been hydrolyzed to produce Sn-OH and an adjacent silanol group (Si-OH). These atomic arrangements are analogous to those proposed for Ti in Ti-Beta and Ti in pure-silica ZSM-5 (called TS-1).[25] For the case of Ti, no NMR data is available; however, EXAFS data provide strong evidence for the open site.[25] Additionally, IR spectra can be used to identify the silanol group adjacent to the Ti center in the open site.

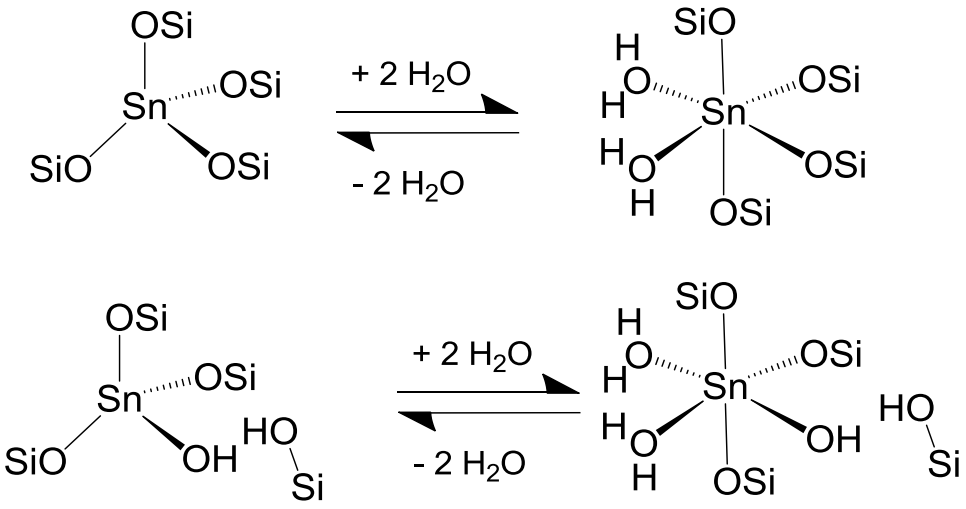


**Figure 2.9 Schematic representations of the closed (top) and open (bottom) sites in Sn-Beta. Left: dehydrated (tetrahedral), right: hydrated (octahedral).**

$^{119}$Sn solid-state NMR studies of the Sn-Beta prepared with $^{119}$Sn enriched starting materials are shown in Figure 2.10, Figure 2.11 and Figure 2.12. These had the structure directing agent (SDA) removed by calcination and were exposed to ambient conditions. The NMR spectrum revealed the presence of octahedral Sn (main resonances at ca. –685 and –700 ppm; Figure 2.10 and Figure 2.11). Upon heating to 393 K under vacuum, water was removed and the dehydrated spectrum showed the presence of tetrahedral Sn (main resonances at ca. -420 to -443 ppm; Figure 2.10 and Figure 2.11). Re-exposure to ambient conditions returned the Sn to its octahedral state. The calcination conditions affected the spectra that were obtained after dehydration, thus suggesting that the ratio of the -420 ppm resonance to -443 ppm resonance could vary with the pre-treatment conditions (compare Figure 2.10 and Figure 2.11).

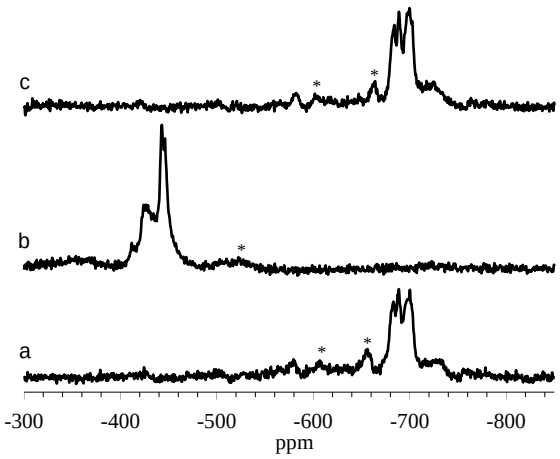


**Figure 2.10 $^{119}$Sn Solid State NMR spectra of Sn-Beta after different treatments. (a) calcined, (b) dehydrated after calcination, (c) rehydrated after step (b). The spinning rate was 14 kHz and spinning sidebands were marked by *.**

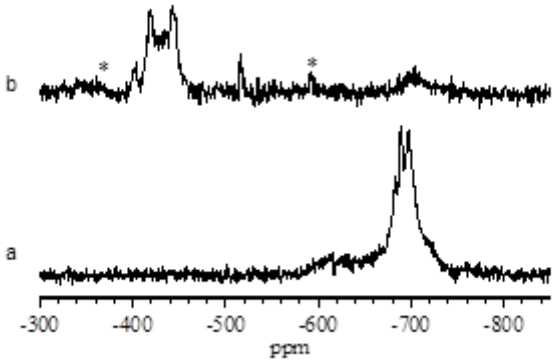


**Figure 2.11 $^{119}$Sn MAS NMR spectra of Sn-Beta as a function of hydration. (a) Sample was calcined with more humid conditions and exposed to ambient conditions, and (b) sample shown in (a) after vacuum drying at 393 K. The spinning rate was 14 kHz and spinning sidebands were marked by *.**

Corma and co-workers have shown that hydrated Sn-Beta has octahedral Sn while dehydration can change the Sn coordination to tetrahedral,[26] having only one resonance. By correlating the intensity of the IR band assigned to the acetonitrile adsorbed on the open site (as a measure of the amount of the open site) to the initial catalytic activity of the Baeyer-Villiger oxidation of cyclic ketones, these workers concluded that the open Sn site was the active center for this reaction. In contrast, $^{119}$Sn NMR showed there were two main resonances, i.e., the tetrahedral Sn centers.

These results could be due to differences in calcination conditions. Diffuse reflectance UV-Vis confirmed the Sn remained within the framework of the zeolite (Figure 2.23). Cross-polarized NMR spectra with variable contact time (Figure 2.12) showed that only one of the Sn environments had a proton source in its neighborhood. Therefore, based on the fact that the Sn atoms were located in the zeolite framework, the resonance at -420 and -443 ppm were assigned to the open and closed site, respectively, for the dehydrated Sn-Beta. Upon hydration, these tetrahedral Sn centers coordinated two additional water molecules to become octahedral (Figure 2.9). Thus, the Sn-Beta, and by analogy Ti-Beta, will have both open and closed sites that may be active reaction centers.

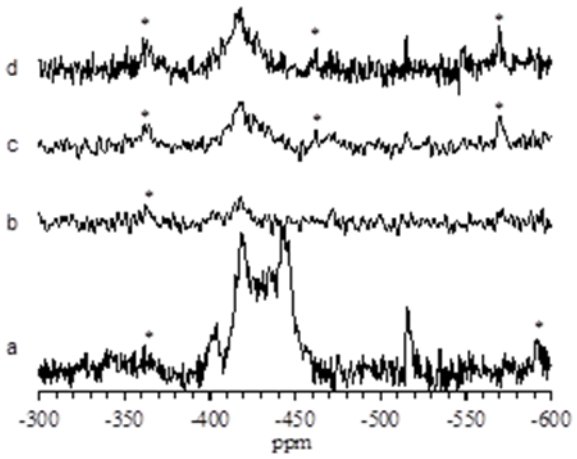


**Figure 2.12 $^{119}$Sn MAS (a) and CPMAS NMR (b-d) spectra for dehydrated Sn-Beta. The cross polarization contact times from 1H to 119Sn were varied: b) 0.2 ms, c) 1.0 ms, d) 2.0 ms. The spinning rate was 14 kHz for the MAS spectrum and 10 kHz for the CPMAS spectra, and spinning sidebands were marked by *.**

TS-1 is not active for the isomerization of glucose; however, this occurs presumably because glucose (kinetic diameter ca. 0.8 nm) is too large to diffuse into the pores of this zeolite (pore diameter ca. 0.55 nm).[1] To test this hypothesis, the isomerization of erythrose to erythrulose was employed as a test reaction using a

reactant that could diffuse into the pores of TS-1. This Ti silicate was active for the isomerization of erythrose, supporting the premise that glucose diffused into the zeolite catalysts in the ring-closed (pyranose) form, and that the ring-closed form is too large to diffuse into TS-1.

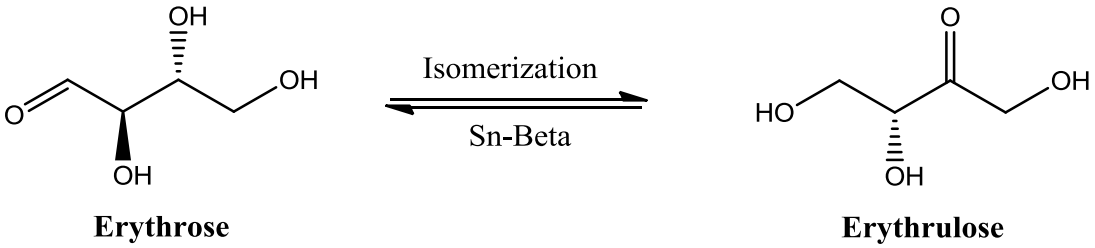


**Erythrose** **Erythrulose**

**Figure 2.13 Isomerization of erythrose to erythrulose with Sn-Beta**

To further investigate the nature of the active Sn site, Sn-containing zeolite beta was prepared using trichloromethyltin as the Sn source (denoted as $CH_3$Sn-Beta, powder X-ray diffraction pattern in Figure 2.24). Calcination of $CH_3$Sn-Beta provided an active glucose isomerization catalyst that was no different from the Sn-Beta samples prepared from tin tetrachloride Figure 2.14. The similar reactivities of these two samples suggested that the amounts of both the open and closed sites were predominantly a function of the high temperature calcination conditions (upon loss of the methyl group the tin center would have an OH group that could then condense with the adjacent silanol group to give a closed site for some of the tin centers in $CH_3$Sn-Beta).

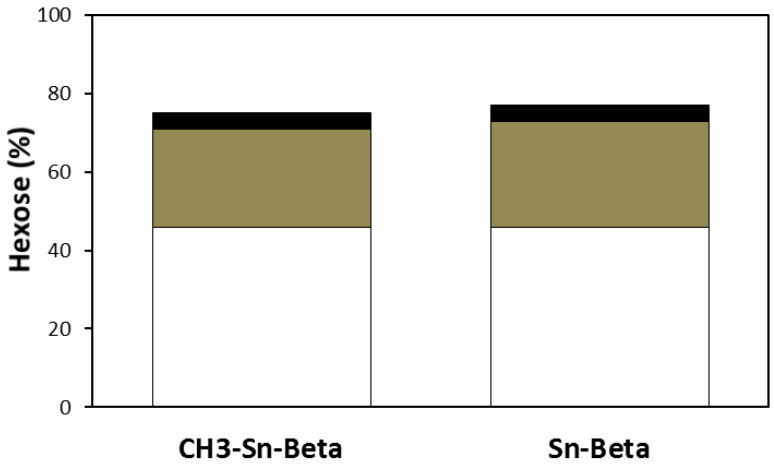


**Figure 2.14 Glucose isomerization reactivity with Sn-Beta and $CH_3$Sn-Beta. White: Glucose; Grey: Fructose; Black: Mannose. Reaction conditions: glucose:Sn = 100:1, 110 $^{o}$C, 45 min.**

In an attempt to alter the distribution of the Sn sites, the as-synthesized $CH_3$Sn-Beta was first exchanged into the sodium form and then calcined (attempt to limit condensation by reducing the number of available silanol groups adjacent to the open Sn center). The reaction rates for this sample were virtually identical to those obtained with the non-exchanged sample. Based upon these results alone, it cannot be conclusively defined which site was in fact the active site or whether both sites were active. These results strongly suggested that the calcination and initial exposure to the reaction environment interconverted the distribution of the tin centers between the open and closed sites, bringing them to an equilibrated state dictated by the reactions conditions or that the reactivity of the two types of sites were the same (highly unlikely). This hypothesis implied that the distribution of open and closed sites was dynamic at reaction conditions, requiring the development of an in-situ method for determining site distributions. Such a characterization technique was not available, and thus theoretical studies from another group (Page 60) were used in order to gain further insights into the nature of the active site.

## 2.4 The Formation of Mannose

In the glucose isomerization into fructose with Sn-Beta in water, mannose is being formed at glucose conversions of 10% or higher.[1] 10% mannose yield is obtained with temperatures ranging in between 363-413 K, with 10% (wt/wt) glucose in water and 1:50 Sn:glucose molar ratio. The small concentration of mannose makes it difficult to understand whether this C-2 epimer of glucose molecule is a side reaction of glucose, fructose or both. Therefore, the formation of mannose was studied to identify the side/s reaction/s. This was done by modeling the conversion and formation of the three hexoses assuming the scheme presented in Figure 2.15, where mannose was reversibly formed from both glucose and fructose. In addition, sink reactions were included for the three hexoses, since retro-adol reactions are seen upon longer reaction times.[27]

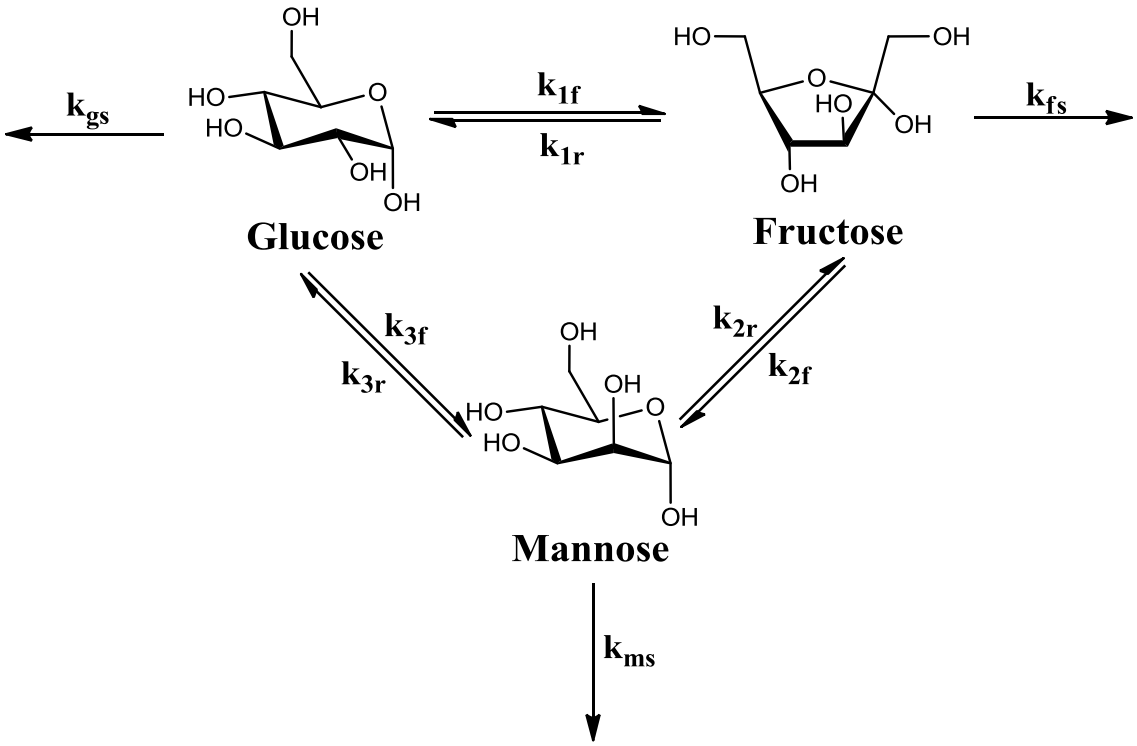


**Figure 2.15 Reaction scheme in the model of the hexoses isomerizations**

In this model, concentration profiles were measured starting from each of the hexoses at 100ºC with a 100:1 hexose:Sn ratio. These were measured in a batch stirred reactor, extracting an aliquot every ten minutes for an hour. Hence, for an ideal, constant volume, batch stirred reaction the mole balances for each of the hexoses, $c_G$ (glucose concentration) $c_F$ (fructose concentration) and $c_M$ (mannose concentration), can be expressed as:

$$\frac{dc_i(t)}{dt} = \nu_i\left(\sum_{j=1}^{n} r_j\right)\frac{M}{V} \qquad \text{Eq. 2.1}$$

where $r_j$ is the net rate (per metal site) of the j reaction shown in Figure 2.15, $\upsilon_i$ is the stoichiometric coefficient of each of the hexoses (-1 for the reactant and 1 for the products), M is the total number of metal sites in the reactor, and V is the reactor volume. Both forward and reverse reactions were assumed first order for each of the hexoses leading to the following glucose, fructose and mannose mole balances:

$$\frac{dc_G(t)}{dt} = \left[-c_G(t)\left(k_{1f} + k_{3f} + k_{gs}\right) + \left(\frac{k_{1f}}{K_1}c_F(t) + \frac{k_{3f}}{K_3}c_M(t)\right)\right]\frac{M}{V} \qquad \text{Eq. 2.2}$$

$$\frac{dc_F(t)}{dt} = \left[-c_F(t)\left(\frac{k_{1f}}{K_1} + k_{2f} + k_{fs}\right) + \left(k_{1f}c_G(t) + \frac{k_{2f}}{K_2}c_M(t)\right)\right]\frac{M}{V} \qquad \text{Eq. 2.3}$$

$$\frac{dc_M(t)}{dt} = \left[-c_M(t)\left(\frac{k_{2f}}{K_2} + \frac{k_{3f}}{K_3} + k_{ms}\right) + \left(k_{2f}c_F(t) + k_{3f}c_M(t)\right)\right]\frac{M}{V} \qquad \text{Eq. 2.4}$$

Where $K_1$, $K_2$ and $K_3$ are the equilibrium constants for the reversible reactions of glucose-fructose, fructose-mannose and glucose-mannose, respectively. The equilibrium constants were taken from the literature at a 100ºC,[1,28,29] being $K_1$ = 1.35, $K_2$ = 0.33 and $K_3$ = 0.45. This is a set of 1$^{st}$ order linear differential equations. Since

the solution to this set of differential equations results in a 3rd order polynomial solution, a numerical method was used. The *Euler Method* is a first-order Runge-Kutta numerical method for solving ordinary differential equations with a given initial value. The value at each time can be calculated with Equation 2.5:

$$c_i(t) = \frac{dc_i(t)}{dt}\Delta t + c_i(t-1) \qquad \text{Eq. 2.5}$$

With an initial value for the six different rate constants and an initial concentration for the hexose reactant, concentrations profiles were calculated with the Euler method. The increment time chosen was of one second, being the total time of one hour (3600 seconds). The rate constants were optimized to fit the experimental concentration values using the Generalized Reduced Gradient (GRG) Nonlinear approach. In the GRG Nonlinear approach the values of the rate constants were changing to optimize a specific objective cell, reaching a solution when the absolute value of the relative change in the objective function (E) is less than 0.0001 for the last 5 iterations. This objective function was defined as the sum of all the squared differences between the experimental and theoretical values:

$$\text{Objective Fuction (E)} = \sum_{i=1}^{6}(c_{exp} - c_{calc})^2 \qquad \text{Eq. 2.6}$$

The whole optimization model is summarized in the following flowchart:

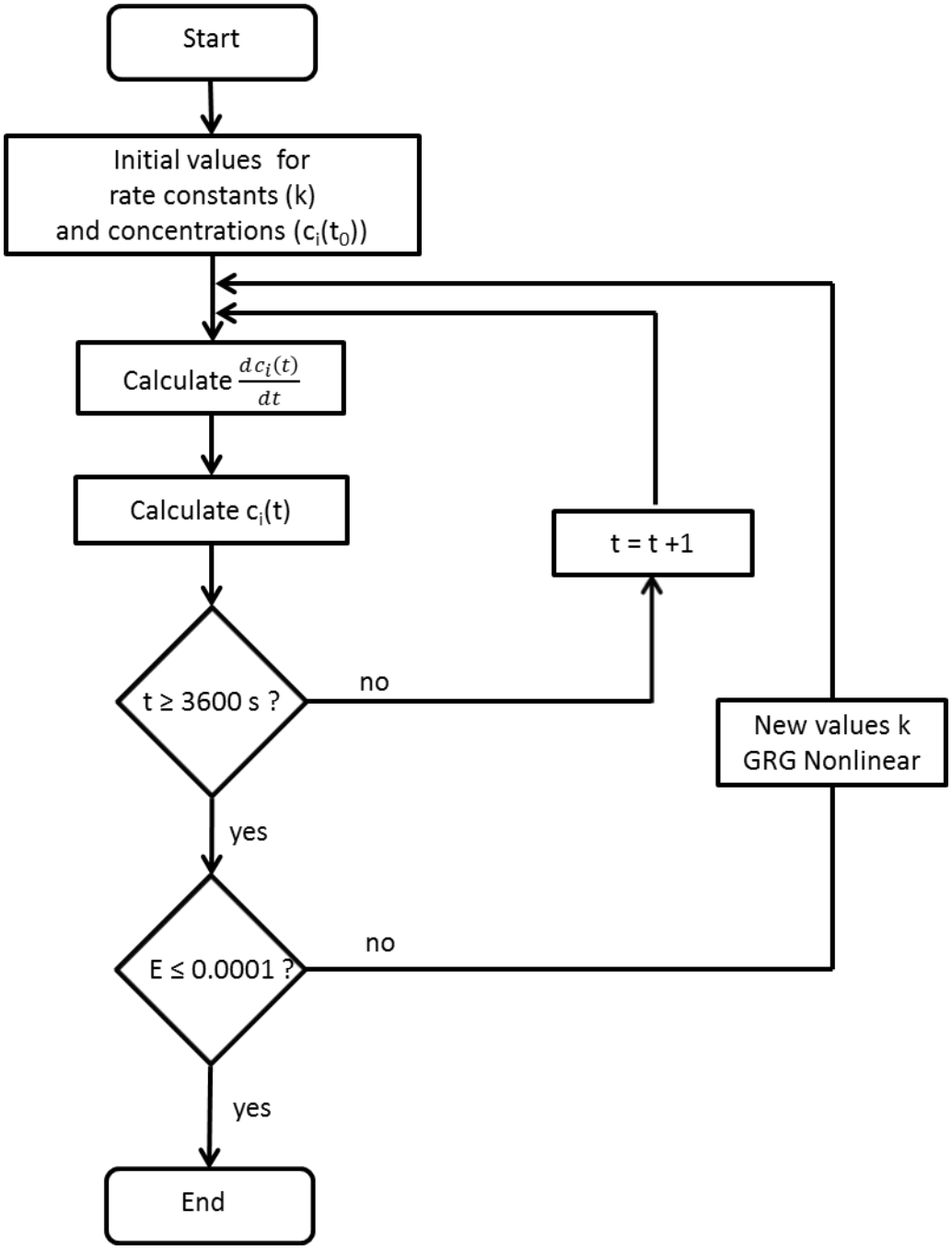


**Figure 2.16 Flowchart for the optimization of the different rate constants.**

This model was applied using the following initial hexoses: glucose, fructose and mannose. The experimental results and the calculated results can be seen in the following figures:

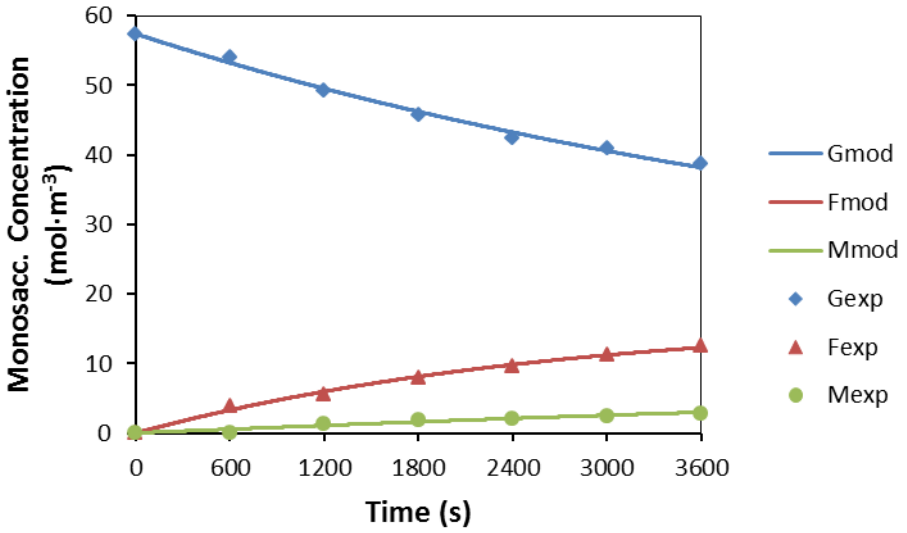


**Figure 2.17 Concentration profiles starting with 1% (wt/wt) glucose in water at 100ºC with a 100:1 glucose:Sn ratio.**

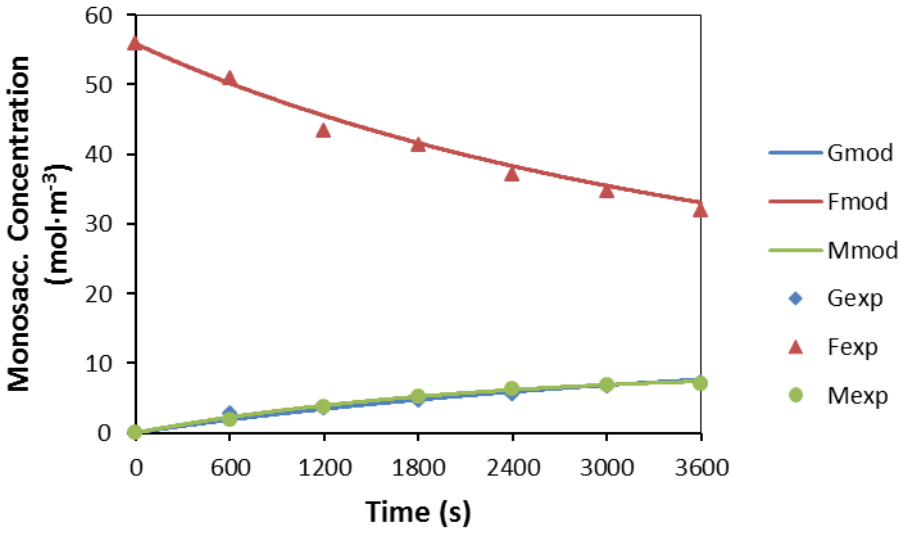


**Figure 2.18 Concentration profiles starting with 1% (wt/wt) fructose in water at 100ºC with a 100:1 fructose:Sn ratio.**

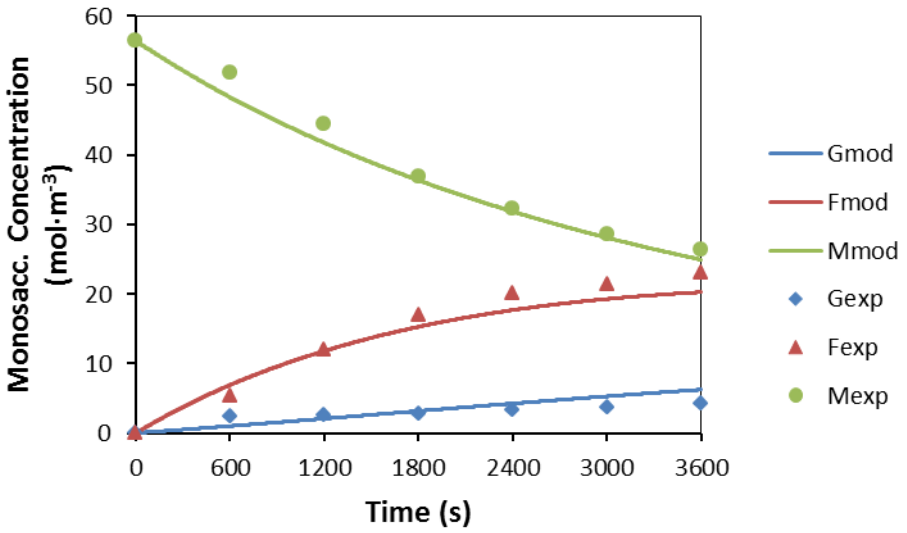


**Figure 2.19 Concentration profiles starting with 1% (wt/wt) mannose in water at 100ºC with a 100:1 mannose:Sn ratio.**

| | First order rate constants ((mol Sn)$^{-1}$·s$^{-1}$·m$^3$) | | | | | |
|---|---|---|---|---|---|---|
| Initial Hexose | $k_{1f}$ | $k_{2f}$ | $k_{3f}$ | $k_{gs}$ | $k_{fs}$ | $k_{ms}$ |
| Glucose | 1.92E-04 | 1.05E-04 | 2.79E-05 | 1.22E-05 | 1.93E-04 | 2.17E-07 |
| Fructose | 1.44E-04 | 1.34E-04 | 0.00E+00 | 1.60E-05 | 8.73E-05 | 2.17E-05 |
| Mannose | 2.06E-04 | 1.39E-04 | 2.12E-05 | 1.22E-05 | 1.83E-04 | 0.00E+00 |

**Table 2-1 First order rate constants calculated with the Euler model and optimized with the GRG Nonlinear approach.**

The experimental values seemed to match well with the model. When glucose and fructose were used as initial hexoses the calculated curve followed the experimental values quite nicely, while in the case of mannose the experimental values were not as precise. As initial values, all rate constants were given 1·00E-4 ((mol Sn)$^{-1}$·s$^{-1}$·m$^3$ to not preference any of the reactions. The initial values of the rate constants could have deviated the optimization of the model into a local minimum in the case were mannose was used as a starting hexose. Experimental error could have also deviated values from the calculated curves. However, in all cases the rate constants in Table 2-1 were higher from glucose into fructose and from fructose into mannose, than from glucose into mannose. The rate constant for the direct conversion

of glucose into mannose was an order of magnitude lower when both glucose and mannose were used as a starting hexose and zero in the case of fructose. These values suggest mannose was formed via fructose intermediate and not from glucose. The sink reaction rate constants were added to the model for better accuracy, but it will be discussed later in Chapter Five.

The formation of mannose with Sn-Beta in water was probed using $^{13}C$ and $^{1}H$ NMR spectroscopies from deuterium as an isotopic tracer in glucose. Following the same experiment previously done by former members in the group,[2] D2-glucose (glucose with deuterium in the C-2 position) was used under the same reactions conditions as in the previous kinetic study (100ºC, 1% (wt/wt) glucose in water, 100:1 glucose:Sn, for 45 minutes). The mannose formed (ca 10% yield) was then separated by means of High-Performance Liquid Chromatography (HPLC). Figure 2.20 and Figure 2.21 show the $^{13}C$ and $^{1}H$ NMR spectra, respectively, of the mannose formed after reaction.

The $^{13}C$ NMR spectrum of the mannose formed after reaction did not show resonances at $\delta$ = 93.9 and 93.5 ppm for the C-1 positions of the $\alpha$ and $\beta$ pyranose forms of mannose ($\alpha$-pyranose and $\beta$-pyranose are present in a ratio of 67:33), as it can be seen in Figure 2.20. This was due to the disruption of the Nuclear Overhauser Enhancement (NOE) by the deuterium atom in the C-1 position of mannose, since enhanced intensities of $^{13}C$-$^{1}H$ pairs were not observed,[30] The $^{1}H$ NMR spectra confirmed this result (Figure 2.21), because there were no resonances at $\delta$ = 4.85 and 5.15 ppm for the H in the C1 position of mannose of the $\alpha$ and $\beta$ pyranose forms of mannose. Since Sn-Beta had formed D1-fructose (fructose with D in the C1 position)

by intramolecular hydride shift from glucose, these results would suggest fructose is then isomerizing into mannose, since it has the D in the C1 position.

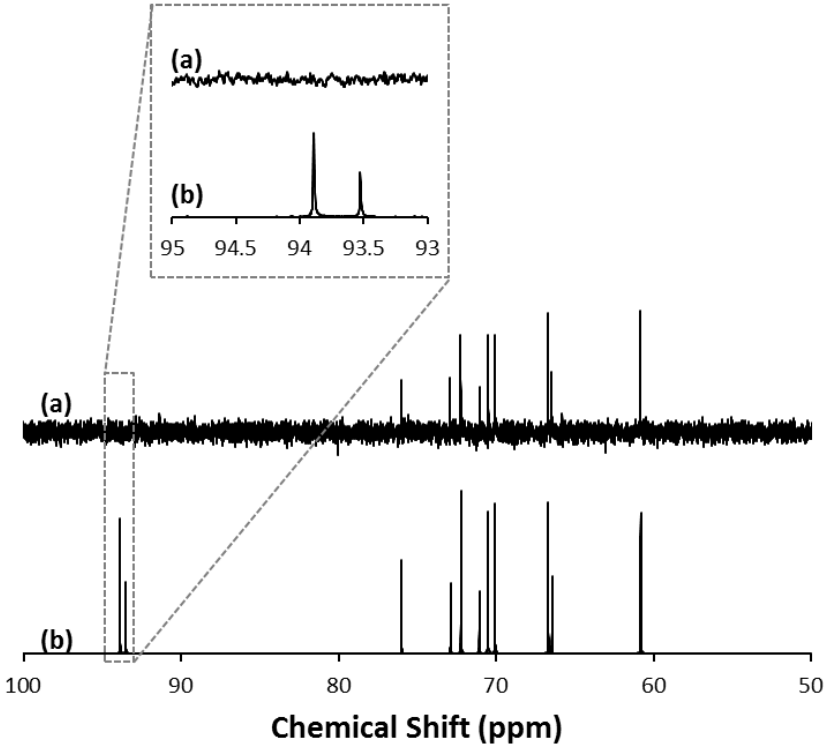


**Figure 2.20 $^{13}$C NMR spectra of (a) mannose formed after 1% (w/w) D2-glucose with Sn-Beta at 373K for 45 min., and (b) mannose.**

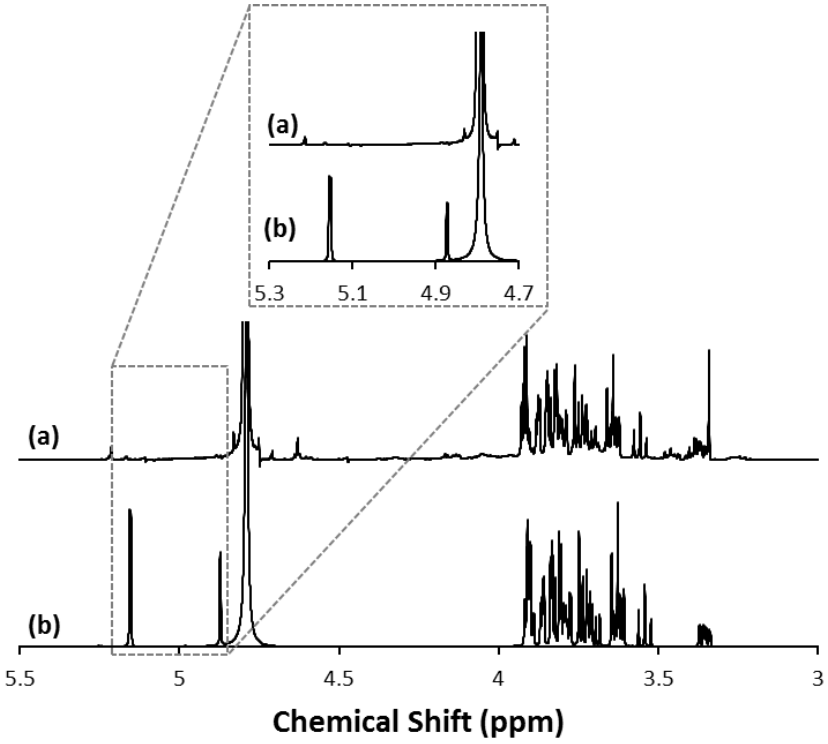


**Figure 2.21 $^{1}$H NMR spectra of (a) mannose formed after 1% (w/w) D2-glucose with Sn-Beta at 373K for 45 min., and (b) mannose.**

If we are to analyze the molecule of fructose in detail, the C1 has two H (name $H_a$ and $H_b$) positioned in the tetrahedral vacancies (Figure 2.22). Analogously to the glucose isomerization into fructose by intramolecular hydride shift, these two H in the C1 of glucose could attack independently the carbonyl (C2) group in fructose by intramolecular hydride shift and form glucose and mannose, respectively. Indeed, when fructose was used as a starting hexose, equimolar amounts of glucose and mannose were obtained (c.a. 12.5% yield), as it can be seen in Figure 2.18. Therefore, all of this data suggest mannose was being made from fructose and not from glucose.

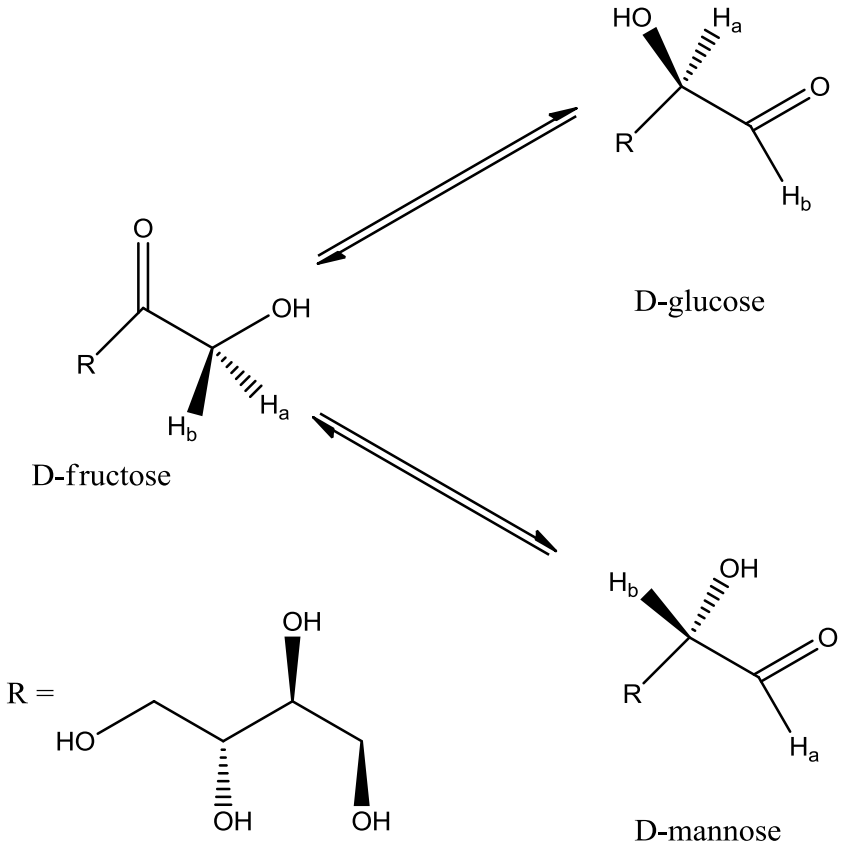


**Figure 2.22 Plausible fructose conversion into mannose and glucose**

## 3. Conclusion

The metalloenzyme D-xylose isomerase can catalyze the isomerization of glucose to fructose. It is shown that Sn-Beta and Ti-Beta can also catalyze this reaction to give similar product distributions to the enzyme and, like the enzyme, Sn-Beta can convert up to 45 wt% aqueous solutions of glucose[1]. The enzyme reaction mechanism involves the cyclic form of glucose binding to the enzyme followed by ring opening.[14] The acyclic form of glucose is then isomerized by a metal-assisted intramolecular hydride transfer.[14] With Sn-Beta (and to a great extent Ti-Beta), it is shown that the reaction mechanism is very similar to that of the enzyme. Evidence is provided to conclude that the glucose partitions into the zeolite in the cyclic form. In the presence of Sn (or Ti), direct NMR evidence of the acyclic fructose is observed.

Acyclic glucose must have first been bound to the Lewis acid center prior to being isomerized to obtain the acyclic fructose. The isomerization is clearly occurring via a Lewis acid-mediated, intramolecular hydride transfer mechanism.[2] Experimental results (kinetic isotope effects) corroborate the conclusion that the rate determining step is the intramolecular hydride transfer and that the open site is likely the active site responsible for isomerization activity. In addition, fructose seems to isomerize to mannose as both kinetic and isotopic experiments provide evidence for the glucose-fructose-mannose pathway and not the glucose-mannose pathway.

It is exciting to learn that the hydrophobic, Lewis acid containing zeolite catalysts can perform this type of reaction mechanism with glucose and presumably other sugars.[6] The fact that zeolite catalysts are quite stable allows them to be used at processing conditions not possible with enzymes, e.g., low pH, high ionic strength, high temperature, providing ways of coupling the isomerization reaction to other types of reactions important to the production of chemicals and fuels from biomass.

## 4. Experimental and Additional Figures

### 4.1 Synthesis of Ti-Beta, TS-1, Sn-Beta and $CH_3$-Sn-Beta

Ti-Beta zeolite was prepared as follows: 7.503 g of tetraethylammonium hydroxide solution (Sigma-Aldrich, 35 wt% in water) was diluted with 15 g of water. Then, 7.016 g of tetraethylorthosilicate (Sigma-Aldrich, 98 wt%) and 0.201 g of titanium (IV) isopropoxide (Sigma-Aldrich, 97%wt) were added to the solution. The mixture was stirred until complete hydrolysis of the tetraethylorthosilicate and titanium (IV) isopropoxide was obtained. Next, the solution was allowed to reach the

desired water ratio by complete evaporation of ethanol, isopropanol, and some water. Finally, 0.670 g of HF solution (Mallinckrodt, 48 wt% in water) was added resulting in a thick gel. The gel composition was $SiO_2$ / 0.021 $TiO_2$ / 0.54 TEAOH / 0.53 HF / 6.6 $H_2O$. This gel was transferred to a Teflon-lined stainless steel autoclave and heated at 140°C for 14 days. The solid was recovered by filtration, extensively washed with water, and dried at 100°C overnight. The solid was calcined at 580ºC for 6 hours to remove the organic content located within the crystalline material.

Sn-Beta zeolites was synthesized following the method reported in the patent literature.[1] TS-1 was crystallized from a clear solution prepared by mixing titanium butoxide (TNBT, Sigma-Aldrich 97 wt%), tetraethylorthosilicate (TEOS, Sigma-Aldrich 97 wt%), tetrapropylammonium hydroxide (TPAOH, 1M, Sigma-Aldrich) and deionized water. The mixture was stirred until complete hydrolysis of the tetraethylorthosilicate and titanium butoxide was obtained, then allowing complete evaporation of ethanol, butanol and some water until the desired water ratio was reached. The gel composition was $SiO_2$ / 0.03 $TiO_2$ / 0.44 TPAOH / 30 $H_2O$. The TS-1 reaction mixture was charged into Teflon-lined autoclaves and allowed to crystallize at 175ºC for 5 days. The autoclave was rotated at 50 RPM. After cooling, the solid was recovered by filtration, extensively washed with water, and dried at 100°C overnight. The material was calcined at 580ºC for 6 hours to remove the organic content located within the crystalline material.

Zeolites were prepared as follows: 7.57 g of tetraethylammonium hydroxide solution (Sigma-Aldrich, 35% (w/w) in water) was diluted with 15 g of water. Next, 7.011 g of tetraethylorthosilicate (Sigma-Aldrich, 98% (w/w)) was added, followed by the addition of 0.121 g of tin (IV) chloride pentahydrate (Sigma-Aldrich, 98% (w/w)), 0.121 $^{119}$tin(IV) chloride pentahydrate (Cambridge Isotopes, 82% enrichment)

or 0.122 g of methyltin trichloride pentahydrate (Sigma Aldrich, 97 wt%), depending if Sn-Beta, $^{119}$Sn-Beta, or $CH_3$-Sn-Beta were synthesized, respectively. The mixture was stirred until complete hydrolysis of the tetraethylorthosilicate was achieved, and then allowed to reach the desired water ratio by complete evaporation of ethanol and some water. Finally, 0.690 g of HF solution (Mallinckrodt, 48% (w/w) in water) was added, resulting in a thick gel. The gel composition was $SiO_2$ / 0.01 $SnCl_4$ / 0.55 TEAOH / 0.54 HF / 7.52 $H_2O$. The gels were transferred to Teflon-lined stainless steel autoclaves and heated at 140 $^oC$ for 25 days. The solids were recovered by filtration, extensively washed with water, and dried at 373 K overnight. The solids were calcined at 580$^oC$ for 6 h to remove the organic content located in the crystalline material. X-ray diffraction confirmed that the solid materials have the Beta zeolite topology (see Figure S2 for the diffraction pattern of $CH_3$-Sn-Beta), and SEM EDS measurements for the Sn-Beta, $^{119}$Sn-Beta and $CH_3$-Sn-Beta samples show a Si:Sn atomic ratio of 125:1, 125:1, and 150:1, respectively.

Si-Beta was prepared by adding 10.01 g of tetraethylammonium fluoride dihydrate (Sigma-Aldrich, 97% (w/w) purity) to 10 g of water and 4.947 g of tetraethylorthosilicate (Sigma-Aldrich, 98% (w/w)). This mixture was stirred overnight at room temperature in a closed vessel to ensure complete hydrolysis of the tetraethylorthosilicate. The targeted $H_2O$:$SiO_2$ ratio was reached by complete evaporation of the ethanol and partial evaporation of the water. The final molar composition of the gel was $SiO_2$ / 0.55 TEAF / 7.25 $H_2O$. The gel was transferred to a Teflon-lined stainless steel autoclave and heated at 413 K in a rotation oven (60 rpm) for 7 days. The solids were recovered by filtration, washed extensively with water, and dried at 373 K overnight. The dried solids were calcined in flowing air (1.67 $cm^3$

$s^{-1}$, Air Liquide, breathing grade) at 853 K (0.0167 K $s^{-1}$) for 10 h to remove the organic content located in the crystalline material.

## 4.2 Isomerization Reactions

Isomerization experiments were carried out in 10 ml thick-walled glass reactors (VWR) heated in a temperature-controlled oil bath placed on top of a digital stirring hotplate (Fisher Scientific). The activation energies were obtained with 1.5 g of an aqueous solution composed of 10 wt% glucose and the corresponding catalyst amount to achieve a 1:100 metal:glucose molar ratio were added to the reactor and sealed. In the study with the mannose formation, 5g of 1% (wt/wt) solution of hexose and the corresponding amount of catalyst were added to achieve 1:100 metal:glucose molar ratio. The reactor was placed in the oil bath and removed at specific times. The reaction was stopped by cooling the reactor in an ice bath, and small aliquots were taken for analysis. Sample analyses were performed by means of high performance liquid chromatography (HPLC) using an Agilent 1200 system (Agilent Technologies Corp.) equipped with PDA UV (320 nm) and evaporative light-scattering (ELS) detectors. Glucose and fructose concentrations were monitored with a Biorad Aminex HPX87C (300 x 7.8 mm) column (Phenomenex), using ultrapure water (pH = 7) as the mobile phase at a flow rate of 0.60 ml/min and a column temperature of 80 $^{o}$C.

## 4.3 Glucose Adsorption Experiments

Sn-BEA or Si-BEA catalyst was mixed with 10 wt% of C13-sugar (glucose or fructose) solution at Sn or Si to sugar (glucose or fructose) molar ratio of 1/100 for two hours at room temperature. The mixture was then centrifuged to separate the solid catalyst from the extra glucose solution. The remaining water was removed by leaving the vessel containing the catalyst open overnight in the hood.

4.4 Characterization

Powder X-ray diffraction (XRD) patterns were collected by using a Scintag XDS 2000 diffractometer using Cu Kα radiation. Scanning electron microscopy (SEM) with Energy Dispersive X-ray Spectroscopy (EDS) measurements were recorded on a LEO 1550 VP FE SEM at an electron high tension (EHT) of 10 kV. UV-Vis measurements were recorded using a Cary 3G spectrophotometer equipped with a diffuse reflectance cell.

Solid-state, magic angle spinning nuclear magnetic resonance (MAS-NMR) measurements were performed using a Bruker Avance 500MHz spectrometer equipped with a 11.7 T magnet and a Bruker 4mm MAS probe. Samples about 60-80 mg in powder were packed into 4mm $ZrO_2$ rotors and spun at 14 kHz for MAS experiments. MAS-NMR experiments were conducted for $^{1}H$, $^{13}C$, $^{23}Na$, and $^{119}Sn$ nuclei of which operating frequencies are 500.2, 125.5, 132.3, 186.5 MHz, respectively. $^{119}Sn$ MAS NMR spectra were obtained with a recycle delay time of 2 s. $^{119}Sn$ cross polarization (CP) MAS spectra were acquired at spinning rate of 10 kHz and using radio frequency (rf) field strength of 62.6 kHz for contact pulse after 4 msec-p/2 pulse on the $^{1}H$ channel and strong $^{1}H$ decoupling during the acquisition. $^{13}C$ CPMAS experiments were carried out at similar rf field strength. NMR spectra are reported with referenced to tetramethylsilane (TMS) for $^{1}H$ and $^{13}C$, 1M aqueous solution of $Na(NO_3)_3$ for $^{23}Na$, and $(CH_3)_3Sn$ but measured with $SnO_2$ at - 604.3 ppm as a second external reference for $^{119}Sn$ nuclei.

For the glucose adsorption experiment analyses, samples (~ 60-80 mg in powder form) were packed into 4mm $ZrO_2$ MAS NMR rotors (sample container made for a Bruker 4mm MAS NMR probe) at ambient conditions.

## 4.5 Additional Figures

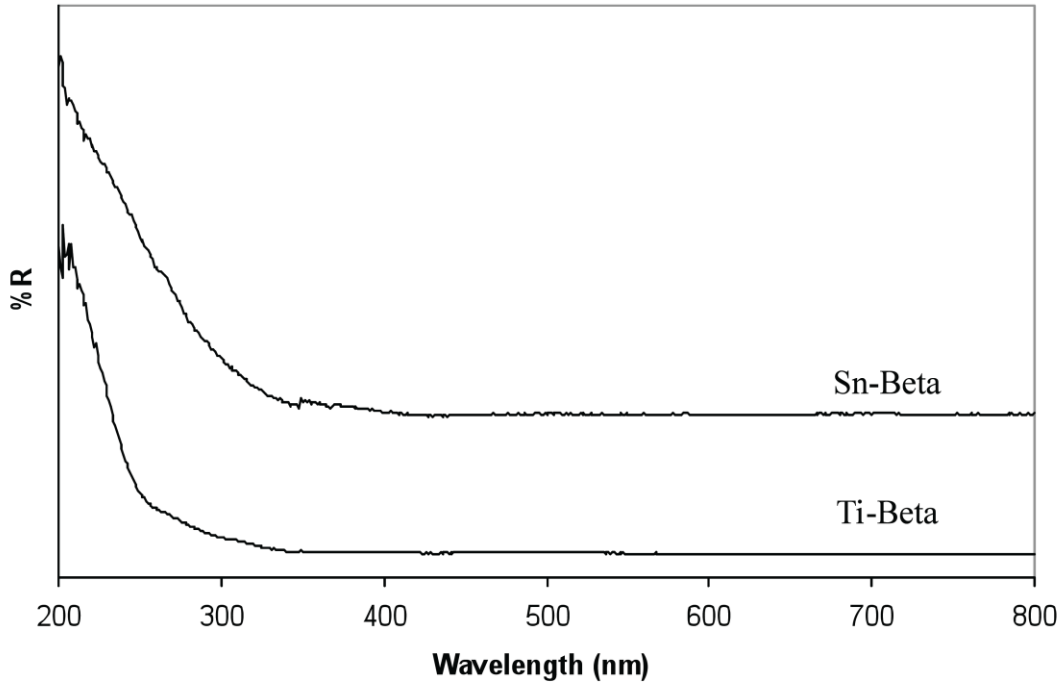


**Figure 2.23 Diffuse reflectance UV-VIS of Sn-beta and Ti-Beta**

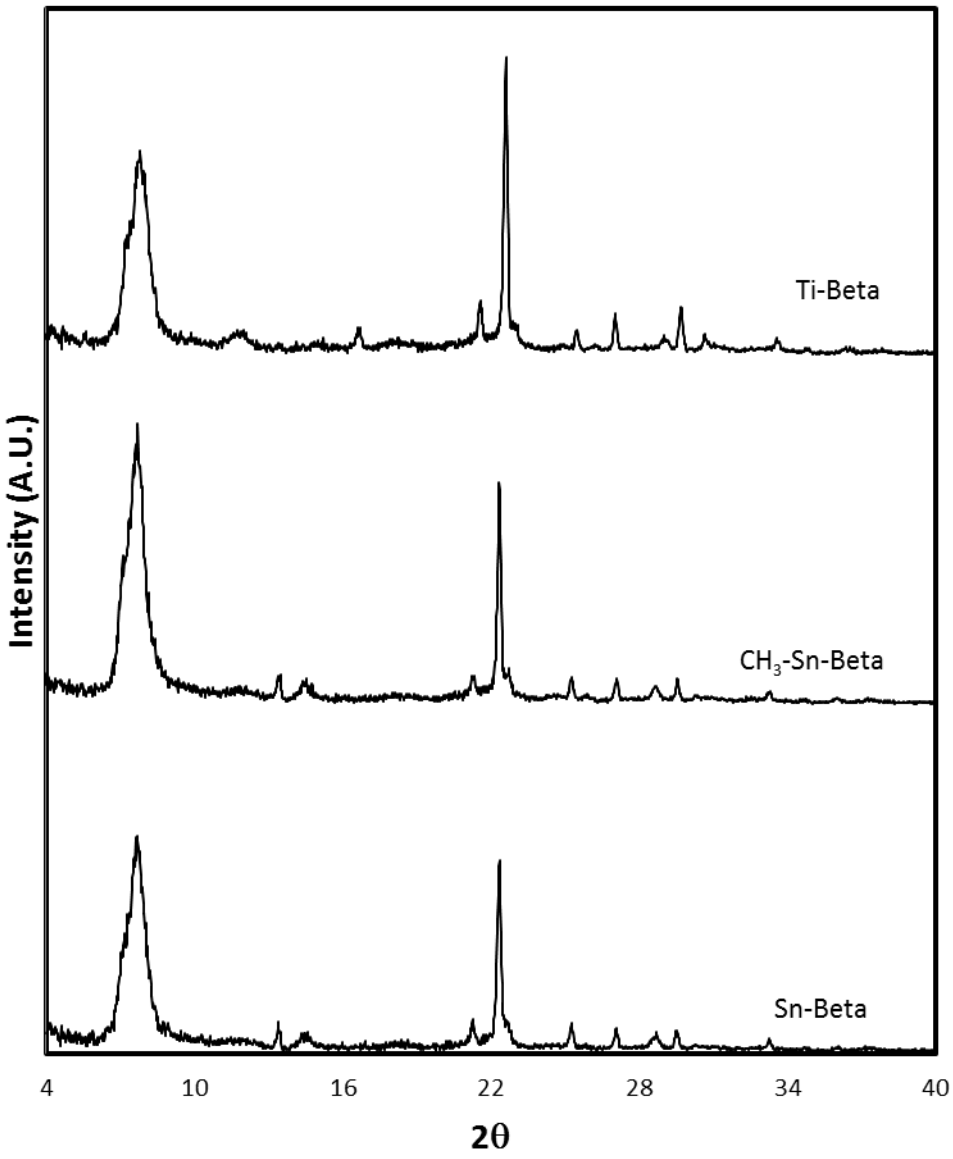


**Figure 2.24 Powder X-Ray Diffraction of Sn-Beta and $CH_3$-Sn-Beta.**

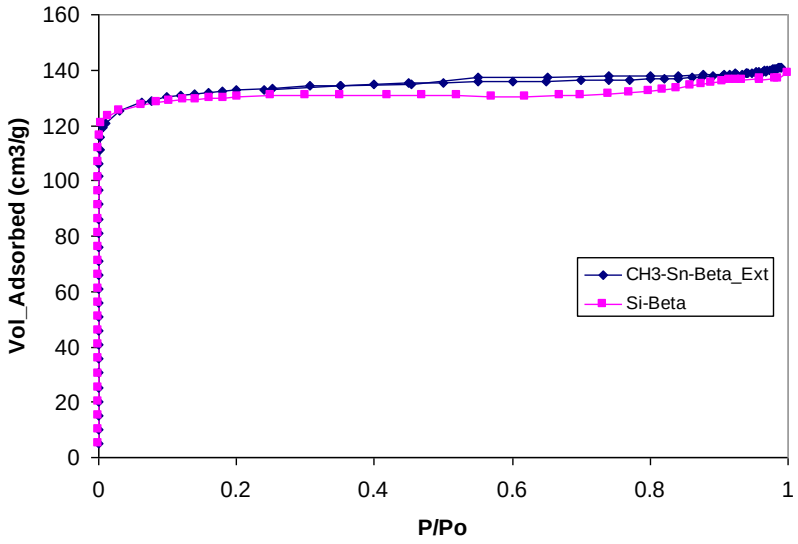


**Figure 2.25 $N_2$ adsorption isotherms of Si-Beta and $CH_3$Sn-Beta extracted.**

## 5. Computational Studies

*Computational studies were done by Rajeev S. Assary and Larry A. Curtiss, from Argonne National Laboratory

Quantum chemical studies were performed to gain further molecular-level understanding of the glucose-fructose isomerization pathways and to compare with experimental kinetics of both Sn-Beta and Ti-Beta. The structures and energies of intermediates and transition states were determined. Based on previous experimental and theoretical studies, it has been suggested that the open site in Sn-Beta, TS-1, and Ti-Beta is the active site for reactions other than the glucose isomerization[24,25,31,32]. The enthalpy profile below and the free energy profile for glucose-fructose isomerization catalyzed by the Sn-Beta open site indicate that, similarly to enzymatic systems, the process can be described as a sequence of ring opening (I to IV), hydride shift (V-VI), and ring closing (VI-IX) events. The initial adsorption of cyclic glucose and ring opening does not require any apparent reaction barriers. The process

requiring significant activation is the intramolecular hydride shift (V to VI) via a transition state ($V^{TS}$), and is consistent with experimental results showing a kinetic isotope effect when the glucose is labeled with deuterium at the C2 position.

The enthalpic profiles for glucose-fructose isomerization catalyzed by three open active site models with and without adjacent silanol groups were also calculated. Based on a single site micro-kinetic model, the activation enthalpy for the glucose-fructose isomerization process was computed to be 18.6, 22.1 and 17.3 kcal/mol for the Sn-Beta open site, the Sn-Beta open site with one silanol group, and Sn-Beta open site with two adjacent silanol groups, respectively. The calculated activation enthalpy for the Sn-Beta open site with one adjacent silanol group is found to be consistent with our experimental value of 21.2 +/- 0.7 kcal/mol , and supports the assignment of the catalytic activity to the open site of Sn-Beta for glucose-fructose isomerization. Overall, these calculations show relatively small energetic differences between the three open sites models, thus suggesting that the presence or absence of adjacent silanol groups does not drastically influence reaction rates. This is in agreement with our experimental results showing that catalysts with $Na^+$ exchanged silanol groups had similar activity as the non-exchanged catalysts.

It was previously shown that the apparent activation energy for the hydride shift associated with the isomerization of glyceraldehyde to dihydroxyacetone is 10 kcal/mol higher for the Sn-Beta closed site than that of an open site[32]. The glucose isomerization over the closed site would require the participation of a water molecule to allow for ring opening of the glucose. Calculations on a closed site with the presence of an explicit water molecule were performed and the computed apparent activation barrier was approximately 30 kcal/mol and is therefore unlikely to be the primary reaction pathway for glucose isomerization over Sn-Beta. These results

support the suggestion that the open site is a catalytically more active site for the glucose-fructose isomerization.

The glucose-fructose isomerization using models of the open sites of Ti-Beta was also investigated. The initial glucose absorption on the open Ti-Beta model site (with one silanol group) is much weaker, and the rate limiting hydride shift is 10 kcal/mol higher in barrier height compared to that catalyzed by the open site of Sn-Beta with one adjacent silanol group. This trend is consistent with previously reported theoretical studies for aldose-ketose isomerization by Sn-Beta and Ti-Beta active site models[32]. The computed activation enthalpy for glucose-fructose isomerization catalyzed by the open site of Ti-Beta, open site of Ti-Beta with one adjacent silanol, and the open site of Ti-Beta with two adjacent silanol groups are 28.0, 34.3, and 36.3 kcal/mol, respectively. The computed activation enthalpies of Ti-Beta with silanol group(s) are consistent with the experimentally measured activation enthalpy (37.1 +/- 1.0 kcal/mol).

Computational results indicate that the acyclic forms of glucose and fructose are equally stabilized by Sn centers (Species V and VI). Gas phase calculations at the G4 level suggest that acyclic fructose is more stable than acyclic glucose by ~ 2 kcal/mol (ketone groups has more intramolecular hydrogen bonding than the aldehyde). Thus, at thermodynamic equilibrium, cyclic and acyclic species of both sugars (Figure 2.26, species I, II, V, VI, VIII, and IX) are expected to be present within the zeolite pores. The enthalpy surfaces support the concept of having acyclic forms strongly coordinated with the Sn active site, which is consistent with the experimental observation of acyclic fructose species by NMR. Note that although the cyclic furanose form of fructose bound to the Sn center has a lower energy (-19 kcal/mol; species VIII) than the bound acyclic form (-9 kcal/mol; Figure 2.26, species

VI), it is still possible to observe the bound acyclic form since a barrier of ~ 10 kcal is required for the cyclization. A similar conclusion can be drawn for glucose.

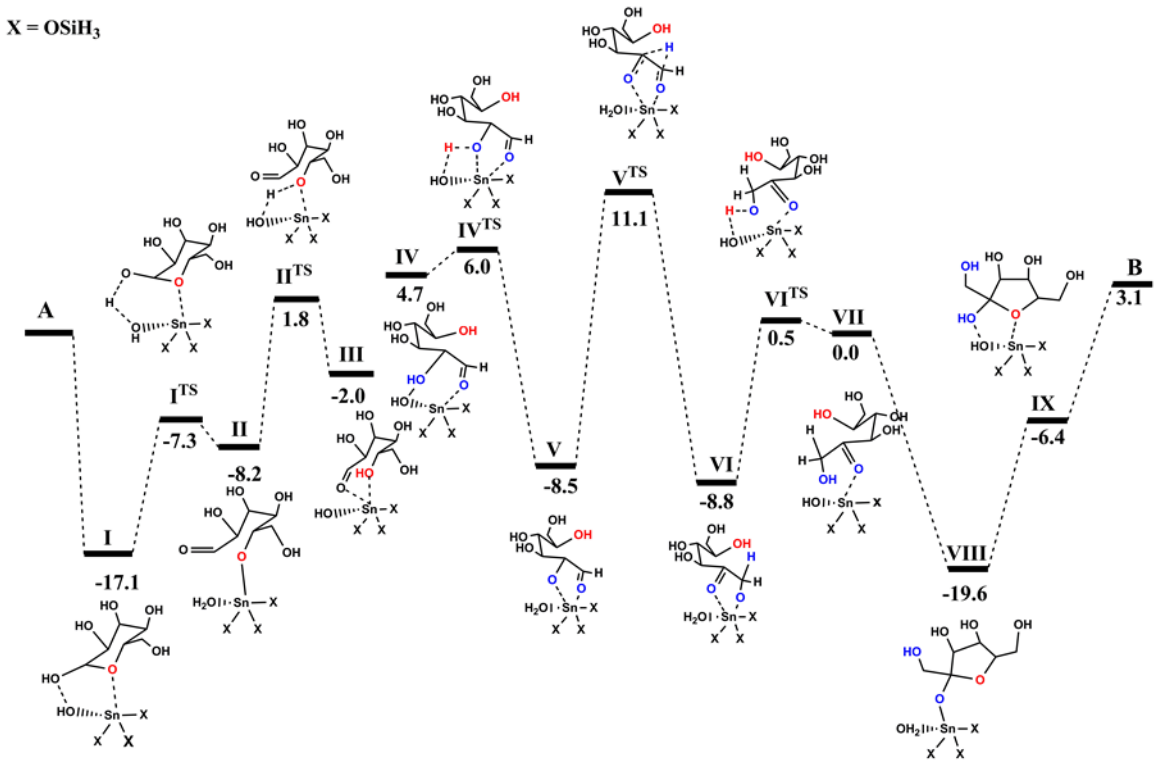


**Figure 2.26 The Computed enthalpy profile (MP2, 298 K in water dielectric) for glucose-fructose isomerization catalyzed by open site of Sn-Beta. The label A denotes the sum of enthalpy of glucose and active site model (Scheme S2, (a)) infinitely separated in aqueous medium, B denotes the same quantity for fructose. All energies are relative to the energy of A and reported in kcal/mol.**

## 6. References


1. Moliner, M., Román-Leshkov, Y. & Davis, M. E. Tin-containing zeolites are highly active catalysts for the isomerization of glucose in water. *Proc. Natl. Acad. Sci. U. S. A.* **107,** 6164–8 (2010).

2. Román-Leshkov, Y., Moliner, M., Labinger, J. a & Davis, M. E. Mechanism of glucose isomerization using a solid Lewis acid catalyst in water. *Angew. Chem. Int. Ed. Engl.* **49,** 8954–7 (2010).

3. Nikolla, E., Rom, Y., Moliner, M. & Davis, M. E. "One-Pot" Synthesis of 5-(Hydroxymethyl)furfural from Carbohydrates using Tin-Beta Zeolite. *ACS Catal.* **1,** 408–410 (2011).

4. Román-Leshkov, Y., Barrett, C. J., Liu, Z. Y. & Dumesic, J. a. Production of dimethylfuran for liquid fuels from biomass-derived carbohydrates. *Nature* **447,** 982–5 (2007).

5. Climent, M. J., Corma, A. & Iborra, S. Converting carbohydrates to bulk chemicals and fine chemicals over heterogeneous catalysts. *Green Chem.* **13,** 520 (2011).

6. Choudhary, V., Pinar, A. B., Sandler, S. I., Vlachos, D. G. & Lobo, R. F. Xylose Isomerization to Xylulose and its Dehydration to Furfural in Aqueous Media. *ACS* 1724–1728 (2011).

7. Lobo, R. F. Synthetic glycolysis. *ChemSusChem* **3,** 1237–40 (2010).

8. De Bruyn, C. A. L. & van Ekenstein, W. A. Action des alcalis sur les sucres, II. Transformation réciproque des uns dans les autres des sucres glucose, fructose et mannose. *Recl. des Trav. Chim. des Pays-Bas* **14,** 203–216 (1895).

9. Osanai, S. No Title. *Top. Curr. Chem.* **215,** 43–76 (2001).

10. Lecomte, J., Finiels, A. & Moreau, C. Kinetic Study of the Isomerization of Glucose into Fructose in the Presence of Anion-modified Hydrotalcites. *Starch - Stärke* **54,** 75–79 (2002).

11. Yang, B. Y. & Montgomery, R. Alkaline degradation of glucose: effect of initial concentration of reactants. *Carbohydr. Res.* **280,** 27–45 (1996).

12. Wit, G. De, Kieboom, A. P. G. & van Bekkum, H. Enolisation and isomerisation of monosaccharides in aqueous, alkaline solution. *Carbohydr. Res.* **74,** 157–175 (1979).

13. Kooyman, C., Vellenga, K. & Wilt, H. G. J. De. The isomerization of d-glucose into d-fructose in aqueous alkaline solutions. *Carbohydr. Res.* **54,** 33–44 (1977).

14. Allen, K. N. *et al.* Isotopic exchange plus substrate and inhibition kinetics of D-xylose isomerase do not support a proton-transfer mechanism. *Biochemistry* **33,** 1481–7 (1994).

15. Kovalevsky, A. Y. *et al.* Metal ion roles and the movement of hydrogen during reaction catalyzed by D-xylose isomerase: a joint x-ray and neutron diffraction study. *Structure* **18,** 688–99 (2010).

16. Corma, A., Domine, M. & Valencia, S. Water-resistant solid Lewis acid catalysts: Meerwein–Ponndorf–Verley and Oppenauer reactions catalyzed by tin-beta zeolite. *J. Catal.* **215,** 294–304 (2003).

17. Corma, A., Domine, M. E., Nemeth, L. & Valencia, S. Al-free Sn-Beta zeolite as a catalyst for the selective reduction of carbonyl compounds (Meerwein-Ponndorf-Verley reaction). *J. Am. Chem. Soc.* **124,** 3194–5 (2002).

18. Taarning, E. *et al.* Zeolite-catalyzed isomerization of triose sugars. *ChemSusChem* **2,** 625–7 (2009).

19. Holm, M. S., Saravanamurugan, S. & Taarning, E. Conversion of sugars to lactic acid derivatives using heterogeneous zeotype catalysts. *Science* **328,** 602–5 (2010).

20. Román-Leshkov, Y. & Davis, M. E. Activation of Carbonyl-Containing Molecules with Solid Lewis Acids in Aqueous Media. *ACS Catal.* **1,** 1566–1580 (2011).

21. Goux, W. J. Complex Isomerization. 4320–4327 (1985).

22. Drew, K. N. 13C-labeled aldopentoses: detection and quatitation of cyclic and acyclic forms by heteronuclear 1D and 2D NMR spectroscopy. *Carbohydr. Res.* **307,** 199–209 (1998).

23. Dworkin, J. P. A kinetic estimate of the free aldehyde content of aldoses. *Carbohydr. Res.* **329,** 359–365 (2000).

24. Boronat, M., Concepcion, P., Corma, a, Renz, M. & Valencia, S. Determination of the catalytically active oxidation Lewis acid sites in Sn-beta zeolites, and their optimisation by the combination of theoretical and experimental studies. *J. Catal.* **234,** 111–118 (2005).

25. Bordiga, S., Bonino, F., Damin, A. & Lamberti, C. Reactivity of Ti(IV) species hosted in TS-1 towards H2O2-H2O solutions investigated by ab initio cluster and periodic approaches combined with experimental XANES and EXAFS data: a review and new highlights. *Phys. Chem. Chem. Phys.* **9,** 4854–78 (2007).

26. Corma, a, Nemeth, L. T., Renz, M. & Valencia, S. Sn-zeolite beta as a heterogeneous chemoselective catalyst for Baeyer-Villiger oxidations. *Nature* **412,** 423–5 (2001).

27. Holm, M. S., Saravanamurugan, S. & Taarning, E. Conversion of sugars to lactic acid derivatives using heterogeneous zeotype catalysts. *Science* **328,** 602–5 (2010).

28. Hayes, M. L., Pennings, N. J., Serianni, A. S. & Barker, R. Rearrangement of the Carbon Skeleton. 6764–6769 (1982).

29. Palleroni, N. & Doudoroff, M. MANNOSE ISOMERASE OF PSEUDOMONAS SACCHAROPHILA. *J. Biol. Chem.* **218,** 535–548 (1956).

30. Neuhaus, D. & Williamson, M. P. *The Nuclear Overhauser Effect in Structural and Conformational Analysis*. 656 (2000).

31. Khouw, C. Catalytic Activity of Titanium Silicates Synthesized in the Presence of Alkali-Metal and Alkaline-Earth Ions. *J. Catal.* **151,** 77–86 (1995).

32. Assary, R. S. & Curtiss, L. a. Theoretical study of 1,2-hydride shift associated with the isomerization of glyceraldehyde to dihydroxy acetone by Lewis acid active site models. *J. Phys. Chem. A* **115,** 8754–60 (2011).

# Chapter 3 : The Glucose Isomerization into Fructose Mechanism with $SnO_2$/Si-Beta

## 1. Introduction

In aqueous media, it has previously been seen that framework Sn centers behave as Lewis acids that bind glucose reactants in their acyclic forms and mediate their isomerization to fructose via an intramolecular hydride shift from the C-2 to the C-1 position.[1,2] Glucose reactants containing a deuterium label on the C-2 position (glucose-D2) formed fructose products deuterated in the C-1 position (fructose-D1),[1,2] reflected in $^{13}$C NMR spectra that showed low-intensity triplet resonances corresponding to these carbon atoms. Low-intensity resonances in $^{13}$C NMR spectra, acquired using $^{1}$H broad-band decoupling, reflect the presence of D atoms that disrupt the Nuclear Overhauser Enhancement (NOE) of $^{13}$C resonances via suppression of $^{13}$C-$^{1}$H couplings. The mechanistic evidence obtained from $^{13}$C and $^{1}$H NMR studies were also consistent with the observed kinetic isotope effect of ca. 2 (at 383 K) when using glucose-D2 reactants.[2] Activation energies measured experimentally (89 kJ mol$^{-1}$) and calculated by MP2-levels of theory for intramolecular hydride shift steps on framework Sn open sites (Sn with three -O(Si) bonds and one -OH group) adjacent to one silanol group (92 kJ mol$^{-1}$) were also similar.[2] These Lewis acid-mediated isomerization pathways on Sn-Beta in aqueous solvent are analogous to those on metalloenzymes such as D-xylose isomerase XI, which contains two divalent metal ions (commonly $Mg^{2+}$ or $Mn^{2+}$) that facilitate the ring-opening of glucose and the hydride shift from C-2 to C-1 positions on the acyclic sugar.[3]

In contrast with the case of glucose isomerization to fructose on framework Sn sites in water, the activity and mechanistic origins of other Sn species in the zeolite remain unclear. In this chapter kinetic and mechanistic studies are used, focusing on

differential glucose conversions to distinguish among isomerization pathways on framework and extraframework Sn sites in zeolite Beta, in both water and methanol. In contrast to framework Sn sites behaving as Lewis acids that isomerize glucose to fructose in water via intramolecular hydride shifts, extraframework $SnO_2$ domains located within hydrophobic zeolite Beta channels mediate glucose isomerization to fructose via base-catalyzed proton abstraction in both water and methanol. Extraframework $SnO_2$ particles located on external zeolite surfaces or on amorphous supports, however, isomerize glucose into fructose in methanol, but not in water. These findings help clarify differences in reactivity among Sn sites of different structure and among extraframework $SnO_2$ particles of different location within porous solids. They also provide the mechanistic origin of fructose when formed as a primary product of glucose conversion with Sn-zeolites

## 2. Results and Discussion.

### 2.1 Site and Structural Characterization of Sn-Containing Samples

The x-ray diffractograms of Si-Beta, Sn-Beta, $SnO_2$/Si-Beta and $SnO_2$/Si-Beta-E (Figure 3.1) show patterns that were consistent with the zeolite Beta structure, while the XRD pattern of $SnO_2/SiO_2$ is consistent with that of an amorphous solid. The XRD pattern of $SnO_2$/Si-Beta also exhibit diffraction lines at 2θ values of $26.7^o$ and $34.0^o$ that are characteristic of bulk $SnO_2$ (Figure 3.1). The presence of some extracrystalline $SnO_2$ aggregates in the $SnO_2$/Si-Beta sample (synthesized using $SnO_2$ as the Sn source) indicate that bulk $SnO_2$ did not completely dissolve or decompose under the hydrothermal conditions used in the synthesis of $SnO_2$/Si-Beta. The absence of large $SnO_2$ domains (as detectable by XRD) in Sn-Beta and $SnO_2$/Si-Beta-E

indicate that mononuclear $SnCl_4$ precursors did not aggregate significantly during hydrothermal synthesis of Sn-Beta, or during the aqueous-phase exchange and subsequent air treatment (853 K) protocols used to synthesize $SnO_2$/Si-Beta-E. Indeed, SEM images of the $SnO_2$/Si-Beta sample, but not of Sn-Beta, show the presence of large (> 10 μm) $SnO_2$ particles (Figure 3.2).

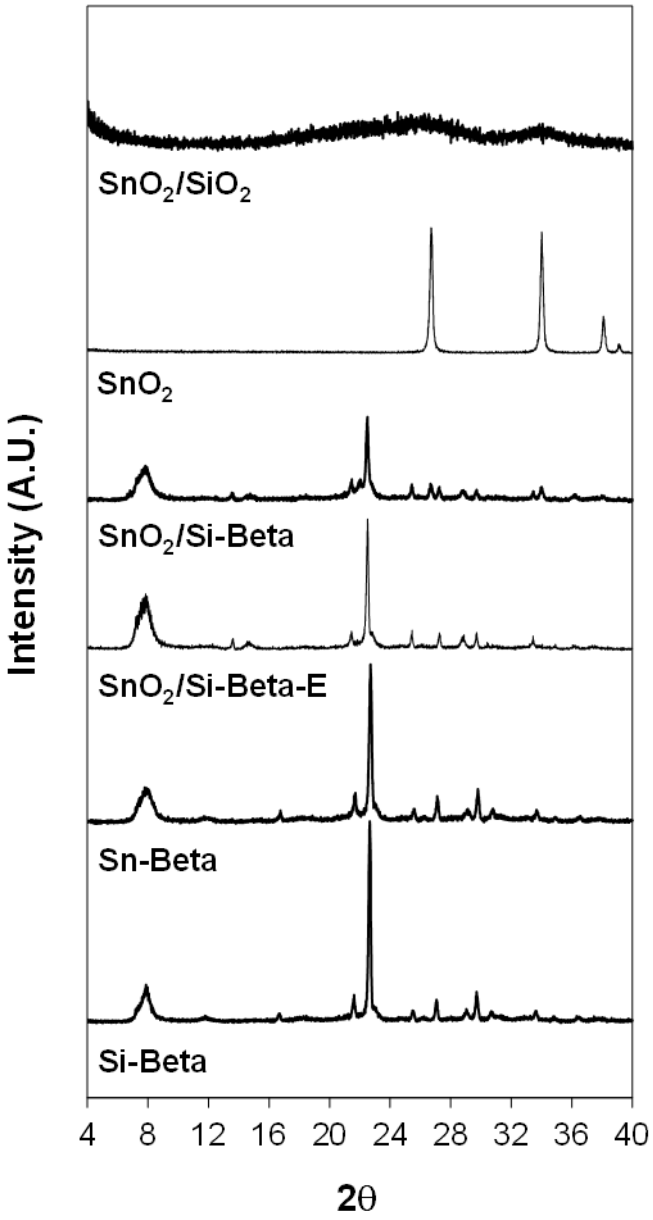


**Figure 3.1 Powder x-ray diffraction patterns of Si-Beta, Sn-Beta, $SnO_2$/Si-Beta-E, $SnO_2$/Si-Beta, $SnO_2$, $SnO_2$/$SiO_2$ (bottom to top).**

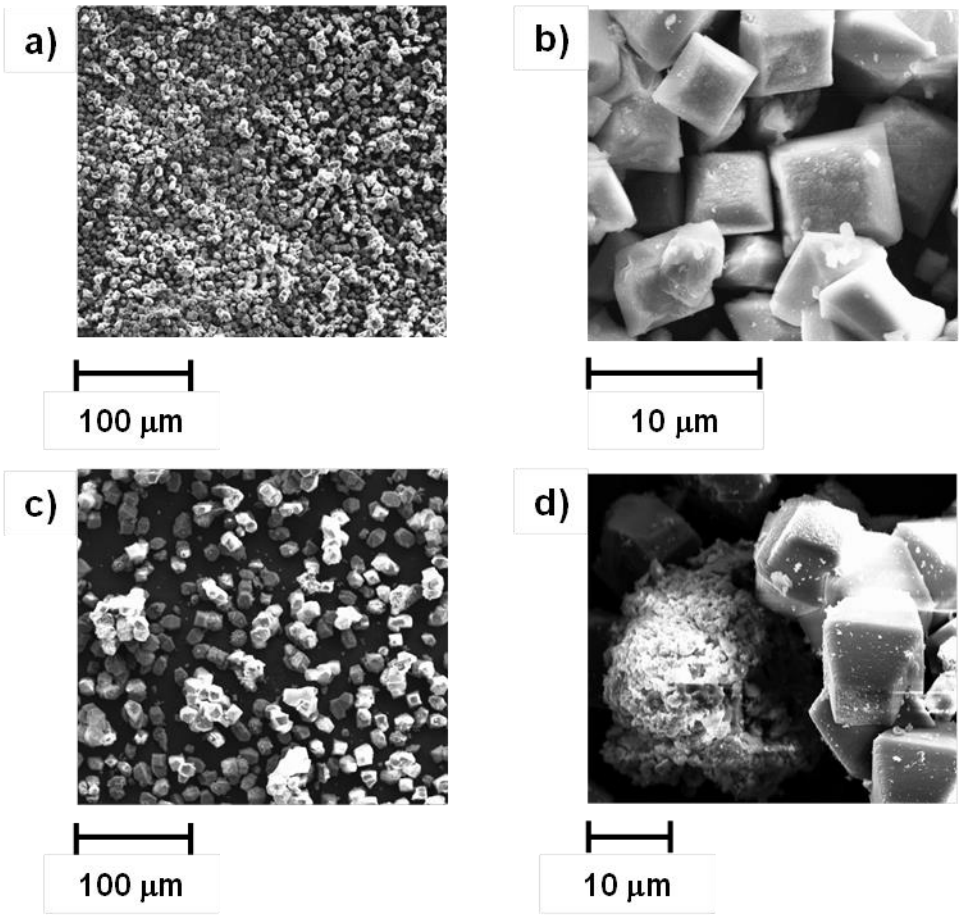


**Figure 3.2 SEM images of (a, b) Sn-Beta and (c, d) $SnO_2$/Si-Beta.**

Total micropore volumes determined by $N_2$ adsorption isotherms (Figure 3.12, Figure 3.13, Figure 3.14 and Figure 3.15) are 0.20 and 0.19 $cm^3\ g^{-1}$ for Sn-Beta and Si-Beta, respectively (Table 3-1). The micropore volume for $SnO_2$/Si-Beta-E, a sample in which $SnO_2$ was deliberately deposited on the exterior surfaces of Beta crystallites, is also 0.20 $cm^3\ g^{-1}$, consistent with its low Sn content (2.1 wt%) and the absence of any intracrystalline $SnO_2$ species that may occlude pore volume. In contrast, the micropore volume is 0.12 $cm^3\ g^{-1}$ for $SnO_2$/Si-Beta (Table 3-1), which is significantly lower than expected if $SnO_2$ were present as extracrystalline phases or located within intracrystralline voids but only occluding space (page 90). These data suggested that some $SnO_2$ domains are located within the pores of $SnO_2$/Si-Beta, preventing access to a fraction of the internal void space in $SnO_2$/Si-Beta crystals.

| **Catalyst** | **Si/Sn**[a] | **$N_2$ micropore volume**[b] ($cm^3\ g^{-1}$) | **$^{119}$Sn MAS NMR resonances**[c] (ppm) | | **UV-Visible band centers**[d] (nm) |
|---|---|---|---|---|---|
| | | | *hydrated* | *dehydrated* | |
| Sn-Beta | 87 | 0.20 | -688, -700 | -424, -443 | 203 |
| $SnO_2$/Si-Beta | 92 | 0.12 | -604 | - | 280 |
| $SnO_2$/Si-Beta-E | 116 | 0.20 | -606 | -602 | 238 |
| $SnO_2/SiO_2$ | 13 | - | -605 | - | 247 |
| $SnO_2$ | - | - | -604 | - | 276 |
| Si-Beta | - | 0.19 | - | - | n.d.* |

[a]Determined by electron microprobe.
[b]Determined by extrapolation of mesopore $N_2$ uptakes to zero pressure (Section S.3, Supporting Information).
[c]Relative to $(CH_3)_4Sn$.
[d]Diffuse reflectance spectra obtained on materials exposed to ambient conditions.
*n.d. not detected

**Table 3-1 Site and structural characterization of samples used in this study.**

$^{119}$Sn NMR spectra of Sn-Beta after calcination and exposure to ambient conditions (hydrated) show main resonances at -688 and -700 ppm (Figure 3.3a). After dehydration, these resonances disappeared and new resonances appeared concomitantly at -424 and -443 ppm (Figure 3.3b), which have been respectively assigned to framework Sn open sites (three framework –O(Si) bonds and one (OH) group) and framework Sn close sites (four framework –O(Si) bonds).[2] The $^{119}$Sn NMR spectrum of hydrated $SnO_2/SiO_2$ (Figure 3.3c) and $SnO_2$/Si-Beta-E (Figure 3.3d) samples exhibit very broad resonances centered near -604 ppm, which do not change upon dehydration (dehydrated $SnO_2$/Si-Beta-E; Figure 3.3e). The position of these resonances is consistent with the chemical shift of octahedrally-coordinated Sn in bulk $SnO_2$ (-604.3 ppm; Figure 3.3g), while their breadth reflect geometric heterogeneities among the octahedral Sn centers in these samples, as expected from the formation of small $SnO_2$ domains from mononuclear $SnCl_4$ precursors. In contrast to $SnO_2$/Si-Beta-E and $SnO_2/SiO_2$, the $^{119}$Sn NMR spectrum of hydrated $SnO_2$/Si-Beta (Figure 3.3f) shows a very sharp resonance at -604 ppm. This sharp resonance reflects

the presence of large $SnO_2$ aggregates on $SnO_2$/Si-Beta, concordant with the diffraction lines for bulk $SnO_2$ that appeared in its XRD pattern (Figure 3.1) and the large $SnO_2$ particles (> 10 μm) detected in its SEM images (Figure 3.2).

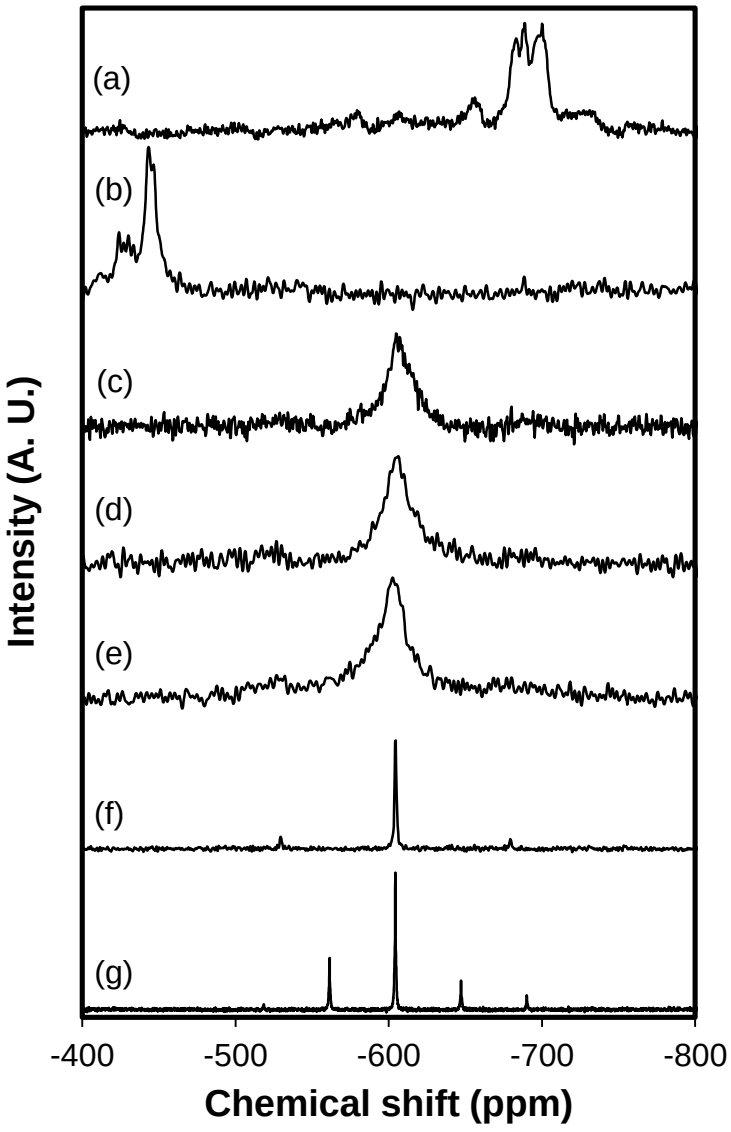


**Figure 3.3 $^{119}$Sn MAS NMR spectra of (a) Sn-Beta (hydrated), (b) Sn-Beta (dehydrated), (c) $SnO_2$/$SiO_2$ (hydrated), (d) $SnO_2$/Si-Beta-E (hydrated), (e) $SnO_2$/Si-Beta-E (dehydrated), (f) $SnO_2$/Si-Beta (hydrated), and (g) bulk $SnO_2$ (hydrated).**

The DRUV spectrum of Sn-Beta (Figure 3.4a) shows a peak centered at 203 nm (Table 3-1) that has been assigned to tetrahedrally coordinated framework Sn,[4,5]

while no features are observed in the spectrum of Si-Beta (Figure 3.16). The DRUV spectra of $SnO_2/SiO_2$ (Figure 3.4b) and $SnO_2$/Si-Beta-E (Figure 3.4c) exhibit peaks centered at 247 and 238 nm (Table 3-1), respectively, which have been assigned to $SnO_2$ species.[6–9] In contrast to $SnO_2/SiO_2$ and $SnO_2$/Si-Beta-E, the DRUV spectra of bulk $SnO_2$ (Figure 3.4) and $SnO_2$/Si-Beta (Figure 3.4e) show broad bands ranging from 235-290 nm with maxima near 280 nm (Table 3-1), which have been assigned to hexacoordinated polymeric Sn species.[5] Relations between UV-Visible absorption wavelengths and the domain sizes of $SnO_2$ nanoparticles have been well-documented;[6–9] quantum confinement effects cause an increase in the band gap energies (and concomitant decreases in UV-Visible absorption wavelengths) of nanoscale semiconducting oxide domains as they decrease in size. Thus, the lower UV-Visible band centers of $SnO_2/SiO_2$ and $SnO_2$/Si-Beta-E, relative to bulk $SnO_2$ and $SnO_2$/Si-Beta-E, indicate the presence of smaller $SnO_2$ domains on the former samples.

Taken together, these characterization data indicated that Sn species are present as framework Sn sites in Sn-Beta, as extraframework $SnO_2$ particles supported on extracrystalline surfaces of $SnO_2$/Si-Beta-E or on amorphous surfaces of $SnO_2/SiO_2$, and as extraframework $SnO_2$ particles located both outside and within microporous voids of $SnO_2$/Si-Beta.

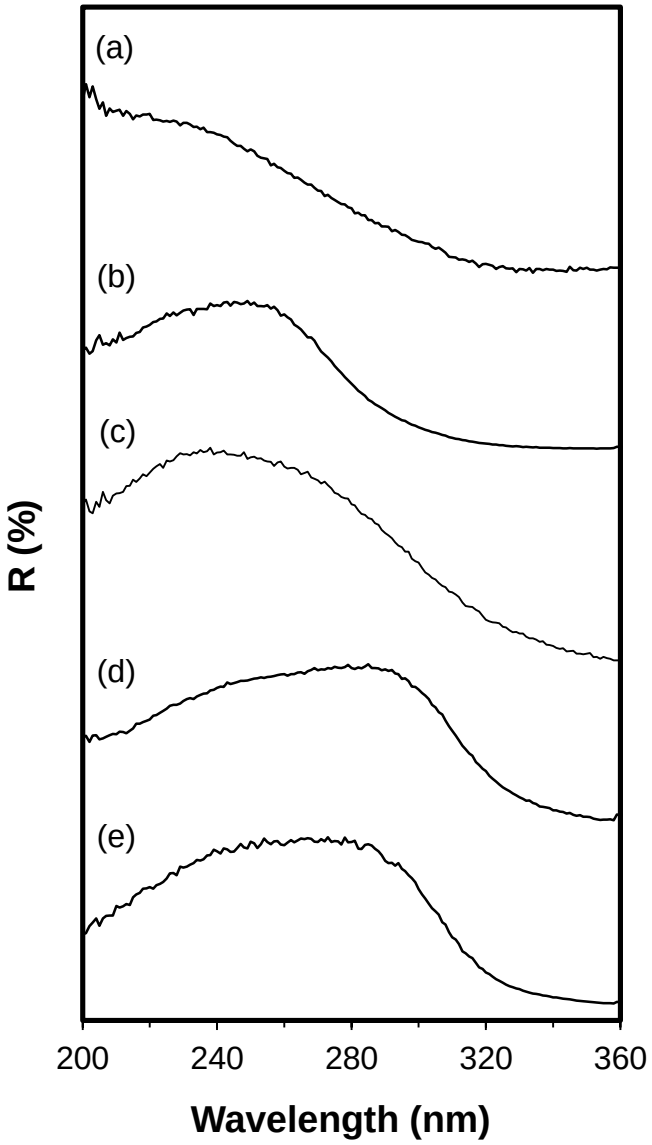


**Figure 3.4 Diffuse reflectance UV-Visible spectra of (a) Sn-Beta, (b) $SnO_2/SiO_2$, (c) $SnO_2$/Si-Beta-E, (d) $SnO_2$/Si-Beta and (e) bulk $SnO_2$; spectra shifted vertically for clarity.**

2.2 Glucose Conversion on Sn-Beta and $SnO_2$-Containing Samples in Water

Fructose was formed as the primary product during differential conversion of glucose on both Sn-Beta and $SnO_2$/Si-Beta in water. Turnover rates (per mol total Sn) were higher on Sn-Beta than on $SnO_2$/Si-Beta throughout the temperature range studied (343-373 K; see Table 3-4). The apparent activation energy was also higher on Sn-Beta (93 $\pm$ 15 kJ $mol^{-1}$;Table 3-2) than on $SnO_2$/Si-Beta (59 $\pm$ 6 kJ $mol^{-1}$;Table 3-2). Although both Sn-Beta and $SnO_2$/Si-Beta are able to isomerize glucose to fructose in water, the different structures of framework and extraframework Sn active

sites and the large difference in apparent activation energies between them suggest that different isomerization mechanisms prevail on these two sites.

| **Catalyst** | **Solvent** | **Turnover rate (373 K)** (/ $10^{-3}$ mol $s^{-1}$ (mol total Sn)$^{-1}$) | **$E_{app}$** (kJ $mol^{-1}$) |
|---|---|---|---|
| Sn-Beta | $H_2O$ | 27.8 ± 5.0 | 93 ± 15 |
| $SnO_2$/Si-Beta | $H_2O$ | 9.7 ± 1.9 | 59 ± 6 |
| | $CH_3OH$ | 16.6 ± 2.3 | 71 ± 15 |
| $SnO_2/SiO_2$ | $H_2O$ | n.d.* | - |
| | $CH_3OH$ | 4.2 ± 0.3 | 102 ± 9 |

*n.d. not detected

**Table 3-2 Turnover rates (373 K) and apparent activation energies ($E_{app}$) for glucose isomerization to fructose and glucose epimerization to mannose on Sn-Beta, $SnO_2$/Si-Beta and $SnO_2/SiO_2$ in $H_2O$ and $CH_3OH$ solvents.**

$^{1}$H and $^{13}$C NMR spectroscopies of products formed from the reaction of a 10 % (w/w) solution of glucose-D2 over $SnO_2$/Si-Beta in water (1 h, 373 K) were used to investigate the isomerization mechanism on $SnO_2$ active sites, as was previously done with Sn-Beta in water.[10] The $^{13}$C NMR spectrum of glucose after reaction (Figure 3.5a) shows resonances at δ = 74.1 and 71.3 ppm for the C-2 positions of β-pyranose and α-pyranose; their low intensity triplets are also present, reflecting the presence of D atoms, which disrupted the Nuclear Overhauser Enhancement (NOE) of $^{13}$C resonances. Thus, the resonance at δ = 74.1 ppm reflects the presence of H atoms at some of the glucose C-2 positions, consistent with the low intensity resonances that appear ca. δ = 3.1 ppm for H atoms at the C-2 position in the corresponding $^{1}$H NMR spectrum (Figure 3.17). These data indicate that the D-label on glucose-D2 underwent isotopic scrambling in the presence of $SnO_2$/Si-Beta in water, as we have previously observed after reaction of glucose-D2 with aqueous NaOH solutions, but not with Sn-Beta in water.[10]

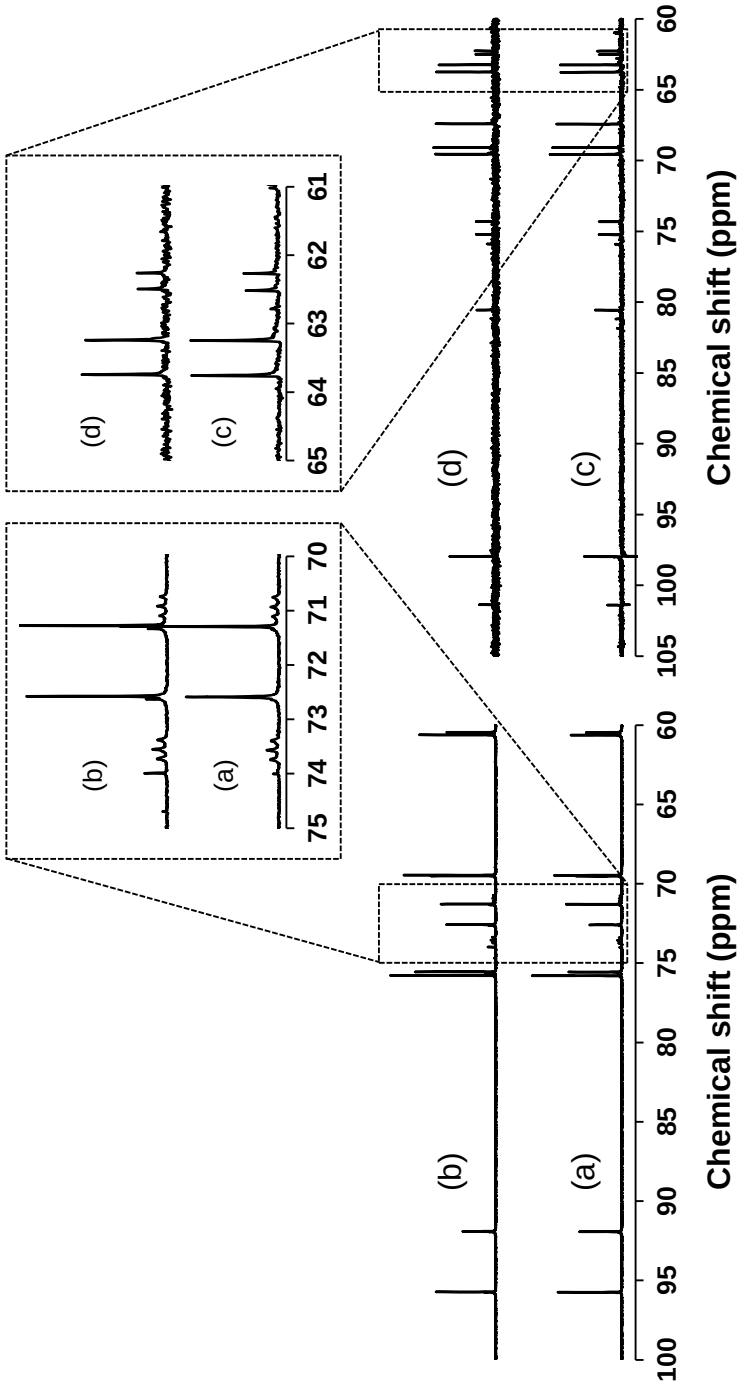


**Figure 3.5 $^{13}$C NMR spectra of sugar fractions (glucose or fructose) obtained after reaction of glucose-D2 with $SnO_2$/Si-Beta in different solvents (water or methanol) at 373 K for 1 h. (a) glucose / water, (b) glucose / methanol, (c) fructose / water, (d) fructose / methanol.**

The $^{13}$C NMR spectrum of fructose products formed from reaction of glucose-D2 with $SnO_2$/Si-Beta in water (Figure 3.5c) showed resonances at $\delta$ = 63.8 and 62.6 ppm for the C-1 position of β-pyranose and β-furanose, respectively. The absence of

low intensity triplets for these resonances indicated that no deuterium atoms were bonded to fructose C-1 carbon atoms.[10] The corresponding $^1$H NMR spectrum (Figure 3.19) shows a resonance at $\delta$ = 3.45 ppm for H-atoms bonded to fructose C-1 carbons, confirming the absence of deuterium at C-1 carbon atoms. In previous work done by former colleagues,[10] similar NMR results were reported for NaOH-catalyzed glucose-D2 isomerizations.

The fructose formed from the glucose isomerization with $SnO_2$/Si-Beta could had been synthesized without any deuterium or with deuterium in the C1 position and then be exchanged with the protons of the aqueous solvent. Glucose isomerization rates were compared, starting from unlabeled glucose and glucose-D2, showing no kinetic isotope effect ($k_H/k_D$ = 1.03, Figure 3.6). In contrast, Sn-Beta does have a considerable kinetic isotope effect, $k_H/k_D$ = 1.98, confirming the intramolecular hydride shift.[1] Thus, the current data show that glucose isomerizes on $SnO_2$ via a proton abstraction mechanism analogous to the homogeneous base catalyst, in which fructose was formed via enolate intermediates generated from the base-catalyzed proton abstraction at the $\alpha$-carbonyl carbon (C-2) position of glucose.

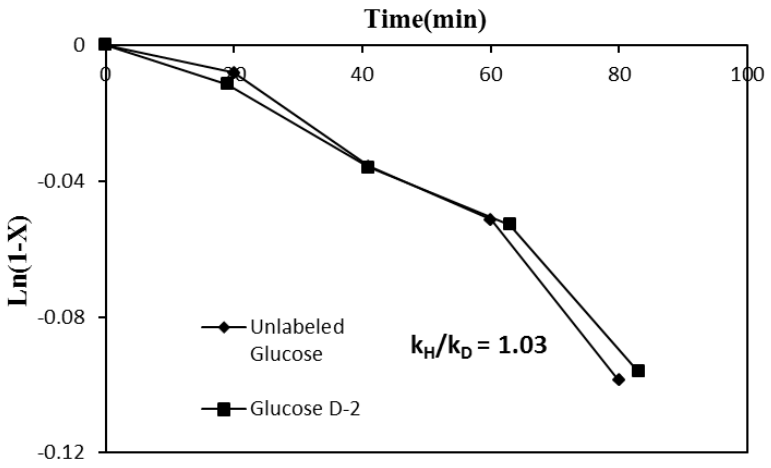


**Figure 3.6 Glucose isomerization rate comparison between unlabeled glucose and glucose-D2 1% (wt/wt) in water at 373K.**

Glucose isomerization via reversible enolization proceeds in aqueous alkaline media with activation energies that are nearly twice as large (~ 120 kJ $mol^{-1}$)[11,12] as observed on $SnO_2$/Si-Beta in water (59 ± 6;Table 3-2). Lower apparent activation energies than expected (by factors of ~ 2) on $SnO_2$/Si-Beta could be consistent with internal mass transfer limitations of the reaction rate.[13] Glucose isomerization rates and activation energies measured on $SnO_2/SiO_2$ and $SnO_2$/Si-Beta-E, for which diffusion to $SnO_2$ surfaces are not expected to limit rates, were used to assess whether reactions may be transport-limited on $SnO_2$/Si-Beta. The conversion of 1 wt% glucose in water mixtures remained below detection limits on $SnO_2/SiO_2$, $SnO_2$/Si-Beta-E and bulk $SnO_2$ (1:50 Sn:glucose molar ratio) after 15 min at 353 K (Table 3-3). These data indicate that bulk water inhibits base-catalyzed glucose isomerization on $SnO_2$ surfaces. Thus, it is suggested that only $SnO_2$ domains located within hydrophobic zeolite Beta pores, which are protected from contact with bulk liquid water and also present in the $SnO_2$/Si-Beta sample, can catalyze glucose isomerization in aqueous solvent.

.

| **Catalyst** | **Glucose Conversion (%)** | |
|---|---|---|
| | *$H_2O$* | *$CH_3OH$* |
| $SnO_2$/Si-Beta | 3.0 | 5.0 |
| $SnO_2$/Si-Beta-E | n.d.* | 3.6 |
| $SnO_2/SiO_2$ | n.d.* | 0.9 |
| $SnO_2$ | n.d.* | n.d.* |

*n.d. not detected

**Table 3-3 Glucose conversion to fructose via base-catalyzed isomerization on $SnO_2$-containing samples in $H_2O$ and $CH_3OH$ solvents. Reaction conditions: 1% (w/w) glucose solutions, 1:50 metal:glucose ratio, 353 K, 15 min.**

## 2.3 Glucose Conversion on $SnO_2$-Containing Samples in Methanol

The differential conversion of 1% (w/w) glucose in methanol over $SnO_2$/Si-Beta formed fructose as the primary product. Turnover rates (per total Sn) were higher (by factors of up to 3; 333-383 K) on $SnO_2$/Si-Beta in methanol than in aqueous solvent (Table 3-4). Glucose also isomerized to fructose on both $SnO_2/SiO_2$ and $SnO_2$/Si-Beta-E when methanol was used as the solvent (Table 3-3), in sharp contrast to the undetectable conversion of glucose on these samples in water under equivalent reaction conditions. These data suggest that contact with bulk methanol does not inhibit isomerization reactivity on $SnO_2$ surfaces and, in turn, that the higher turnover rates on $SnO_2$/Si-Beta in methanol than in water (Table 3-4) reflect, to an extent, additional contributions from glucose conversion on extracrystalline $SnO_2$ particles.

.

| **Catalyst** | **Solvent** | **Turnover rate** ($/ 10^{-3}$ mol $s^{-1}$ (mol Sn)$^{-1}$) | | | | | |
|---|---|---|---|---|---|---|---|
| | | ***333 K*** | ***343 K*** | ***353 K*** | ***363 K*** | ***373 K*** | ***383 K*** |
| Sn-Beta | $H_2O$ | - | 2.5 ± 1.9 | 3.8 ± 1.2 | 16.4 ± 6.1 | 27.8 ± 5.0 | - |
| $SnO_2$/Si-Beta | $H_2O$ | 1.3 ± 0.2 | 2.0 ± 0.3 | 3.5 ± 0.3 | 4.8 ± 0.7 | 9.7 ± 1.9 | 20.7 ± 2.7 |
| | $CH_3OH$ | 1.8 ± 0.2 | 3.6 ± 0.9 | 9.2 ± 2.1 | 14.1 ± 3.2 | 16.6 ± 2.3 | 19.2 ± 2.9 |
| $SnO_2/SiO_2$ | $H_2O$ | n.d.* | n.d.* | n.d.* | n.d.* | n.d.* | n.d.* |
| | $CH_3OH$ | - | 0.2 ± 0.04 | 0.7 ± 0.1 | 2.0 ± 0.3 | 4.2 ± 0.3 | - |

*n.d. not detected

**Table 3-4 Turnover rates for glucose conversion on Sn-Beta, $SnO_2$/Si-Beta and $SnO_2/SiO_2$ in $H_2O$ and $CH_3OH$ solvents.**

In contrast to turnover rates measured over $SnO_2$/Si-Beta in water, turnover rates over $SnO_2$/Si-Beta in methanol depended differently on temperature in the 333-363 K and 363-383 K ranges (Figure 3.7). This behavior might have reflected temperature-dependent contributions to measured isomerization rates from $SnO_2$ particles of different size and location (i.e., extracrystalline or intracrystalline). The apparent activation energy estimated from initial rate data in methanol between 333-

363 K is 71 ± 15 kJ $mol^{-1}$, which is similar to that determined in water between 343-373 K (59 ± 6 kJ $mol^{-1}$;Table 3-2). The activation energy for glucose isomerization to fructose on $SnO_2/SiO_2$ in methanol was 102 ± 9 kJ $mol^{-1}$ (Figure 3.8), which was similar to the values of ~ 120 kJ $mol^{-1}$ reported for base-catalyzed glucose isomerization in aqueous alkaline media.[11,12] The lower activation energies on $SnO_2$/Si-Beta in water and in methanol, compared to $SnO_2/SiO_2$ in methanol, suggested that isomerization rates may, in part, be limited by internal mass transfer restrictions on $SnO_2$/Si-Beta,[13] as might be expected from the significant decrease in micropore volume accessible to $N_2$ (~ 40%;Table 3-2).

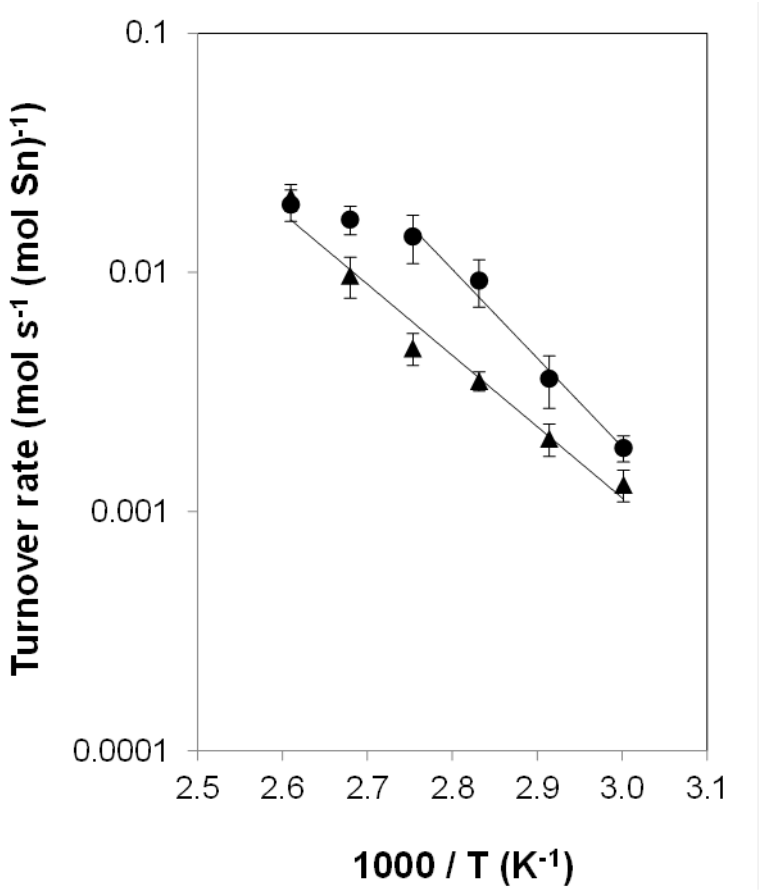


**Figure 3.7 Temperature dependence of turnover rates on $SnO_2$/Si-Beta for glucose isomerization to fructose in water (triangles) and methanol (circles).**

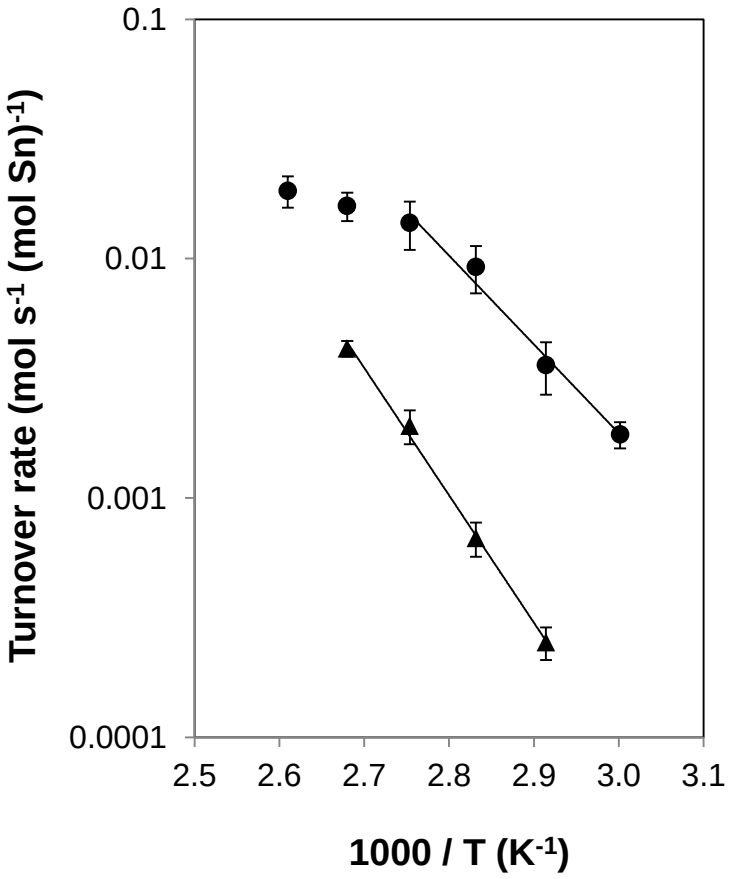


**Figure 3.8 Temperature dependence of turnover rates for glucose isomerization to fructose in methanol on $SnO_2$/Si-Beta (circles) and $SnO_2$-$SiO_2$ (triangles).**

The mechanism of glucose isomerization on $SnO_2$/Si-Beta in methanol was probed using $^{13}C$ and $^{1}H$ NMR spectroscopies of the products formed from the reaction of glucose-D2 reactants, as in the case of $SnO_2$/Si-Beta in water. Both $^{13}C$ (Figure 3.5b) and $^{1}H$ NMR (Figure 3.20) spectra of the glucose after reaction in methanol provided evidence for H/D scrambling at the C-2 position. Fructose products did not retain the deuterium label on their C-1 positions, as reflected in resonances present at $\delta$ = 63.8 and 62.6 ppm in their $^{13}C$ NMR spectrum (Figure 3.5d) and at $\delta$ = 3.45 ppm in their $^{1}H$ NMR spectrum (Figure 3.21). These spectral features, which reflect the presence or absence of D-atoms at specific carbon atoms in glucose and fructose products, are similar when glucose is reacted with $SnO_2$/Si-Beta in

methanol and in water. As in water, the glucose isomerization into fructose with $SnO_2$/Si-Beta did not have a kinetic isotope effect ($k_H/k_D$ = 1.07, Figure 3.9), confirming the loss of the deuterium in the C-2 position of glucose and the enolate intermediate prior to the formation of fructose.

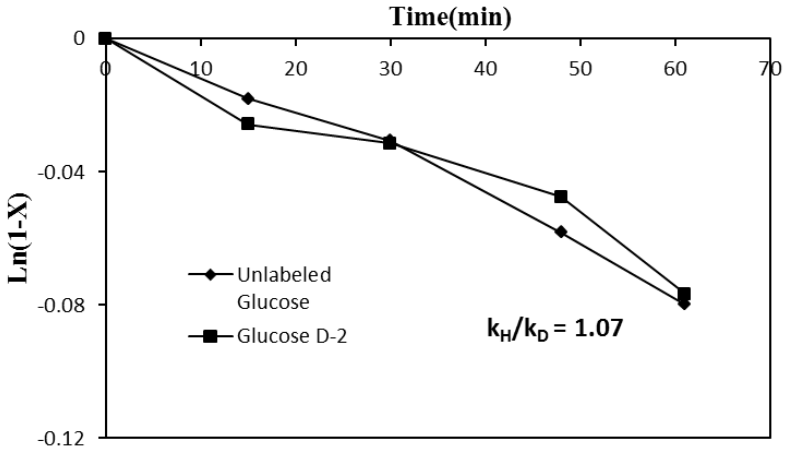


**Figure 3.9 Glucose isomerization rate comparison between unlabeled glucose and glucose-D2 1%(wt/wt) in methanol at 373K.**

It is observed from these isotopic labeling studies that $SnO_2$ particles can isomerize glucose to fructose via the base-catalyzed proton abstraction mechanism. Glucose isomerization to fructose on $TiO_2$ and $ZrO_2$ particles has been attributed previously to a base-catalyzed mechanism, but solely based on differences in fructose yields and the numbers of basic sites on these catalysts (determined by $CO_2$ temperature-programmed desorption).[14] Glucose isomerization in methanol occurs irrespective of $SnO_2$ location within or outside of pore structures, but in water apparently requires that $SnO_2$ domains to be confined within hydrophobic microporous channels in order to prevent their contact with bulk liquid water. Although turnover rates (per total Sn) were larger by factors of ~ 3 (333-383 K) on $SnO_2$/Si-Beta in methanol than aqueous solvent, the order-of-magnitude higher solubility of glucose in water (~ 50 wt%) than in methanol (~ 1-2 wt%) implies that

significantly higher yields and productivities can be achieved for glucose isomerization in aqueous media.

2.4 Glucose Conversion on Sn-Beta in Methanol.

The reactivity of glucose on Sn-Beta in methanol led to high glucose conversions with unknown additional side products. Glucose conversion was of 35.3% after 10 min at 373K (Table 3-5), with a carbon balance of 81.1%. Even at lower temperatures, 353K, and higher tin to glucose ratio, 1:100, the carbon balance was of 92.8% after 10 minutes at 12.0% glucose conversion. These results made it difficult to obtain glucose turnover rates to fructose, since other side products are being formed and it is unclear how these are formed. However, deuterium in the C-1 position of fructose was observed by $^{13}C$ NMR. The absence of the resonances at $\delta$ = 63.8 and 62.6 ppm for β-pyranose and β-furanose reflect that in Sn-Beta glucose does also isomerize into fructose by an intramolecular hydride shift. The other products are discussed in Chapter 5.

| | | *15 minutes* | | | *30 minutes* | | | *45 minutes* | | |
|---|---|---|---|---|---|---|---|---|---|---|
| **Catalyst** | **Solvent** | $X_G(\%)$ | $Y_F(\%)$ | $Y_M(\%)$ | $X_G(\%)$ | $Y_F(\%)$ | $Y_M(\%)$ | $X_G(\%)$ | $Y_F(\%)$ | $Y_M(\%)$ |
| Sn-Beta | $CH_3OH$ | 35.3 | 11.8 | 4.6 | 49.3 | 11.6 | 6.3 | 58.0 | 11.6 | 5.5 |

**Table 3-5 Glucose conversion and fructose and mannose yields in $CH_3OH$ solvents. Reaction conditions: 1% (w/w) glucose solutions, 1:50 metal:glucose ratio and 373 K.**

| | | *10 minutes* | | | *20 minutes* | | | *30 minutes* | | |
|---|---|---|---|---|---|---|---|---|---|---|
| **Catalyst** | **Solvent** | $X_G(\%)$ | $Y_F(\%)$ | $Y_M(\%)$ | $X_G(\%)$ | $Y_F(\%)$ | $Y_M(\%)$ | $X_G(\%)$ | $Y_F(\%)$ | $Y_M(\%)$ |
| Sn-Beta | $CH_3OH$ | 12.0 | 4.8 | 0.0 | 20.4 | 9.1 | 1.8 | 23.2 | 10.3 | 3.9 |

**Table 3-6 Glucose conversion and fructose and mannose yields in $CH_3OH$ solvents. Reaction conditions: 1% (w/w) glucose solutions, 1:100 metal:glucose ratio and 353 K.**

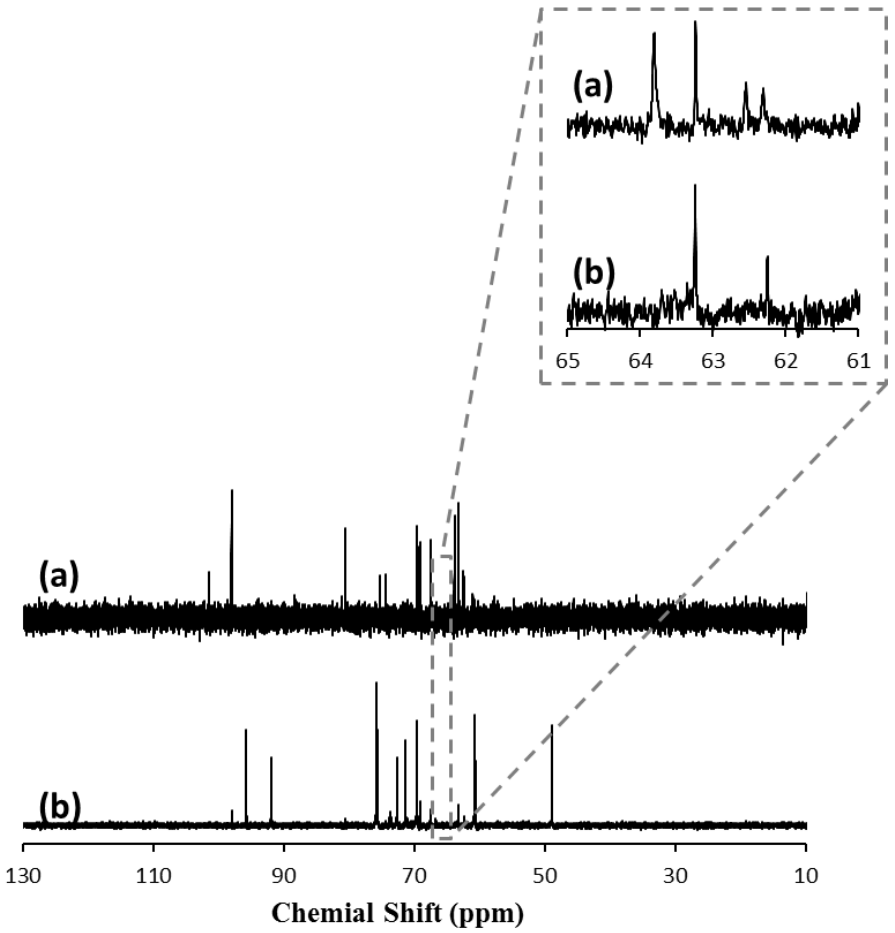


**Figure 3.10 $^{13}$C NMR Spectra of (a) fructose, (b) product mixture from glucose-D2 with Sn-Beta, after 15 minutes at 100°C at a glucose:Sn ratio of 100:1.**

## 3. Conclusion

Glucose initially undergoes isomerization to fructose on both framework Sn sites and extraframework $SnO_2$ sites (Figure 3.11). Framework Sn centers within the hydrophobic pores of zeolite Beta (Sn-Beta) behave as Lewis acid sites that catalyze isomerization via intramolecular hydride shifts between C-1 and C-2 carbon atoms on acyclic glucose. In contrast, basic sites on extraframework $SnO_2$ domains catalyze glucose isomerization via the abstraction of protons at C-2 carbon atoms to form enolate intermediates (Figure 3.11). Extraframework Sn species appear to be reactive only when confined in hydrophobic zeolite Beta channels ($SnO_2$/Si-Beta) and not when in contact with bulk water at external zeolite crystal surfaces ($SnO_2$/Si-Beta-E)

and on amorphous supports ($SnO_2/SiO_2$). In methanol $SnO_2$ domains are able to catalyze glucose isomerization irrespective of their location, within or outside of hydrophobic zeolite Beta pores, indicating that methanol does not inhibit the base-catalyzed isomerization on $SnO_2$. These findings demonstrate clearly that the sole observation of glucose-to-fructose isomerization on Sn-zeolite samples, in the absence of any isotopic labeling studies or unambiguous Sn site characterization, does not provide sufficient evidence for the incorporation of Sn atoms into zeolite frameworks.

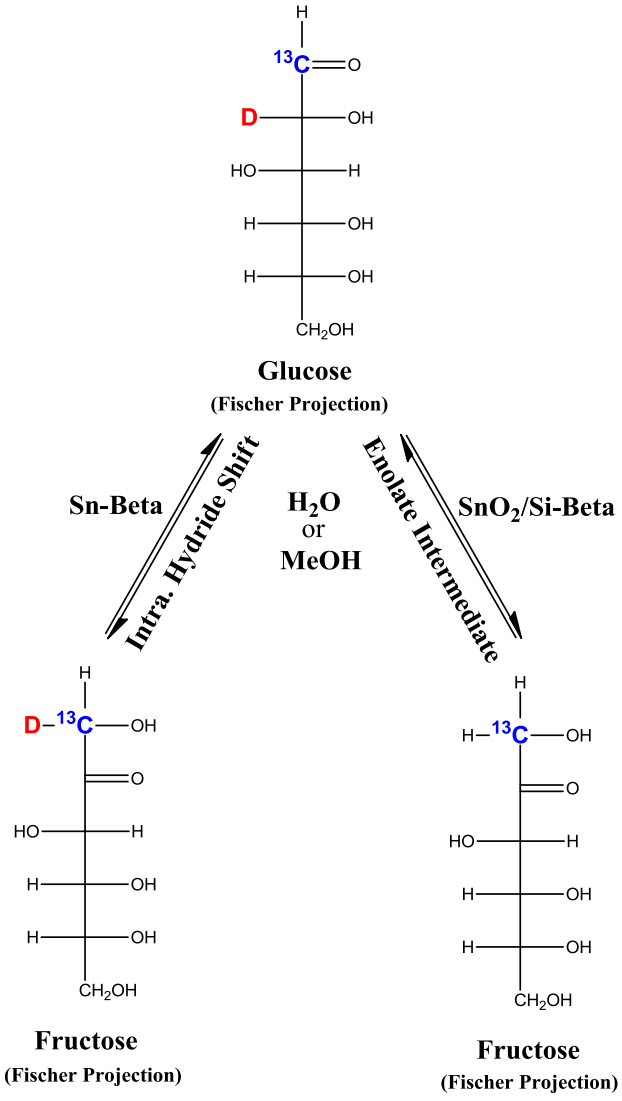


**Figure 3.11 Reaction network of glucose with Sn-Beta and $SnO_2$/Si-Beta in water and methanol solvents.**

## 4. Experimental Procedure and Additional Figures

### 4.1 Synthesis of Si-Beta, Sn-Beta, $SnO_2$/Si-Beta and $SnO_2$-$SiO_2$

Si-Beta was prepared by adding 10.01 g of tetraethylammonium fluoride dihydrate (Sigma-Aldrich, 97% (w/w) purity) to 10 g of water and 4.947 g of tetraethylorthosilicate (Sigma-Aldrich, 98% (w/w)). This mixture was stirred overnight at room temperature in a closed vessel to ensure complete hydrolysis of the tetraethylorthosilicate. The targeted $H_2O$:$SiO_2$ ratio was reached by complete evaporation of the ethanol and partial evaporation of the water. The final molar composition of the gel was $SiO_2$ / 0.55 TEAF / 7.25 $H_2O$. The gel was transferred to a Teflon-lined stainless steel autoclave and heated at 413 K in a rotation oven (60 rpm) for 7 days. The solids were recovered by filtration, washed extensively with water, and dried at 373 K overnight. The dried solids were calcined in flowing air (1.67 $cm^3$ $s^{-1}$, Air Liquide, breathing grade) at 853 K (0.0167 K $s^{-1}$) for 10 h to remove the organic content located in the crystalline material.

Sn-Beta was synthesized according to previously reported procedures.[8] 7.57 g of tetraethylammonium hydroxide solution (Sigma-Aldrich, 35% (w/w) in water) were added to 7.011 g of tetraethylorthosilicate (Sigma-Aldrich, 98% (w/w)), followed by the addition of 0.121 g of tin (IV) chloride pentahydrate (Sigma-Aldrich, 98% (w/w)). The mixture was stirred until tetraethylorthosilicate was completely hydrolyzed and then allowed to reach the targeted $H_2O$:$SiO_2$ ratio by complete evaporation of ethanol and partial evaporation of water. Finally, 0.690 g of HF solution (Mallinckrodt, 52% (w/w) in water) was added, resulting in the formation of a thick gel. The final molar composition of the gel was 1 $SiO_2$ / 0.01 $SnCl_4$ / 0.55 TEAOH / 0.54 HF / 7.52 $H_2O$. Si-Beta was added as seed material (5 wt% of $SiO_2$ in gel) to this gel and then mixed with it. The final gel was transferred to a Teflon-lined

stainless steel autoclave and heated at 413 K in a static oven for 40 days. The solids were recovered, washed, dried and calcined using the procedure described above for Si-Beta.

Si-Beta containing extraframework $SnO_2$ ($SnO_2$/Si-Beta) was prepared using the same procedure as Sn-Beta, but substituting tin (IV) chloride pentahydrate with 0.052 g of tin (IV) dioxide (Sigma-Aldrich, -325 mesh; aggregate particle size < 44 μm) as the source of tin in the synthesis gel. The gel was transferred to a Teflon-lined stainless steel autoclave and heated at 413 K in a static oven for 25 days. The recovered solids were washed, dried and calcined using the same procedure as for Si-Beta and Sn-Beta.

Si-Beta containing extraframework $SnO_2$ particles located on external crystallite surfaces ($SnO_2$/Si-Beta-E) was synthesized by first adding 0.059 g of tin (IV) chloride pentahydrate (Sigma-Aldrich, 98% (w/w)) to 10 g of water. This solution was stirred with 1.0 g of Si-Beta in its as-made form for 16 h at ambient temperature. The solids were recovered by centrifugation and dried at 373 K overnight. Finally, the dried solids were calcined in flowing air (1.67 $cm^3$ $s^{-1}$, Air Liquide, breathing grade) at 853 K (0.0167 K $s^{-1}$) for 10 h.

$SnO_2$ was dispersed on silica ($SnO_2$/$SiO_2$) by first adding 0.5 g of tin (IV) chloride pentahydrate (Sigma-Aldrich, 98% (w/w)) to 30 g of water. 2 g of fumed silica (Sigma-Aldrich, 0.2-0.3 mm average particle size) were added to the mixture and stirred for 24 hours at room temperature. The solids were recovered, washed, dried and calcined using the same procedure as for crystalline zeolites.

## 4.2 Characterization Methods

Atomic Si and Sn contents were determined using a JEOL 8200 electron microprobe operated at 15 kV and 25 nA in a focused beam mode with a 40 μm spot

size. Scanning electron microscopy (SEM) images were recorded on a LEO 1550 VP field emission SEM at an electron high tension of 10 kV on zeolite samples after sputtering with carbon to minimize the effects of charging. The crystalline structures of zeolite samples were determined from powder X-ray diffraction (XRD) patterns collected using a Rigaku Miniflex II diffractometer and Cu Kα radiation. Diffuse reflectance UV-Visible (DRUV) spectra were recorded using a Cary 3G spectrophotometer equipped with a diffuse reflectance cell; zeolite samples were calcined in air at 853 K for 10 hours and exposed to ambient conditions prior to acquiring spectra.

$N_2$ adsorption isotherms at 77 K were obtained using a Quantachrome Autosorb iQ automated gas sorption analyzer. Zeolite samples (typically 0.03-0.04 g) were pelleted and sieved to retain 150-600 μm particles. Samples were degassed at 353 K (0.167 K $s^{-1}$) for 1 h, 393 K (0.167 K $s^{-1}$) for 3 h and 623 K (0.167 K $s^{-1}$) for 8 h prior to recording dry sample weight. $N_2$ uptake was recorded between relative pressures of $10^{-7}$ and 1 at 77 K. Total micropore volumes were estimated from linear extrapolation of mesopore $N_2$ uptakes to zero pressure and the density of liquid nitrogen.

Solid-state magic angle spinning nuclear magnetic resonance (MAS NMR) spectra were recorded using a Bruker Avance 500 MHz spectrometer equipped with a 11.7 T magnet and a Bruker 4mm MAS probe. Powdered samples (0.06-0.08 g) were packed into 4 mm $ZrO_2$ rotors with Kel-F caps and spun at 14 kHz. $^{119}$Sn NMR spectra were recorded at an operating frequency of 186.5 MHz and are referenced to $(CH_3)_4Sn$. Unless otherwise specified, spectra were acquired on hydrated samples, which were exposed to ambient conditions after calcination in flowing air at 853 K but prior to packing NMR rotors. Samples were dehydrated by heating the packed

NMR rotors to 423 K in vacuum and holding overnight prior to acquiring NMR spectra.

Liquid $^{1}H$ and $^{13}C$ NMR spectra were recorded using a Varian INOVA 500 MHz spectrometer equipped with an auto-x pfg broad band probe. Proton and carbon chemical shifts are reported relative to the residual solvent signal. $^{1}H$ NMR spectra were acquired with 256 scans while $^{13}C$ NMR spectra were acquired with 1000 scans.

## 4.3 Reaction Procedures

Reactions with D-glucose (Sigma-Aldrich, ≥99%) were conducted in 10 ml thick-walled glass reactors (VWR) that were heated in a temperature-controlled oil bath placed on top of a digital stirring hotplate (Fisher Scientific). For each catalyst and solvent combination, different metal:glucose molar ratios were used. Reactions on Sn-Beta in water were typically carried out using 1.0 g of a 10% (w/w) glucose solution and a 1:100 Sn:glucose molar ratio. Reactions on Sn-Beta in methanol were typically carried out using 1.0 g of a 1% (w/w) glucose solution and a 1:100 Sn:glucose molar ratio. Reactions on $SnO_2$/Si-Beta in water and methanol were typically carried out using 1.0 g of a 1% (w/w) glucose solution and a 1:20 Sn:glucose molar ratio. Reactions on $SnO_2$-$SiO_2$ were performed using 1.5 g of a 1% (w/w) glucose solution and a 1:10 Sn:glucose molar ratio.

Reactors were placed in the oil bath for specific time intervals and quenched by cooling in an ice bath. Small aliquots were extracted, filtered with 0.2 μm PTFE syringe filter, and mixed with D-mannitol (Sigma-Aldrich, ≥98%) solutions used as an internal standard for quantification (10% (w/w) mannitol for experiments with Sn-Beta in water; 1.5% (w/w) mannitol otherwise). Samples were analyzed by high performance liquid chromatography (HPLC) using an Agilent 1200 system (Agilent)

equipped with PDA UV (320 nm) and evaporative light scattering (ELS) detectors. Glucose, fructose, mannose and mannitol fractions were separated with a Hi-Plex Ca column (6.5 x 300 mm, 8 μm particle size, Agilent) held at 358 K, using ultrapure water as the mobile phase at a flow rate of 0.01 mL $s^{-1}$. Turnover rates were calculated by normalizing the total moles of glucose converted by the total moles of Sn on the catalyst. For liquid NMR analysis of products formed from isotopic labeling studies using D-glucose-D2 (Cambridge Isotope Laboratories, ≥98%) and D-glucose-$^{13}$C-C1 (Cambridge Isotope Laboratories, ≥98%), glucose, mannose and fructose fractions were first separated by HPLC, isolated by evaporation of $H_2O$, and dissolved in $D_2O$ (Cambridge Isotope Laboratories, 99.9%).

4.4 $N_2$ Adsorption Isotherms and DRUV

$N_2$ adsorption isotherms (77 K) are shown for Si-Beta (Figure 3.12), Sn-Beta (Figure 3.13), $SnO_2$/Si-Beta-E (Figure 3.14) and $SnO_2$/Si-Beta (Figure 3.15). Total micropore volumes were determined from linear extrapolation of $N_2$ uptakes in mesopore regions ($P/P_0$ ~ 0.1-0.4) to zero relative pressure and from the liquid $N_2$ molar density (0.029 mol $cm^{-3}$). This method gave values of 0.19, 0.20, 0.20 and 0.12 $cm^3$ $g^{-1}$ for Si-Beta, Sn-Beta, $SnO_2$/Si-Beta-E and $SnO_2$/Si-Beta, respectively. The value for $SnO_2$/Si-Beta (0.12 $cm^3$ $g^{-1}$) is lower than expected if $SnO_2$ domains (2.67 wt%, 6.95 g $cm^{-3}$) were located in extracrystalline phases of Si-Beta (0.185 $cm^3$ $g^{-1}$) or occluded volume within Si-Beta voids (0.181 $cm^3$ $g^{-1}$), suggesting that $SnO_2$ particles within the pores of $SnO_2$/Si-Beta also prevent access to a fraction of the intracrystalline void volume.

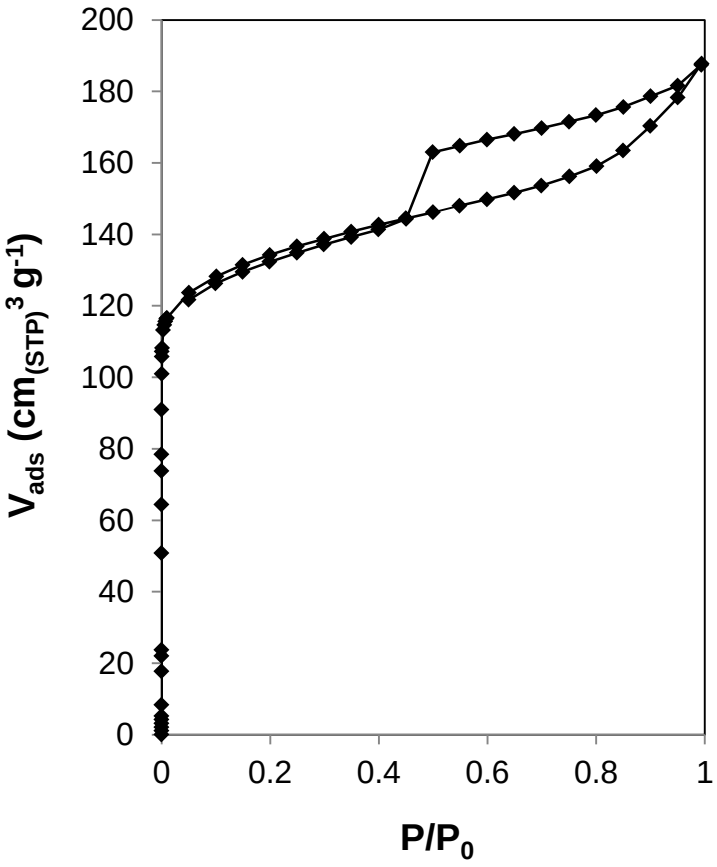


**Figure 3.12 $N_2$ adsorption isotherm (77 K) for Si-Beta.**

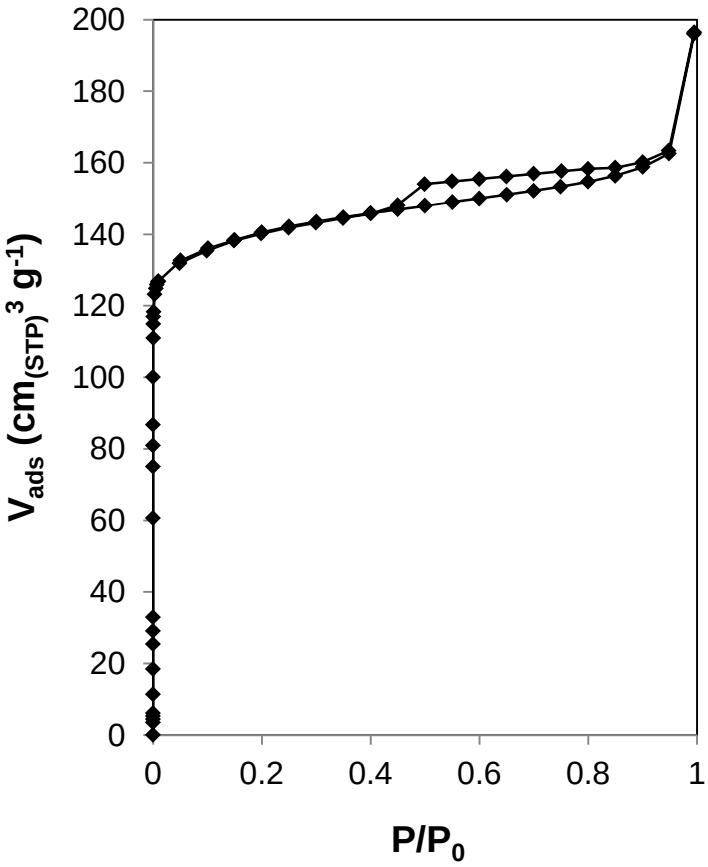


**Figure 3.13 $N_2$ adsorption isotherm (77 K) for Sn-Beta.**

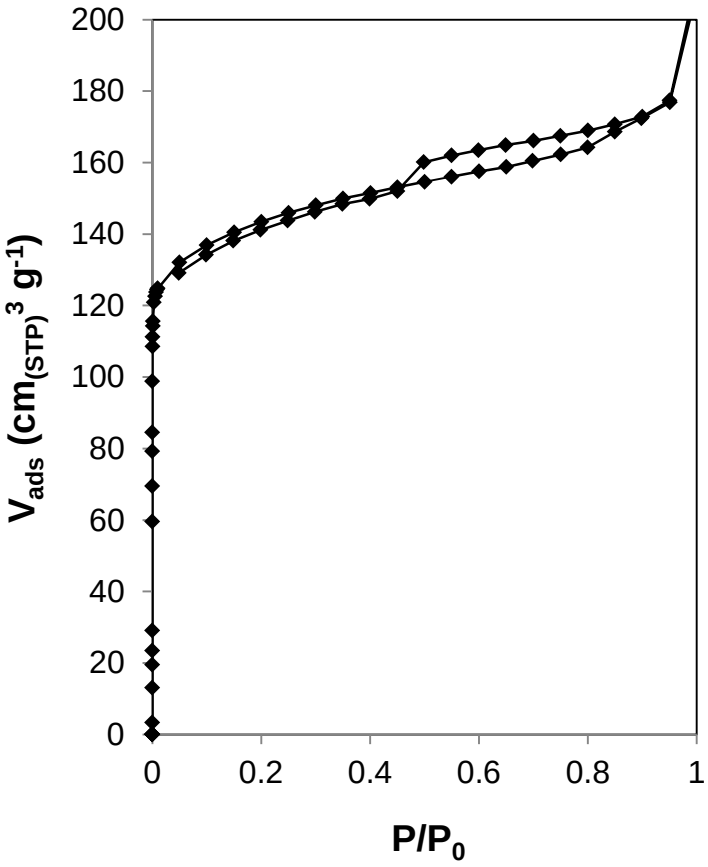


**Figure 3.14 $N_2$ adsorption isotherm (77 K) for $SnO_2$/Si-Beta-E.**

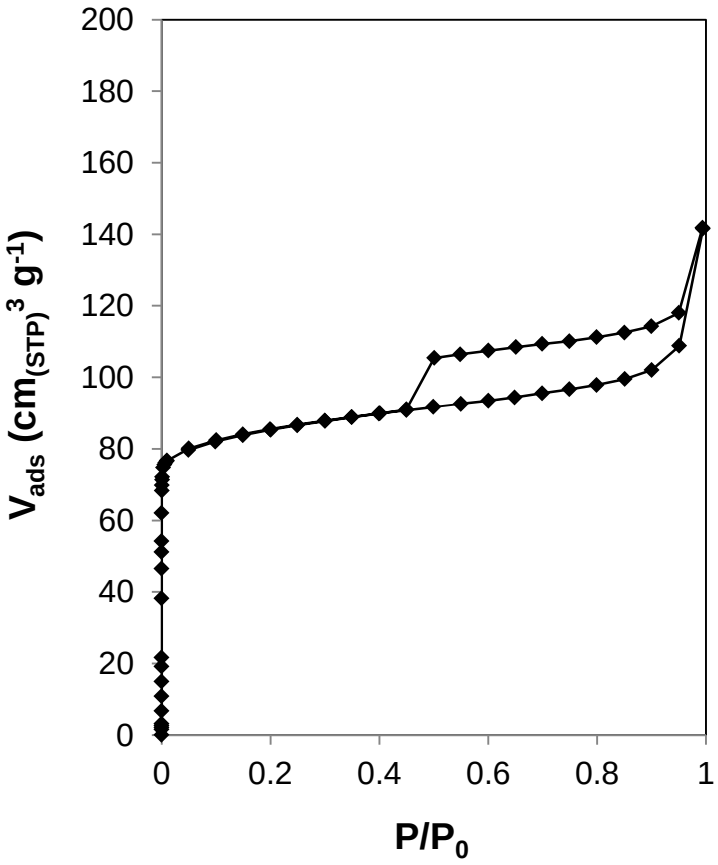


**Figure 3.15 $N_2$ adsorption isotherm (77 K) for $SnO_2$/Si-Beta.**

The DRUV spectrum of Si-Beta is shown in Figure S.7; the DRUV spectra for all other samples in this study are shown in Figure 3.4 of the main text.

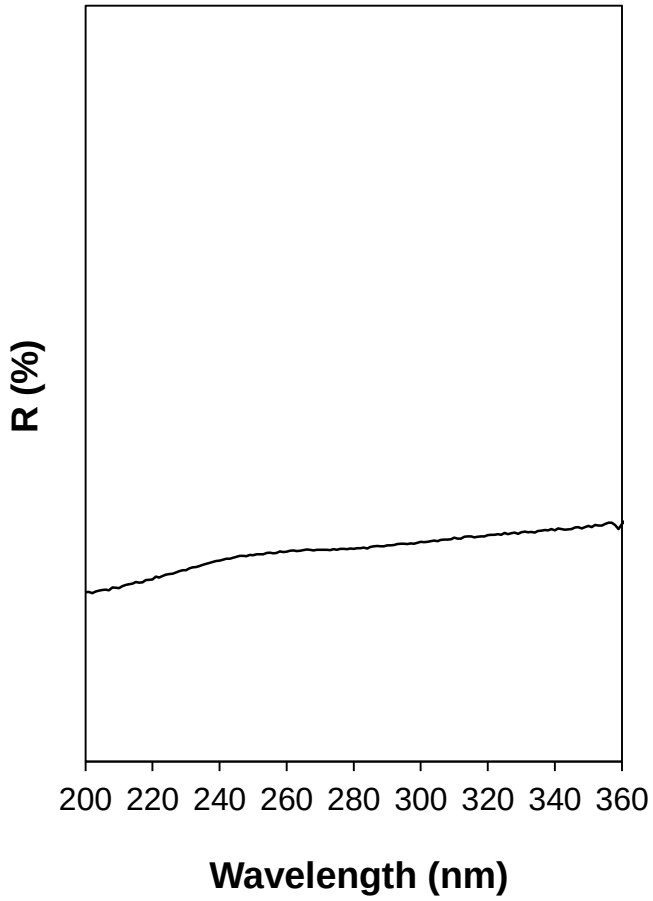


**Figure 3.16 DRUV spectrum of Si-Beta.**

4.5 $^{1}H$ and $^{13}C$ NMR Spectra of Sugars after Reaction of Glucose-D2 with $SnO_2$/Si-Beta in Water

The $^{1}H$ NMR spectrum of the glucose fraction after reaction of glucose-D2 with $SnO_2$/Si-Beta in water is shown in Figure 3.17. The resonance near $\delta$ = 3.1 ppm reflects the presence of a proton at the C-2 position in glucose. This suggests that D-atoms initially located at the C-2 position have been scrambled isotopically, as expected from the formation of enolate species via $SnO_2$-catalyzed proton abstraction at the $\alpha$-carbonyl carbon atom of glucose. We have previously reported the scrambling of D-atoms at the C-2 position when glucose-D2 is isomerized via the proton-transfer mechanism in aqueous NaOH (resonance at $\delta$ = 74.1 ppm, Figure 3.13d), but not when isomerized via the intramolecular hydride shift mechanism on Sn-Beta in water (no resonance at $\delta$ = 74.1 ppm, Figure 3.13c).

Enolate intermediates can form unlabeled glucose via reprotonation, or unlabeled fructose via isomerization. The resonance $\delta$ = 3.45 ppm in the fructose fraction after reaction glucose-D2 with $SnO_2$/Si-Beta in water (Figure 3.19) confirms the presence of a proton at the C-1 position in fructose. We have previously reported that the deuterium atoms are retained at C-1 positions in fructose when isomerization occurs on Sn-Beta (no resonances at $\delta$ = 63.8 and 62.6 ppm, Figure 3.13f), but are not retained when isomerization occurs on aqueous NaOH (resonances at $\delta$ = 63.8 and 62.6 ppm, Figure 3.13g).

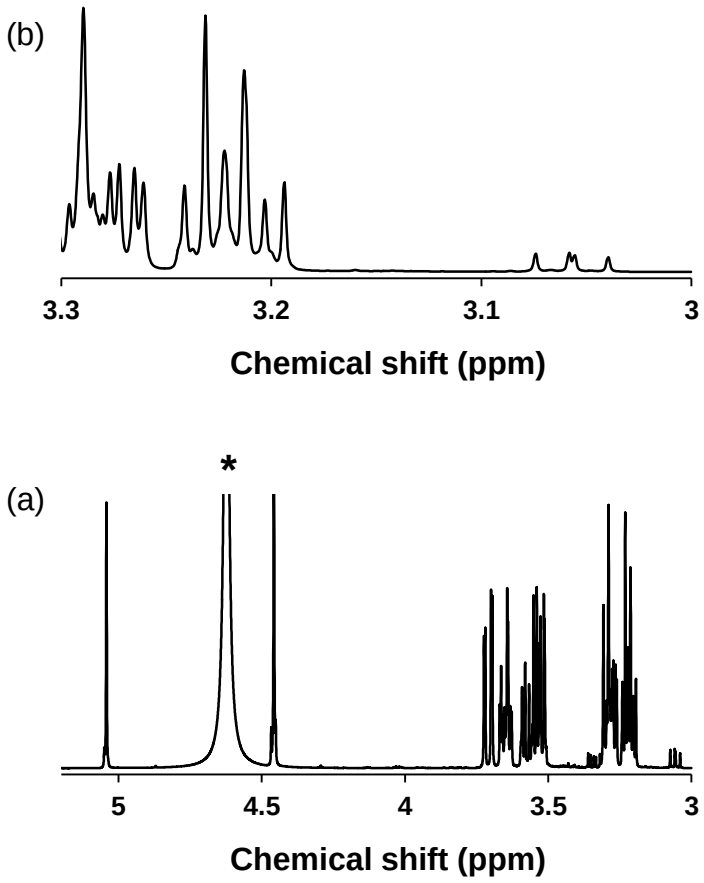


**Figure 3.17 $^{1}$H NMR spectrum of glucose fraction after reaction of glucose-D2 with $SnO_2$/Si-Beta in water at 373 K for 1h. (a) δ: 3-5.2 ppm; * denotes $H_2O$. (b) δ: 3-3.3 ppm.**

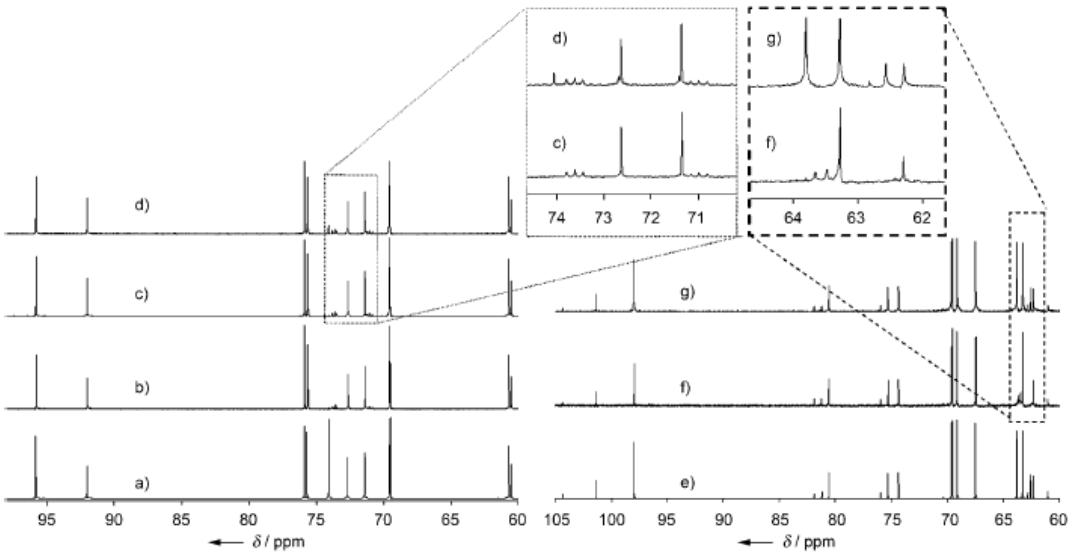


**Figure 3.18 $^{13}$C NMR spectra of a) unlabeled glucose, b) labeled glucose-D2, c) glucose fraction obtained after reacting glucose-D2 with Sn-Beta, d) glucose fraction obtained after reacting labeled glucose-D2 with NaOH, e) unlabeled fructose, f) fructose fraction obtained after reacting labeled glucose-D2 with Sn-Beta, and g) fructose fraction after reacting labeled glucose-D2 with NaOH. Reproduced with permission from reference 1 (Y. Roman-Leshkov, M. Moliner, J. A. Labinger and M. E. Davis, Angew. Chem.-Int. Edit., 2010, 49, 8954-8957), copyright 2010, Wiley-VCH Verlag GmbH & Co. KGaA, Weinheim.**

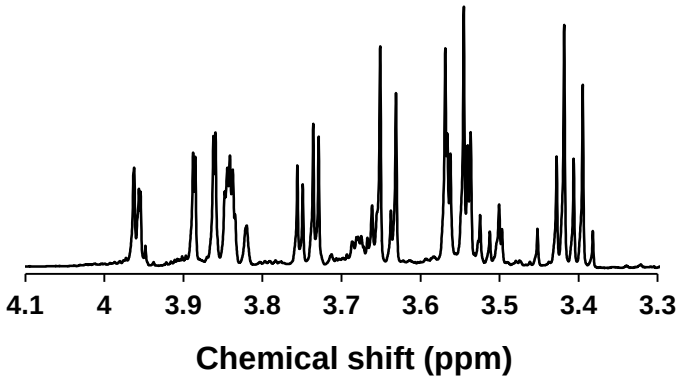


**Figure 3.19 $^{1}$H NMR spectrum of fructose fraction after reaction of glucose-D2 with $SnO_2$/Si-Beta in water at 373 K for 1 h.**

4.6 $^{1}$H NMR Spectra of Sugars After Reaction of Glucose-D2 with $SnO_2$/Si-Beta in Methanol.

The $^{1}$H NMR spectrum of the glucose fraction after reaction of glucose-D2 with $SnO_2$/Si-Beta in methanol is shown in Figure 3.20. The resonance at $\delta$ = 3.1 ppm is assigned to a proton at the C-2 position in glucose, indicating isotopic scrambling

of some of the D-atoms in glucose. These observations are consistent with the formation of enolate species via $SnO_2$-catalyzed proton abstraction at the α-carbonyl carbon atom of glucose-D2, which can reprotonate to form unlabeled glucose or isomerize to form unlabeled fructose. The resonance δ = 3.45 ppm in the fructose fraction after reaction glucose-D2 with $SnO_2$/Si-Beta in methanol (Figure 3.21) confirms the presence of a proton at the C-1 position in fructose, in contrast to the deuterium expected if isomerization were to occur via an intramolecular hydride shift.

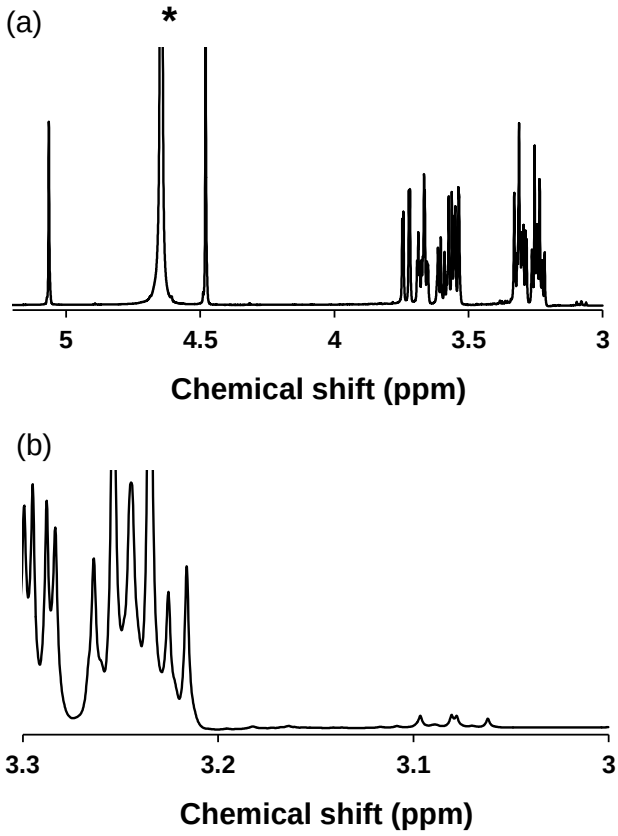


**Figure 3.20 $^1$H NMR spectrum of glucose fraction after reaction of glucose-D2 with SnO2/Si-Beta in methanol at 373 K for 1 h. (a) δ: 3-5.2 ppm; * denotes $H_2O$. (b) δ: 3-3.3 ppm.**

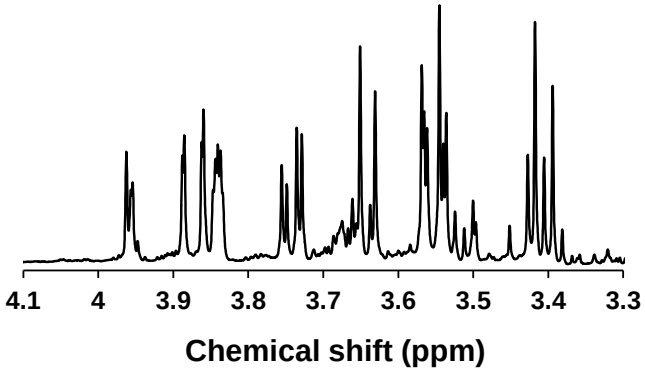


**Figure 3.21 $^{1}$H NMR spectrum of fructose fraction after reaction of glucose-D2 with $SnO_2$/Si-Beta in methanol at 373 K for 1 h.**

## 5. References


1. Román-Leshkov, Y., Moliner, M., Labinger, J. a & Davis, M. E. Mechanism of glucose isomerization using a solid Lewis acid catalyst in water. *Angew. Chem. Int. Ed. Engl.* **49,** 8954–7 (2010).

2. Bermejo-Deval, R. *et al.* Metalloenzyme-like catalyzed isomerizations of sugars by Lewis acid zeolites. *Proc. Natl. Acad. Sci. U. S. A.* **109,** 9727–32 (2012).

3. Kovalevsky, A. Y. *et al.* Metal ion roles and the movement of hydrogen during reaction catalyzed by D-xylose isomerase: a joint x-ray and neutron diffraction study. *Structure* **18,** 688–99 (2010).

4. Moliner, M., Román-Leshkov, Y. & Davis, M. E. Tin-containing zeolites are highly active catalysts for the isomerization of glucose in water. *Proc. Natl. Acad. Sci. U. S. A.* **107,** 6164–8 (2010).

5. Mal, N. K. & Ramaswamy, A. V. Hydroxylation of phenol over Sn-silicalite-1 molecular sieve: solvent effects. *J. Mol. Catal. A Chem.* **105,** 149–158 (1996).

6. Bhagwat, M., Shah, P. & Ramaswamy, V. Synthesis of nanocrystalline SnO2 powder by amorphous citrate route. *Mater. Lett.* **57,** 1604–1611 (2003).

7. Chiodini, N., Paleari, A., DiMartino, D. & Spinolo, G. SnO2 nanocrystals in SiO2: A wide-band-gap quantum-dot system. *Appl. Phys. Lett.* **81,** (2002).

8. Gu, F. *et al.* Synthesis and luminescence properties of SnO2 nanoparticles. *Chem. Phys. Lett.* **372,** 451–454 (2003).

9. Pang, G. *et al.* Controlling the Particle Size of Calcined SnO2 Nanocrystals. *Nano Lett.* **1,** 723–726 (2001).

10. Román-Leshkov, Y., Moliner, M., Labinger, J. a & Davis, M. E. Mechanism of glucose isomerization using a solid Lewis acid catalyst in water. *Angew. Chem. Int. Ed. Engl.* **49,** 8954–7 (2010).

11. Vuorinen, T. & Sjöström, E. Kinetics of alkali-catalyzed isomerization of D-glucose and D-fructose in ethanol-water solutions. *Carbohydr. Res.* **108,** 23–29 (1982).

12. Kooyman, C., Vellenga, K. & Wilt, H. G. J. De. The isomerization of d-glucose into d-fructose in aqueous alkaline solutions. *Carbohydr. Res.* **54,** 33–44 (1977).

13. Davis, M. E. & Davis, R. J. *Fundamentals of Chemical Reaction Engineering*. 207–208 (2003).

14. Watanabe, M., Aizawa, Y., Iida, T., Nishimura, R. & Inomata, H. Catalytic glucose and fructose conversions with TiO2 and ZrO2 in water at 473K: Relationship between reactivity and acid–base property determined by TPD measurement. *Appl. Catal. A Gen.* **295,** 150–156 (2005).

# Chapter 4 : Active Sites in Sn-Beta for Glucose Isomerization to Fructose and Epimerization to Mannose

## 1. Introduction

We have previously seen that tetravalent Lewis acidic metal centers ($Sn^{+4}$ and $Ti^{+4}$) isolated within hydrophobic, pure-silica molecular sieves with the zeolite beta framework topology (Sn-Beta and Ti-Beta, respectively) catalyze the isomerization of glucose to fructose in aqueous media.[1–4] Framework Sn sites mediate the ring opening of glucose and coordinate with glucose O1 and O2 atoms prior to isomerization via an intramolecular hydride shift from the C2 to C1 position (1, 2 intramolecular hydride shift) in the ring-opened glucose chain.[1] This glucose isomerization reaction pathway is analogous to that observed in metalloenzymes such as D-xylose isomerase XI that contains two divalent Lewis acid metal centers (e.g., $Mg^{2+}$ or $Mn^{2+}$) confined within a hydrophobic pocket.[5–7] Extraframework SnOx clusters located within hydrophobic micropores of pure-silica zeolite beta, but not at external crystallite surfaces or on amorphous supports, are also able to isomerize glucose to fructose in aqueous solutions.[2] However, unlike the framework Sn centers, these extraframework intrazeolitic SnOx clusters act as solid bases that catalyze glucose isomerization via a LdB-AvE (Lobry de Bruyn-Alberda van Ekenstein) rearrangement that involves enolate intermediates,[2,8] and the hydrophobic surrounding voids protect SnOx surface sites from inhibition or deactivation that otherwise occurs in the presence of liquid water.

Homogeneous Lewis acids such as molybdate anions[9–11] and nickel(II) diamine complexes[12–14] have been reported to catalyze the epimerization of glucose to mannose by the Bilik reaction. With the use of $^{13}C$ as an isotopic tracer $^{13}C$- mannose formed exclusively $^{13}C2$-glucose, being the mannose epimerization into glucose by

1,2 intramolecular carbon shift. Hayes *et al.*[9] suggested that with dimolybdate anionic complexes involving the carbonyl oxygen and the hydroxylic oxygen of the aldose at the C2, C3 and C4 are formed, leading to bond formation between the C1 and C3 and cleavage of the C2-C3 cleavage to produce the epimer.

Framework Sn centers in Sn-Beta were proposed by Corma *et al.*[15] to be present in both "open" and "closed" forms that respectively correspond to a partially hydrolyzed Sn site ((HO)-Sn-$(OSi)_3$) and a non-hydrolyzed Sn site (Sn-$(OSi)_4$) (Figure 4.1a and 1b, respectively). The open site was proposed to be more active in the Baeyer-Villiger oxidation of cyclic ketones.[15] Similarly, the open site has also been proposed to be active in the isomerization of glucose into fructose,[1] with the open and closed sites being inter-convertible during calcination and reaction conditions. While we were able to observe the presence of the open and closed sites via $^{119}$Sn NMR, the previous experimental data could not conclusively distinguish which site (or both) is the active site for glucose isomerization.[1] Computational results suggest that isomerization pathways are catalyzed with lower barriers on open than on closed sites.[1] Khouw and Davis[16] exchanged $Na^+$ onto the silanol groups (Si-OH) adjacent to open Ti sites ((HO)-Ti-$(OSi)_3$) in TS-1 and completely inhibited the catalytic activity for alkane oxidation with hydrogen peroxide, providing conclusive evidence that open Ti sites are the active sites for alkane oxidation. Thus, it is possible that the silanol group adjacent to the open Sn site in Sn-Beta could influence the rates and selectivities of glucose isomerization catalysis. Recently, Rai *et al.*[17] used density functional theory calculations to show that the isomerization of glucose to fructose proceeds via a lower energy pathway when glucose binds to an open Sn site in a monodentate mode that involves the silanol group adjacent to the open Sn site, relative to a pathway where glucose binds to the Sn site in a bidentate mode that lacks

the involvement of the neighboring silanol group. Conversely, the bidentate binding mode results in a lower energy pathway for the epimerization of glucose to mannose than the monodentate binding mode.[17] If the epimerization pathway is lower in energy than the isomerization pathway when silanol groups adjacent to Sn sites are not involved in the mechanism, a detail that is not addressed in the paper by Rai *et al.*[17], it would suggest that the active site in Sn-Beta may be altered in a way that precludes the involvement of the neighboring silanol in the reaction pathway.

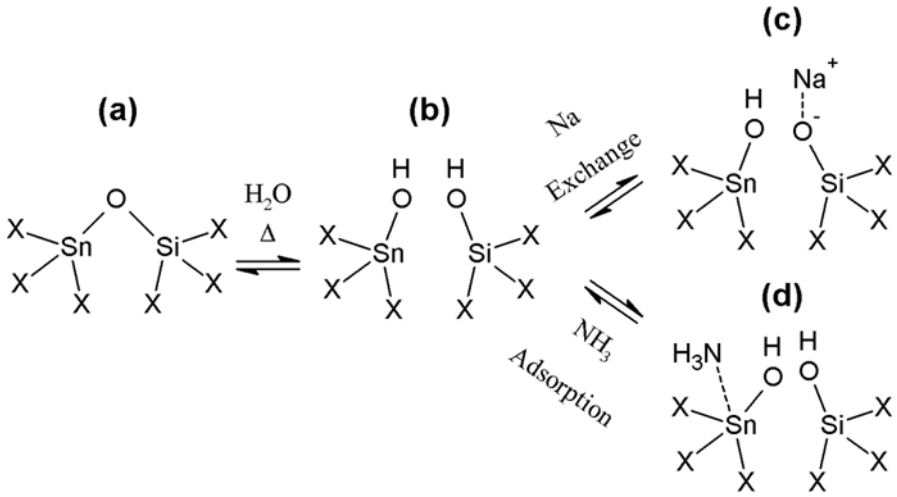


**Figure 4.1 Schematic representation of the (a) "closed" and (b) "opeed" sites in Sn-Beta, as well as (c) Na-exchanged open site and (d) $NH_3$ dosed open site, all in their dehydrated state. "X" denotes framework O-Si units.**

In this chapter the structure of the framework Sn site in Sn-Beta is examined. The mechanistic role of the silanol group adjacent to the open Sn site is analyzed by exchanging its proton with a sodium cation. Evidence is provided that Na-exchanged Sn-Beta catalyzes the epimerization of glucose to mannose via 1, 2 intramolecular carbon shift with high selectivity in methanol and in concentrated aqueous NaCl solutions. In water, the selectivity to isomerization to fructose via 1, 2 intramolecular hydride shift increases with time because $Na^+$ ions are removed during reaction and neighboring silanol groups are restored. These data clearly show that the open Sn site

is the active site for both glucose isomerization and epimerization reactions, with the former prevailing on open sites with adjacent silanol groups in their proton form and the latter on open sites where the adjacent silanol is exchanged with $Na^+$.

## 2. Results and Discussion

### 2.1 Summary of Microporous Materials

Successive sodium ion exchanges were performed by stirring calcined Sn-Beta in a solution of 1 M $NaNO_3$ and $10^{-4}$ M NaOH in distilled water, obtaining three different sodium exchanged Sn-Beta (Sn-Beta-1Ex, Sn-Beta-2Ex, and Sn-Beta-3Ex, respectively). The triple exchanged Sn-Beta (Sn-Beta-3Ex) was acid washed (Sn-Beta-AW) in 1 M $H_2SO_4$. Sn-Beta was also synthesized with $NaNO_3$ present in the synthesis gel with different ratios of Si/Na (Si/Na = 100, 60 and 30). Ammonia, $NH_3$, was adsorbed on Sn-Beta (Sn-Beta-$NH_3$) and also regenerated (Sn-Beta-$NH_3$-Cal) by calcination. The syntheses of all of these materials are discussed in detail at the end of this chapter in the Experimental Procedure.

### 2.2 Characterization of Microporous Materials

The powder X-ray patterns of Sn-Beta, Sn-Beta-1Ex, Sn-Beta-2Ex, Sn-Beta-3Ex, Sn-Beta-AW, Sn-Beta-$NH_3$, Sn-Beta-$NH_3$-Cal and Na-Sn-Beta (Si/Na = 100, 60 and 30) (Figure 4.2 and Figure 4.3) show that each of the samples is highly crystalline and has the zeolite beta framework topology. No diffraction lines were observed at 2θ values of $26.7^o$ and $34.0^o$ that are characteristic of bulk $SnO_2$. SEM images (Figure 4.4) indicate that the crystallite size of Sn-Beta is between 5-8 μm, and does not change significantly after exchange with $NaNO_3$/NaOH or treatment with $NH_3$. Na-Sn-Beta-30 (Figure 4.5) and other materials with gel Na/Sn > 30 (results not

presented here because of the high impurity content) contain an impurity that consists of dark, amorphous (determined by powder X-ray diffraction) particles that are not observed in Na-Sn-Beta-60 and Na-Sn-Beta-100. Thus, synthesis gels with high amounts of Na resulted in contaminating amorphous solids that had high contents of Na and Sn, with a Si/Sn and Na/Sn ratio of 15 and 2.28, respectively (measured by EDS). Bellussi *et al.*[18] proposed that the insertion of titanium into the silicate framework (TS-1) is inhibited when alkali metal ions are present in the synthesis gel due to the formation of alkali titanates. Here, it is possible that the Sn atoms in the synthesis gels form alkali stannates that are part of the amorphous phase impurity, thereby lowering the Sn and Na content of the crystalline Na-Sn-Beta that is formed.

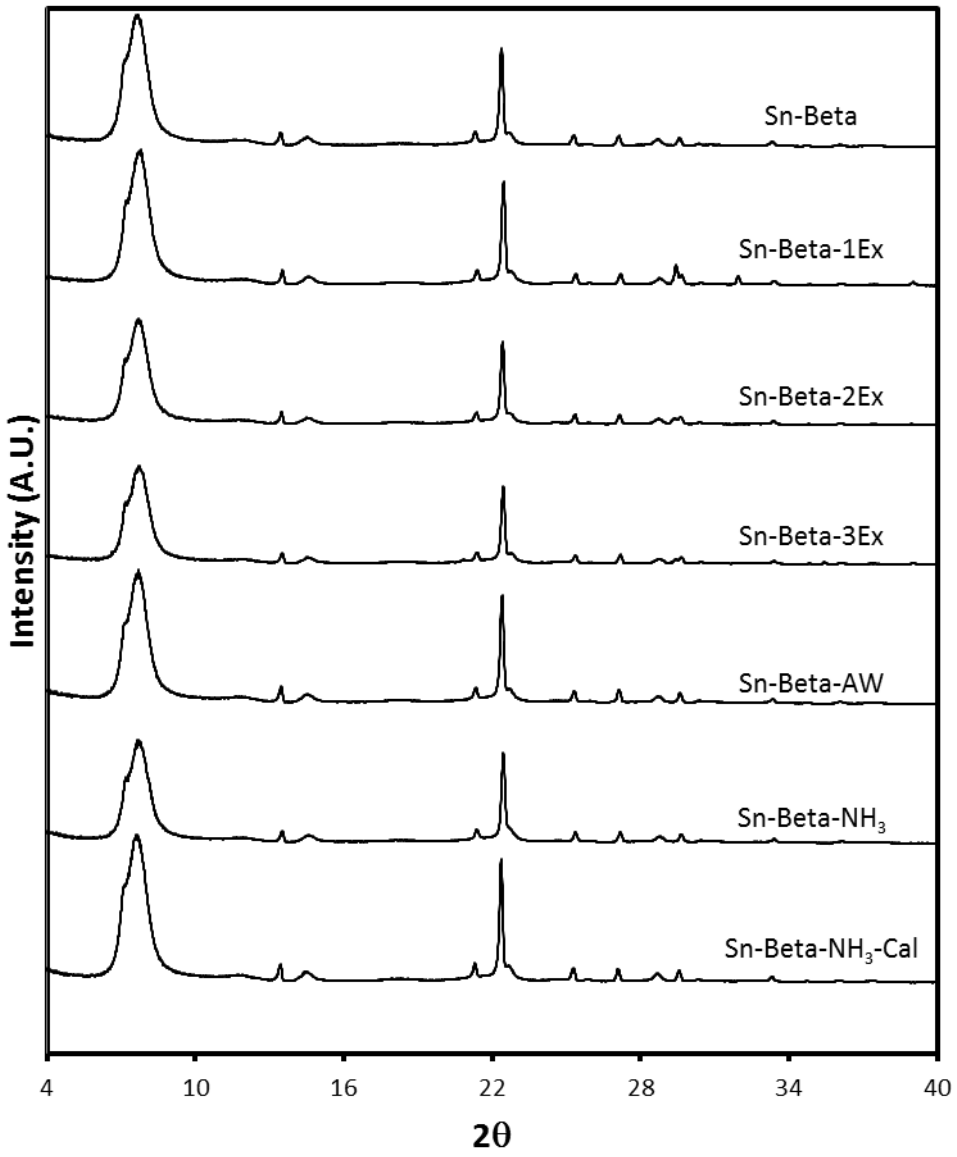


**Figure 4.2 Powder X-ray powder diffraction patterns of Sn-Beta, Sn-Beta-1Ex, Sn-Beta-2Ex, Sn-Beta-3Ex, Sn-Beta-AW, Sn-Beta-$NH_3$ and Sn-Beta-$NH_3$-Cal (top to bottom).**

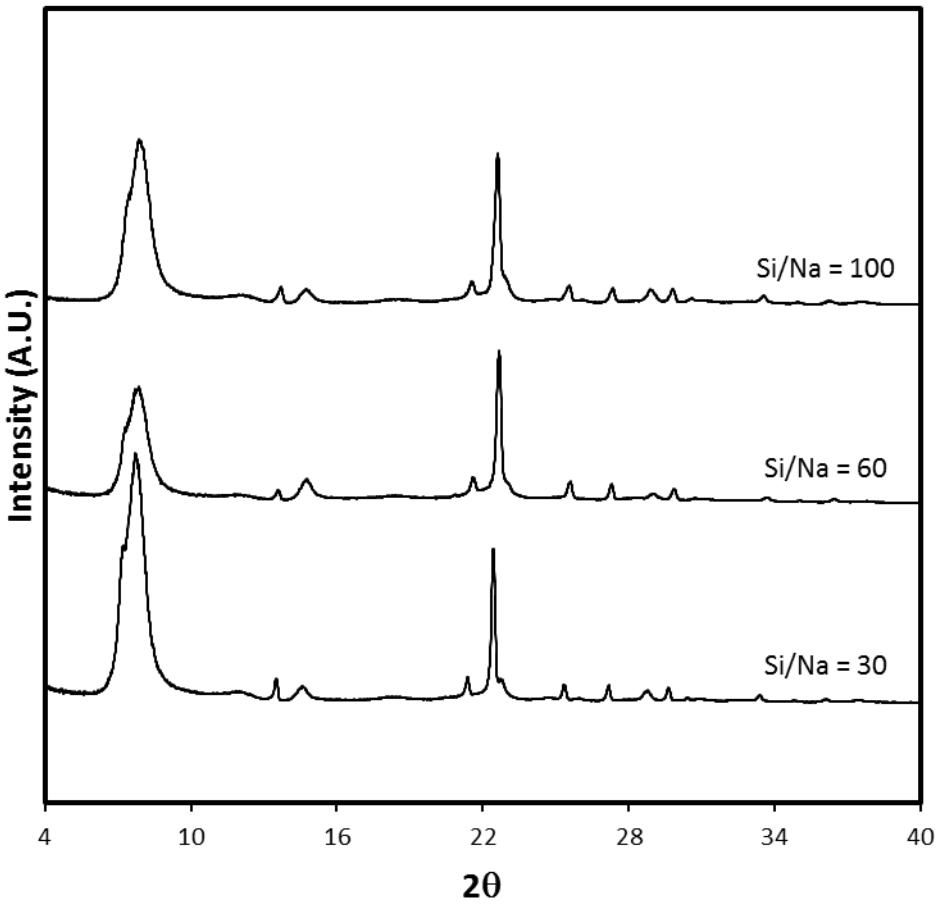


**Figure 4.3 Powder X-ray powder diffraction patterns of Sn-Beta with Si/Na synthesis gel composition of 100, 60, and 30.**

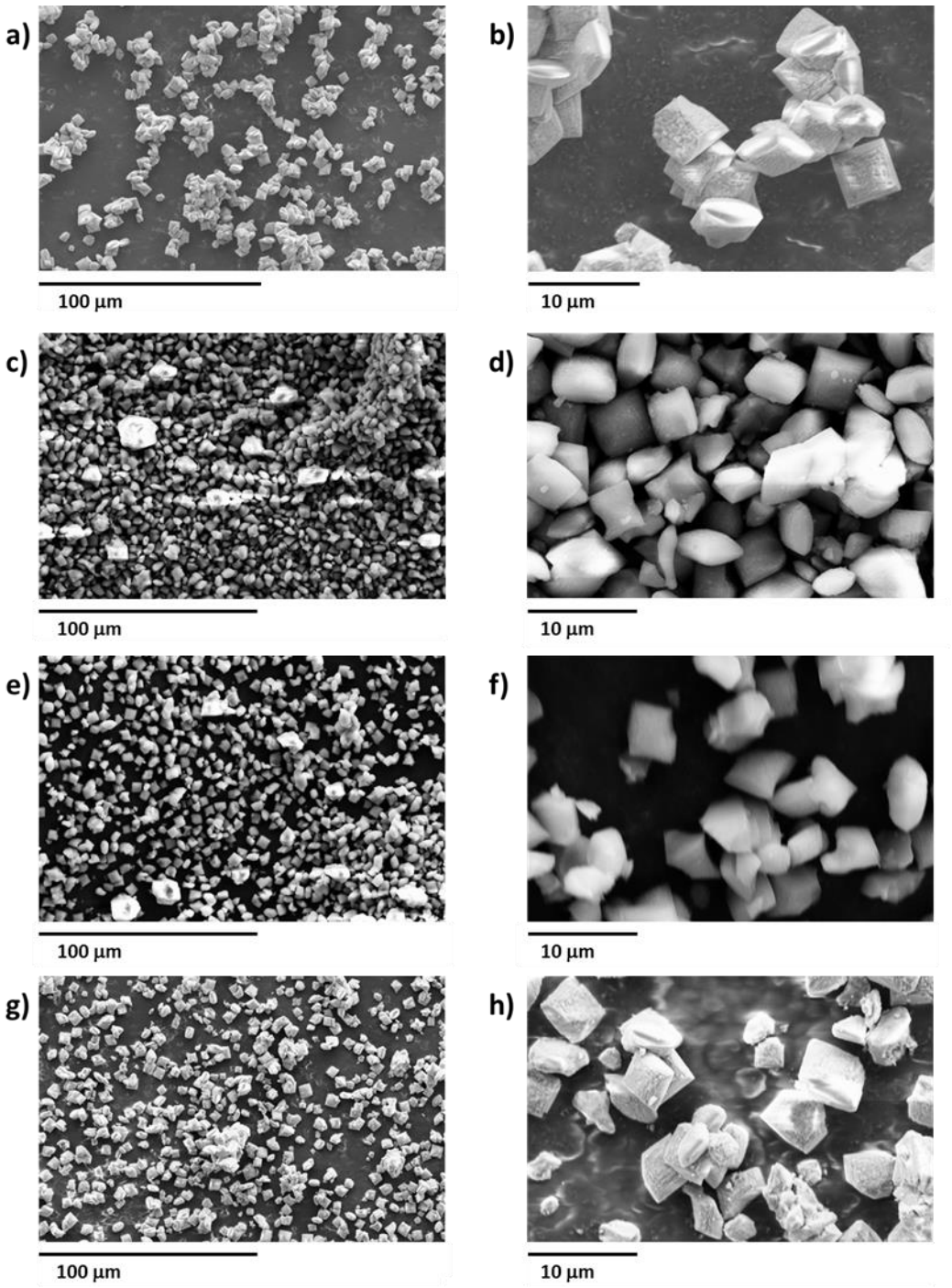


**Figure 4.4 SEM images of (a, b) Sn-Beta, (c, d) Sn-Beta-1Ex, (e, f) Sn-Beta-3Ex, and (g, h) Sn-Beta-$NH_3$.**

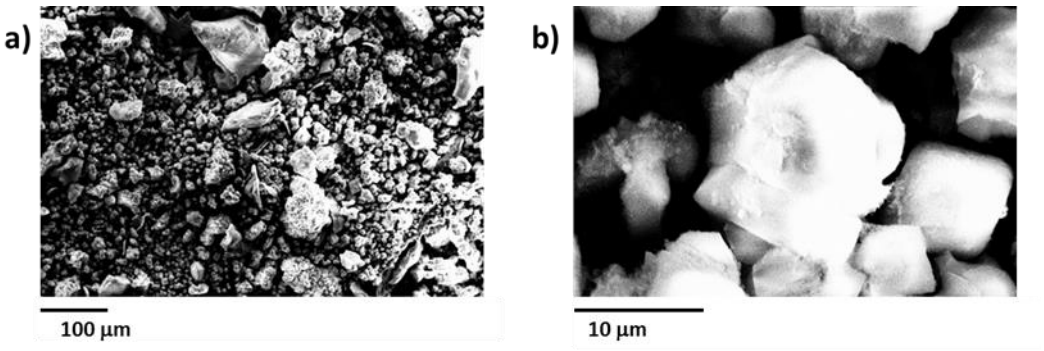


**Figure 4.5 SEM images of Na-Sn-Beta-30.**

The total micropore volumes of the samples were determined from Ar adsorption isotherms (87K), and the results are listed in Table 4-1. There is a decrease in the micropore volume of all Na exchanged materials that might be due to the presence of excess $NaNO_3$ that remains on the solid after Na exchange. The final wash in the exchange procedure was performed with 1M $NaNO_3$ because the use of distilled water for the final rinse results in partial $Na^+$ removal. The FTIR spectra (Figure 4.23) of the Na exchanged materials indeed show a broad shoulder in the 1300 to 1500 $cm^{-1}$ IR range that contains the IR band observed for the $NO_3^-$ ion.[19] Sn-Beta-AW has the same micropore volume (0.19 $cm^3g^{-1}$) as the parent Sn-Beta material, showing that the measured decrease in microporosity for the Na-exchanged materials is not due to a loss of crystallinity, but due to the excess $NaNO_3$. Na-Sn-Beta-60 and Na-Sn-Beta-100 exhibit a similar micropore volume to Sn-Beta (Table 4-1), but Na-Sn-Beta-30 has a micropore volume of 0.14 $cm^3g^{-1}$. This significant decrease in micropore volume is likely due to the amorphous particle impurities. The ammonia-dosed Sn-Beta showed a slight decrease in the micropore volume, giving 0.17 $cm^3$ $g^{-1}$, which was recovered after calcination (0.19 $cm^3g^{-1}$).

| Catalyst | Si/Sn[a] | Na/Sn[a] | Ar micropore volume[b] ($cm^3\ g^{-1}$) | IR bands *($cm^{-1}$)* |
|---|---|---|---|---|
| Sn-Beta | 95 | 0.00 | 0.19 | 2315, 2307, 2276 and 2266 |
| Sn-Beta-1Ex | 115 | 3.80 | 0.16 | 2310, 2280 and 2274 |
| Sn-Beta-2Ex | 159 | 4.38 | 0.15 | 2310, 2280 and 2274 |
| Sn-Beta-3Ex | 140 | 4.85 | 0.16 | 2310, 2280 and 2274 |
| Sn-Beta-AW | 104 | 0.27 | 0.19 | 2315, 2307, 2276 and 2266 |
| Na-Sn-Beta-100 | 113 | 0.12 | 0.18 | n.d. |
| Na-Sn-Beta-60 | 127 | 0.26 | 0.19 | n.d. |
| Na-Sn-Beta-30 | 91 | 0.94 | 0.15 | 2310, 2280 and 2274 |
| Sn-Beta-$NH_3$ | 105 | 0.00 | 0.17 | 2306 and 2270 |
| Sn-Beta-$NH_3$-Cal | 117 | 0.00 | 0.19 | 2315, 2307, 2276 and 2266 |

[a]Determined by Energy Dispersive X-ray Spectroscopy (EDS).The highest measured Si/Sn standard deviation for three scans of different parts of the same material was ± 30, while the highest Na/Sn standard deviation was of ± 1.25. These maximal standard deviations may be used to estimate the uncertainty of measurement for all samples.
[b]Determined from the Ar adsorption isotherm (87K).
[C]n.d., not determined

**Table 4-1 Site and structural characterization of samples used in this study.**

Table 4-1 lists the Sn and Na contents for all of the samples in this study. The Na/Sn ratio increased with the number of consecutive sodium ion exchanges, with the highest ratio being 4.38 after three consecutive exchanges with $NaNO_3$/NaOH. Na/Sn ratios above unity likely reflect the presence of sodium nitrate deposited on the sample and some Na exchange occurring at silanol groups other than the ones adjacent to open Sn centers. Acid treatment removed most of the sodium from the zeolite, as the Na/Sn ratio in Sn-Beta-AW decreased to 0.27. The Na/Sn ratio also increased in the solids synthesized in the presence of sodium (Na-Sn-Beta-100, 60 and 30) as the sodium concentration increased in the synthesis gels.

## 2.3 Structural Characterization of the Sn Sites in Sn-Beta

The nature of Lewis acidic Sn sites in Sn-Beta and post-synthetically treated Sn-Beta samples was probed by monitoring changes in IR bands of the stretching vibrations of the C≡N group (2260-2340 $cm^{-1}$)[20] of deuterated acetonitrile during temperature-programmed desorption experiments (Figure 4.6, Figure 4.24, Figure

4.25, Figure 4.26 and Figure 4.27). The IR spectra for Sn-Beta exposed to $CD_3CN$ (Figure 4.6) show bands at 2315, 2307, 2276, and 2266 $cm^{-1}$. The $CD_3CN$ IR bands at 2276 and 2266 $cm^{-1}$ have been assigned to $CD_3CN$ coordinated to silanol groups and physisorbed $CD_3CN$, respectively, while the bands at 2315 and 2307 $cm^{-1}$ fall in the range that has been assigned to $CD_3CN$ coordinated to Lewis acid sites.[20,21] These results are consistent with Corma *et al.,*[15] who assigned the 2316 $cm^{-1}$ band to $CD_3CN$ bound at the open Sn site, and the 2308 $cm^{-1}$ band to $CD_3CN$ bound at a weaker Lewis acid site proposed to be the closed Sn site.

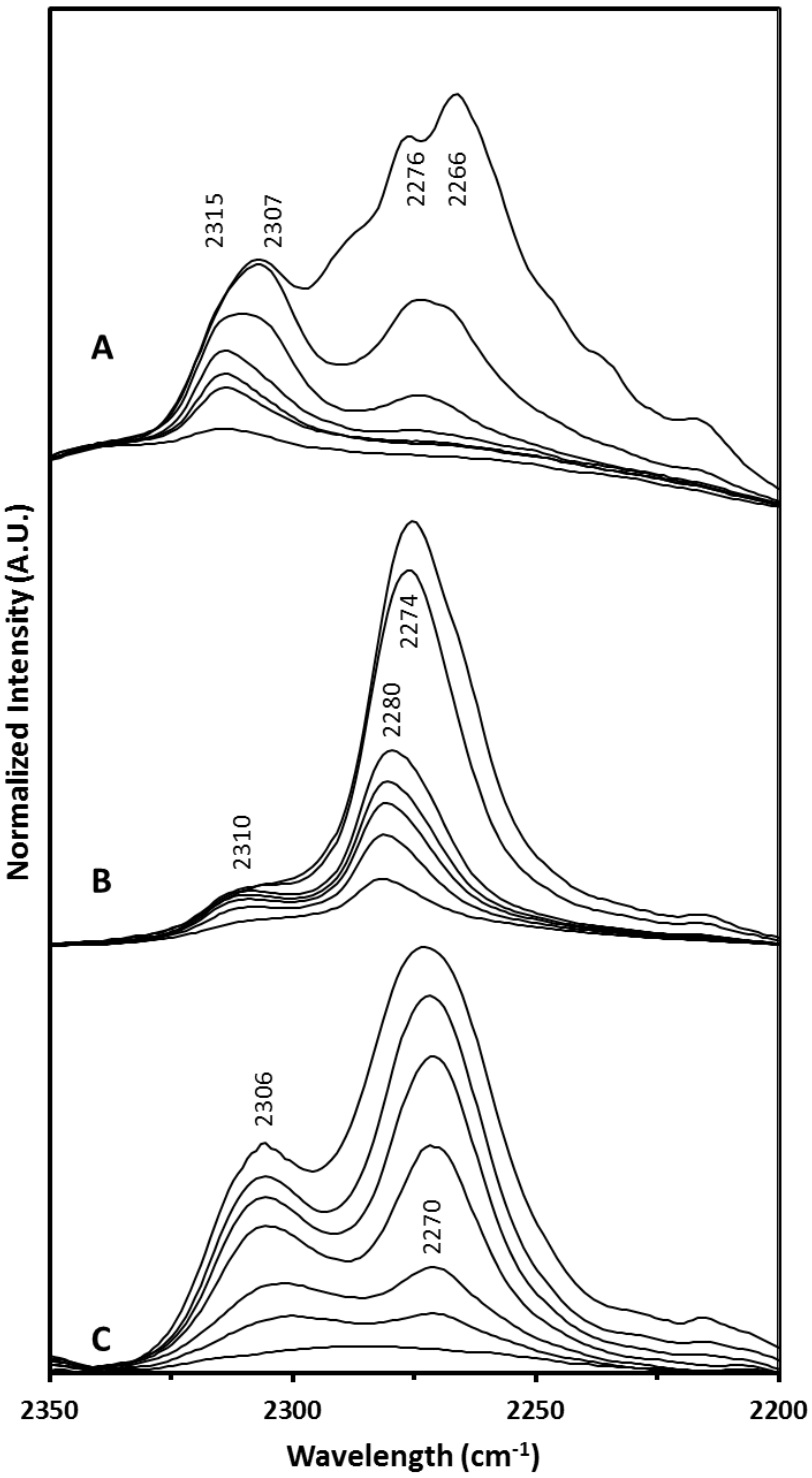


**Figure 4.6 Baseline corrected IR spectra with decreasing $CD_3CN$ coverage on (a) Sn-Beta, (b) Sn-Beta-3Ex, and (c) Sn-Beta-$NH_3$.**

After $NaNO_3$/NaOH treatments (Figure 4.24, Figure 4.25 and Figure 4.6), the $CD_3CN$ bands associated with $CD_3CN$ bound to the open and closed sites disappear or diminish in intensity, while a single broad IR band with low intensity appears and is centered between 2310-2312 $cm^{-1}$. Corma et al.[22] showed that a broad band centered at 2310 $cm^{-1}$ in Sn-MCM-41 may be deconvoluted into multiple bands that correspond to different Sn environments. Similarly, the broad band observed in Na-exchanged Sn-Beta samples may have multiple contributions from the residual non-exchanged Sn-sites. Interestingly, a more prominent band appears at 2280 $cm^{-1}$ in these Na-exchanged Sn-Beta materials (Figure 4.24, Figure 4.25 and Figure 4.6), which we tentatively associate with the Lewis acid site responsible for the reactivity of these samples. Despite the lower frequency of this new band (2280 $cm^{-1}$) compared to the open Sn site (2315 $cm^{-1}$), which may suggest a weaker interaction[20] of $CD_3CN$ with the Lewis acid centers in Na-exchanged Sn-Beta, the $CD_3CN$ that gives rise to this band desorbs more slowly than $CD_3CN$ bound to the closed site (2307 $cm^{-1}$) and at comparable rates to $CD_3CN$ bound to the open site (Figure 4.6a and b). These findings suggest that, in addition to direct lone pair donation of $CD_3CN$ to the Lewis acidic Sn center, secondary interactions of $CD_3CN$ with the site or its surrounding environment may influence the binding strength and the $\nu(C\equiv N)$ of $CD_3CN$. When the Na exchange procedure was performed on Si-Beta, the resulting material did not show strongly-bound $CD_3CN$ at 2280 $cm^{-1}$ (Figure 4.26), confirming that this IR band is not a result of $CD_3CN$ adsorbed to Na-exchanged terminal silanol groups, and requires the Lewis acidity of a framework Sn site. The synthetic Na-Sn-Beta-30 sample showed a similar desorption profile to that of the Na-exchanged Sn-Beta (Figure 4.27), suggesting that $Na^+$ ions introduced to the framework Sn sites during synthesis lead to a similar change in site properties as $Na^+$ ions introduced post-synthetically.

$CD_3CN$ adsorption onto Sn-Beta-$NH_3$ gives rise to IR bands at 2306 and 2270 $cm^{-1}$(Figure 4.6c). $CD_3CN$ associated with the previously unobserved 2270 $cm^{-1}$ band desorbs at a rate similar to that of $CD_3CN$ bound to the closed site of Sn-Beta. While the IR band assigned to $CD_3CN$ bound to the closed site at 2306 $cm^{-1}$ (as confirmed by $^{119}Sn$ NMR, vide infra) was present in Sn-Beta-$NH_3$, the IR band of $CD_3CN$ bound to the open site at 2315 $cm^{-1}$ was not observed (Figure 4.6c). These data indicate that $NH_3$ remains bound to open Sn sites in Sn-Beta-$NH_3$, but not to closed Sn sites, after exposure to ambient air and treatment prior to $CD_3CN$ exposure (vacuum at 373 K, 2h) (Figure 4.7), consistent with proposals that open Sn sites are stronger Lewis acid sites.[15] We propose that open Sn sites with bound $NH_3$ (Figure 4.1d) are more electron-rich, and in turn bind $CD_3CN$ more weakly, than its analog in Sn-Beta (Figure 4.1b). The open Sn site with pre-adsorbed $NH_3$ (Figure 4.1d) seems to be a likely candidate for the IR band at 2270 $cm^{-1}$ (Figure 4.6c), which reflects weakly-bound $CD_3CN$ that disappears much more rapidly than the IR band at 2315 $cm^{-1}$ for $CD_3CN$ bound more strongly at open Sn sites (Figure 4.6a). On the other hand, the presence of the 2306 $cm^{-1}$ IR band after $CD_3CN$ adsorption onto the Sn-Beta-$NH_3$ suggests that any $NH_3$ initially bound to the closed site (Figure 4.7b) desorbs after exposure to ambient air or vacuum treatment at 373 K (Figure 4.7c), and results in a closed Sn site of similar structure to that in untreated Sn-Beta.

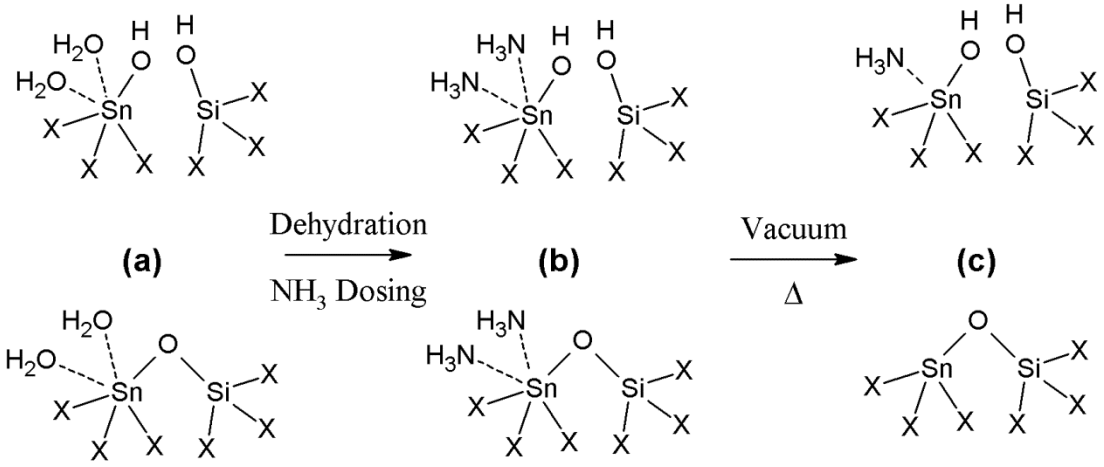


**Figure 4.7 Schematic representation of the $NH_3$ dosed Sn-Beta sample history that explains its characterization behavior. The hydrated open and closed sites (a) are dehydrated and saturated with ammonia (b). After exposure to ambient atmosphere and heated evacuation (373 or 393 K for IR and NMR studies, respectively), only the open site is expected to retain the coordinated ammonia (c). "X" denotes framework O-Si units.**

The $^{119}$Sn NMR spectra of $^{119}$Sn-Beta after calcination and exposure to ambient conditions, which allows the Sn centers to become hydrated, shows a main resonance centered at -688 ppm (Figure 4.8a) that has been assigned to octahedrally coordinated Sn in the framework.[1,2,23] Upon dehydration at 383 K to remove the coordinating water, the Sn resonances shift to -423 and -443 ppm (Figure 4.8d) that are characteristic of tetrahedrally-coordinated Sn. We have shown previously through $^{1}$H-$^{119}$Sn CPMAS NMR that the open and closed sites correspond to the resonances centered at -423 and -443 ppm, respectively, because only the -423 ppm resonance was detected when cross-polarization occurred from nearby protons.[1]

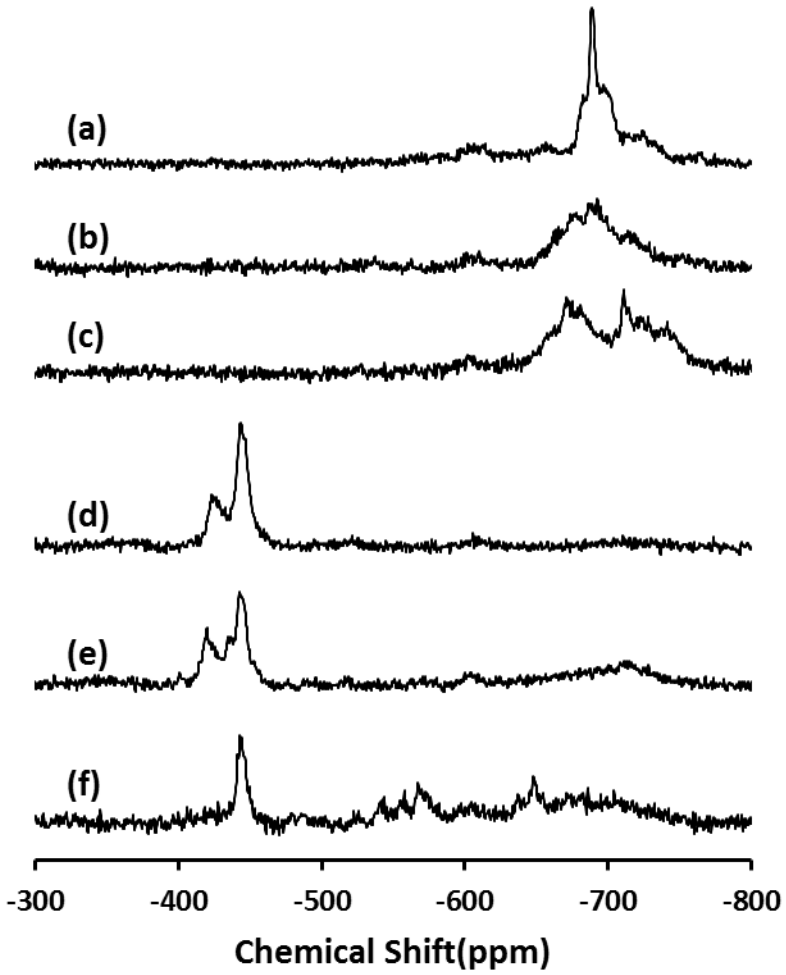


**Figure 4.8 $^{119}$Sn MAS Solid State NMR spectra of $^{119}$Sn-Beta after different treatments: (a) calcination, (b) three Na-exchanges after calcination, (c) $NH_3$ adsorption after calcination, (d) dehydration after calcination, (e) dehydration after three Na-exchanges and (f) dehydration after $NH_3$ adsorption.**

Three Na-exchanges performed on $^{119}$Sn-Beta result in a decreased intensity of the sharp -688 ppm resonance observed in $^{119}$Sn-Beta (Figure 4.8a), and instead result in a broad shoulder that appears to begin at -650 ppm and merge into the broader features of the $^{119}$Sn-Beta spectrum (Figure 4.8b). Dehydration of this sample (vacuum treatment at 398 K, 2h) leads to a shift of the resonance associated with the tetrahedral open site at -423 ppm (Figure 4.8d) to -419 ppm (Figure 4.8e). The expanded chemical shift range in the -400 to -480 ppm region of $^{119}$Sn MAS Solid State NMR spectra of the dehydrated samples can be found in Figure 4.28. A small shoulder develops at -435 ppm and was confirmed not to be a spinning sideband of

another resonance (Figure 4.8e). The closed site resonance at -443 ppm (Figure 4.8d) is not shifted by the Na-exchange (-443 ppm, Figure 4.8e). The $^{1}H$-$^{119}Sn$ CPMAS NMR of $^{119}Sn$-Beta dehydrated after three Na-exchanges shows a resonance at -419 ppm, indicating that these Sn centers have a proton source nearby that cross-polarizes the $^{119}Sn$ atom (Figure 4.29). This observation suggests that Na exchanges only one of the two available protons present in the silanol and stannanol groups in the dehydrated open Sn site (Figure 4.1b). The silanol proton is the more likely position for Na exchange (Figure 4.1c) because the proposed mechanisms for glucose isomerization and epimerization on Sn-Beta require bonding to glucose through the stannanol group.[17] Note that some difficulties in optimizing $^{1}H$-$^{119}Sn$ CPMAS conditions has been experienced, partly due to poor rf pulse coverage over 300 ppm during contact period at high spinning speed (14 kHz in this case). Because of the poor cross-polarization efficiency, the $^{1}H$-$^{119}Sn$ CPMAS spectra (e.g., Figure 4.29b) were averaged over 30,000 transients, and the resonances detected in the tetrahedral range of the dehydrated Na-exchanged $^{119}Sn$-Beta do not allow us to characterize the origin of the small - 435 ppm shoulder (Figure 4.8e).

Adsorption of ammonia onto $^{119}Sn$-Beta gives rise to two groups of broad resonances centered at -669 and -708 ppm (Figure 4.8c). Dehydration of this sample (evacuation at 398 K, 2h) gives rise to a resonance for the closed tetrahedral site (-443 ppm, Figure 4.8f), but not for the open tetrahedral site found in $^{119}Sn$-Beta (-423 ppm, Figure 4.8d). New resonances are detected in -500 to -600 ppm range that suggest the presence of a different Sn coordination environment, which may have come from the open site of Sn-Beta as depicted in Figure 4.1d. The $^{1}H$-$^{119}Sn$ CPMAS NMR spectrum of the $^{119}Sn$-Beta dehydrated after ammonia adsorption confirms that there is no

proton source in the neighborhood of the closed site (-443 ppm), or of any tetrahedrally-coordinated Sn sites, after these treatments (Figure 4.30).

These $^{119}$Sn NMR results are consistent with the interpretations of the IR spectra of Sn-Beta-$NH_3$ after $CD_3CN$ adsorption, and lead to propose the Sn structures and coordinations in Figure 4.7. These findings suggest that the open Sn site is a stronger Lewis acid site than the closed Sn site (Figure 4.7a), and that it retains the adsorbed $NH_3$ (Figure 4.7b) after vacuum treatment at 373 K (Figure 4.7c). Open Sn sites that coordinate one $NH_3$ ligand would appear as penta-coordinated Sn sites in $^{119}$Sn NMR spectra, which it is *speculated* that it could give rise to the resonances detected in -500 to -600 ppm range (Figure 4.8f); however, we have not conclusively assigned these resonances at this time. Penta-coordinated open Sn sites with one $NH_3$ ligand would also bind $CD_3CN$ more weakly than open Sn sites without coordinated $NH_3$, and may give rise to the 2270 $cm^{-1}$ $CD_3CN$ band observed in IR spectra (Figure 4.6c). These NMR data also suggest that $NH_3$ bound to the closed Sn sites desorbs upon dehydration (Figure 4.7c), such that the behavior of the closed Sn sites in Sn-Beta-$NH_3$ is similar to their behavior in Sn-Beta samples that have not been treated with $NH_3$.

## 2.4 Mannose Formation with Na containing Sn-Beta

Fructose is the predominant product formed when Sn-Beta reacts with 1% aqueous glucose solutions at a 1:100 Sn:glucose ratio at 353 K for 30 min (Table 4-2 and Table 4-5). At the noted glucose conversions, the carbon balances obtained are similar to those reported previously by our group.[3] Experiments performed for the same reaction time and temperature with the sodium exchanged Sn-Beta samples led

to similar glucose conversions (6.0-6.8%, Table 4-2) as with Sn-Beta (6.4%,Table 4-2), however, the mannose yield increased systematically from 0.4% to 3.3% and the fructose yields decreased from 5.0% to ~ 2% with increasing Na content. Similar results were observed with increasing Na content for Na-Sn-Beta samples synthesized directly (Table 4-2), suggesting that these selectivity differences do not depend on the method used to introduce $Na^+$ cations into Sn-Beta.

| Catalyst | Solvent | $X_{Gluc.}$(%) | $Y_{Fruc.}$(%) | $Y_{Mann.}$(%) |
|---|---|---|---|---|
| Sn-Beta | $H_2O$ | 6.4 | 5.0 | 0.4 |
| | $CH_3OH$ | 23.2 | 10.3 | 3.9 |
| Sn-Beta-1Ex | $H_2O$ | 6.0 | 2.1 | 1.8 |
| | $CH_3OH$ | 12.6 | 3.2 | 5.0 |
| Sn-Beta-2Ex | $H_2O$ | 6.1 | 1.8 | 2.5 |
| | $CH_3OH$ | 12.2 | 2.1 | 6.7 |
| Sn-Beta-3Ex | $H_2O$ | 6.8 | 2.3 | 3.3 |
| | $CH_3OH$ | 12.4 | 0.0 | 7.9 |
| Sn-Beta-AW | $H_2O$ | 5.4 | 3.9 | 0.0 |
| | $CH_3OH$ | 16.9 | 6.1 | 2.8 |
| Na-Sn-Beta-100 | $H_2O$ | 6.8 | 5.1 | 1.1 |
| | $CH_3OH$ | 19.4 | 8.4 | 3.3 |
| Na-Sn-Beta-60 | $H_2O$ | 7.3 | 4.0 | 2.7 |
| | $CH_3OH$ | 17.2 | 8.0 | 3.0 |
| Na-Sn-Beta-30 | $H_2O$ | 5.8 | 1.1 | 3.5 |
| | $CH_3OH$ | 6.8 | 0.0 | 4.6 |
| Sn-Beta-$NH_3$ | $H_2O$ | 3.8 | 1.9 | 2.4 |
| | $CH_3OH$ | 3.0 | 0.0 | 1.9 |
| Sn-Beta-$NH_3$-Cal. | $H_2O$ | 5.0 | 3.2 | 0.0 |
| | $CH_3OH$ | 17.6 | 7.2 | 2.6 |

**Table 4-2 Glucose conversion (X) and fructose and mannose yields (Y) in $H_2O$ and $CH_3OH$ solvents. Reaction conditions: 1% (w/w) glucose solutions, 1:100 metal:glucose ratio, 353 K, 30 min.**

Equivalent reaction conditions led to higher glucose conversions on Sn-Beta and the Na-containing Sn-Beta samples in methanol than in water (Table 4-2 and Table 4-5), with glucose conversions of 23.2% for Sn-Beta and 12.2-12.6% for Na-

exchanged Sn-Beta (Table 4-2). As in the case of water solvent, Sn-Beta samples with increasing Na/Sn ratio led to mannose yields that increased systematically from 3.9% to 7.9% and to fructose yields that decreased systematically from 10.3% to 0.0% (Table 4-2). Similarly, increasing the sodium content in the synthesis gel of Sn-Beta led to samples that produced higher mannose yields and lower fructose yields (0.0% fructose for Na-Sn-Beta-30, Table 4-2). The large black particles of the amorphous phase impurity formed from synthesis gels with Si/Na ratios less than 30 were isolated from the crystalline solids and did not react with glucose in water, but were able to catalyze glucose-fructose isomerization in methanol.

The sodium containing Sn-Beta catalysts showed a higher selectivity towards mannose when the reaction was performed in methanol than in water. Furthermore, the fructose to mannose ratio in aqueous media significantly increased as the reaction progressed (Table 4-2 and Table 4-5). These results suggested to us that sodium decationation could be occurring in aqueous media at a rate that would cause the reactivity to change over the timeframe of the experiment. Thus, we investigated the effects of adding sodium salt to the aqueous reaction solution in order to maintain the sodium content in the solid more effectively during reaction (Table 4-3 and Table 4-6). When glucose was reacted with Sn-Beta in aqueous NaCl solutions, mannose and fructose were produced in nearly equal yields (4.1% and 4.5%, respectively; Table 4-3 and Table 4-6), and the solid had a Na/Sn ratio of 2.65 after reaction (Table 4-3 and Table 4-6) indicating that $Na^+$ was exchanging into the solid during reaction. Sn-Beta pre-exchanged with Na (Sn-Beta-3Ex) maintained mannose selectivity during the course of the reaction when NaCl was added to the aqueous reaction solutions. These results indicate that the presence of a sodium cation, whether added synthetically or exchanged onto the material prior to or during the reaction, shifts the

reaction selectivity of Sn-Beta from the 1, 2 intramolecular hydride shift-mediated isomerization that yields fructose to the 1, 2 intramolecular carbon shift mediated-epimerization that yields mannose. When water is used as the solvent for the reaction, the $Na^+$ ion in the Sn active site is replaced by a proton and the catalyst reverts to a state that favors the formation of fructose, while in methanol the $Na^+$ ion is retained for a longer time and the catalyst maintains its tendency to form mannose. The addition of excess sodium salt to aqueous reaction mixtures increases the extent to which Na exchanges onto the solid, in turn maintaining the selectivity of Sn-Beta towards mannose during the course of reaction.

| Catalyst | Solvent | $X_{Gluc.}(\%)$ | $Y_{Fruc.}(\%)$ | $Y_{Mann.}(\%)$ |
|---|---|---|---|---|
| Sn-Beta[a] | $H_2O$-NaCl | 9.8 | 4.5 | 4.1 |
| Sn-Beta-1Ex | $H_2O$-NaCl | 10.9 | 2.6 | 5.2 |
| Sn-Beta-2Ex | $H_2O$-NaCl | 10.7 | 2.5 | 6.0 |
| Sn-Beta-3Ex | $H_2O$-NaCl | 11.5 | 0.0 | 7.5 |

[a]After reaction the catalyst had a Si/Sn and a Na/Sn ratio of 115 and 2.65, respectively, determined by Energy Dispersive X-ray Spectroscopy (EDS). The highest measured Si/Sn standard deviation for three scans of different parts of the same material was ± 30, while the highest Na/Sn standard deviation was of ± 1.25. These maximal standard deviations may be used to estimate the uncertainty of measurement for all samples.

**Table 4-3 Glucose conversion (X) and fructose and mannose yields (Y) with 0.2g NaCl/g $H_2O$. Reaction conditions: 1% (w/w) glucose solutions, 1:100 metal:glucose ratio, 353 K, 30 min.**

The Sn-Beta sample that was dosed with $NH_3$ showed lower glucose conversions in both water and methanol solvents (3.0-3.8%, Table 4-2) than Sn-Beta and the Na-containing Sn-Beta samples. Higher glucose conversions were observed with Sn-Beta-$NH_3$ in water, with a resulting dark yellow post-reaction solution that may indicate the presence of humins formed from $NH_4OH$ that possibly could be formed *in situ* from the desorption of $NH_3$. Upon calcination of the ammonia-dosed sample, the reactivity was nearly fully recovered in methanol and water (17.6% and 5.0% glucose conversion, respectively, Table 4-2). The suppression of isomerization

reactivity on Sn-Beta-$NH_3$ (Table 4-2) occurs together with the disappearance of the open site $CD_3CN$ IR band at 2315 $cm^{-1}$ (Figure 4.6c) and with the disappearance of the open site $^{119}Sn$ NMR resonance at -419 ppm (Figure 4.8f) in the dehydrated $NH_3$-dosed Sn-Beta. These data corroborate our proposal that the open site is the active site in the hydride-shift mediated glucose to fructose isomerization pathway in the absence of sodium, and is the active site for the epimerization of glucose to form mannose in the presence of sodium.

2.5 Sodium Removal from Sn-Beta

The Sn-Beta-3Ex sample was acid washed to remove $Na^+$ from the sample (Sn-Beta-AW) and probed whether the effects of sodium on the reactivity of Sn-Beta were reversible. Sn-Beta-AW had much less sodium (Na/Sn = 0.27) than Sn-Beta-3Ex (Na/Sn = 4.85). The glucose conversion and the fructose and mannose yields observed with Sn-Beta-AW were very similar to that of the parent Sn-Beta (Table 4-2). The decrease in mannose yield and concurrent increase in fructose yield after the acid treatment demonstrates that the effects of sodium addition are reversible, and are not a result of a permanent poisoning of the site active for glucose-fructose isomerization.

The effect of the reaction solvent on the recyclability of the catalyst was probed by reacting Sn-Beta-3Ex with glucose in water and methanol under the previously stated reaction conditions (353 K for 30 min in a 1% (w/w) glucose solution) and washing once with the solvent used in the reaction. This cycle was repeated twice and the reaction results after each cycle are shown in Table 4-4. The Na/Sn ratio of the material decreased in each cycle, with a greater extent of sodium loss in the case of aqueous media. A decrease in sodium content in the zeolite after

each cycle also led to a decrease in the mannose yield and corresponding increase in the fructose yield (Table 4-4), consistent with the proposal that open Sn sites with Na-exchanged silanol groups are active sites for the epimerization reaction.

| Cycle | Si/Sn[a] | Na/Sn[a] | Solvent | $X_{Gluc.}$(%) | $Y_{Fruc.}$(%) | $Y_{Mann.}$(%) |
|---|---|---|---|---|---|---|
| 1 | 115 | 4.38 | $H_2O$ | 8.5 | 1.7 | 4.5 |
| 2 | 136 | 0.93 | $H_2O$ | 8.6 | 4.6 | 3.9 |
| 3 | 123 | 0.26 | $H_2O$ | 9.0 | 6.4 | 1.2 |
| 1 | 115 | 4.38 | $CH_3OH$ | 9.4 | 0.0 | 6.5 |
| 2 | 132 | 1.26 | $CH_3OH$ | 10.2 | 1.5 | 6.0 |
| 3 | 119 | 0.82 | $CH_3OH$ | 13.7 | 3.7 | 6.2 |

[a]Determined by Energy Dispersive X-ray Spectroscopy (EDS). The highest measured Si/Sn standard deviation for three scans of different parts of the same material was ± 30, while the highest Na/Sn standard deviation was of ± 1.25. These maximal standard deviations may be used to estimate the uncertainty of measurement for all samples.

**Table 4-4 Glucose conversion (X) and fructose and mannose yields (Y) with Sn-Beta-3Ex in $CH_3OH$ and $H_2O$. After the first cycle the catalysts was washed with the solvent used in the reaction and reused under the same reaction and solvent conditions as the previous cycle. Reaction conditions: 1% (w/w) glucose solutions, 1:100 metal:glucose ratio, 353 K, 30 min.**

## 3.6 Glucose Isomerization and Epimerization Mechanisms

1% (w/w) glucose labeled with $^{13}C$ at the C1 position ($^{13}C$-C1-glucose) was reacted at 353 K for 30 min with Sn-Beta in water, aqueous NaCl solutions (0.2g NaCl/g $H_2O$), and methanol as solvents to determine the mechanism of glucose isomerization to fructose and epimerization to mannose. All $^{13}C$ NMR spectra in Figure 4.9 show the presence of $^{13}C$ in the C1 position (resonances at $\delta$ = 95.8 and 92.0 ppm) of the $\beta$ and $\alpha$ pyranose forms of the starting labeled glucose, respectively. The fructose formed from reactions with Sn-Beta in all three solvents showed $^{13}C$ in the C1 position (resonances at $\delta$ = 63.8 and 62.6 ppm) for $\beta$-pyranose and $\beta$-furanose forms of fructose, as expected from isomerization mediated by 1, 2 intramolecular hydride shift.[1] The $^{13}C$ label was only observed in the C1 position (resonances at $\delta$ =

93.9 and 93.5 ppm) of α and β pyranose forms of mannose with water and methanol solvents in Sn-Beta, indicating that mannose was not formed by a 1, 2 intramolecular carbon shift. In contrast, the $^{13}C$ label appeared in the C2 position (resonances at δ = 70.5 and 71.1 ppm) of the α and β pyranose forms of mannose with Sn-Beta in aqueous NaCl solutions, indicating that mannose was formed by the 1, 2 intramolecular carbon shift mechanism of the Bilik reaction.[9]

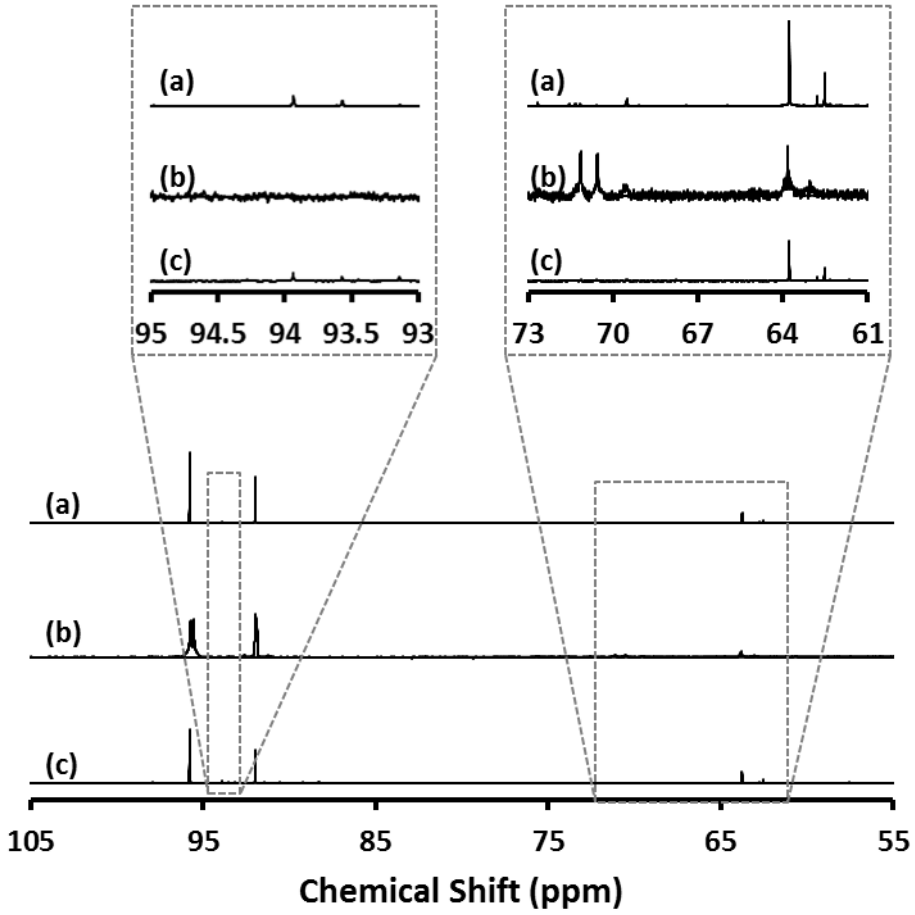


**Figure 4.9 $^{13}C$ NMR spectra for reactant and products with Sn-Beta in a 1% (w/w) $^{13}C1$-glucose solution at 353 K for 30 min with the following solvent mixtures (a) $H_2O$, (b) NaCl-$H_2O$ and (c) $CH_3OH$.**

The experiment performed with Sn-Beta was also conducted with Sn-Beta-3Ex in water, aqueous NaCl solutions (0.2g NaCl/g $H_2O$), and methanol as solvents, and the resulting $^{13}C$ NMR spectra are shown in Figure 4.10. In water, the fructose

products retained the $^{13}C$ label in the C1 position (resonances at $\delta$ = 63.8 and 62.6 ppm), with a lower intensity relative to Sn-Beta, and the mannose product showed the $^{13}C$ label only in the C2 position (resonances at $\delta$ = 70.5 and 71.1 ppm). These results (along with reaction data for earlier reaction times in Table S.2) suggest that in water, Sn-Beta-3Ex initially forms mannose through the 1, 2 intramolecular carbon shift, but the loss of sodium from the active site results in the formation of fructose without carbon rearrangement. When methanol or concentrated aqueous NaCl solutions were used as solvents, mannose with $^{13}C$ in the C2 position was observed as the main product. These results confirm that the switch in reaction mechanism from isomerization to epimerization of sodium-exchanged materials is not directly dependent on the solvent, but rather on the presence of sodium in the active site.

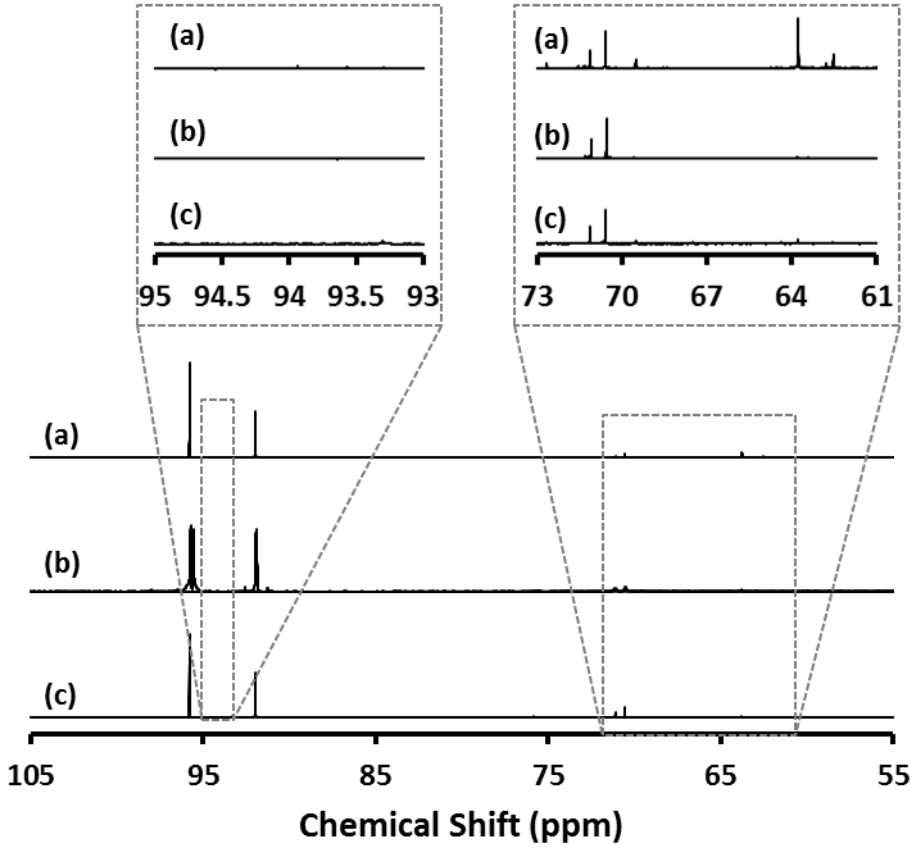


**Figure 4.10 $^{13}$C NMR spectra for reactant and products with Sn-Beta-3Ex in a 1% (w/w) $^{13}$C1-glucose solution at 353 K for 30 min with the following solvent mixtures (a) $H_2O$, (b) NaCl-$H_2O$ and (c) $CH_3OH$.**

Glucose epimerization into mannose can proceed via reversible enolization upon abstraction of α-carbonyl protons (LdB-AvE rearrangement), or via an intramolecular carbon shift between C1-C2 positions.[24] In order to confirm that the Sn-Beta containing $Na^+$ was not epimerizing glucose to mannose by abstraction of the α-carbonyl proton, glucose with deuterium at the C2 position (glucose-D2) was used as a reactant. The mannose formed with Sn-Beta-3Ex after 30 minutes at 353 K with 1% (w/w) glucose solution in methanol did not show resonances at δ = 93.9 and 93.5 ppm (Figure 4.11) that correspond to the C1 positions of the α and β pyranose forms of mannose, respectively, due to the disruption of the Nuclear Overhauser Effect

(NOE). This NMR evidence indicates that with the sodium cation in the active site of Sn-Beta, the carbon in the C2 position of glucose moves along with its deuterium to the C1 position by the 1, 2 intramolecular carbon shift to form mannose, as it has been observed previously.[2]

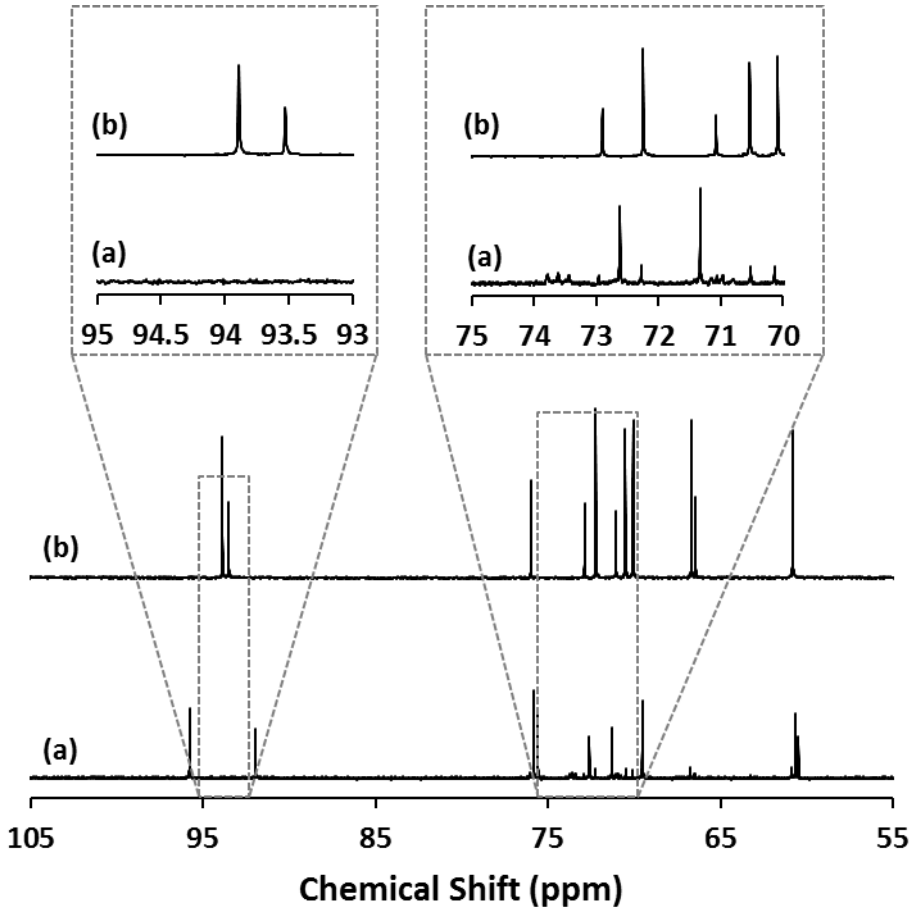


**Figure 4.11 $^{13}$C NMR spectra for (a) reactant and products with Sn-Beta-3Ex in a 1% (w/w) $^{13}$C1-glucose solutions at 353 K for 30 min in $CH_3OH$ and (b) mannose.**

## 3. Conclusion

The proton containing partially hydrolyzed Sn site in zeolite beta, characterized by an IR band at 2315 $cm^{-1}$ from adsorbed $CD_3CN$ and a $^{119}$Sn NMR resonance at -423 ppm in the dehydrated state (denoted as the open site) is the active site involved in the isomerization of glucose into fructose via a Lewis-acid mediated

hydride-shift mechanism; whereas a sodium containing open site analog, characterized by an IR band at 2280 $cm^{-1}$ adsorbed $CD_3CN$ and a $^{119}Sn$ NMR resonance at - 419 ppm in the dehydrate state, is the active site in the epimerization of glucose into mannose via a 1, 2 intramolecular carbon shift. The sodium cation can be introduced into the active site of the zeolite, either by ion exchange of Sn-Beta or by incorporation of low amounts of sodium into the synthesis gel, with both methods resulting in samples that give higher epimerization selectivity relative to Sn-Beta. Acid wash of sodium containing materials gives nearly full recovery of initial activity of the parent Sn-Beta, showing that the alterations to the tin site by the sodium ion are reversible. The addition of NaCl to aqueous reaction solutions also enhanced the selectivity towards epimerization of glucose into mannose. These results, in combination with reusability studies in water and methanol, support the finding that the sodium cation is more prone to decationize in water than in methanol under reaction conditions.

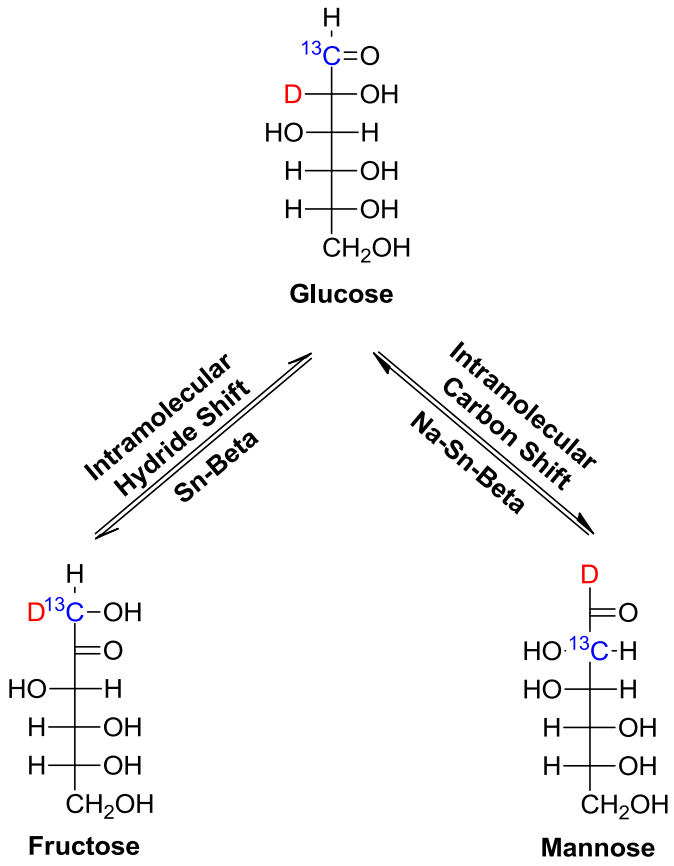


**Figure 4.12 Schematic representation of the isomerization of glucose to fructose with Sn-Beta (left) and epimerization of glucose to mannose with Sn-Beta in the presence of sodium (right).**

## 4. Experimental Procedure and Additional Figures

### 4.1 Synthesis of Sn-Beta, $^{119}$Sn-Beta, Na-Sn-Beta and Si-Beta.

Sn-Beta and $^{119}$Sn-Beta were synthesized according to previously reported procedures.[1] 15.25 g of tetraethylammonium hydroxide solution (Sigma-Aldrich, 35% (w/w) in water) were added to 14.02 g of tetraethylorthosilicate (Sigma-Aldrich, 98% (w/w)), followed by the addition of 0.172 g of tin (IV) chloride pentahydrate (Sigma-Aldrich, 98% (w/w)) or of 0.121 g of $^{119}$Sn enriched tin (IV) chloride pentahydrate (Cambridge Isotopes, 82% isotopic enrichment). The mixture was stirred until tetraethylorthosilicate was completely hydrolyzed and then allowed to reach the targeted $H_2O$:$SiO_2$ ratio by complete evaporation of ethanol and partial evaporation of

water. Finally, 1.53 g of HF solution (Sigma Aldrich, 54% (w/w) in water) was added, resulting in the formation of a thick gel. The final molar composition of the gel was 1 $SiO_2$ / 0.0077 $SnCl_4$ / 0.55 TEAOH / 0.54 HF / 7.52 $H_2O$. As-synthesized Si-Beta (vide infra) was added as seed material (5 wt% of $SiO_2$ in gel) to this gel and mixed. The final gel was transferred to a Teflon-lined stainless steel autoclave and heated at 413 K in a static oven for 40 days. The recovered solids were centrifuged, washed extensively with water, and dried at 373 K overnight. The dried solids were calcined in flowing air (1.67 $cm^3$ $s^{-1}$, Air Liquide, breathing grade) at 853 K (0.0167 K $s^{-1}$) for 10 h to remove the organic content located in the crystalline material. $^{119}$Sn-Beta was calcined twice under the same conditions.

Na-Sn-Beta was synthesized using the same procedure as Sn-Beta, but with the addition of $NaNO_3$ (Sigma Aldrich, $\geq$ 99.0%) to the synthesis gel. The final molar composition of the gel was 1 $SiO_2$ / x $NaNO_3$ / 0.0077 $SnCl_4$ / 0.55 TEAOH / 0.54 HF / 7.52 $H_2O$, where "x" was 0.010, 0.017 and 0.033 (Na-Sn-Beta-100, 60 and 30, respectively). The gel was transferred to a Teflon-lined stainless steel autoclave and heated at 413 K in a static oven for 25 days. The recovered solids were washed, dried and calcined using the same procedure as for Sn-Beta. Synthesis gels with Si/Na ratio lower than 30 yielded a heterogeneous material with small black particles dispersed among the zeolite. These black particles were separated from the zeolite by hand, and were found to be amorphous, having a Si/Sn and Na/Sn ratio of 15 and 2.28, respectively.

Si-Beta was prepared by adding 10.01 g of tetraethylammonium fluoride dihydrate (Sigma-Aldrich, 97% (w/w) purity) to 10 g of water and 4.947 g of tetraethylorthosilicate (Sigma-Aldrich, 98% (w/w)). This mixture was stirred overnight at room temperature in a closed vessel to ensure complete hydrolysis of the

tetraethylorthosilicate. The targeted $H_2O:SiO_2$ ratio was reached by complete evaporation of the ethanol and partial evaporation of the water. The final molar composition of the gel was $SiO_2$ / 0.55 TEAF / 7.25 $H_2O$. The gel was transferred to a Teflon-lined stainless steel autoclave and heated at 413 K in a rotation oven (60 rpm) for 7 days. The solids were recovered by filtration, washed extensively with water, and dried at 373 K overnight. The dried solids were calcined in flowing air (1.67 $cm^3$ $s^{-1}$, Air Liquide, breathing grade) at 853 K (0.0167 K $s^{-1}$) for 10 h to remove the organic content located in the crystalline material.

## 4.2 $Na^+$ and $H^+$ Ion Exchange of Zeolite Samples

Each ion exchange step was carried out for 24 hours at ambient temperature, using 45 mL of exchange or wash solution per 300 mg of starting solids. For the procedures involving multiple ion-exchange steps, the ion-exchange solution was replaced every 24 hours without intermediate water washing. One, two, and three successive sodium ion exchanges (Sn-Beta-1Ex, Sn-Beta-2Ex, and Sn-Beta-3Ex, respectively) were performed by stirring calcined Sn-Beta in a solution of 1 M NaNO3 (Sigma Aldrich, ≥99.0%) and 10-4 M NaOH (Alfa Aesar 97%) in distilled water. The final material was recovered by centrifugation, and washed three times with 1 M NaNO3 in distilled water. Acid washed Sn-Beta (Sn-Beta-AW), was made by stirring the triply-exchanged Sn-Beta (Sn-Beta-3Ex) in 1 M H2SO4 (Macron Fine Chemicals, > 51%) for 1 h at ambient temperature, followed by separation by filtration and washing with 1 L of distilled water in 100 mL batches. Finally the material was dried in room temperature air and calcined in flowing air (1.67 $cm^3$ $s^{-1}$, Air Liquide, breathing grade) at 853 K (0.0167 K $s^{-1}$). We note that the dehydration of sodium-exchanged materials resulted in changes in their catalytic properties;

therefore, to ensure comparable saturation of the samples with water, 24 h prior to reaction testing, all samples were placed in a chamber whose humidity was controlled by a saturated NaCl solution.

## 4.3 Ammonia Adsorption onto Sn-Beta

Ammonia gas dosing experiments were performed on Sn-Beta samples after drying in a Schlenk flask at 473 K for 2 h under vacuum. The dried Sn-Beta was cooled under dynamic vacuum to ambient temperature, and the flask was backfilled to 101 kPa of anhydrous ammonia gas (Matheson Tri-Gas, 99.99%). After 24 h, the excess ammonia was evacuated and the sample was exposed to atmosphere (Sn-Beta-NH3). The ammonia-saturated material was regenerated by calcination (Sn-Beta-NH3-Cal) in flowing air (1.67 $cm^3$ $s^{-1}$, Air Liquide, breathing grade) for 6 h at 853 K (0.0167 K $s^{-1}$).

## 4.4 Argon Adsorption

Ar adsorption isotherms at 87 K were obtained using a Quantachrome Autosorb iQ automated gas sorption analyzer. Zeolite samples were degassed at 353 K (0.167 K $s^{-1}$) for 1 h, 393 K (0.167 K $s^{-1}$) for 3 h and 623 K (0.167 K $s^{-1}$) for 8 h prior to recording dry sample weight. For Sn-Beta-$NH_3$, the temperature during the degassing procedure never exceeded 473 K (0.167 K $s^{-1}$). Relative pressures ($P/P_0$) were measured between $10^{-7}$ and 1 at 87 K with precise volumetric Ar doses. Total micropore volume of each sample was determined from linear extrapolation of its Ar uptake in the mesopore regions ($P/P_0$ ~ 0.1-0.4) to zero relative pressure and from the liquid Ar molar density (0.035 mol $cm^{-3}$).

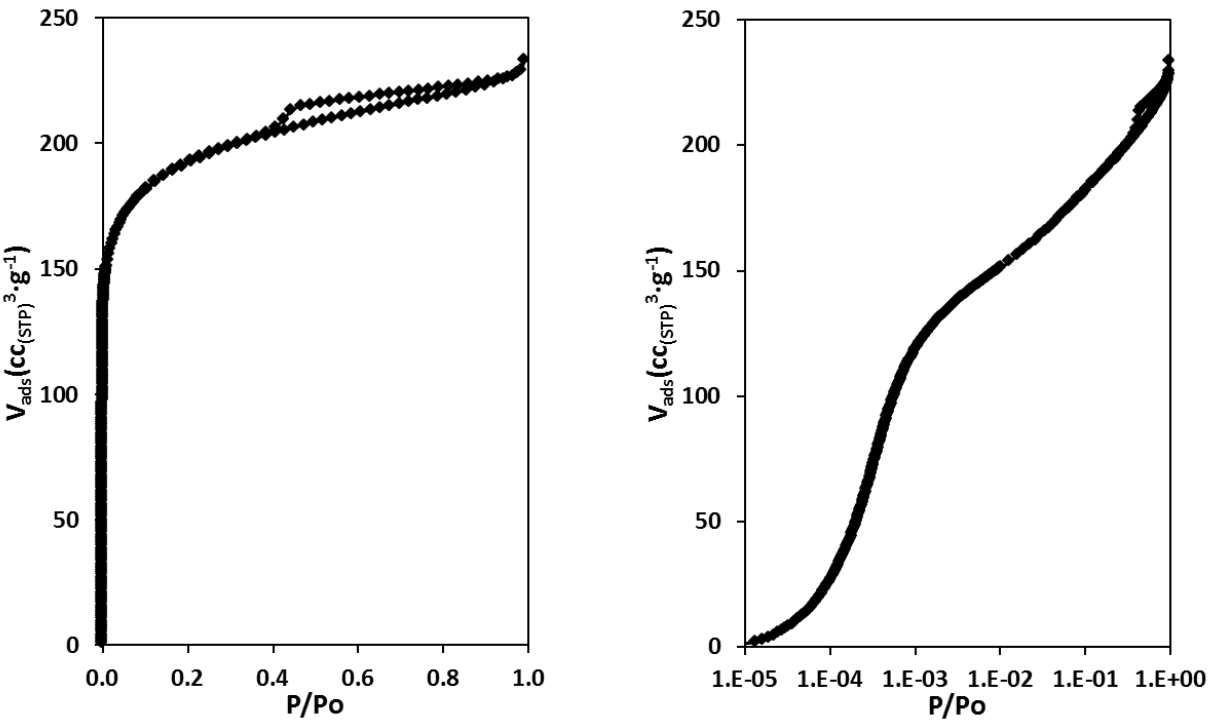


Figure 4.13 Ar adsorption isotherm (87 K) for Sn-Beta.

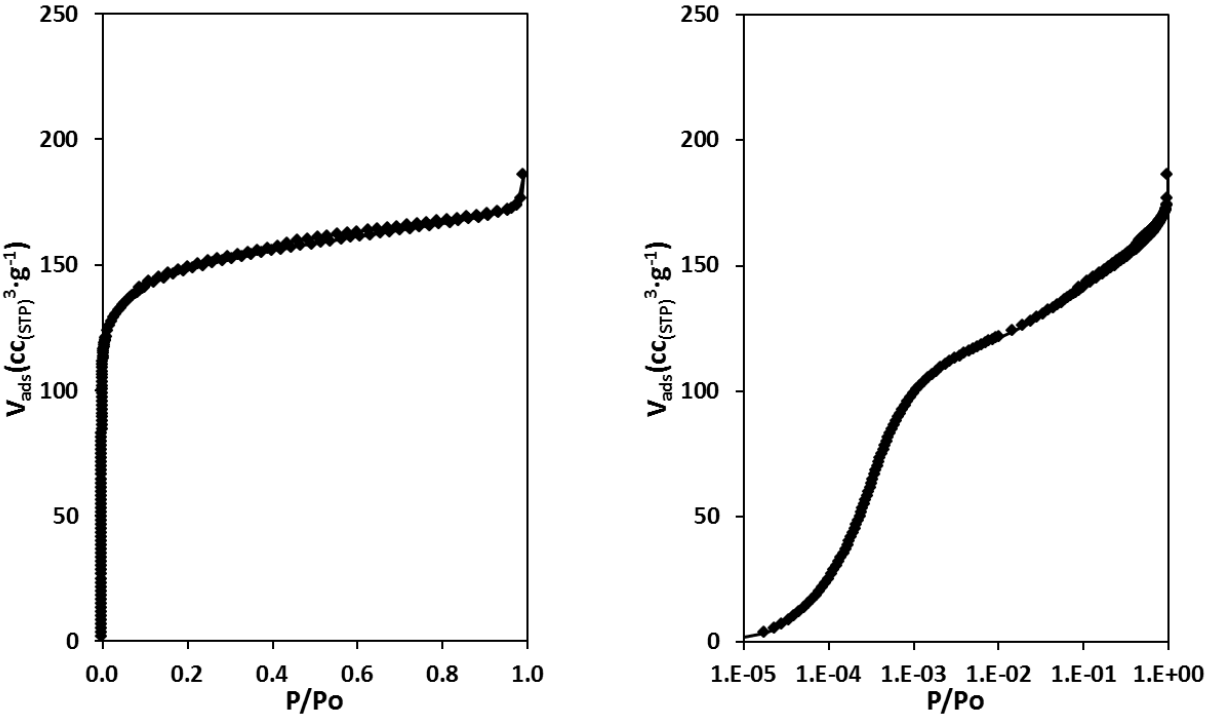


Figure 4.14 Ar adsorption isotherm (87 K) for Sn-Beta-1Ex.

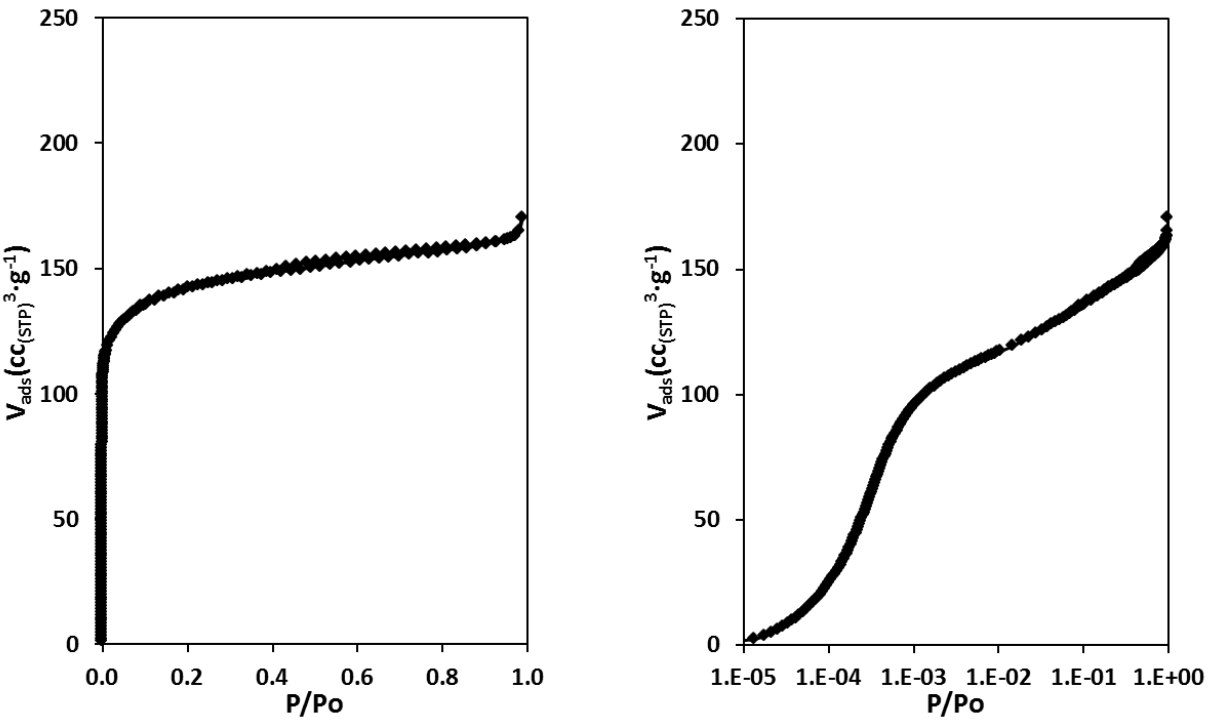


**Figure 4.15 Ar adsorption isotherm (87 K) for Sn-Beta-2Ex.**

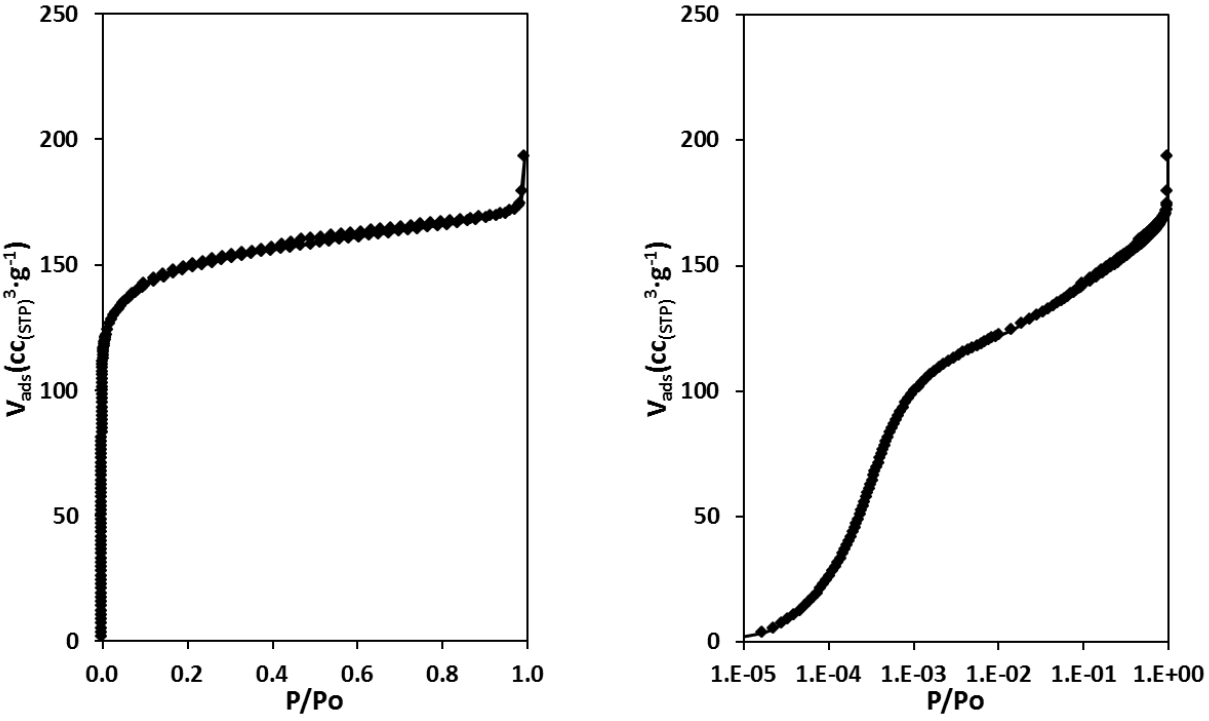


**Figure 4.16 Ar adsorption isotherm (87 K) for Sn-Beta-3Ex.**

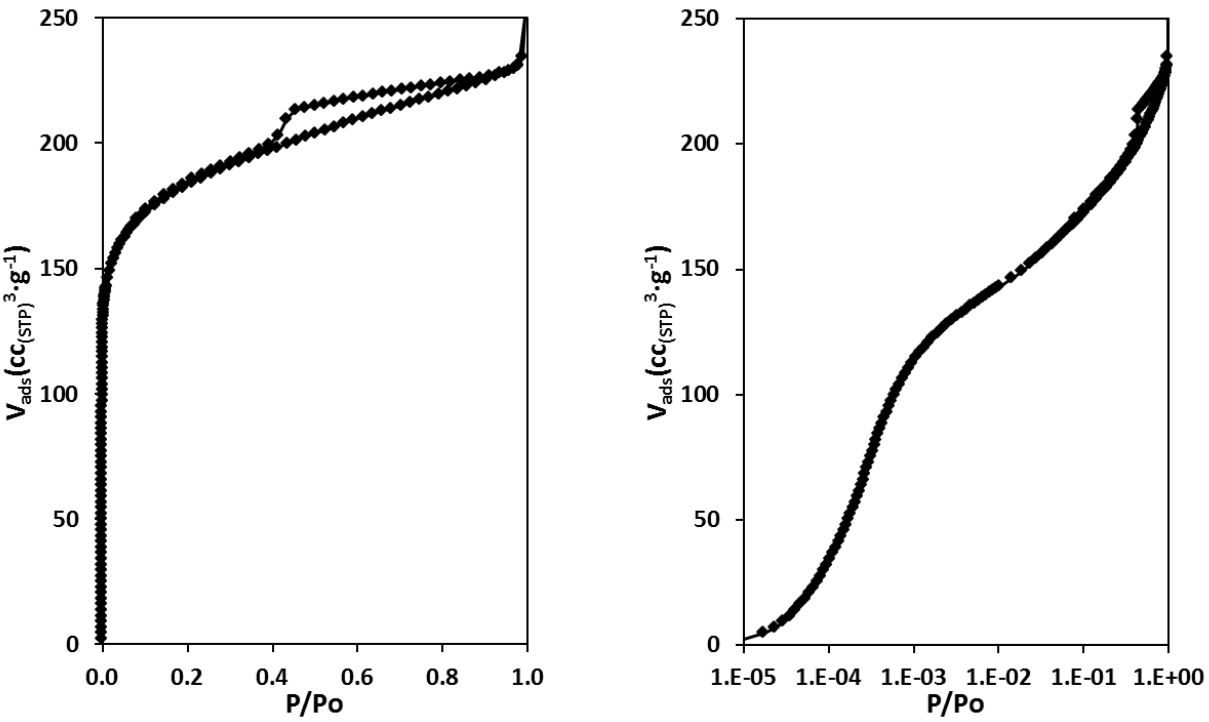


**Figure 4.17 Ar adsorption isotherm (87 K) for Sn-Beta-AW.**

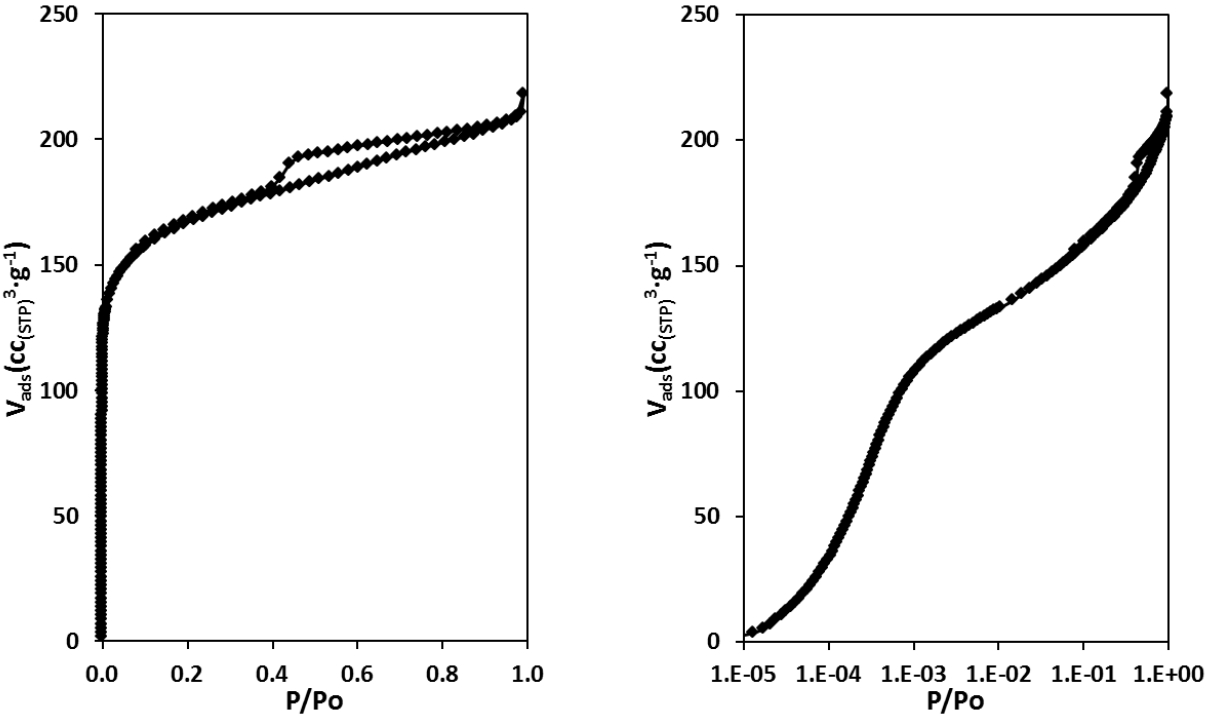


**Figure 4.18 Ar adsorption isotherm (87 K) for Sn-Beta-$NH_3$.**

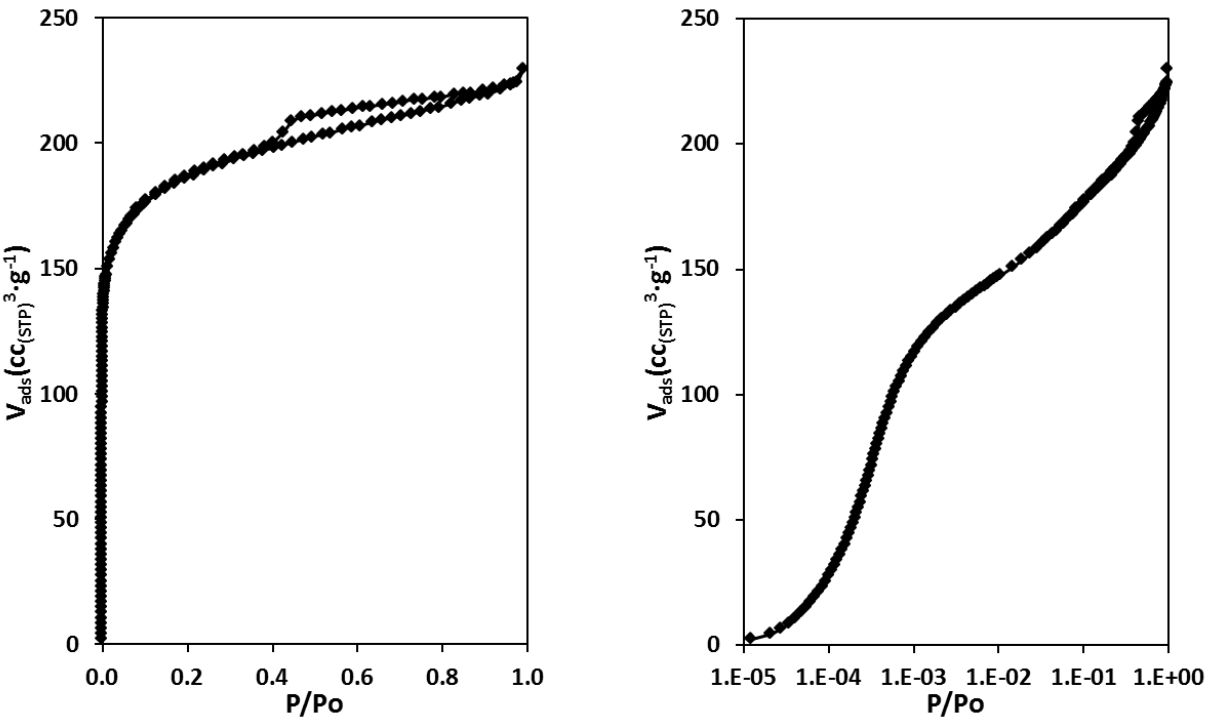


**Figure 4.19 Ar adsorption isotherm (87 K) for Sn-Beta-$NH_3$-Cal.**

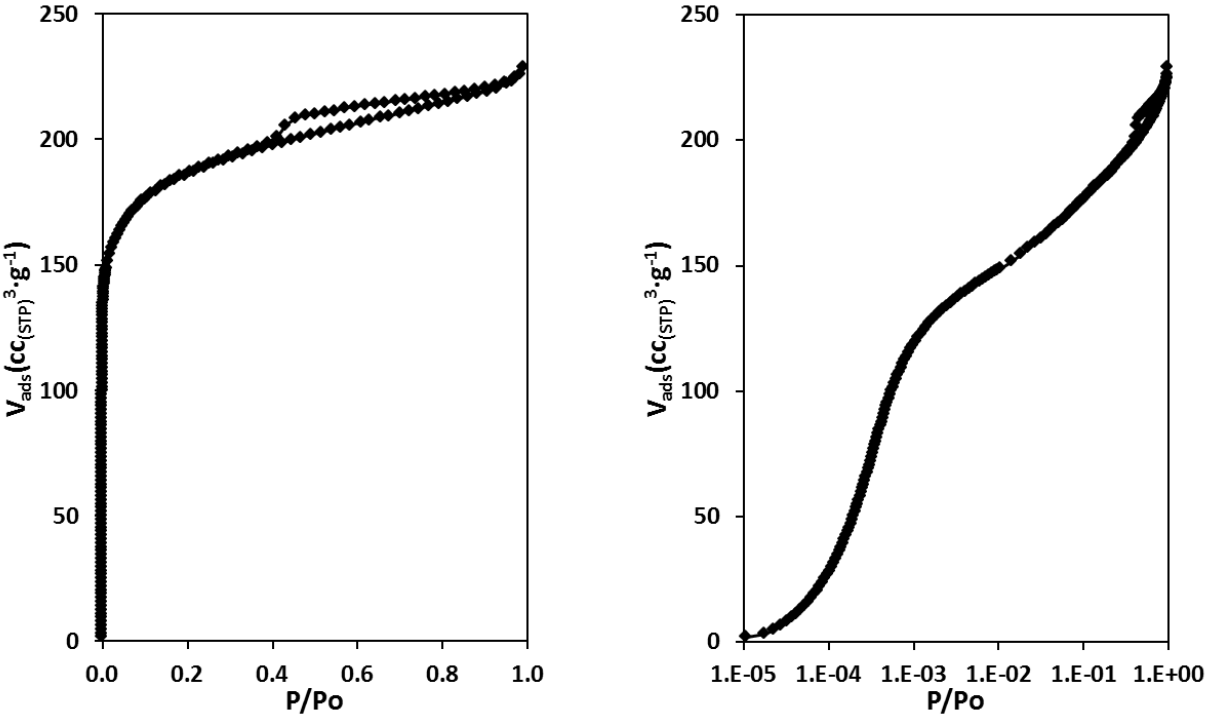


**Figure 4.20 Ar adsorption isotherm (87 K) for Na-Sn-Beta-100.**

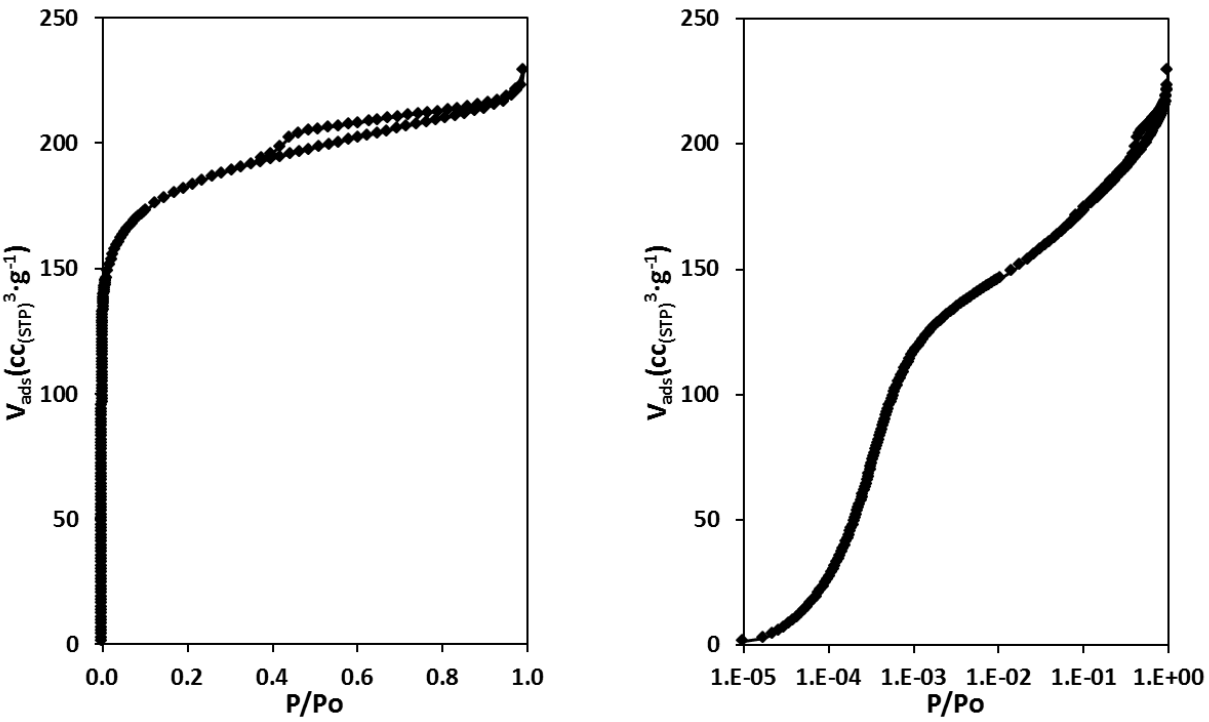


**Figure 4.21 Ar adsorption isotherm (87 K) for Na-Sn-Beta-60.**

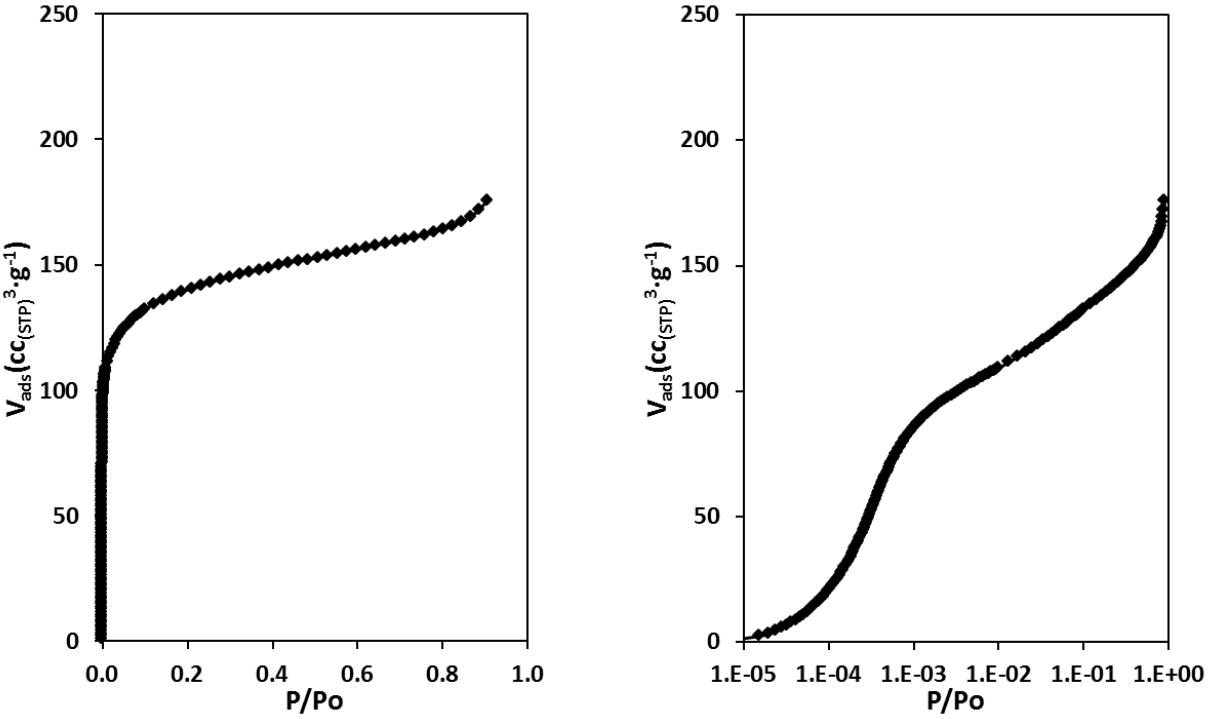


**Figure 4.22 Ar adsorption isotherm (87 K) for Na-Sn-Beta-30.**

## 4.5 Scanning Electron Microscopy and X-ray Diffraction Characterization Methods

Scanning electron microscopy (SEM) with Energy Dispersive X-ray Spectroscopy (EDS) measurements were recorded on a LEO 1550 VP FE SEM at an electron high tension (EHT) of 15 kV. The crystalline structures of zeolite samples were determined from powder X-ray diffraction (XRD) patterns collected using a Rigaku Miniflex II diffractometer and Cu Kα radiation.

## 4.6 Infra-Red Spectroscopy

Deuterated acetonitrile dosing and desorption experiments were performed according to the procedure described elsewhere.[25] A Nicolet Nexus 470 Fourier transform infrared (FTIR) spectrometer with a Hg-Cd-Te (MCT) detector was used to record spectra in 4000-650 $cm^{-1}$ range with a 2 $cm^{-1}$ resolution. Self-supporting wafers (10-20 mg $cm^{-2}$) were pressed and sealed in a heatable quartz vacuum cell with removable KBr windows. The cell was purged with air (1 $cm^3$ $s^{-1}$, Air Liquide, breathing grade) while heating to 373 K (0.0167 K $s^{-1}$), where it was held for 12h, followed by evacuation at 373 K for > 2h (< 0.01 Pa dynamic vacuum; oil diffusion pump), and cooling to 308 K under dynamic vacuum. $CD_3CN$ (Sigma-Aldrich, 99.8% D-atoms) was purified by three freeze (77 K), pump, thaw cycles, then dosed to the sample at 308 K until the Lewis acid sites were saturated. At this point, the first FTIR spectrum in the desorption series was recorded. The cell was evacuated down to 13.3 Pa, and the second spectrum was recorded. Then, the cell was evacuated under dynamic vacuum while heating to 433 K (0.0167 K $s^{-1}$). Concurrently, a series of FTIR spectra were recorded (2 min for each spectrum) at 5 minute intervals. The resulting spectra were baseline-corrected, and the most illustrative spectra were chosen for presentation. The spectra are not normalized by the number of Sn sites.

Spectral artifacts known as "interference fringes" were removed using a computational method based on digital filtering techniques and Fourier analysis.[26]

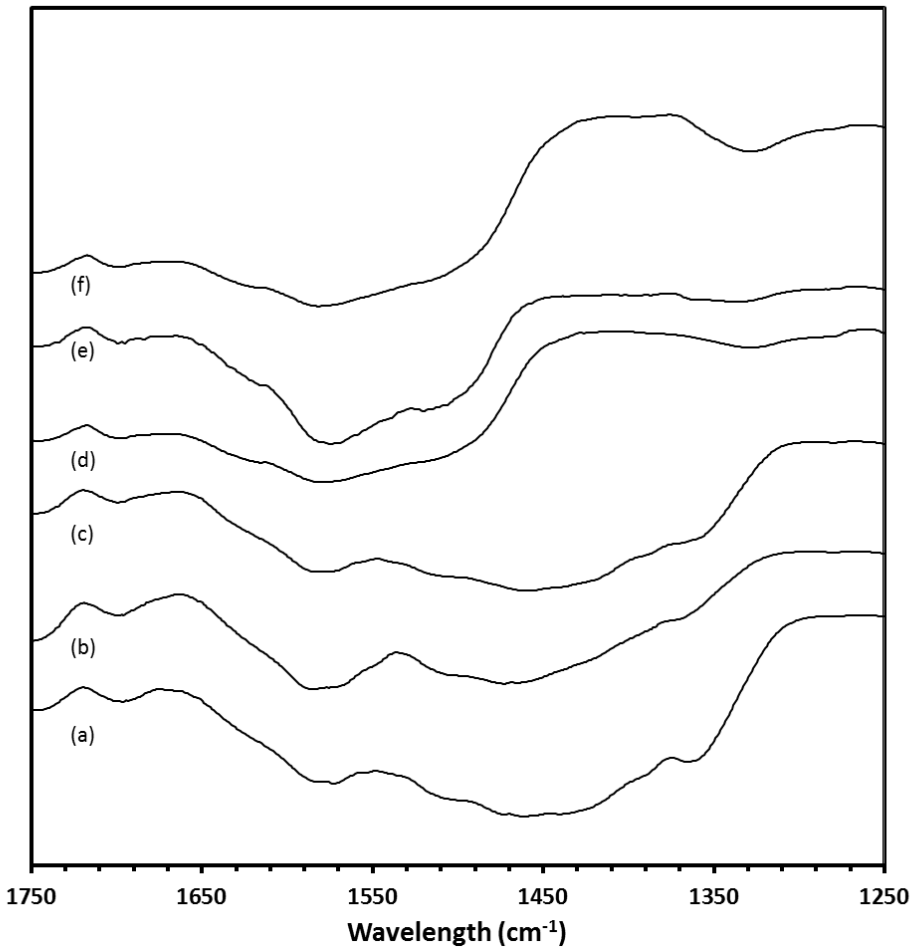


**Figure 4.23 IR spectra of (a) Sn-Beta, (b) Sn-Beta-AW, (c) Sn-Beta-$NH_3$-Cal, (d) Sn-Beta-1Ex, (e) Sn-Beta-2Ex, and (f) Sn-Beta-3Ex showing the presence or absence of a broad nitrate ion absorption band in the 1300 $cm^{-1}$ -1500 $cm^{-1}$ range[19]**

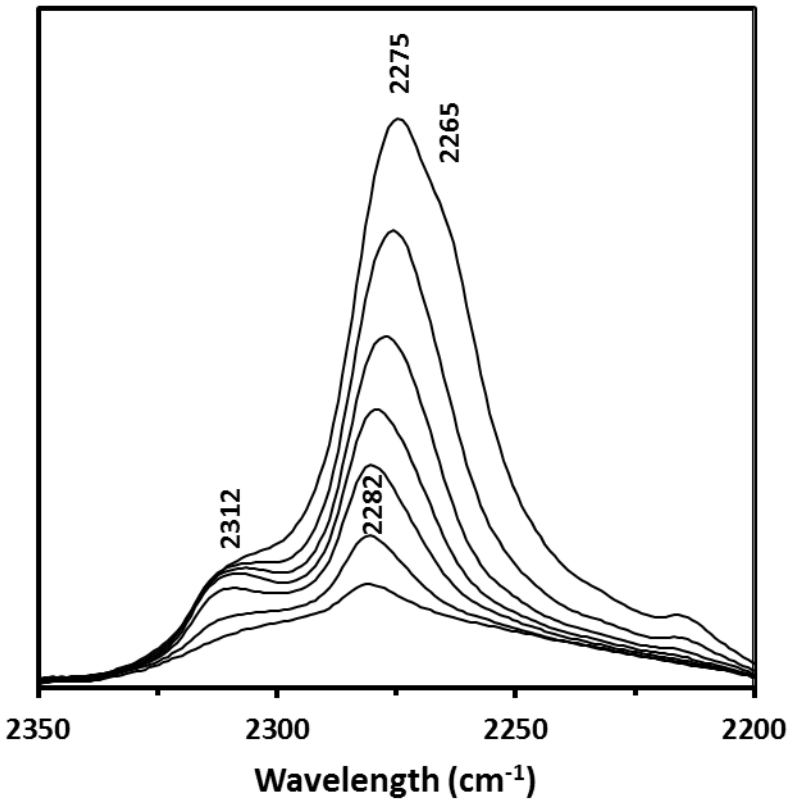


**Figure 4.24 Baseline corrected IR spectra with decreasing $CD_3CN$ coverage on Sn-Beta-1Ex.**

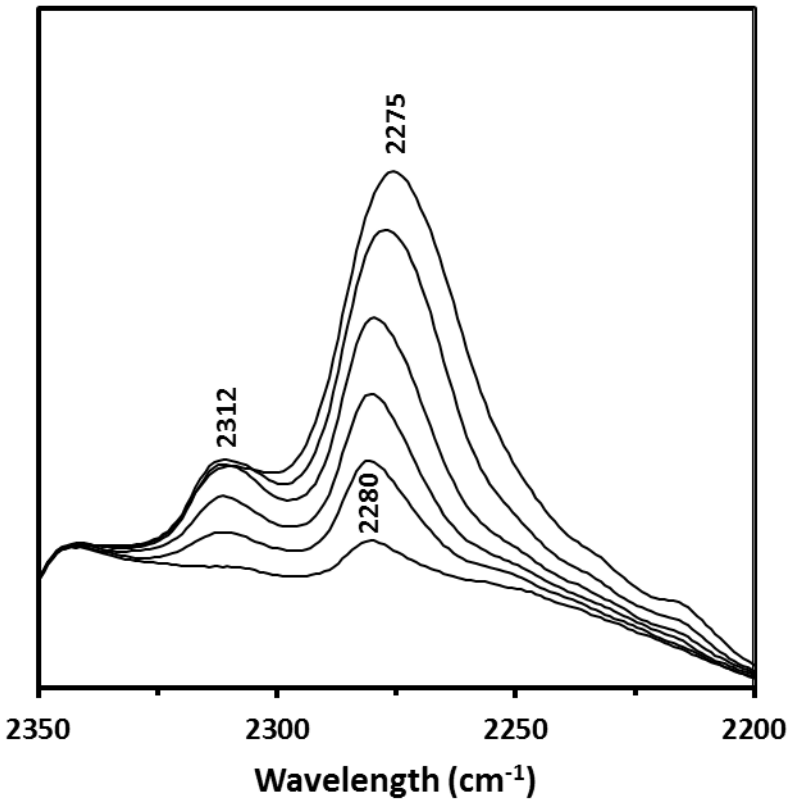


**Figure 4.25 Baseline corrected IR spectra with decreasing $CD_3CN$ coverage on Sn-Beta-2Ex.**

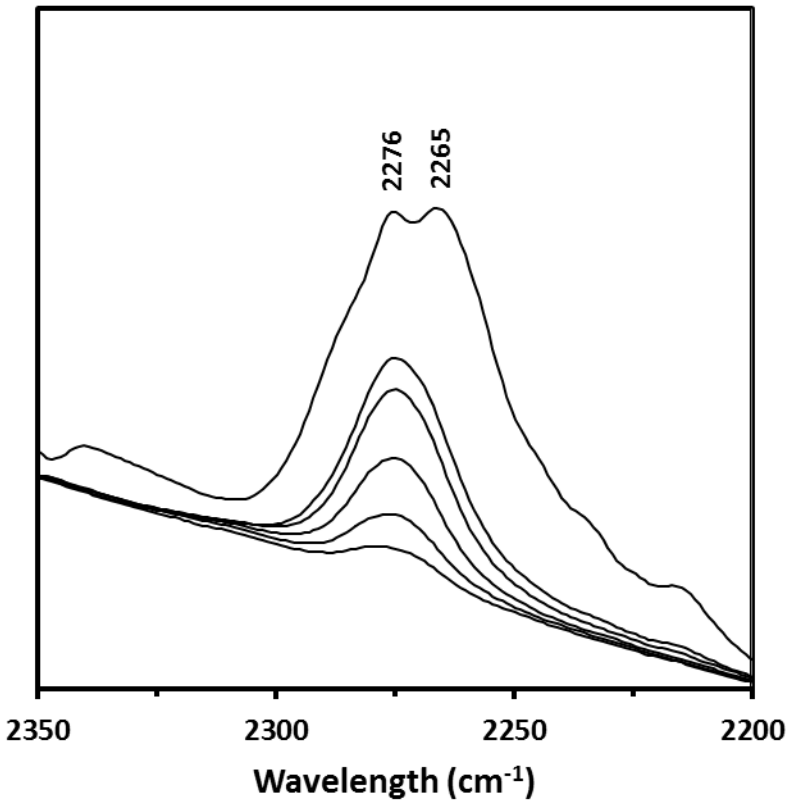


**Figure 4.26 Baseline corrected IR spectra with decreasing $CD_3CN$ coverage on Si-Beta-3Ex.**

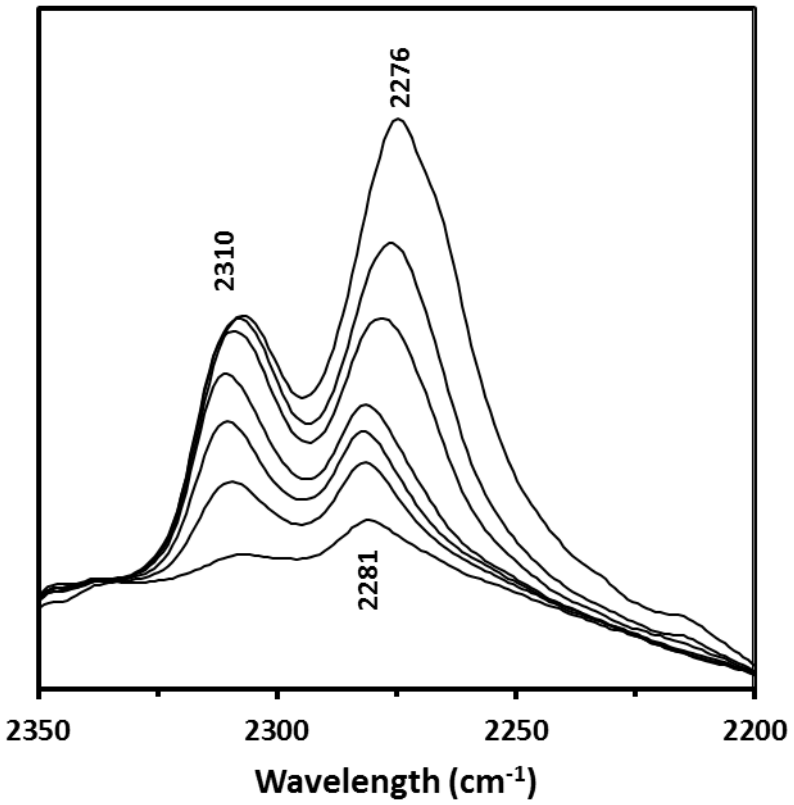


**Figure 4.27 Baseline corrected IR spectra with decreasing acetonitrile coverage on Na-Sn-Beta-30. This spectrum was collected after a 2h 773 K vacuum activation.**

## 4.7 $^{119}$Sn Solid-State NMR and Liquid NMR

Solid-state magic angle spinning nuclear magnetic resonance (MAS-NMR) measurements were performed using a Bruker Avance 500MHz spectrometer equipped with a 11.7 T magnet and a Bruker 4mm broad band dual channel MAS probe. The operating frequencies were 500.2 MHz and 186.5 MHz for $^{1}$H and $^{119}$Sn nuclei, respectively. Approximately 60-80 mg of powder were packed into 4mm $ZrO_2$ rotors and spun at 14 kHz for MAS or cross polarization (CP) MAS experiments at ambient condition. $^{119}$Sn{$^{1}$H} CP condition was optimized at radiofrequency pulse power of 62.5 kHz $\pm$ $\nu_r$ , where $\nu_r$ is spinning frequency, and spectra were recorded using 2 ms contact time. The recycle delay times were 20 sec and 2 sec for $^{119}$Sn MAS

and CPMAS experiments, respectively. Signal averaging over 8,000 scans was performed for the CPMAS spectrum of $^{119}$Sn-Beta dehydrated after $NH_3$ dosing, while averaging over 30,000 scans was performed for the CPMAS spectrum of $^{119}$Sn-Beta dehydrated after three Na-exchanges.

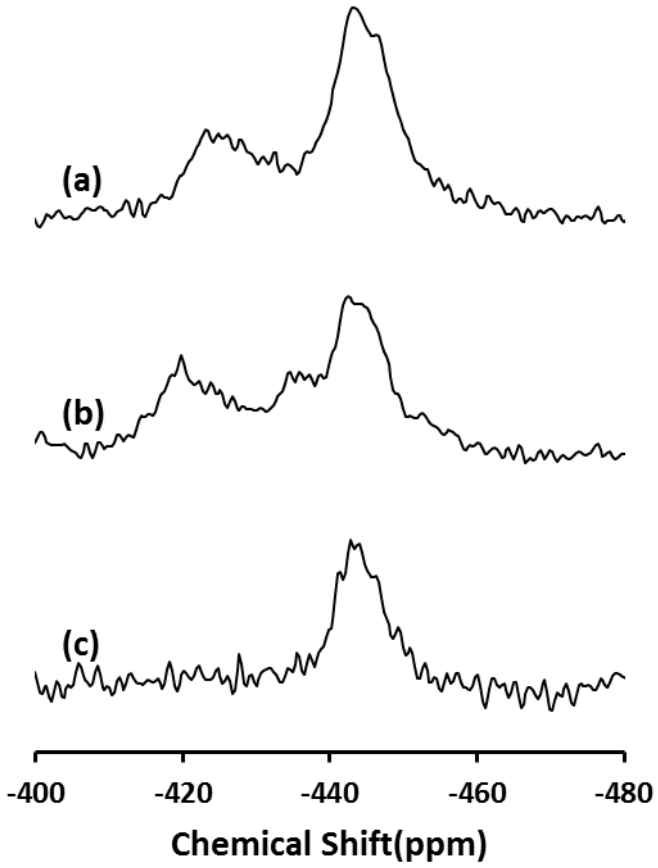


**Figure 4.28 Expanded chemical shift range in the -400 to -480 ppm region of $^{119}$Sn MAS Solid State NMR spectra of $^{119}$Sn-Beta after different treatments: (a) dehydration after calcination, (b) dehydration after three Na-exchanges and (c) dehydration after $NH_3$ adsorption.**

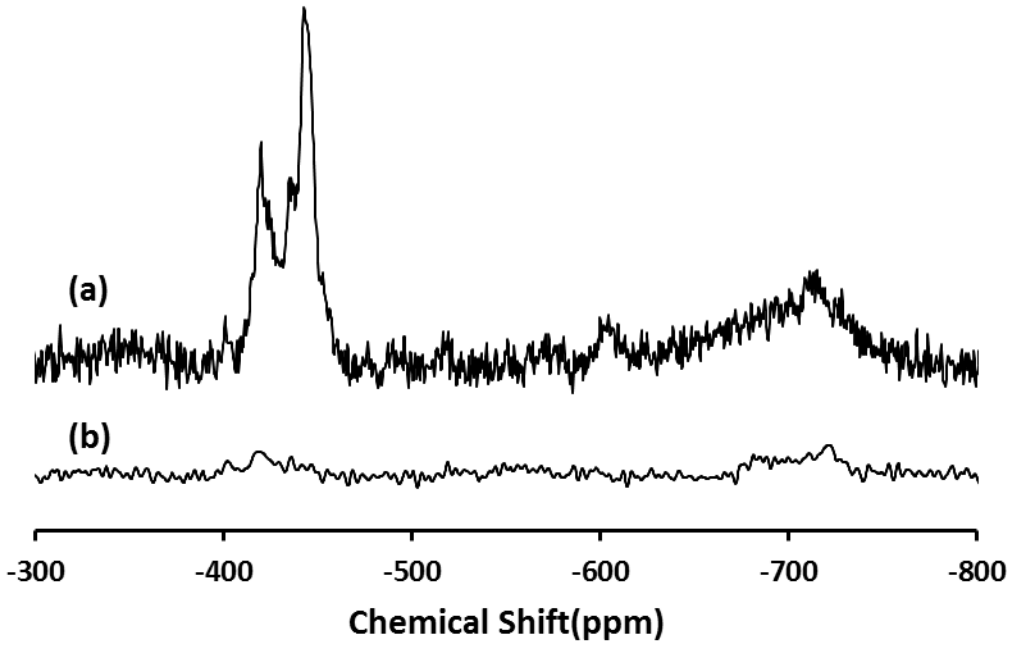


**Figure 4.29 $^{119}$Sn NMR of three times Na-exchanged $^{119}$Sn-Beta dehydrated at 397 K for 2h: (a) MAS spectrum and (b) CPMAS spectrum with 2ms contact time.**

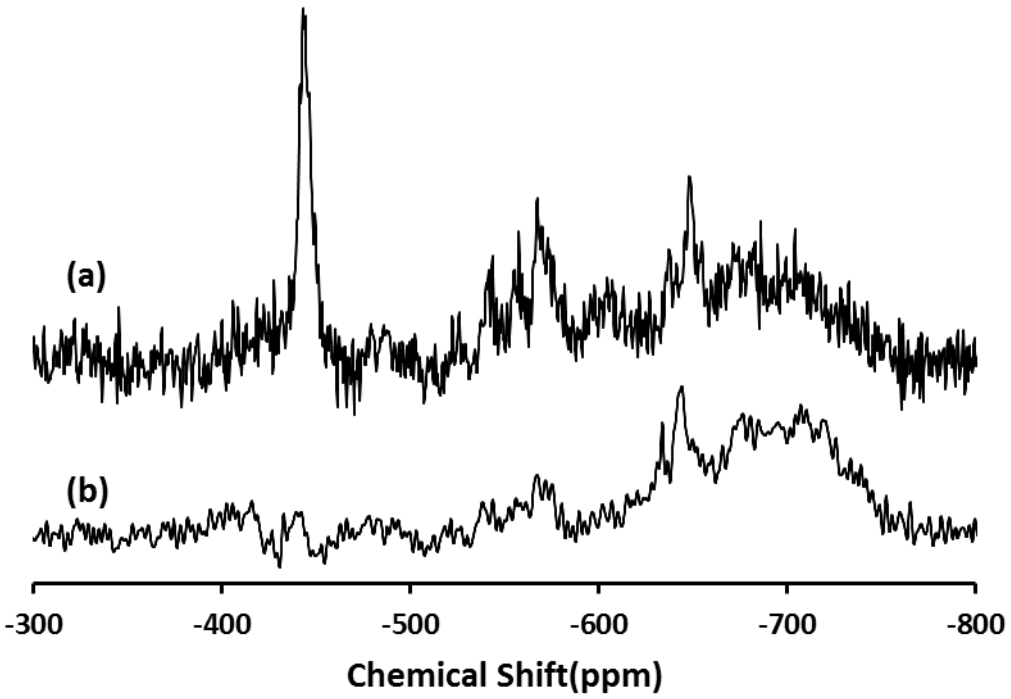


**Figure 4.30 $^{119}$Sn NMR of $NH_3$-dosed $^{119}$Sn-Beta dehydrated at 397 K for 2h: (a) MAS spectrum and (b) CPMAS spectrum with 2ms contact time.**

Liquid $^{13}C$ Nuclear Magnetic Resonance, NMR, spectra were recorded using a Varian INOVA 500 MHz spectrometer equipped with an auto-x pfg broad band probe. Carbon chemical shifts are reported relative to the residual solvent signal. $^{13}C$ NMR spectra were acquired with 2000 scans.

4.8 Reaction Procedures

Reactions with D-glucose (Sigma-Aldrich, ≥99%) were conducted in 10 ml thick-walled glass reactors (VWR) that were heated in a temperature-controlled oil bath. Reactions were prepared with a 1:100 Sn:glucose molar ratio using 5.0 g of a 1% (w/w) glucose solution with approximately 20 mg of catalyst. For reactions performed to investigate the effects of addition of NaCl to aqueous glucose reactant solution, 0.2 g of NaCl were added per 1.0 g of 1% (w/w) glucose solution. Reactors were placed in the oil bath at 353 K and approximately 50 mg aliquots were extracted at 10, 20 and 30 minutes. These reaction aliquots were mixed with 50 mg of a 1% (w/w) D-mannitol (Sigma-Aldrich, ≥98%) solution as an internal standard for quantification, diluted with 0.3 ml of $H_2O$ and filtered with a 0.2 μm PTFE syringe filter.

Recyclability experiments were performed with Sn-Beta-3Ex reacted with glucose in water and methanol under the previously stated reaction conditions (353 K for 30 min in a 1% (w/w) with 1:100 Sn:glucose molar ratio) and washed once with the solvent used in the reaction. The solids were centrifuged and dried with room temperature air.

Reaction aliquots were analyzed by high performance liquid chromatography (HPLC) using an Agilent 1200 system (Agilent) equipped with PDA UV (320 nm)

and evaporative light scattering (ELS) detectors. Glucose, fructose, mannose and mannitol fractions were separated with a Hi-Plex Ca column (6.5 x 300 mm, 8 μm particle size, Agilent) held at 358 K, using ultrapure water as the mobile phase at a flow rate of 0.6 mL $s^{-1}$.

Reactions with labeled $^{13}C$ glucose at the C1 position (Cambridge Isotope Laboratories,1-$^{13}C$ D-glucose, 98-99%) and deuterium (D) in the C2 position of glucose (Cambridge Isotope Laboratories, D-glucose-D2, > 98%) were conducted under the same conditions as those with D-glucose. The reaction was ended by quenching after 30 minutes. The reaction solution was filtered and rotavaporated to separate the solvent from the reactant-product mixture. These recovered solids were dissolved in deuterium oxide and analyzed using $^{13}C$ NMR.

## 4.9 Glucose Conversion and Fructose and Mannose Yields

Table 4-2 and Table 4-3 of the main text provide glucose conversion and fructose and mannose yields at 30 minutes of reaction. The following tables provide the same type of data for 10 and 20 minute times of reaction.

| | | *10 minutes* | | | *20 minutes* | | |
|---|---|---|---|---|---|---|---|
| **Catalyst** | **Solvent** | $X_{Gluc.}(\%)$ | $Y_{Fruc.}(\%)$ | $Y_{Mann.}(\%)$ | $X_{Gluc.}(\%)$ | $Y_{Fruc.}(\%)$ | $Y_{Mann.}(\%)$ |
| Sn-Beta | $H_2O$ | 1.0 | 1.0 | 0.0 | 3.4 | 2.9 | 0.4 |
| | $CH_3OH$ | 12.0 | 4.8 | 0.0 | 20.4 | 9.1 | 1.8 |
| Sn-Beta-1Ex. | $H_2O$ | 2.9 | 0.0 | 1.0 | 3.6 | 0.8 | 1.6 |
| | $CH_3OH$ | 8.9 | 0.0 | 2.3 | 10.6 | 2.8 | 3.6 |
| Sn-Beta-2Ex. | $H_2O$ | 2.2 | 0.0 | 0.8 | 4.9 | 0.0 | 2.4 |
| | $CH_3OH$ | 7.9 | 0.0 | 2.4 | 10.5 | 0.0 | 4.4 |
| Sn-Beta-3Ex. | $H_2O$ | 4.4 | 0.0 | 1.3 | 5.8 | 0.0 | 3.2 |
| | $CH_3OH$ | 8.2 | 0.0 | 2.7 | 11.7 | 0.0 | 5.0 |
| Sn-Beta-AW | $H_2O$ | 2.4 | 0.0 | 0.0 | 3.8 | 2.3 | 0.0 |
| | $CH_3OH$ | 9.9 | 2.2 | 2.2 | 12.1 | 4.7 | 2.7 |
| Na-Sn-Beta-100 | $H_2O$ | 2.8 | 0.0 | 1.5 | 4.1 | 2.9 | 1.1 |
| | $CH_3OH$ | 9.2 | 3.2 | 2.1 | 14.0 | 6.3 | 2.7 |
| Na-Sn-Beta-60 | $H_2O$ | 1.8 | 0.0 | 1.3 | 4.3 | 2.5 | 1.9 |
| | $CH_3OH$ | 8.1 | 2.7 | 2.7 | 13.3 | 6.2 | 2.7 |
| Na-Sn-Beta-30 | $H_2O$ | 3.0 | 0.0 | 2.2 | 3.1 | 0.0 | 2.9 |
| | $CH_3OH$ | 5.1 | 0.0 | 2.5 | 5.1 | 0.0 | 3.6 |
| Sn-Beta-$NH_3$ | $H_2O$ | 0.0 | 0.0 | 0.0 | 2.3 | 0.0 | 2.0 |
| | $CH_3OH$ | 2.7 | 0.0 | 1.4 | 2.7 | 0.0 | 1.5 |
| Sn-Beta-$NH_3$-Cal | $H_2O$ | 1.7 | 0.0 | 0.0 | 2.8 | 1.7 | 0.0 |
| | $CH_3OH$ | 11.0 | 2.5 | 1.7 | 14.8 | 5.0 | 2.5 |

**Table 4-5 Glucose conversion (X) and fructose and mannose yields (Y) in $H_2O$ and $CH_3OH$ solvents. Reaction conditions: 1% (w/w) glucose solutions, 1:100 metal:glucose ratio, 353 K, 10 and 20 min.**

| | | *10 minutes* | | | *20 minutes* | | |
|---|---|---|---|---|---|---|---|
| **Catalyst** | **Solvent** | $X_{Gluc.}(\%)$ | $Y_{Fruc.}(\%)$ | $Y_{Mann.}(\%)$ | $X_{Gluc.}(\%)$ | $Y_{Fruc.}(\%)$ | $Y_{Mann.}(\%)$ |
| Sn-Beta | $H_2O$-NaCl | 5.1 | 1.9 | 2.1 | 9.6 | 3.4 | 3.2 |
| Sn-Beta-1Ex. | $H_2O$-NaCl | 3.5 | 0.0 | 3.0 | 6.3 | 1.5 | 4.4 |
| Sn-Beta-2Ex. | $H_2O$-NaCl | 4.0 | 0.0 | 3.0 | 5.8 | 1.4 | 5.0 |
| Sn-Beta-3Ex. | $H_2O$-NaCl | 3.7 | 0.0 | 3.6 | 9.6 | 0.0 | 6.4 |

**Table 4-6 Glucose conversion (X) and fructose and mannose yields (Y) with 0.2g NaCl/g $H_2O$. Reaction conditions: 1% (w/w) glucose solutions, 1:100 metal:glucose ratio, 353 K, 10 and 20 min.**

## 5. References

1. Bermejo-Deval, R. *et al.* Metalloenzyme-like catalyzed isomerizations of sugars by Lewis acid zeolites. *Proc. Natl. Acad. Sci. U. S. A.* **109,** 9727–32 (2012).

2. Bermejo-Deval, R., Gounder, R. & Davis, M. E. Framework and Extraframework Tin Sites in Zeolite Beta React Glucose Differently. *ACS Catal.* **2,** 2705–2713 (2012).

3. Moliner, M., Román-Leshkov, Y. & Davis, M. E. Tin-containing zeolites are highly active catalysts for the isomerization of glucose in water. *Proc. Natl. Acad. Sci. U. S. A.* **107,** 6164–8 (2010).

4. Nikolla, E., Rom, Y., Moliner, M. & Davis, M. E. "One-Pot" Synthesis of 5-(Hydroxymethyl)furfural from Carbohydrates using Tin-Beta Zeolite. *ACS Catal.* **1,** 408–410 (2011).

5. Collyer, C. A., Henrick, K. & Blow, D. M. Mechanism for aldose-ketose interconversion by D-xylose isomerase involving ring opening followed by a 1,2-hydride shift. *J. Mol. Biol.* **212,** 211–35 (1990).

6. Bhosale, S. H., Rao, M. B. & Deshpande, V. V. Molecular and industrial aspects of glucose isomerase. *Microbiol. Rev.* **60,** 280–300 (1996).

7. Kovalevsky, A. Y. *et al.* Metal ion roles and the movement of hydrogen during reaction catalyzed by D-xylose isomerase: a joint x-ray and neutron diffraction study. *Structure* **18,** 688–99 (2010).

8. Roy, S., Bakhmutsky, K., Mahmoud, E., Lobo, R. F. & Gorte, R. J. Probing Lewis Acid Sites in Sn-Beta Zeolite. *ACS Catal.* **3,** 573–580 (2013).

9. Hayes, M. L., Pennings, N. J., Serianni, A. S. & Barker, R. Epimerization of aldoses by molybdate involving a novel rearrangement of the carbon skeleton. *J. Am. Chem. Soc.* **104,** 6764–6769 (1982).

10. Petrus, L. Reactions of saccharides catalyzed by molybdate ions . XV . Mechanism of the epimerization reaction. *Chem. zvesti* **29,** 690–693 (1975).

11. Bílik, V., Petrus, L. & Zemek, J. Reactions of saccharides catalyzed by molybdate ions . XIX .* Molybdate complexes and epimerization of aldoses as a function of pH. *Chem. zvesti* **32,** 242–251 (1978).

12. Tanase, T. *et al.* C-2 epimerization of aldoses promoted by combinations of metals and diamines involving a novel rearrangement of the carbon skeleton. *J. Chem. Soc. Chem. Commun.* **2,** 659 (1987).

13. Tanase, T., Shimizu, F., Yano, S. & Yoshikawa, S. Novel C-2 epimerization of aldoses and stereoselective uptake of one of the epimeric aldoses by nickel(II) complexes. *J. Chem. Soc. Chem. Commun. Chem. Commun.* 1001–1003 (1986). doi:10.1039/C39860001001

14. Tanase, T. *et al.* Novel C-2 epimerization of aldoses promoted by nickel(II) diamine complexes, involving a stereospecific pinacol-type 1,2-carbon shift. *Inorg. Chem.* **27,** 4085–4094 (1988).

15. Boronat, M., Concepcion, P., Corma, a, Renz, M. & Valencia, S. Determination of the catalytically active oxidation Lewis acid sites in Sn-beta zeolites, and their optimisation by the combination of theoretical and experimental studies. *J. Catal.* **234,** 111–118 (2005).

16. Khouw, C. Catalytic Activity of Titanium Silicates Synthesized in the Presence of Alkali-Metal and Alkaline-Earth Ions. *J. Catal.* **151,** 77–86 (1995).

17. Rai, N., Caratzoulas, S. & Vlachos, D. G. Role of Silanol Group in Sn-Beta Zeolite for Glucose Isomerization and Epimerization Reactions. *ACS Catal.* **3,** 2294–2298 (2013).

18. Perego, C., Carati, A., Ingallina, P., Mantegazza, M. A. & Bellussi, G. Production of titanium containing molecular sieves and their application in catalysis. *Appl. Catal. A Gen.* **221,** 63–72 (2001).

19. Miller, F. a. & Wilkins, C. H. Infrared Spectra and Characteristic Frequencies of Inorganic Ions. *Anal. Chem.* **24,** 1253–1294 (1952).

20. Pelmenschikov, A. G., van Santen, R. A., Jänchen, J. & Meijer, E. CD3CN as a probe of Lewis and Bonsted acidity. *J. Phys. Chem.* **97,** 11071–11074 (1993).

21. Tvaru, Z. & Sobalı, Z. Determination and properties of acid sites in H-ferrierite A comparison of ferrierite and MFI structures. *Microporous Mesoporous Mater.* **24,** 223–233 (1998).

22. Boronat, M. *et al.* Reactivity in confined spaces of zeolites: the interplay between spectroscopy and theory to develop structure-activity relationships for catalysis. *Phys. Chem. Chem. Phys.* **11,** 2876–2884 (2009).

23. Corma, a, Nemeth, L. T., Renz, M. & Valencia, S. Sn-zeolite beta as a heterogeneous chemoselective catalyst for Baeyer-Villiger oxidations. *Nature* **412,** 423–5 (2001).

24. Osanai, S. No Title. *Top. Curr. Chem.* **215,** 43–76 (2001).

25. Gounder, R. & Davis, M. E. Monosaccharide and disaccharide isomerization over Lewis acid sites in hydrophobic and hydrophilic molecular sieves. *J. Catal.* **308,** 176–188 (2013).

26. Faggin, M. F. & Hines, M. A. Improved algorithm for the suppression of interference fringe in absorption spectroscopy. *Rev. Sci. Instrum.* **75,** (2004).

# Chapter 5 : Glucose Conversion into Carboxylic Acids with Sn-Bea and $SnO_2$/Si-Beta

## 1. Introduction

Lactic acid is considered as one of the chemical building blocks of food, pharmacy, cosmetics and chemical industries,[1] being its main focus the production of biodegradable plastics.[2] The singularity of having both carboxyl and functional groups, facilitates the formation of linear polyesters through intramolecular or self-esterification. The molecule itself is chiral, having different internal planes of symmetry. The polymerization of L-lactic acid, poly-L-lactide (PLLA), is known to result in the highest degree of crystallinity, while polymerization of a racemic mixture of lactic acid becomes into poly-D,L-lactide (PDLLA) which is amorphous.[3] High degree of crystallinity is required for the applications of polylactic acid.

The drawbacks affiliated with the biological synthetic route of lactic acid, by means of glucose fermentation, has grown recent interest in developing an efficient catalytic chemical synthesis route.[4] The calcium hydroxide used to maintain the fermentation broth at neutral pH, together with the post sulfuric acid added to reform the acid is not ideal, from an environmental standpoint. Following the biological glycolysis pathway, both homogeneous and heterogeneous catalyst have achieved high lactic acid yields and selectivities in aqueous and alcohol solvents, resulting the latter in alkyl lactates.[5] In alkaline media, chemical conversion of carbohydrates to lactate salts proceeds at low yields (< 30%), due to the harsh reaction conditions (573K).[6] More efficient homogenous catalyst have been used, such as a dual-cation system of Al(III) and Sn(II),[7] cation Pb(II)[7] or lanthanide triflates,[8] resulting in 81%, 71% and 90% lactic acid yields, respectively. Metal oxides in combination of alkaline hydrothermal or superheated water conditions are also active catalysts in the

conversion of monosaccharides to lactic acid. A mixture in aluminum oxide and zirconium oxide lead to 34% yield of lactic acid under superheated water conditions.[9] Higher lactic acid selectivities were seen with platinum supported over carbon, 47%,[10] and copper oxide, 59%.[11]

Zeolite frameworks with isolated Lewis acid centers have shown a unique ability in the formation of lactic acid from C3- and C6-sugars.[5] Sn-Beta has a higher methyl lactate yield over Ti-Beta and Zr-Beta at 160ºC, being 43%, 31% and 33%, respectively.[12] Surprisingly, with Sn-Beta a higher lactic acid yield is achieved starting from sucrose, 64%, a disaccharide composed of monosaccharides glucose and fructose. The overall reaction pathway is believed to be following the one seen in Figure 5.1, similarly to the glycolysis pathway.[13] Firstly, is the isomerization of glucose into fructose, by intramolecular hydride shift. Secondly, is the retro-aldol reaction of fructose into the two C3-sugars glyceraldehyde and dihydroxyacetone, being the rate determining step, which these two can also isomerize by intramolecular hydride shift. Then glyceraldehyde dehydrates into pyruvaldehyde. Finally, isomerization of these species by intramolecular hydride shift will lead to the formation of lactic acid in water and methyl lactate in methanol. Analogously, glucose could go through retro-aldol C4-C5 to form vinyl glycolitic acid in water or methyl vinyl glycolate in methanol. In addition, fructose dehydration will lead to 5-hydroxymethylfurfural (HMF).

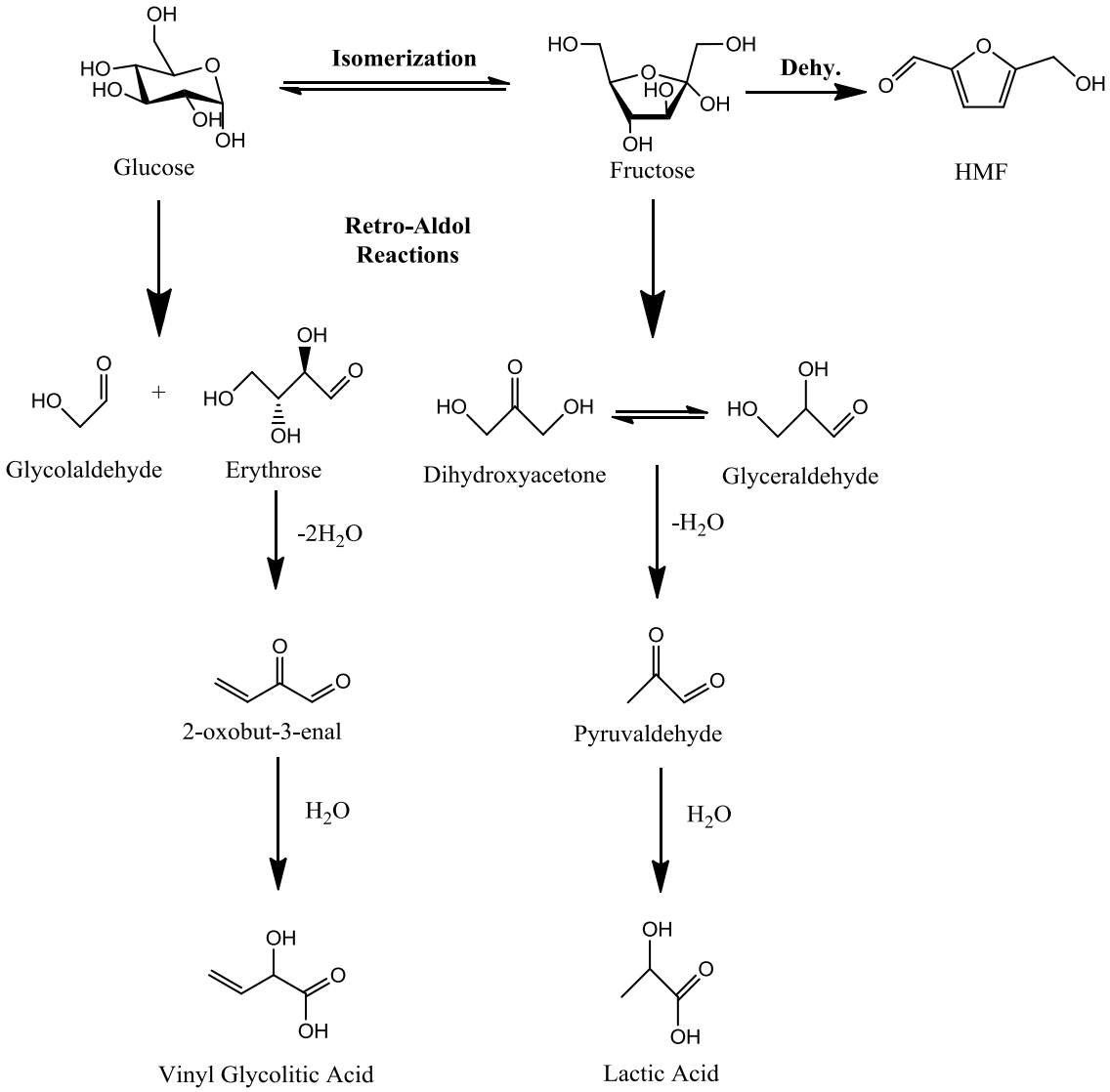


**Figure 5.1 Reaction pathway to form vinyl glycolytic acid, lactic acid and HMF.**

The conversion of $C_3$-sugars into lactic acid, in water, or alkyl lactates, in alcohol, can be done at much lower temperatures.[14] At 80ºC full conversion of dihydroxyacetone into methyl lactate in methanol and a 90% yield of lactic acid in water is obtained with Sn-Beta. Both $C_3$- and $C_6$-sugars lead to lower yields of lactic acid in water, which could be emerging from the degradation of the sugars by the Brønsted acidity of the carboxylic acid. Protonation of the different intermediates by the carboxylic acid will decrease the selectivity of lactic acid.[15,16] An example of this

is pyruvaldehyde, a highly reactive intermediate, whose aldehyde group hydrates in water and could go through other molecular transformations,[17] instead of the intramolecular hydride shift to finally form lactic acid.

The rate limiting step in the conversion of C3-sugars into lactic acid with Sn-Beta is suggested to be its dehydration into pyruvaldehyde.[18] Higher rates are observed for the 1,2-hydride shift of pyruvaldehyde to lactic acid or methyl lactate, in contrast to the dehydration of glyceraldehyde to pyruvaldehyde. The hydride shift is analogous to the one taking place between dihydroxyacetone to glyceraldehyde and glucose to fructose. The Lewis acid centers in Sn-Beta have the ability to redistribute the oxidation states between among the carbon atoms of the same molecule. Similarly, in between the carbon atoms of two distinct molecules, there is an intermolecular redistribution of the oxidation states by Meerwein-Ponndorf-Verley aldehyde and ketone reduction and Oppenauer alcohol oxidation (MPVO) reactions, as has been described in Chapter 1.

Conventional zeolites are also active in the conversion of $C_3$-sugars into lactate derivatives.[14,19] Higher reaction temperatures (110-120ºC) and post-synthesis treatments are needed with conventional zeolite Y and Beta. The formation of Lewis acid sites by steaming the zeolite shifts the Brønsted acid sites to extraframework alumina, diminishing the formation of pyruvaldehyde dimethyl acetal and increasing the selectivity towards methyl lactate.[14] Since Brønsted acidity in zeolite Y is not active in the 1,2-hydride shift, further acetylation of pyruvaldehyde occurs. Al-Beta zeolite with Si/Al ratio of 65 can be treated under steaming conditions at 750ºC for 20 hours, changing the methyl lactate yield from 3% to 32% with dihydroxyacetone at 115ºC.[14]

In this chapter the formation of lactic acid from glucose was studied with Sn-Beta and extraframework $SnO_2$ deposited on Si-Beta ($SnO_2$/Si-Beta) in both water and methanol solvents. The formation of lactic acid was measured over a period of 8 hours. In addition, $^{13}C$ isotopic labeling in the $C_1$ and $C_2$ position of the monosaccharides was monitored by $^{13}C$ NMR to identify the molecular rearrangements. While intermediates were identified through these studies, they were not added to the carbon balance as these were detected in trace amounts. Since the catalysts used were fully characterized in previous chapters, Sn-Beta (Chapter 2, 3 and 4) and $SnO_2$/Si-Beta (Chapter 3), there physical and chemical properties can be seen in those.

## 2. Results and Discussion

### 2.1 Glucose Conversion and Product Distribution

The formation of lactic acid required lower glucose to Sn ratio and longer reaction times than those seen in previous chapters. This is due to retro-aldol reaction, the C-C cleavage in the monosaccharides, which is believed to be the rate limiting step.[12] The glucose conversion and product distribution was measured with a 1% (wt/wt) glucose solution in water and methanol at 100ºC and 120ºC with Sn-Beta and $SnO_2$/Si-Beta for eight hours. The difference in activity previously seen between the two catalysts, Chapter 3, led to the use of different glucose to tin ratios, being *c.a.* 30 for Sn-Beta and 15 for $SnO_2$/Si-Beta. Figure 5.2 and Figure 5.3 show the glucose reacted per tin atom in the zeolite over the course of eight hours for 100ºC and 120ºC, respectively. In all cases an increase in activity was seen at higher temperatures and with methanol as a solvent. Sn-Beta exhibits a higher glucose conversion, demonstrating the higher Lewis acidity of the isolated Sn sites in the framework. Gorte *et al.*[20] have shown with adsorbed deuterated acetonitrile in the IR how Sn-Beta

has a higher Lewis acid strength in comparison to extraframework $SnO_2$ in Si-Beta. The catalytic activity of metal oxides is known to be found at its defect sites.[21] In this case it is hard to compare the strength of the defect site in the metal oxide with the "open" site of zeolite Sn-Beta, considered the active site, since the number and distribution of these is unknown in each catalyst. In the case of Sn-Beta in methanol, full glucose conversion was reached after two hours and one hour, respectively, indicating the high reactivity of the isolated tin centers in a non-aqueous solvent. This would suggest that some of the Lewis acid sites in Sn-Beta are not completely hydrophobic, being susceptible to water attack and consequently deactivation.

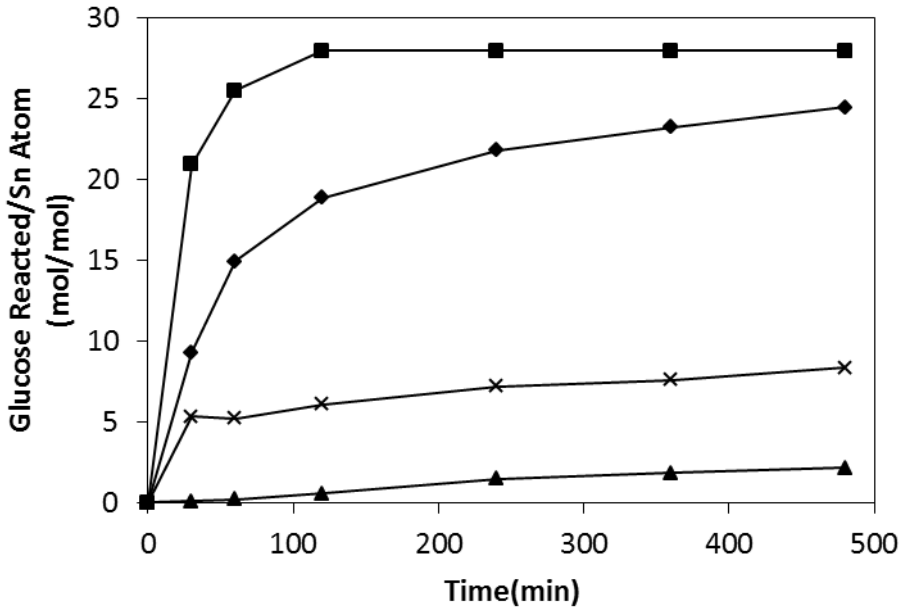


**Figure 5.2 Glucose reacted per tin atom for 8 hours at 100ºC with Sn-Beta in water (diamond), Sn-Beta in methanol (square), $SnO_2$/Si-Beta in water (cross) and $SnO_2$/Si-Beta in methanol (triangle).**

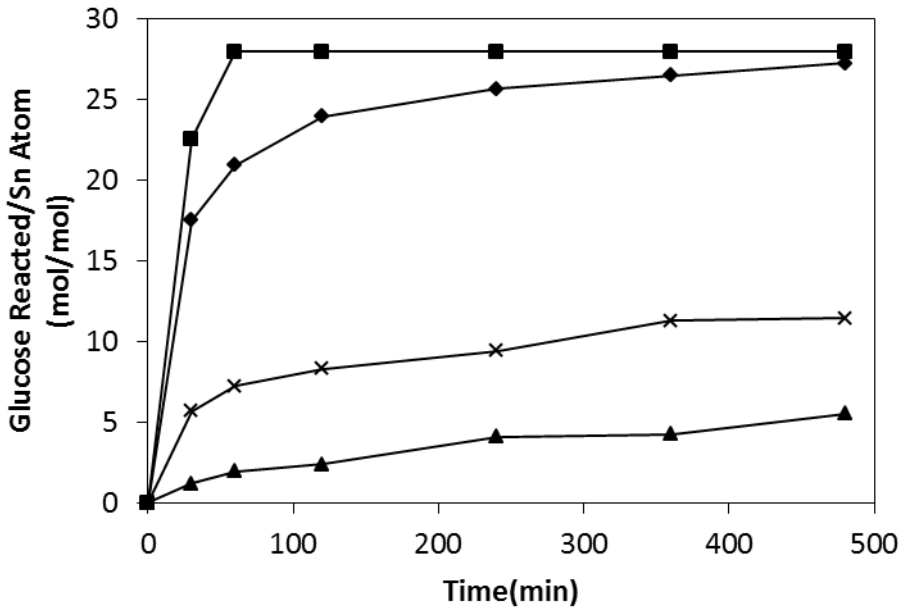


**Figure 5.3 Glucose reacted per tin atom for 8 hours at 120ºC with Sn-Beta in water (diamond), Sn-Beta in methanol (square), $SnO_2$/Si-Beta in water (cross) and $SnO_2$/Si-Beta in methanol (triangle).**

In Figure 5.4 and Figure 5.5 the product distributions can be seen from a 1% glucose (wt/wt) aqueous solution with Sn-Beta at 100ºC and 120ºC. The carbon balances were similar to previous results in our group,[22] with no carboxylic acids analyzed. At 110ºC the carbon balance was almost 80% at approximately 35% glucose conversion in 90 min with 10% (wt/wt) aqueous glucose solution and 50:1 glucose to tin ratio.[22] In this study, comparable results were obtained for 120 min at 100ºC and 30 min at 120ºC. Mannose (Mann) also reached a maximum yield at 120 min (9.1%) at 100ºC and 60 min (7.4%) at 120ºC. The disappearance of mannose could also be due to the formation of fructose. As it was described in Chapter 2, mannose would preferentially isomerize to fructose than epimerize to glucose with Sn-Beta.

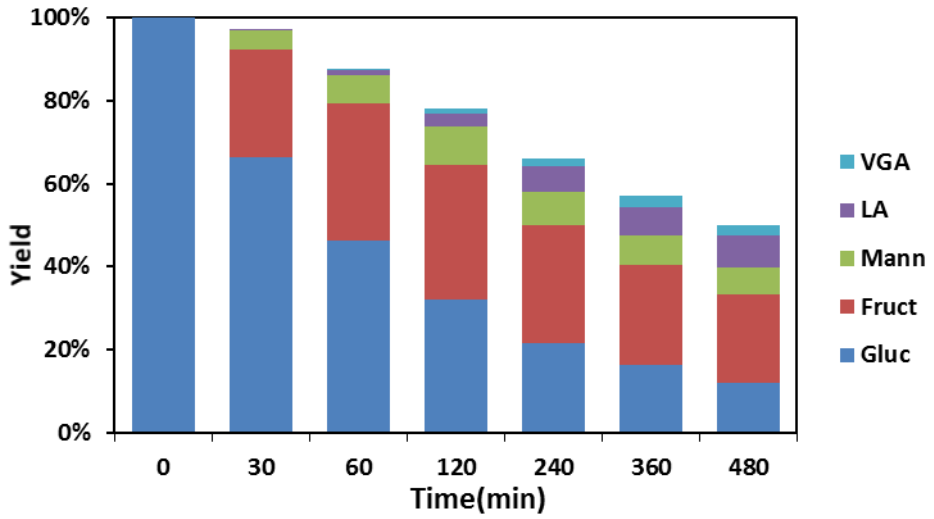


**Figure 5.4 Monosaccharides and carboxylic acids distribution from a 1% (wt/wt) glucose solution in water with Sn-Beta at 100ºC with glucose to tin ratio of 30.**

The formation of carboxylic acid acids with Sn-Beta in water was seen at both temperatures 100ºC and 120ºC (Figure 5.4 and Figure 5.5, respectively) being higher for lactic acid (LA) than for vinylglycolic acid (VGA). Lactic acid was formed at glucose conversions higher than 34% (for 100ºC), with at least 25% fructose yields, proving the formation of lactic acid is related to the presence of fructose in the solution. The maximum lactic acid yields were of 8% and 16 % for 100ºC and 120ºC, respectively. The carbon to carbon bond formation in aldol-reaction is known to be exothermic,[23] which would be in agreement with our results for the reverse process, retro-aldol. However, since we are not in the equilibrium the formation of lactic acid seems to be controlled by kinetics. Analogously, vinylglycolic acid yields were higher at 120ºC (5%) than at 100ºC (2%). The higher formation of lactic acid was in accordance with the simulation studies in Chapter 2, with higher rate constants for the fructose sink than the glucose sink. Holm *et al.*[12] reported 29% yield of lactic acid at 160ºC with similar glucose to Sn ratios (*c.a.* 30:1), but having the reaction vessel purged with argon.

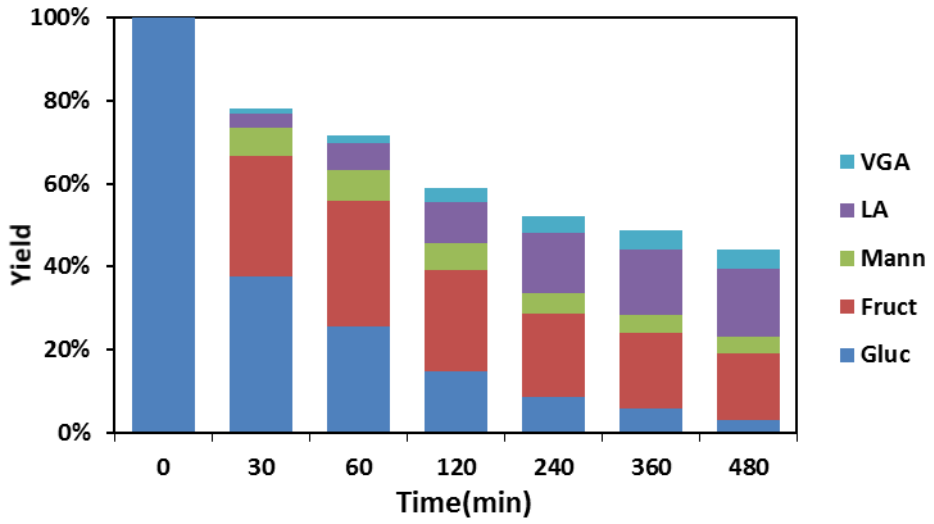


**Figure 5.5 Monosaccharides and carboxylic acids distribution from a 1% (wt/wt) glucose solution in water with Sn-Beta at 120ºC with glucose to tin ratio of 30.**

With Sn-Beta the solvent was changed to methanol, leading to higher glucose conversions and carboxylic acid yields. The fructose analyzed was a mixture of fructose and methyl fructoside, which reached maximum yields at 30 min for 100ºC (27%) and 120ºC (9%). The maximum methyl lactate yields were of 8% and 22% for 100ºC and 120ºC, respectively. These results were much lower than those reported by Holm *et al.*,[12] with 43% methyl lactate yields at 160ºC. Higher yields of methyl vinylglycolate were formed in methanol than in water, reaching 6% at 120ºC. As in water, the formation of carboxylates is greatly influenced by the temperature of the reaction, being higher as the temperature is increased. It has been suggested that alkyl lactates are much more stable than carboxylic acids, having no Brønsted acidity that could lead to the dehydration/hydration of other species,[12] such as HMF. The product distribution was approximately the same after 240 min, suggesting the deactivation of the Lewis acid sites in Sn-Beta or the deposition of different organic products in the zeolite pores blocking the intra-diffusion of the molecules.

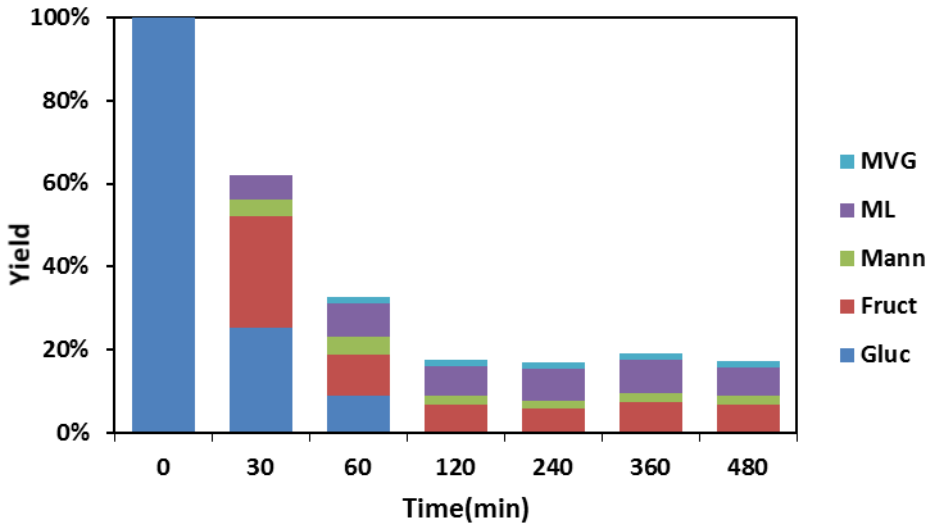


**Figure 5.6 Monosaccharides and carboxylic acids distribution from a 1% (wt/wt) glucose solution in methanol with Sn-Beta at 100ºC with glucose to tin ratio of 30.**

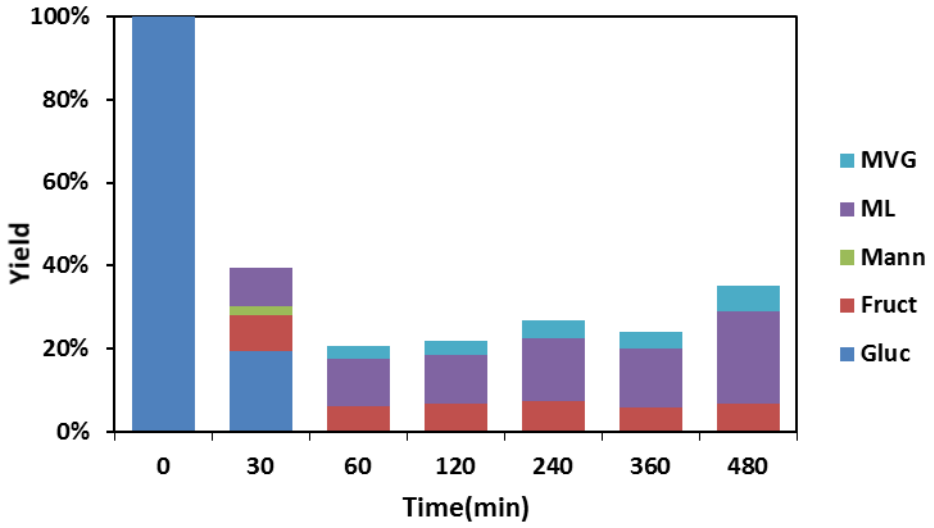


**Figure 5.7 Monosaccharides and carboxylic acids distribution from a 1% (wt/wt) glucose solution in methanol with Sn-Beta at 120ºC with glucose to tin ratio of 30.**

The conversion of 1% (wt/wt) glucose in water over $SnO_2$/Si-Beta formed fructose as the primary product. $SnO_2$/Si-Beta can isomerize glucose to fructose through the base enolate intermediate.[24] $SnO_2$ needs to be located within the zeolite micropores to provide a hydrophobic environment to which water will not deactivate the Lewis acid sites. Glucose will then isomerize into fructose inside of the pores.

However, the product yields were quite low since the clusters are not as active as the isolated framework Sn sites in Sn-Beta, as it can be seen in Figure 5.8 and Figure 5.9. Also, these $SnO_2$ clusters occupy part of the micropore volume restricting the diffusion of glucose inside of the zeolite, as apparent activation energies were half of those with the homogenous catalyst sodium hydroxide.[24] Increasing the temperature of the reaction from 100ºC to 120ºC raised the fructose yield from 10% to 30%, resulting in traces of lactic acid. Therefore, lactic acid could only be formed during much longer reaction times than eight hours at 120ºC.

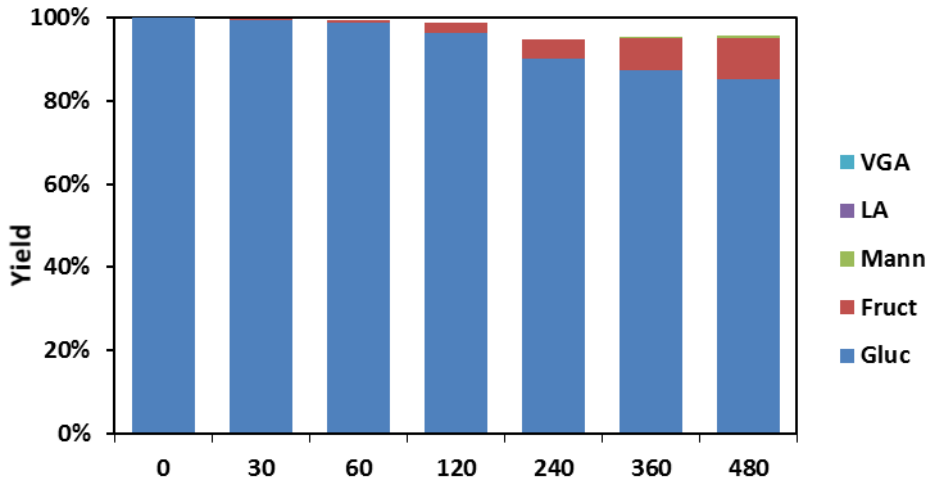


**Figure 5.8 Monosaccharides and carboxylic acids distribution from a 1% (wt/wt) glucose solution in water with $SnO_2$/Si-Beta at 100ºC with glucose to tin ratio of 15.**

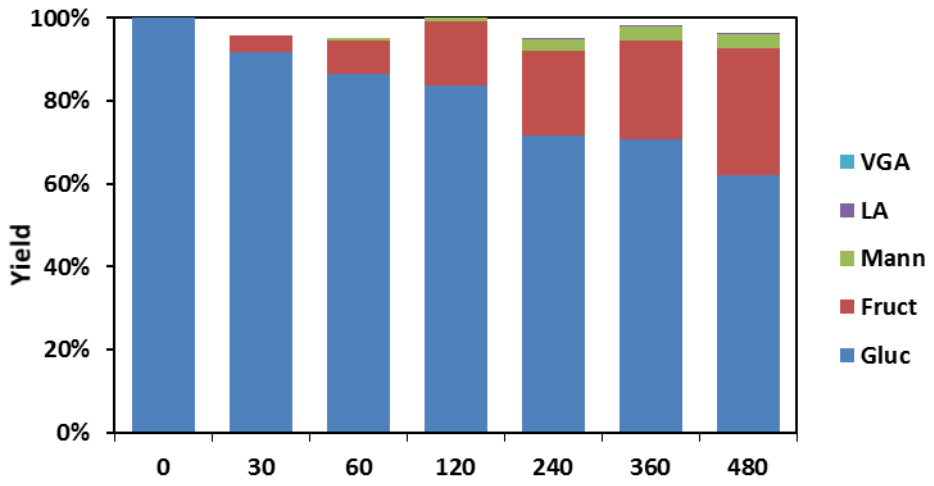


**Figure 5.9 Monosaccharides and carboxylic acids distribution from a 1% (wt/wt) glucose solution in water with $SnO_2$/Si-Beta at 120ºC with glucose to tin ratio of 15.**

In methanol $SnO_2$/Si-Beta was much more active in the isomerization of glucose and retro-aldol reactions. The isomerization mechanism of glucose to fructose with $SnO_2$/Si-Beta in methanol is analogous to the one in water, base enolate intermediate.[24] In this case, $SnO_2$ is active in both the inside and outside of the micropores, since methanol does not seem to inhibit the active sites of $SnO_2$ as water does. This was reflected in the higher glucose conversions, reaching 57% and 79% at 100ºC and 120ºC, respectively, after 480 minutes.

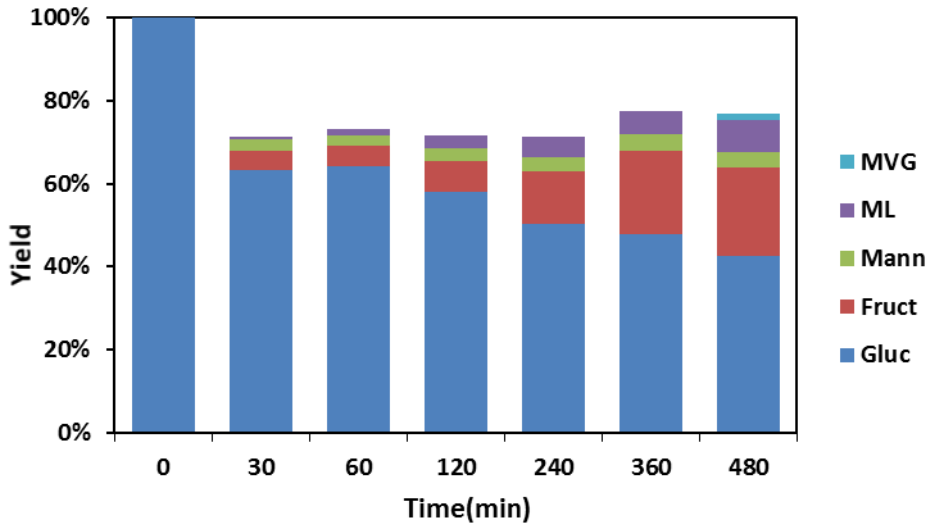


**Figure 5.10 Monosaccharides and carboxylic acids distribution from a 1% (wt/wt) glucose solution in methanol with $SnO_2$/Si-Beta at 100ºC with glucose to tin ratio of 15.**

The formation of carboxylates from a 1% (wt/wt) glucose solution in methanol confirms that $SnO_2$/Si-Beta is also active in the retro-aldol reaction of both glucose and fructose. The raise in temperature does also increase formation of carboxylates with $SnO_2$/Si-Beta, with methyl lactate and methyl vinylglycolate yields of 8% and 2% at 100ºC and 11% and 2% at 120ºC, respectively. This could also be in agreement with the retro-aldol reaction being the rate-limiting step, although further rate analysis among the different intermediates would be required to confirm these findings. When these results are compared with Sn-Beta in water, the product distribution seems quite similar at equal glucose conversion. With Sn-Beta in water, at 74% glucose conversion, 6% and 2% yields of lactic acid and vinylglycolic acid, respectively, were obtained after 60 minutes at 120ºC, with a carbon balance of 71%. Similarly, with $SnO_2$/Si-Beta in methanol, at 77% glucose conversion, 9% and 2% yields of methyl lactate and methyl vinylglycolate, respectively, were obtained after 360 min at 120ºC, with a carbon balance of 67%. Therefore, the $SnO_2$ in Si-Beta does not seem to show

a change in the product distribution in comparison to Sn-Beta, only a lower activity in the synthesis of carboxylic acids.

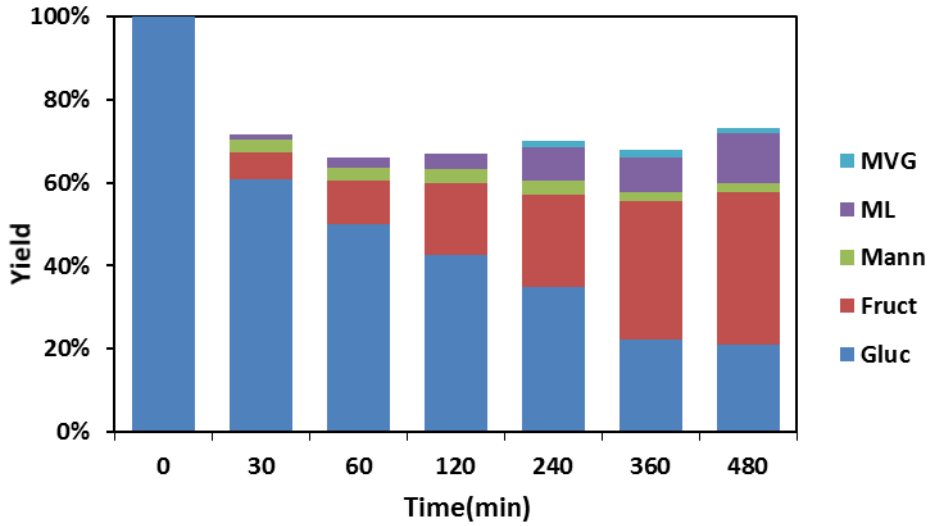


**Figure 5.11 Monosaccharides and carboxylic acids distribution from a 1% (wt/wt) glucose solution in methanol with $SnO_2$/Si-Beta at 120ºC with glucose to tin ratio of 15.**

2.2 Carboxylate Formation Mechanism

Since the product distribution is quite similar for both catalysts, Sn-Beta and $SnO_2$/Si-Beta, the molecular mechanism of the carboxylates formation was studied using $^{13}C$ as an isotopic tracer. Starting from $^{13}C$1-glucose and $^{13}C$2-fructose, $^{13}C$ NMR was used to identify some of the molecular transformations occurring along the pathway described in Figure 5.1. The reaction conditions were similar to the ones seen in the previous section, with the exception of the reaction time, which was approximated to reach 70% conversion. This study was only performed in the cases of Sn-Beta in water, Sn-Beta in methanol and $SnO_2$/Si-Beta in methanol. $SnO_2$/Si-Beta in water was not analyzed due to the low activity at 100ºC and 120ºC.

The $^{13}C$ NMR spectra of the different products in solution can be seen in the figures below. In Figure 5.12 and Figure 5.13 the $^{13}C$ NMR spectra show a high

number of resonance bands that can be related to the $^{13}C$ labeling of different molecules. In the following figures the chemical shifts were focused on the plausible intermediates suggested by Holm *et al.*,[12] which were not identified by High Performance Liquid Chromatography (HPLC). In addition, other chemical shifts appear that were not identified. This coincides with the low carbon balances seen in the previous experiments.

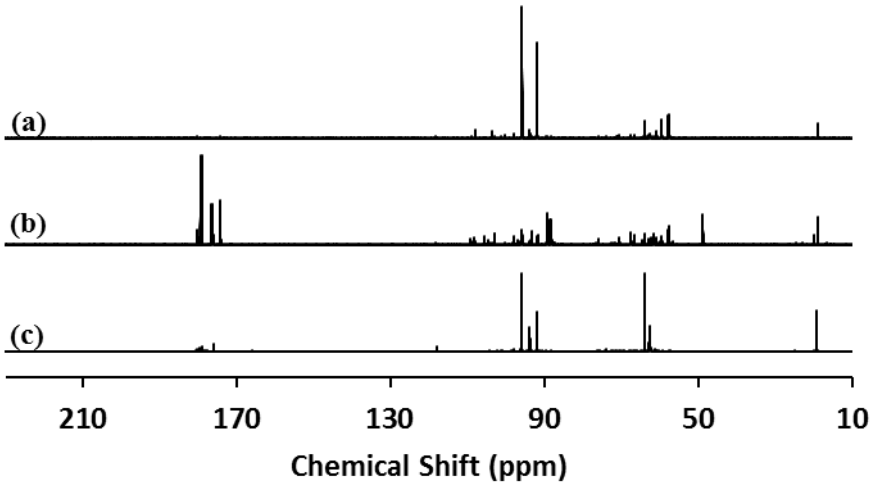


**Figure 5.12 $^{13}C$ NMR spectra of product mixture using $^{13}C1$-glucose with (a) $SnO_2$/Si-Beta in methanol, (b) Sn-Beta in methanol and (c) Sn-Beta in water. Reaction conditions: 1% (wt/wt) monosaccharide with a monosacc/Sn ratio of 30 and 15 for Sn-Beta and $SnO_2$/Si-Beta, respectively.**

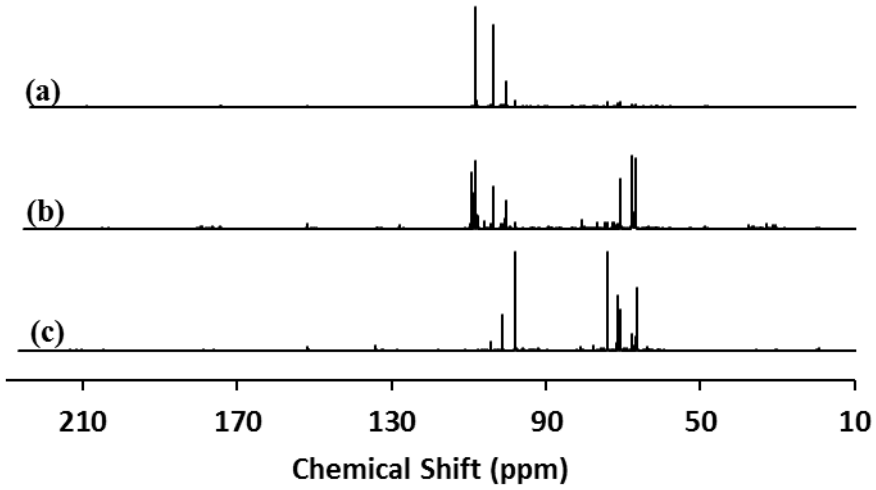


**Figure 5.13 $^{13}$C NMR spectra of product mixture using $^{13}$C2-fructose with (a) $SnO_2$/Si-Beta in methanol, (b) Sn-Beta in methanol and (c) Sn-Beta in water. Reaction conditions: 1% (wt/wt) monosaccharide with a monosacc/Sn ratio of 30 and 15 for Sn-Beta and $SnO_2$/Si-Beta, respectively.**

In Figure 5.14 the presence of methyl fructoside can be observed, formed with $SnO_2$/Si-Beta and Sn-Beta in methanol as a solvent. The resonances δ = 57.7, 59.6 and 60.8 ppm are for the C1 position of β-pyranose, β-furanose and α-pyranose, respectively, of methyl fructoside, which were synthesized from the starting $^{13}$C1-glucose solution. Similarly, resonances δ = 108.2, 103.7 and 100.7 ppm are for the C1 position of β-pyranose, β-furanose and α-pyranose, respectively, of methyl fructoside, which were synthesized from the starting $^{13}$C2-fructose solution. In the case of Sn-Beta in water, fructose was not methylated due to the absence of methanol. Methyl glucoside was not observed in any of the samples.

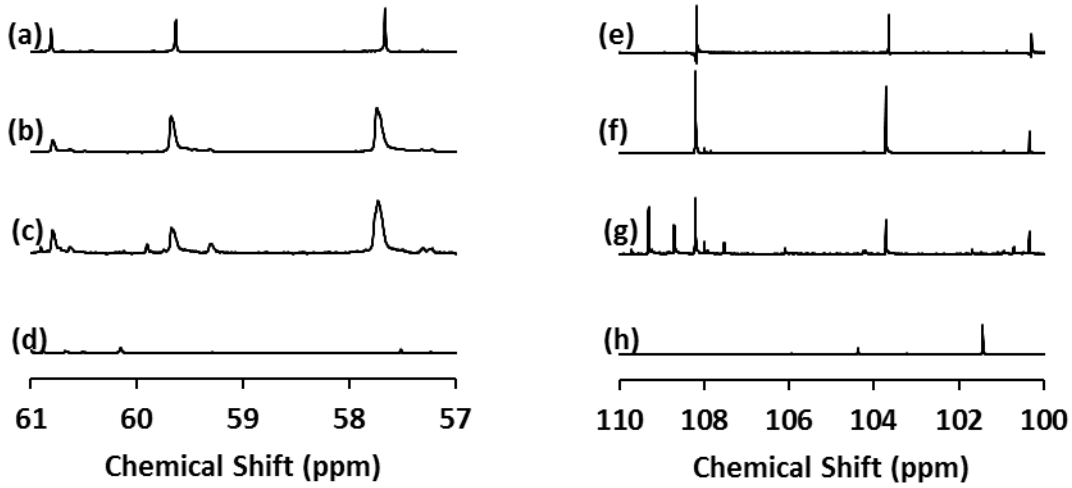


**Figure 5.14 $^{13}$C NMR spectra of (a) methyl fructoside, (b) product mixture using $^{13}$C1-glucose with $SnO_2$/Si-Beta in methanol , (c) product mixture using $^{13}$C1-glucose with Sn-Beta in methanol, (d) product mixture using $^{13}$C1-glucose with Sn-Beta in water, (e) methyl fructoside, (f) product mixture using $^{13}$C2-fructose with $SnO_2$/Si-Beta in methanol, (g) product mixture using $^{13}$C2-fructose with Sn-Beta in methanol and (h) product mixture using $^{13}$C2-fructose with Sn-Beta in water. All product mixtures were obtained from the following reaction conditions: 1% (wt/wt) monosaccharide with a monosacc/Sn ratio of 30 and 15 for Sn-Beta and $SnO_2$/Si-Beta, respectively.**

In Figure 5.15 the presence of dihydroxyacetone in solution is studied. The terminal hydroxyls at δ = 64.8 ppm seem to appear from the starting $^{13}$C1 glucose solution, while no ketone at δ = 212.1 ppm was observed from the starting $^{13}$C2 fructose solution. The appearance of the terminal hydroxyl in the $^{13}$C NMR spectrum does not give sufficient evidence that dihydroxyacetone was present in solution. This suggests that either dihydroxyacetone was not formed as an intermediate or that after retro-aldol reaction of fructose, dihydroxyacetone rapidly isomerizes into glyceraldehyde.

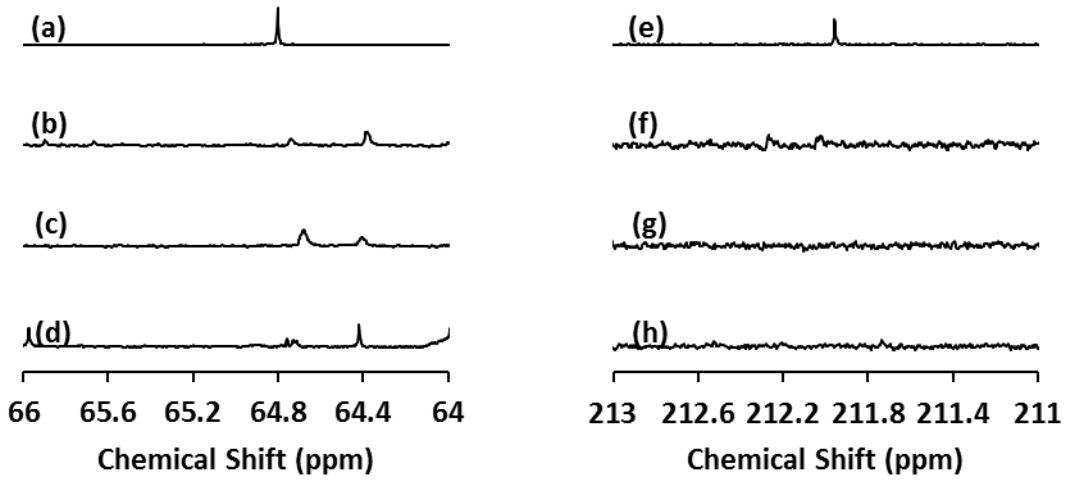


**Figure 5.15 $^{13}$C NMR spectra of (a) dihydroxyacetone, (b) product mixture using $^{13}$C1-glucose with $SnO_2$/Si-Beta in methanol , (c) product mixture using $^{13}$C1-glucose with Sn-Beta in methanol, (d) product mixture using $^{13}$C1-glucose with Sn-Beta in water, (e) dihydroxyacetone, (f) product mixture using $^{13}$C2-fructose with $SnO_2$/Si-Beta in methanol, (g) product mixture using $^{13}$C2-fructose with Sn-Beta in methanol and (h) product mixture using $^{13}$C2-fructose with Sn-Beta in water. All product mixtures were obtained from the following reaction conditions: 1% (wt/wt) monosaccharide with a monosacc/Sn ratio of 30 and 15 for Sn-Beta and $SnO_2$/Si-Beta, respectively.**

Figure 5.16 confirmed the presence of glyceraldehyde as an intermediate with $SnO_2$/Si-Beta and Sn-Beta in methanol, and Sn-Beta in water. The resonance at $\delta$ = 89.6 ppm is for the aldehyde carbon in glyceraldehyde, which was synthesized from starting $^{13}$C1-glucose solution. Aldehydes can be hydrated in solution, leading to lower chemical shifts in the $^{13}$C NMR spectrum (an aldehyde has a chemical shift between 210-220 ppm). The resonance at $\delta$ = 74.1 ppm is for the hydroxyl at the C2 in glyceraldehyde, which was synthesized from starting $^{13}$C2-fructose solution. These results support the retro-aldol reaction from fructose. However, thermodynamically the formation of dihydroxyacetone is favored over glyceraldehyde.[25–27] Similarly to the intramolecular hydride shift from glucose to fructose, dihydroxyacetone can isomerize into glyceraldehyde with Sn-Beta,[14] and vice versa. Assary *et al.*[28] calculated the activation energies for the isomerization of glyceraldehyde to

dihydroxyacetone, being 13.8 kcal/mol for the "open" site and 23.3 kcal/mol for the "closed" site. These results were obtained by the same authors that calculated the glucose isomerization into fructose with the open site of Sn-Beta and one silanol group, being 22.1 kcal/mol. The presence of glyceraldehyde over dihydroxyacetone might be explained by an unknown secondary reaction converting the dihydroxyacetone.

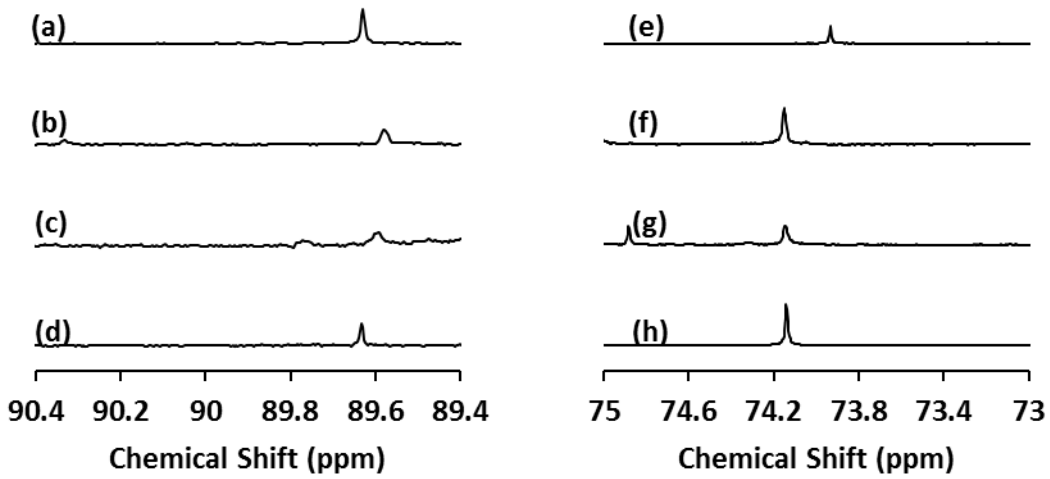


**Figure 5.16 $^{13}$C NMR spectra of (a) glyceraldehyde, (b) product mixture using $^{13}$C1-glucose with $SnO_2$/Si-Beta in methanol , (c) product mixture using $^{13}$C1-glucose with Sn-Beta in methanol, (d) product mixture using $^{13}$C1-glucose with Sn-Beta in water, (e) glyceraldehyde, (f) product mixture using $^{13}$C2-fructose with $SnO_2$/Si-Beta in methanol, (g) product mixture using $^{13}$C2-fructose with Sn-Beta in methanol and (h) product mixture using $^{13}$C2-fructose with Sn-Beta in water. All product mixtures were obtained from the following reaction conditions: 1% (wt/wt) monosaccharide with a monosacc/Sn ratio of 30 and 15 for Sn-Beta and $SnO_2$/Si-Beta, respectively.**

Pyruvaldehyde was present in solution with $SnO_2$/Si-Beta and Sn-Beta in methanol, and Sn-Beta in water as it can be seen in the $^{13}$C NMR spectra of Figure 5.17. The methyl group of pyruvaldehyde seemed to be present in all cases as the resonance at $\delta$ = 24.4 ppm was seen from the starting $^{13}$C1-glucose solution. Also, the hydrated form of the ketone was present by the resonance at $\delta$ = 89.5 ppm from the starting $^{13}$C2-fructose solution. The intensities of the resonance bands of pyruvaldehyde in Figure 5.17 seem lower than the resonance bands of glyceraldehyde

in Figure 5.16. H-USY-6 zeolite can also isomerize triose sugars glyceraldehyde and dihydroxyacetone into lactic acid and methyl lactate, being the dehydration of glyceraldehyde to pyruvaldehyde the rate limiting step.[18] This could also be true for Sn-Beta, but further rate analysis would be needed with Sn-Beta to confirm that the dehydration of glyceraldehyde to pyruvaldehyde is also the rate limiting step in conversion of triose sugars into lactic acid and methyl lactate.

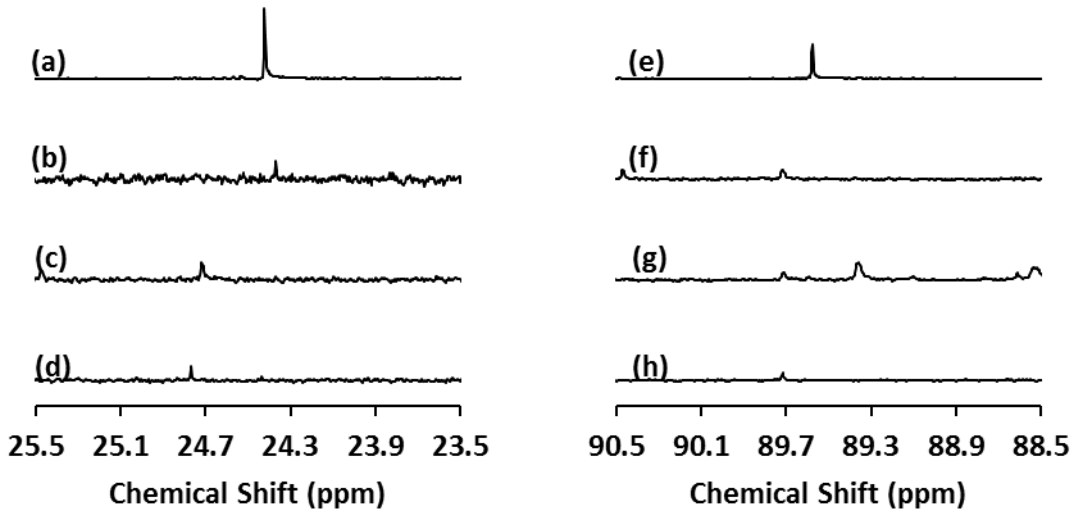


**Figure 5.17 $^{13}$C NMR spectra of (a) pyruvaldehyde, (b) product mixture using $^{13}$C1-glucose with $SnO_2$/Si-Beta in methanol , (c) product mixture using $^{13}$C1-glucose with Sn-Beta in methanol, (d) product mixture using $^{13}$C1-glucose with Sn-Beta in water, (e) pyruvaldehyde, (f) product mixture using $^{13}$C2-fructose with $SnO_2$/Si-Beta in methanol, (g) product mixture using $^{13}$C2-fructose with Sn-Beta in methanol and (h) product mixture using $^{13}$C2-fructose with Sn-Beta in water. All product mixtures were obtained from the following reaction conditions: 1% (wt/wt) monosaccharide with a monosacc/Sn ratio of 30 and 15 for Sn-Beta and $SnO_2$/Si-Beta, respectively.**

Figure 5.18 confirms the presence of lactic acid with Sn-Beta in water, methyl lactate with $SnO_2$/Si-Beta and Sn-Beta in methanol. The $^{13}$C NMR spectra shows the methyl group ($\delta$ = 19.1 ppm) of lactic acid and methyl lactate from the starting $^{13}$C1-glucose solution. The starting $^{13}$C2-fructose solution results in the isotopic labeling of the carbon bonded to the hydroxyl group ($\delta$ = 68.5 ppm) in lactic acid and methyl lactate.

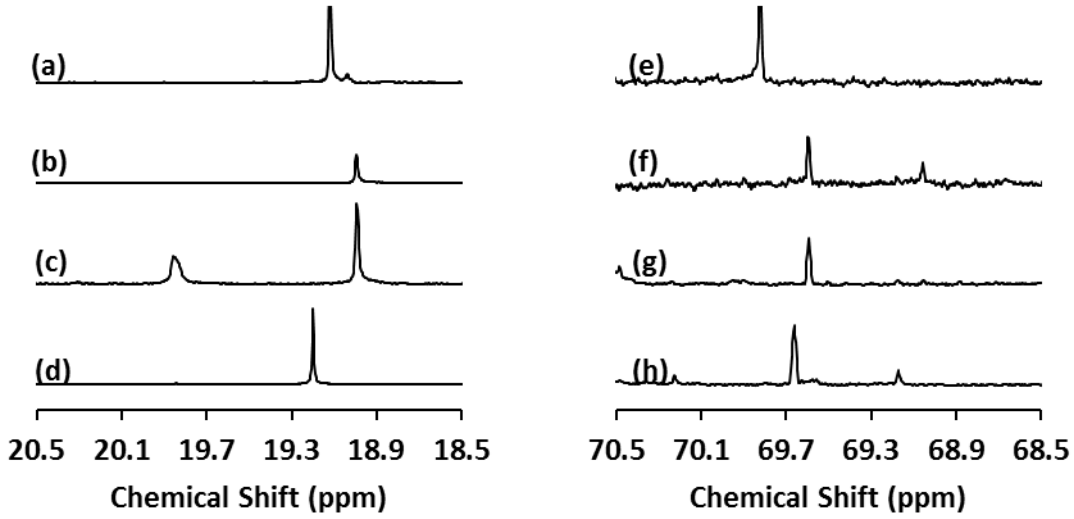


**Figure 5.18 $^{13}$C NMR spectra of (a) lactic acid, (b) product mixture using $^{13}$C1-glucose with $SnO_2$/Si-Beta in methanol , (c) product mixture using $^{13}$C1-glucose with Sn-Beta in methanol, (d) product mixture using $^{13}$C1-glucose with Sn-Beta in water, (e) lactic acid, (f) product mixture using $^{13}$C2-fructose with $SnO_2$/Si-Beta in methanol, (g) product mixture using $^{13}$C2-fructose with Sn-Beta in methanol and (h) product mixture using $^{13}$C2-fructose with Sn-Beta in water. All product mixtures were obtained from the following reaction conditions: 1% (wt/wt) monosaccharide with a monosacc/Sn ratio of 30 and 15 for Sn-Beta and $SnO_2$/Si-Beta, respectively.**

The previous $^{13}$C NMR spectra allow us to infer that the two carbons from starting glucose backbone do stay together, along the reaction pathway leading for the synthesis of lactic acid with Sn-Beta and $SnO_2$/Si-Beta, as it can be seen in Figure 5.19. The C1 in glucose is reduced from an aldehyde to a methyl as it was confirmed by the formation of a methyl group in pyruvaldehyde and lactic acid. The C2 hydroxyl in glucose to lactic acid is oxidized to a ketone, during fructose and dihydroxyacetone, and later reduced upon the formation of lactic acid. This mechanism is analogous to glycolysis.[13]

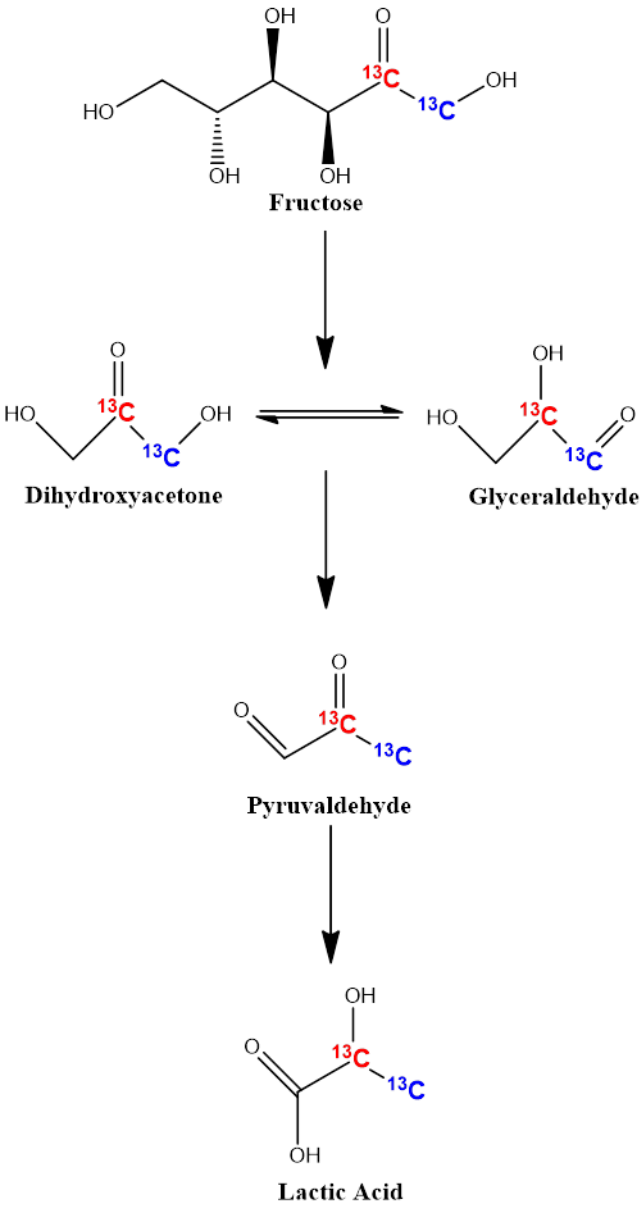


**Figure 5.19 Plausible mechanism for the synthesis of lactic acid with Sn-Beta and $SnO_2$/Si-Beta.**

In contrast to the synthesis of lactic acid with Sn-Beta and $SnO_2$/Si-Beta, two different vinylglycolic acid molecules are present in solution with both Sn-Beta and $SnO_2$/Si-Beta catalysts, as it can be seen in Figure 5.20 and Figure 5.21. The starting $^{13}$C1-glucose solution resulted in the different labeling of two vinylglycolic acid molecules in water or methyl vinylglycolate molecules in methanol, having the isotopic labeling in the methylene ($\delta$ = 118.1 ppm, Figure 5.20) and in the carboxylate

(δ = 174.2 ppm, Figure 5.21) of vinylglycolic acid. Similarly, the starting $^{13}$C2-fructose solution formed two different vinylglycolic acid molecules, having the isotopic labeling in the methine (δ = 133.6 ppm, Figure 5.20) and in the hydroxyl carbon (δ = 71.5 ppm, Figure 5.21).

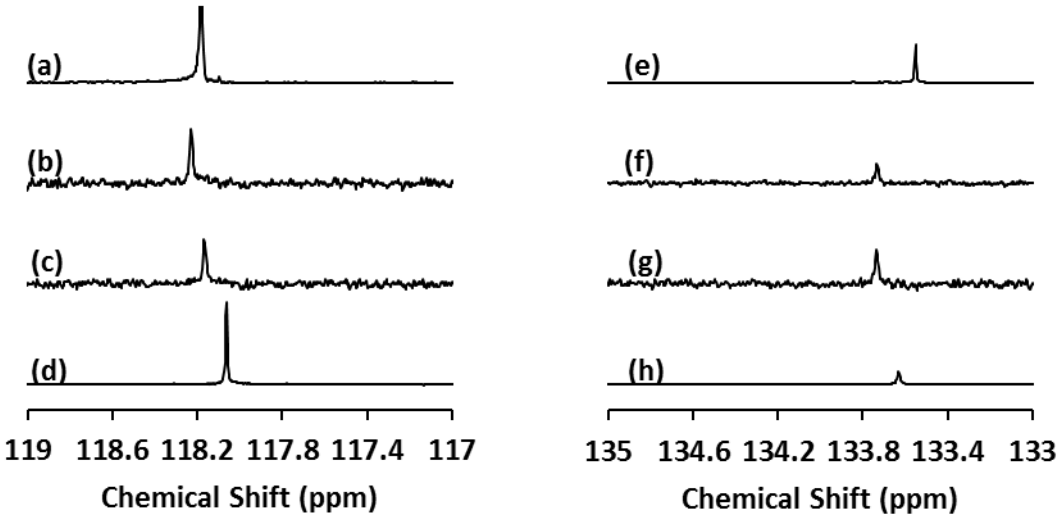


**Figure 5.20 $^{13}$C NMR spectra of (a) methyl vinylglycolate, (b) product mixture using $^{13}$C1-glucose with $SnO_2$/Si-Beta in methanol , (c) product mixture using $^{13}$C1-glucose with Sn-Beta in methanol, (d) product mixture using $^{13}$C1-glucose with Sn-Beta in water, (e) methyl vinylglycolate, (f) product mixture using $^{13}$C2-fructose with $SnO_2$/Si-Beta in methanol, (g) product mixture using $^{13}$C2-fructose with Sn-Beta in methanol and (h) product mixture using $^{13}$C2-fructose with Sn-Beta in water. All product mixtures were obtained from the following reaction conditions: 1% (wt/wt) monosaccharide with a monosacc/Sn ratio of 30 and 15 for Sn-Beta and $SnO_2$/Si-Beta, respectively.**

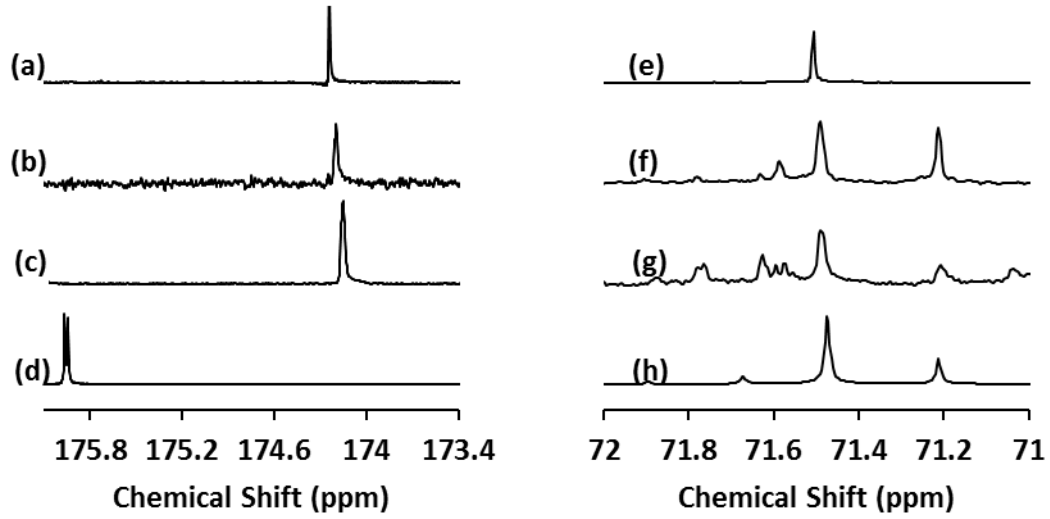


**Figure 5.21 $^{13}$C NMR spectra of (a) methyl vinylglycolate, (b) product mixture using $^{13}$C1-glucose with $SnO_2$/Si-Beta in methanol , (c) product mixture using $^{13}$C1-glucose with Sn-Beta in methanol, (d) product mixture using $^{13}$C1-glucose with Sn-Beta in water, (e) methyl vinylglycolate, (f) product mixture using $^{13}$C2-fructose with $SnO_2$/Si-Beta in methanol, (g) product mixture using $^{13}$C2-fructose with Sn-Beta in methanol and (h) product mixture using $^{13}$C2-fructose with Sn-Beta in water. All product mixtures were obtained from the following reaction conditions: 1% (wt/wt) monosaccharide with a monosacc/Sn ratio of 30 and 15 for Sn-Beta and $SnO_2$/Si-Beta, respectively.**

The detection of erythrose and 2-oxobut-3-enal (Figure 5.1) could aid in reasoning the mechanistic pathway leading to the formation of vinylglycolic acid, but its low amount made it difficult to identify the intermediates in $^{13}$C NMR. A plausible explanation for the two molecules could be explained in Figure 5.22. Similarly to lactic acid, glucose in its open form could go through C4-C5 cleavage to form erythrose and consequently vinylglycolic acid. On the other hand, redistribution in the oxidation states of erythrose could also shift the aldehyde to the carbon atom in the opposite end of the carbon skeleton (Figure 5.22) and consequently form vinylglycolic acid.

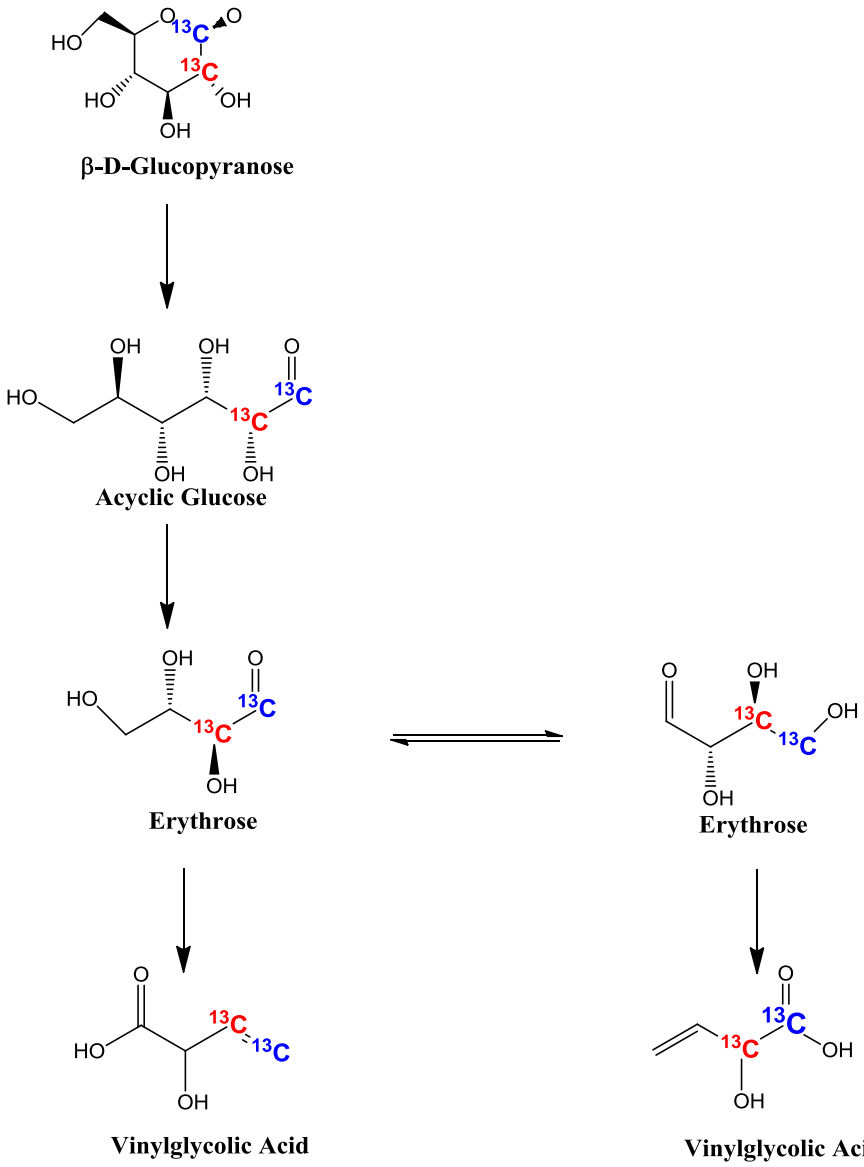


**Figure 5.22 Plausible mechanism for the synthesis of vinylglycolic acid with Sn-Beta or $SnO_2$/Si-Beta.**

After analyzing the formation of the two main carboxylic acids there were other secondary products observed in solution. One of them was 5-(Hydroxymethyl)furfural, HMF. Both the C1 (δ = 180.4 ppm) and C2 (δ = 151.7 ppm) of mannose were observed from the starting $^{13}$C1-glucose and $^{13}$C2-fructose solutions, respectively, with both Sn-Beta and $SnO_2$/Si-Beta, as it can be seen in Figure 5.23.

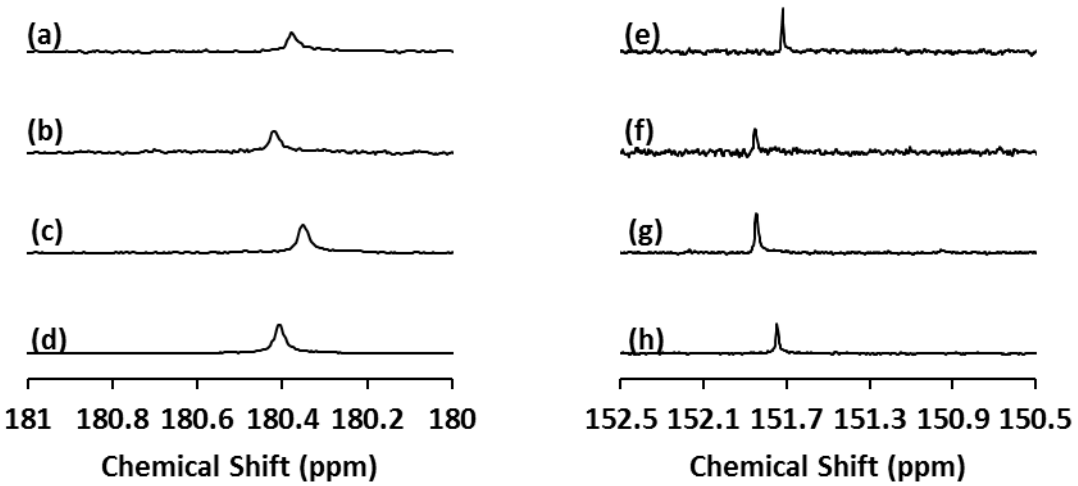


**Figure 5.23 $^{13}$C NMR spectra of (a) HMF, (b) product mixture using $^{13}$C1-glucose with $SnO_2$/Si-Beta in methanol , (c) product mixture using $^{13}$C1-glucose with Sn-Beta in methanol, (d) product mixture using $^{13}$C1-glucose with Sn-Beta in water, (e) HMF, (f) product mixture using $^{13}$C2-fructose with $SnO_2$/Si-Beta in methanol, (g) product mixture using $^{13}$C2-fructose with Sn-Beta in methanol and (h) product mixture using $^{13}$C2-fructose with Sn-Beta in water. All product mixtures were obtained from the following reaction conditions: 1% (wt/wt) monosaccharide with a monosacc/Sn ratio of 30 and 15 for Sn-Beta and $SnO_2$/Si-Beta, respectively.**

The low carbon balances seen with Sn-Beta and $SnO_2$/Si-Beta reflects the formation of byproducts which have not been quantified. One of these products can be seen in Figure 5.24b. This product was separated by HPLC and resulted in a molecular weight of 134 g/mol. This molecule has similar $^{13}$C NMR spectra as 2-deoxy-d-ribose (Figure 5.24a), with the same molecular weight. This 2-deoxy-d-ribose isomer ($C_5O_4H_{10}$) and other similar molecules were present in all of the $^{13}$C NMR spectra previously discussed. Holm *et al*,[18] reported the formation of levulinic acid and trace amounts of other products in solution such as formaldehyde, glycolaldehyde, glycolic acid and furfural derivatives. Levulinic acid, formaldehyde and furfural derivatives were also seen in this study by $^{1}$H NMR analysis, as well as other non-identified resonance bands for saturated alkanes (R-H, 1-2ppm). Therefore, Sn-Beta seems to be doing the reactions seen in the formation of lactic acid

(intramolecular hydride shift, retro-aldol and dehydration) to other parts of the carbon backbone that lead to different products.

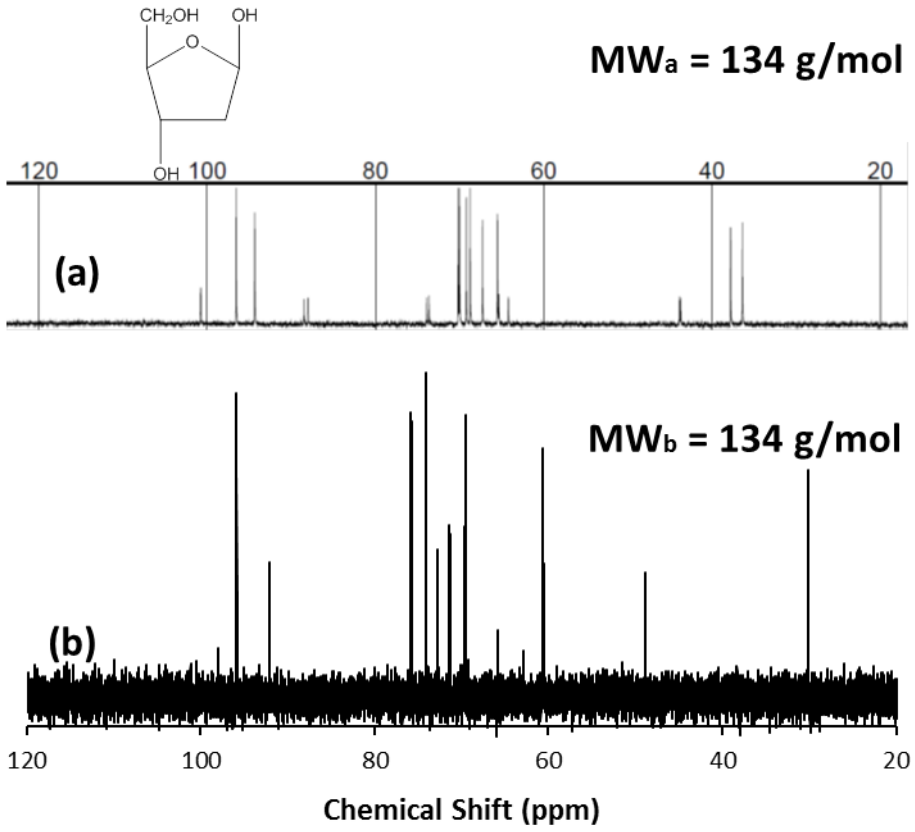


**Figure 5.24 $^{13}$C NMR spectra (a) 2-deoxy-d-ribose (b) unknown product separated with HPLC, having a molecular weight of 134 g/mol.**

## 3. Conclusion

Framework Sn centers within the hydrophobic pores of zeolite beta, Sn-Beta and extraframework $SnO_2$ clusters deposited on zeolite beta, $SnO_2$/Si-Beta, are active in the glucose and fructose retro-aldol reactions that lead to the formation of vinylglycolic acid and lactic acid, respectively. Sn-Beta has a superior activity over $SnO_2$/Si-Beta, leading to higher carboxylic acid yields. The activity in aqueous solvent is lower than in methanol, resulting in trace amounts of lactic acid with $SnO_2$/Si-Beta in water. However, in methanol the $SnO_2$ clusters deposited on the exterior surface of zeolite beta are active and catalyze the retro-aldol reactions. Lactic

acid and vinylglycolic acid are formed with $SnO_2$/Si-Beta in an analogous mechanistic pathway as with Sn-Beta, without carbon rearrangement.

## 4. Experimental Procedure

### 4.1 Synthesis of Sn-Beta and $SnO_2$/Si-Beta

The synthesis of Sn-Beta and $SnO_2$/Si-Beta was done following the procedure in Chapter 3.

### 4.2 Reaction Conditions

Reactions with D-glucose (Sigma-Aldrich, ≥99%) were conducted in 10 ml thick-walled glass reactors (VWR) that were heated in a temperature-controlled oil bath. Reactions were prepared with a 1:30 and 1:15 Sn:glucose molar ratio with Sn-Beta and $SnO_2$/Si-Beta, using 5.0 g of a 1% (w/w) glucose solution with approximately 20 mg of catalyst. Reactors were placed in the oil bath at 353 K and approximately 50 mg were extracted at different times. These aliquots were mixed with deuterium oxide ($D_2O$, Cambridge Isotope Laboratories, 98-99%). The samples were then analyzed with WET ($^1H$) NMR analysis with previous glucose, fructose, mannose, lactic acid and methyl vinylglycolate calibration, using a Varian INOVA 400 MHz spectrometer equipped with a multinuclear autotune acquired with T1 10 seconds and 128 scans.

Reactions with labeled $^{13}C$ glucose at the C1 position (Cambridge Isotope Laboratories,1-$^{13}C$ D-glucose, 98-99%) and $^{13}C$ fructose at the C2 position of fructose (Cambridge Isotope Laboratories,2-$^{13}C$ D-fructose, 98-99%) were conducted under the same conditions as those with D-glucose. The reaction was ended differently for each, estimating for a 70% conversion. The reaction solution was filtered and rotavaporated to separate the solvent from the reactant-product mixture.

These recovered solids were redissolved in deuterium oxide and analyzed using $^{13}C$ NMR.

## 5. References


1. Datta, R. & Henry, M. Lactic acid: recent advances in products, processes and technologies — a review. *J. Chem. Technol. Biotechnol.* **81,** 1119–1129 (2006).

2. Climent, M. J., Corma, A. & Iborra, S. Converting carbohydrates to bulk chemicals and fine chemicals over heterogeneous catalysts. *Green Chem.* **13,** 520 (2011).

3. Lunt, J. Large-scale production, properties and commercial application of polylactic acid polymers. *Polym. Degrad. Stab.* **3910,** 145–152 (1998).

4. Román-Leshkov, Y. & Davis, M. E. Activation of Carbonyl-Containing Molecules with Solid Lewis Acids in Aqueous Media. *ACS Catal.* **1,** 1566–1580 (2011).

5. Taarning, E. *et al.* Zeolite-catalyzed biomass conversion to fuels and chemicals. *Energy Environ. Sci.* **4,** 793 (2011).

6. Yan, X., Jin, F., Tohji, K., Moriya, T. & Enomoto, H. Production of lactic acid from glucose by alkaline hydrothermal reaction. *J. Mater. Sci.* **42,** 9995–9999 (2007).

7. Wang, Y. *et al.* Chemical synthesis of lactic acid from cellulose catalysed by lead(II) ions in water. *Nat. Commun.* **4,** 2141 (2013).

8. Wang, F.-F., Liu, C.-L. & Dong, W.-S. Highly efficient production of lactic acid from cellulose using lanthanide triflate catalysts. *Green Chem.* **15,** 2091–2095 (2013).

9. Zeng, W., Cheng, D., Chen, F. & Zhan, X. Catalytic Conversion of Glucose on Al–Zr Mixed Oxides in Hot Compressed Water. *Catal. Letters* **133,** 221–226 (2009).

10. Onda, A., Ochi, T., Kajiyoshi, K. & Yanagisawa, K. A new chemical process for catalytic conversion of d-glucose into lactic acid and gluconic acid. *Appl. Catal. A Gen.* **343,** 49–54 (2008).

11. Wang, Y. *et al.* Selective conversion of glucose into lactic acid and acetic acid with copper oxide under hydrothermal conditions. *AIChE J.* **59,** 2096–2104 (2013).

12. Holm, M. S., Saravanamurugan, S. & Taarning, E. Conversion of sugars to lactic acid derivatives using heterogeneous zeotype catalysts. *Science* **328,** 602–5 (2010).

13. Lobo, R. F. Synthetic glycolysis. *ChemSusChem* **3,** 1237–40 (2010).

14. Taarning, E. *et al.* Zeolite-catalyzed isomerization of triose sugars. *ChemSusChem* **2,** 625–7 (2009).

15. Holm, M. S. *et al.* Sn-Beta catalysed conversion of hemicellulosic sugars. *Green Chem.* (2012). doi:10.1039/c2gc16202d

16. Osmundsen, C. M., Holm, M. S., Dahl, S. & Taarning, E. Tin-containing silicates: structure-activity relations. *Proc. R. Soc. A Math. Phys. Eng. Sci.* (2012). doi:10.1098/rspa.2012.0047

17. Holm, M. S., Saravanamurugan, S. & Taarning, E. Conversion of sugars to lactic acid derivatives using heterogeneous zeotype catalysts. *Science* **328,** 602–5 (2010).

18. West, R. M. *et al.* Zeolite H-USY for the production of lactic acid and methyl lactate from C3-sugars. *J. Catal.* **269,** 122–130 (2010).

19. Janssen, K. P. F., Paul, J. S., Sels, B. F. & Jacobs, P. A. in *From Zeolites to Porous MOF Mater. - 40th Anniv. Int. Zeolite Conf. Proc. 15th Int. Zeolite Conf.* (Ruren Xu Zi Gao, J. C. & Yan, W.) **170,** 1222–1227 (Elsevier, 2007).

20. Roy, S., Bakhmutsky, K., Mahmoud, E., Lobo, R. F. & Gorte, R. J. Probing Lewis Acid Sites in Sn-Beta Zeolite. *ACS Catal.* **3,** 573–580 (2013).

21. Corma, A. & Zones, S. *Zeolites and Catalysis*. (Wiley-VCH Verlag GmbH & Co. KGaA, 2010). doi:10.1002/9783527630295

22. Moliner, M., Román-Leshkov, Y. & Davis, M. E. Tin-containing zeolites are highly active catalysts for the isomerization of glucose in water. *Proc. Natl. Acad. Sci. U. S. A.* **107,** 6164–8 (2010).

23. Arnett, E. M., Fisher, F. J., Nichols, M. A. & Ribeiro, A. A. Thermochemistry of a structurally defined aldol reaction. *J. Am. Chem. Soc.* **111,** 748–749 (1989).

24. Bermejo-deval, R., Gounder, R. & Davis, M. E. Framework and Extraframework Tin Sites in Zeolite Beta React Glucose Differently. *ACS Catal.* **2,** 2705–2713 (2012).

25. Yaylayan, V. A., Harty-Majors, S. & Ismail, A. I. Investigation of DL-glyceraldehyde-dihydroxyacetone interconversion by FTIR spectroscopy.pdf. *Carbohydr. Res.* **318,** 20–25 (1999).

26. Simonetti, D. a. & Dumesic, J. a. Catalytic Production of Liquid Fuels from Biomass-Derived Oxygenated Hydrocarbons: Catalytic Coupling at Multiple Length Scales. *Catal. Rev.* **51,** 441–484 (2009).

27. Davis, L. The Structure of Dihydroxyacetone. *Bioorg. Chem.* **2,** 197–201 (1973).

28. Assary, R. S. & Curtiss, L. a. Theoretical study of 1,2-hydride shift associated with the isomerization of glyceraldehyde to dihydroxy acetone by Lewis acid active site models. *J. Phys. Chem. A* **115,** 8754–60 (2011).

# Chapter 6 : Summary and Future Direction

## 1. Conclusion

In this thesis, framework and extraframework tin sites in zeolite Beta catalyzing the reaction of glucose are studied. With Sn-Beta (and to a great extent Ti-Beta), it is shown that the glucose isomerization into fructose mechanism is very similar to that of the metalloenzymes D-xylose isomerase. Evidence is provided to conclude that the glucose partitions into the zeolite in the cyclic form. In the presence of Sn (or Ti), direct NMR and IR evidence of the acyclic fructose are observed. Acyclic glucose must have first been bound to the Lewis acid center, prior to being isomerized to obtain the acyclic fructose. The isomerization is occurring via a Lewis acid-mediated, intramolecular hydride transfer mechanism. Experimental results (kinetic isotope effects) corroborate the conclusion that the rate determining step is the intramolecular hydride transfer and that the "open" site is likely the active site responsible for isomerization activity. The "open" and "close" sites seem to reach an equilibrium distribution upon calcination. The mannose formed with Sn-Beta seems to be isomerizing from fructose and not from glucose.

The basic sites on extraframework $SnO_2$ domains catalyze the glucose isomerization into fructose, via the abstraction of protons at C-2 carbon atoms to form enolate intermediates. In aqueous environment, extraframework Sn species appear only to be reactive when they are confined in the hydrophobic zeolite Beta channels ($SnO_2$/Si-Beta); however, at the external zeolite crystal surfaces ($SnO_2$/Si-Beta-E) and on amorphous supports ($SnO_2/SiO_2$) water does seem to inhibit the isomerization of glucose into fructose. In methanol, $SnO_2$ domains are able to catalyze glucose isomerization irrespective of their location, within or outside of the hydrophobic zeolite Beta pores, indicating that methanol does not inhibit the base-catalyzed

isomerization on $SnO_2$. These findings can provide sufficient evidence for the type of Sn site in zeolite Beta, framework or extraframework, without the use of $^{119}$Sn Solid-State NMR.

The proton containing partially hydrolyzed Sn site in zeolite beta, characterized by an IR band at 2315 $cm^{-1}$ from adsorbed $CD_3CN$ and a $^{119}$Sn NMR resonance at -423 ppm in the dehydrated state (denoted as the open site) is the active site involved in the isomerization of glucose into fructose via a Lewis-acid mediated hydride-shift mechanism; whereas a sodium containing open site analog, characterized by an IR band at 2280 $cm^{-1}$ adsorbed $CD_3CN$ and a $^{119}$Sn NMR resonance at -419 ppm in the dehydrate state, is the active site in the epimerization of glucose into mannose via a 1, 2 intramolecular carbon shift. The sodium cation can be introduced into the active site of the zeolite, either by ion exchange of Sn-Beta or by incorporation of low amounts of sodium into the synthesis gel, with both methods resulting in samples that give higher epimerization selectivity relative to Sn-Beta. Acid wash of sodium containing materials gives nearly full recovery of initial activity of the parent Sn-Beta, showing that the alterations to the tin site by the sodium ion are reversible. The addition of NaCl to aqueous reaction solutions also enhanced the selectivity towards epimerization of glucose into mannose. These results, in combination with reusability studies in water and methanol, support the finding that the sodium cation is more prone to decationize in water than in methanol under reaction conditions.

The formation of lactic acid and vinylglycolic acid from glucose can be catalyzed by framework Sn centers within the hydrophobic pores of zeolite beta, Sn-Beta, and/or extraframework $SnO_2$ clusters deposited on zeolite beta, $SnO_2$/Si-Beta. Sn-Beta has a superior activity over $SnO_2$/Si-Beta, leading to higher carboxylic acid

yields. The activity in aqueous solvent is lower than in methanol, resulting in trace amounts of lactic acid with $SnO_2$/Si-Beta in water. However, in methanol the $SnO_2$ clusters deposited on the exterior surface of zeolite beta are active and catalyze the retro-aldol reactions. Lactic acid and vinylglycolic acid are formed with $SnO_2$/Si-Beta in an analogous mechanistic pathway as with Sn-Beta, without carbon rearrangement.

The different framework and extraframework Sn sites are fully characterized and we know which site will isomerize or epimerize glucose into fructose or mannose, respectively. However, it is unknown why do each of these Sn sites choose to follow such different mechanistic pathway. Therefore, further research to solve in detail the interaction of the hexoses with the active sites could elucidate the reason for these mechanisms.

## 2. Future Work

### 2.1 Sn-Beta Post-Treatment

#### *2.1.1 Sn-Beta SDA Exchange*

Zeolite post-treatment has been known to alter and condition the activity and selectivity of a catalyst, providing unique chemical and physical properties.[1] Organic molecules are used in the synthesis of zeolites as stucture-directing agents (SDA) or templates. These molecules are within the zeolite micropores after their synthesis. To remove these organics calcination is commonly employed, leaving behind an organic-free zeolite able to diffuse orther molecules, such as reactants. However, severe calcination conditions can change or modify the features desired in the synthesis of molecular sieves. Therefore, the removal of the organics has been investigated through other procedures. Mineral and organic acids have been used to remove by extraction the SDA present in the micropores after zeolite synthesis.[2,3] The amount of

SDA removed by this treatment is reliant in its size and strength of interaction with the molecular sieve framework, correlating well with the temperature at which the SDA combusts in thermogravimetric analyses experiments.[2]

Throughout Chapter 2 it was discussed how upon calcination the "open" and "closed" sites of Sn-Beta might equilibrate within the high temperature conditions (400-600ºC). To hinder the changes that might uccur during calcination, the SDA in Sn-Beta was removed by extraction with glacial acetic acid (water-free acetic acid) at 80ºC for 24 hours. This was then tested with 1% glucose (wt/wt) at 100ºC for 30 minutes at a Sn:glucose ratio of 1:50, forming only mannose, Figure 6.1 HAcEx. This same reaction was performed with $^{13}C$ in the C1 position of glucose, confirming an 1,2 intramolecular carbon shift, as the $^{13}C$ NMR spectrum displayed the resonance bands at $\delta$ = 70.5 and 71.1 ppm, corresponding to the C2-positions of the $\alpha$ and $\beta$ pyranose forms of mannose, respectively. The catalyst seems to behave similarly to the sodium exchanged Sn-Beta in methanol solvent (Chapter 4), were mannose was selectively formed over fructose through a 1,2 intramolecular carbon shift. These results led to think that not all of the SDA (tetraethylamonium hydroxide, TEAOH) had been removed from Sn-Beta after acetic acid extraction, having some attached to the "open" site. Similarly to sodium exchanged Sn-Beta, tetraethylammonium cation ($TEA^+$) could be counterbalancing the neighbouring $Si\text{-}O^-$ in the "open" site.

Sn-Beta was exchanged with ammonium cations tetraethylammonium ($TEA^+$) and tetramethylammonium ($TMA^+$) in hydroxide solution, TEAOH and TMAOH, respectively. These exchanged materials were then tested with 1% (wt/wt) glucose in water and methanol solvent at 100ºC, as it can be seen in Figure 6.1 and Figure 6.2. Comparing these exchanged materials with Sn-Beta extracted with acetic acid, a

resemblance is seen in their activity and selectivity. In aqueous environment, glucose conversion does not surpass 17%, obtaining  after 2 hours almost aproximately 11% mannose yields in all cases. Sn-Beta exchanged with $TMA^+$ seems to have a higher initial activity than exchanged with $TEA^+$, implying the possibility of some steric hindrance with bigger ammonium cations. Only a small ammount of fructose is observed after Sn-Beta extracted with acetic acid was used in water solvent. Acetic acid from the extraction treatment could be remaining in the zeolite, catalyzing the isomerization into fructose. In solvent methanol the behaviour is also similar in all three cases, with a higher selectivity towards fructose in comparison to water. Methanol might be interacting in a different way with the active site, promoting the isomerization into fructose.

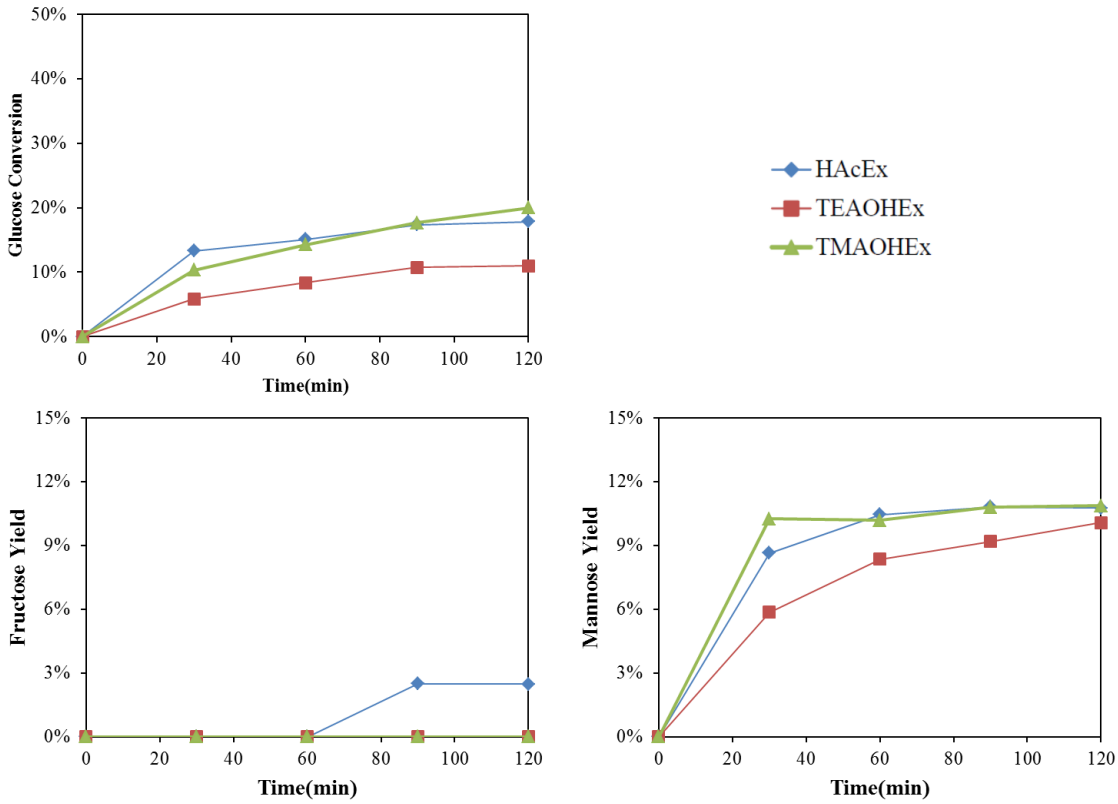


**Figure 6.1 Glucose conversion and fructose and mannose yields with Sn-Beta extracted with acetic acid (HAcEx), Sn-Beta exchanged with TEAOH (TEAOHEx) and Sn-Beta exchanged with TMAOH (TMAOHEx). Reactions conditions: 1% (wt/wt) in water, 100ºC and glucose:Sn ratio of 50:1.**

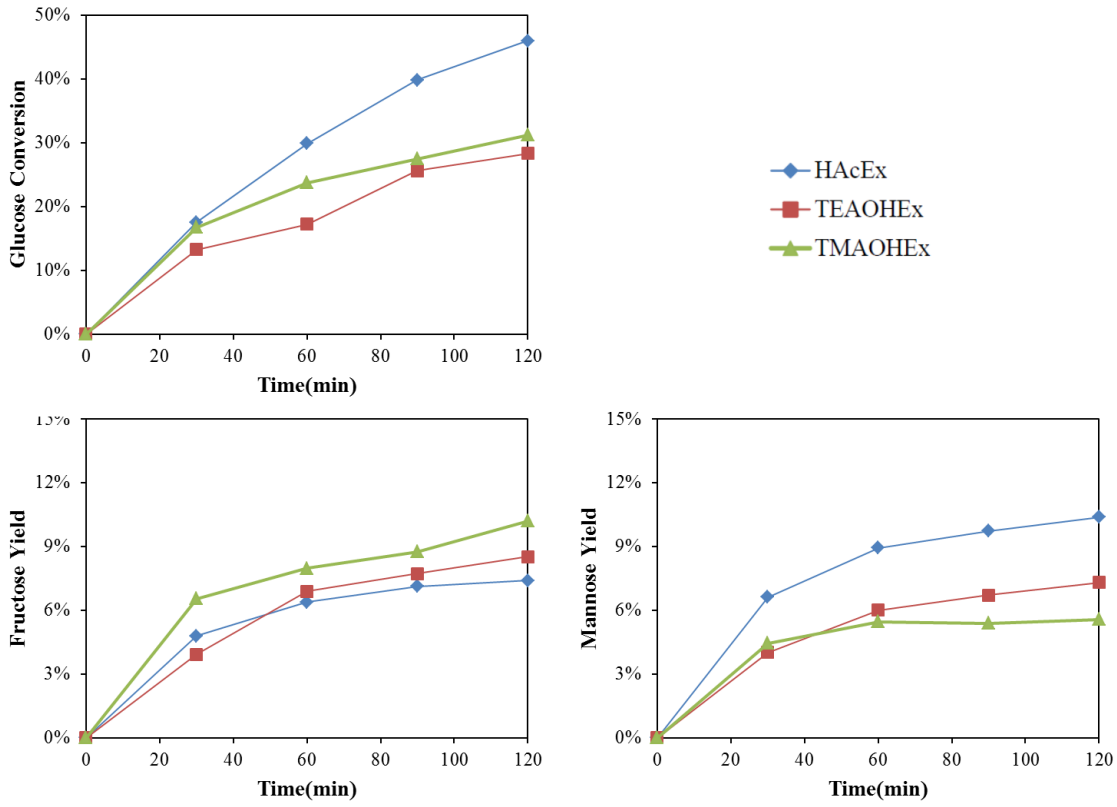


**Figure 6.2 Glucose conversion and fructose and mannose yields with Sn-Beta extracted with acetic acid (HAcEx), Sn-Beta exchanged with TEAOH (TEAOHEx) and Sn-Beta exchanged with TMAOH (TMAOHEx). Reactions conditions: 1% (wt/wt) in water, 100ºC and glucose:Sn ratio of 50:1. The TMAOH and TEAOH exchange was performed under same conditions as those from Corma et al.[4]**

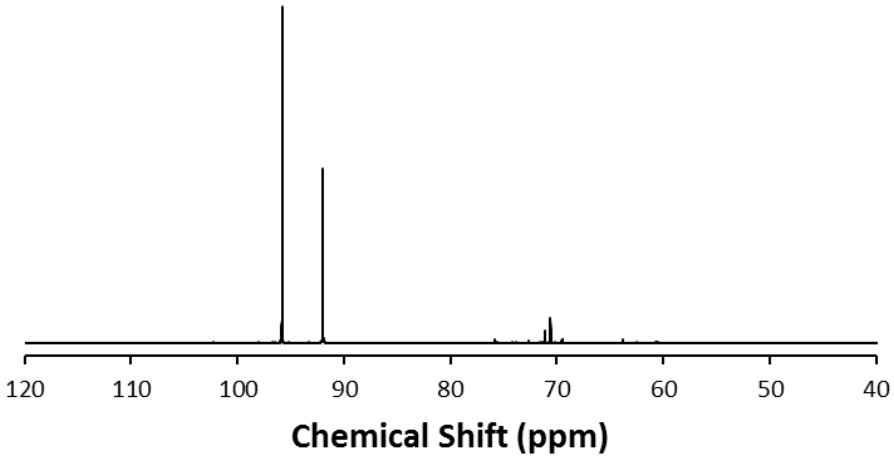


**Figure 6.3 $^{13}$C NMR spectra of product mixture from a 1% (wt/wt) $^{13}$C1-glucose in water at 100ºC after 30 minutes using Sn-Beta extracted with acetic acid at a glucose:Sn ratio of 50:1.**

These preliminary results could allow us to gain a precise understanding of the active site in Sn-Beta. The results suggest that after extraction with acetic acid, Sn-Beta has the $TEA^+$ cation bonded through charge-balancing interactions to the "open" site. Jones *et al.*[2] reported that for the cases of borosilicates, aluminosilicates and zincosilicates, only organics that can combust in thermogravimetric analysis (TGA) at temperatures below 400ºC can be removed by solvent extraction. If all Sn sites were to have $TEA^+$, TGA analysis of extracted Sn-Beta should confirm a minimum weight loss correspondent to those sites. In addition, IR with adsorbed acetonitrile could tell us the Lewis acid encountered in the active site of Sn-Beta.

Releasing the $TEA^+$ from the active site of Sn-Beta without calcination could lead to a different activity. The as-synthesized Sn-Beta could be initially formed without "closed" sites and upon calcination an "open" site could be "closing". This idea could only be tested by the removal of the $TEA^+$ cation from the active sites of Sn-Beta. After acetic acid extraction of Sn-Beta, sulfuric acid ($H_2SO_4$) wash was performed. This did not change the activity, as it did with the sodium exchanged materials, forming only mannose. Other possibilities could be by sodium exchange of Sn-Beta extracted with acetic acid and then $Na^+$ de-cationation with an acid wash.

### *2.1.2 Surface Modification and Hierarchical Sn-Beta*

In the presence of water the catalytic activity of a Lewis acid is diminished.[5] In Chapters 3-5, it can be seen that the glucose conversion with Sn-Beta is higher in methanol than in water. This could be due to the Sn site distribution, where the Sn sites in the mouth pore and at the external surfaces are hindered in the presence of

water, owing to their lower hydrophobicity. To increase the activity of these sites in water a surface treatment could be done to enhance the hydrophobic environment of these tin sites. Surface silylation can increase the hydrophobicity without significantly reducing the acid site density in conventional zeolites.[1,6–8] The addition of a hydrophobic layer on Sn-Beta could enhance the activity of Sn-Beta without the formation of the methylated products observed in methanol solvent. The most common silylating agents are hexamethyldisilazane, trymethylchlorosilane and triphenylchlorosilane.[8]

Another post-treatment method to enhance the activity of Sn-Beta in water could be to combine desilication and surface silylation. Hierarchical zeolites are known to be formed by desilication,[9–13] introducing needed mesoporosity to enhance the accessibility of the active sites in the zeolite. Since glucose diffuses into the zeolite in the cyclic form,[14] the desilication could facilitate the diffusion of glucose in the zeolite prior to reaching the active site. Desilication in the titanium zeolite TS-1 has shown to increase the diffusion of aromatics, resulting in higher activity using acetone[15] or water[16] as solvents. However, in the case of Sn-Beta, additional surface silylation might be needed after desilication to protect the outer Sn sites from deactivation in water.

## 2.2 Calcination

The calcination of a zeolite can change completely its activity. While extensive research has been done on the calcination treatment of conventional zeolites,[17–20] very little work has been reported on the calcination treatment of Lewis acid zeolites.[16,21] The main effect of steaming is the de-alumination of the framework into extraframework aluminum,[17–20] decreasing the concentration of Brønsted acid sites in the zeolite. Similarly, Sn-Beta was calcined under different steaming

conditions (Figure 6.4), changing the framework Sn sites (c.a. -700 ppm in $^{119}$Sn NMR) to extraframework $SnO_2$ sites (-600 ppm in $^{119}$Sn NMR). Calcination under dry air conditions results in pure framework Sn sites (Figure 6.4a), while additional steaming at 25ºC induces the formation of some extraframework $SnO_2$ (Figure 6.4b). However, when the as-synthesized Sn-Beta was calcined under steaming conditions of 80ºC a higher amount of extraframework was observed (Figure 6.4c).

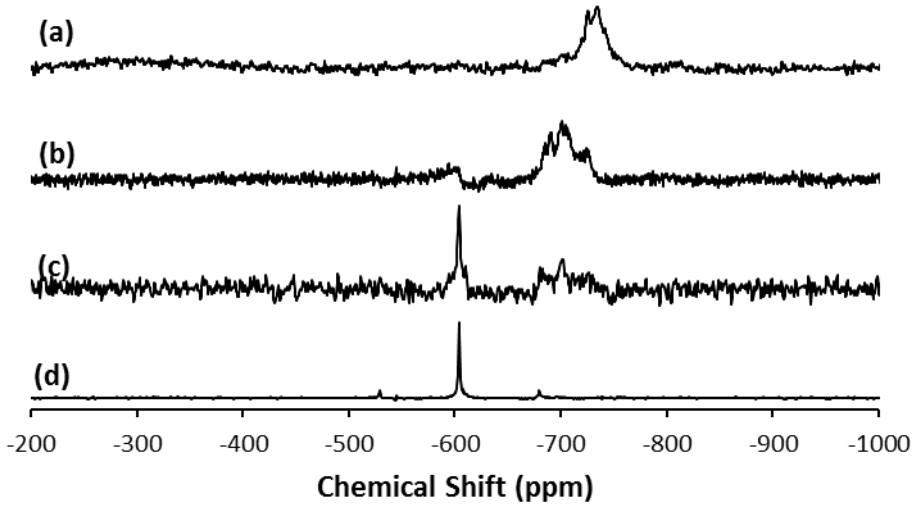


**Figure 6.4 As-synthesized Sn-Beta calcined with (a) dry air, (b) air saturated with water at 25ºC after step (a), (c) air saturated with water at 80ºC, and (d) argon. Steaming was performed by Raj Gounder and catalyst was synthesized by Ricardo Bermejo-Deval. All calcinations were done under following conditions: 1ºC/min to 150ºC, hold at 150ºC for 3 hours, 1ºC/min to 580ºC and hold at 580ºC for 12 hours.**

Changing the gas in the calcination treatment from dry air to argon produced no framework Sn sites and all extraframework Sn sites (Figure 6.4d). The argon treatment and steam treatment in zeolite Beta could be a way of synthesizing another $SnO_2$/Si-Beta catalyst with higher activity than the one synthesized with $SnO_2$ clusters during the synthesis gel. Since these $SnO_2$ clusters would be formed in the zeolite Beta pores during calcinations, the amount extrazeolitic $SnO_2$ clusters that are inactive in water would be decreased.[22]

## 3. References


1. Corma, A. & Zones, S. *Zeolites and Catalysis*. (Wiley-VCH Verlag GmbH & Co. KGaA, 2010). doi:10.1002/9783527630295

2. Jones, C. W., Tsuji, K., Takewaki, T., Beck, L. W. & Davis, M. E. Tailoring molecular sieve properties during SDA removal via solvent extraction. *Microporous Mesoporous Mater.* **48,** (2001).

3. Jones, C. W., Hwang, S.-J., Okubo, T. & Davis, M. E. Synthesis of Hydrophobic Molecular Sieves by Hydrothermal Treatment with Acetic Acid. *Chem. Mater.* **13,** 1041–1050 (2001).

4. Camblor, M. A. et al. Infrared Spectroscopy Investigation of Titanium in Zeolites. A new Assingment of the 960 band. *J. Chem. Soc. Chem. Commun.* **1557,** (1993).

5. Román-Leshkov, Y. & Davis, M. E. Activation of Carbonyl-Containing Molecules with Solid Lewis Acids in Aqueous Media. *ACS Catal.* **1,** 1566–1580 (2011).

6. Zapata, P. a, Faria, J., Ruiz, M. P., Jentoft, R. E. & Resasco, D. E. Hydrophobic zeolites for biofuel upgrading reactions at the liquid-liquid interface in water/oil emulsions. *J. Am. Chem. Soc.* **134,** 8570–8 (2012).

7. Lew, C. M. *et al.* Hydrofluoric-acid-resistant and hydrophobic pure-silica-zeolite MEL low-dielectric-constant films. *Langmuir* **25,** 5039–44 (2009).

8. Huang, M. & Adnot, A. Silylation of H-ZSM-5: An X-ray photoelectron and infrared spectroscopy study. **89,** 4231–4237 (1993).

9. Verboekend, D. & Pérez-Ramírez, J. Design of hierarchical zeolite catalysts by desilication. *Catal. Sci. Technol.* **1,** 879 (2011).

10. Thibault-Starzyk, F. *et al.* Quantification of enhanced acid site accessibility in hierarchical zeolites – The accessibility index. *J. Catal.* **264,** 11–14 (2009).

11. Dapsens, P. Y., Mondelli, C. & Pe, J. Biobased Chemicals from Conception toward Industrial Reality : Lessons Learned and To Be Learned. (2012).

12. Gil, B., Mokrzycki, Ł., Sulikowski, B., Olejniczak, Z. & Walas, S. Desilication of ZSM-5 and ZSM-12 zeolites: Impact on textural, acidic and catalytic properties. *Catal. Today* **152,** 24–32 (2010).

13. Miltenburg, a. *et al.* Alkaline Modification of MCM-22 to a 3D Interconnected Pore System and its Application in Toluene Disproportionation and Alkylation. *Top. Catal.* **52,** 1190–1202 (2009).

14. Bermejo-Deval, R. *et al.* Metalloenzyme-like catalyzed isomerizations of sugars by Lewis acid zeolites. *Proc. Natl. Acad. Sci. U. S. A.* **109,** 9727–32 (2012).

15. Chao, P.-Y., Tsai, S.-T., Tsai, T.-C., Mao, J. & Guo, X.-W. Phenol Hydroxylation over Alkaline Treated TS-1 Catalysts. *Top. Catal.* **52,** 185–192 (2009).

16. Xin, H. *et al.* Enhanced Catalytic Oxidation by Hierarchically Structured TS-1 Zeolite. *J. Phys. Chem. C* **114,** 6553–6559 (2010).

17. Maier, S. M., Jentys, A. & Lercher, J. a. Steaming of Zeolite BEA and Its Effect on Acidity: A Comparative NMR and IR Spectroscopic Study. *J. Phys. Chem. C* **115,** 8005–8013 (2011).

18. De Lucas, A., Canizares, P., Durán, A. & Carrero, A. Dealumination of HZSM-5 zeolites: Effect of steaming on acidity and aromatization activity. *Appl. Catal. A Gen.* **154,** 221–240 (1997).

19. Otomo, R., Yokoi, T., Kondo, J. N. & Tatsumi, T. Applied Catalysis A : General Dealuminated Beta zeolite as effective bifunctional catalyst for direct transformation of glucose to 5-hydroxymethylfurfural. *"Applied Catal. A, Gen.* **470,** 318–326 (2014).

20. Bokhoven, J. A. Van, Koningsberger, D. C., Kunkeler, P. & Bekkum, H. Van. Stepwise Dealumination of Zeolite Beta at Specific T-Sites Observed with 27 Al MAS and 27 Al MQ MAS NMR. **8,** 12842–12847 (2000).

21. Ke, X., Xu, L., Zeng, C., Zhang, L. & Xu, N. Synthesis of mesoporous TS-1 by hydrothermal and steam-assisted dry gel conversion techniques with the aid of triethanolamine. *Microporous Mesoporous Mater.* **106,** 68–75 (2007).

22. Bermejo-deval, R., Gounder, R. & Davis, M. E. Framework and Extraframework Tin Sites in Zeolite Beta React Glucose Differently. *ACS Catal.* **2,** 2705–2713 (2012).